CRANFIELD INSTITUTE OF TECHNOLOGY

School of Mechanical Engineering

Ph.D. Thesis

Academic Year 1986-87

MOHAMMED EL-NABAWEY A. GAHEEN

STATIC AND DYNAMIC FINITE ELEMENT ANALYSIS OF PNEUMATIC TYRES INCLUDING ANISOTROPIC AND NONLINEAR EFFECTS

SUPERVISORS	PROFESSOR	R.A. COOKSON
	DR.	A.M. EL-ZAFRANY
EXTERNAL EXAMINER	DR.	C.W. BARSON
	MANAGER	
	TYRE RESEARCH DEPT	
	DUNLOP	

April 1987

TO MY PARENTS

ACKNOWLEDGMENTS

The author would like to express his sincere appreciation and gratitude to all these kind people without whom this work would have never been completed.

The author cannot find enough words to express his gratitude and his true feelings towards Professor Roy Cookson, the Head of the Applied Mechanics Group. His kind encouragement, valuable advice, and continuous help will not be forgotten.

The author would like to express his sincere thanks to Dr. Ali El-Zafrany, without whose useful advice, guidance and continuous encouragement, this thesis would not have come to fruition.

The author is extremely grateful to the kind people of his Country, EGYPT, for their support which includes their generous sponsorship.

The author is indebted to the DUNLOP Company, Birmingham, for providing him with data and experimental results, for the radial tyre investigated in this work.

The author would like to thank the Staff of the Automotive Studies Group, for their kind cooperation. Particularley Mr. Healy, for his help during the experimental work.

This work would not have been possible without the facilities and the good service made avaible by the C.I.T. Computer Centre.

The author's life on the Cranfield Campus would have become extremely difficult without the presence of many good friends.

The author would like to thank the Committee of Vice-Chancellors and Principals for their ORS awards.

Finally, nothing could have been achieved without the support, patience, love and kindness of the author's wife and children.

SUMMARY

This thesis introduces a versatile finite element package, which is tailored for the static and dynamic analysis of radial tyres. A new axisymmetric solid-of-revolution element which takes into consideration, large deformation, the influence of composite orthotropic material and the viscoelasticity and the nonlinearity of the material properties, has been developed for a general loaded tyre. The finite element package has been verified by comparing its results with available analytical, numerical and experimental results. A full static and dynamic investigation has been carried out for a commercial tyre 175 HR 14 and results obtained by using the package have been compared with available experimental results developed by DUNLOP or carried out at Cranfield.

The package has proved to be reliable, flexible, efficient, economic and accurate. The numerical instability problems which are prevalent in this type of analysis have been overcome by the derivation of a developed Newton-Raphson iterative scheme.

CONTENTS

		Page No
1.	INTRODUCTION	1
2.	LITERATURE REVIEW	5
	2.1 Macroscopic Analysis of Tyres	5
	2.2 Microscopic Analysis of Tyres	6
	2.3 Finite Element Methods	14
	2.4 Rubber Analysis	16
3.	LINEAR FINITE ELEMENT ANALYSIS AND MESH GENERATION FOR PNEUMATIC TYRES	19
	3.1 Introduction	19
	3.2 The Elastic Constants of a Composite Laminate	20
	3.3 Stress-Strain Relation for Reinforced Layers	25
	3.4 Rubber Analysis	26
	3.5 Finite Element Formulation	28
	3.6 Loading Analysis	38
	3.7 Boundary Conditions	41
	3.8 Mesh Generation	43
	3.9 Mesh Plotting	46
4.	NONLINEAR FINITE ELEMENT ANALYSIS OF A RADIAL TYRE	48
	4.1 Introduction	48
	4.2 Analysis of Material Nonlinearity	48
	4.3 Analysis of Large Deformation for Axisymmetric Loading	51
	4.4 Analysis of Large Deformation with General Loading	60
	4.5 Application to Nonlinear Analysis of Tyre	63

5. VISCOELASTIC STRESS ANALYSIS 65

5.1 Introduction 65
5.2 Mechanical Representation of Viscoelastic Behaviour 65
5.3 Viscoelastic Stress Analysis 66
5.4 Solution Algorithm 73

6. LINEAR AND NONLINEAR DYNAMIC ANALYSIS OF RADIAL TYRES 75

6.1 Introduction 75
6.2 Derivation of Stiffness and Mass Matrices 77
6.3 Dynamic Eigenvalue Problem 79

7. FINITE ELEMENT PROGRAMMING 86

7.1 Introduction 86
7.2 Preprocessing Modules 87
7.3 Analysis Modules 91
7.4 Postprocessing Modules 100

8. RESULTS AND DISCUSSION 104

8.1 Package Verification 104
8.2 The Case Study of the Radial Tyre 107
8.3 Static Analysis of the Tyre 110
8.4 Viscoelastic Analysis of the Tyre 113
8.5 Dynamic Analysis of the Tyre 114
8.6 General Discussion 115

9. CONCLUSIONS 118

REFERENCES 121

TABLES

No.		Page No
7.1	Gaussian Quadrature Parameters	133
8.1	Comparison Between the Computed and Analytical Solution for Pressurised Cylinder	134
8.2	Comparison of the Results Between The Package and the MARC Package for a Composite Pressurised Cylinder	134
8.3	The Natural Frequencies of a Cylinder	134
8.4	Material Properties of 175-HR-14 Radial Tyre	135
8.5	The Eigenvalue and Natural Frequencies of the 175-HR-14 Radial Tyre	136
8.6	Radial and Axial Displacements of Pressurised Cylinder Using N-R, M-N-R and D-N-R.	137

FIGURES

No.		Page No
3.1	Cord ana Rubber Ply Lamenate	138
3.2	Elastic Modulus Representation in Direction 1	138
3.3	Elastic Modulus Representation in Direction 2	138
3.4	Elastic Modulus Representation in Direction 3	139
3.5	Lamina Under Shearing Load	139
3.6	Loaded Lamina Under Unidirectional Load	139
3.7	Rotation of Coordinates	140
3.8	Use of One-D Element for Equivalent Nodal Force of a Uniformly Distributed Pressure.	140
3.9	Representation of Pressure Distribution for Externally Loaded Tyre.	140
3.10	Generation of Quadrilateral Elements in Quadrilateral Block.	141
4.1	Interpolative Procedure	142
5.1	Time Dependent Behaviour of Stress and Strain	143
5.2	Spring-Dashpot model	144
5.3	Tyre-Time Dependent Model	144
7.1	Package Structure	145
7.2	Schematic Diagram of the Preprocessing Module	146
7.3	Schematic Diagram of the Mesh Generation Module	147
7.4	Schematic Diagram of the Analysis Module	148
7.5	Static Analysis Module	149
7.6	Iterative Procedure for Material Nonlinearity	150
7.7	Increment Load Procedure and Fourier Series Expansion	151
7.8	Iterative Procedure for Large Deformation Analysis	152
7.9	Interpolative Procedure of Viscoelastic Analysis	153
7.10	Simple Iteration Technique	154
7.11	Flow Chart of Dynamic Condensation	155

7.12	Subspace Iteration	156
7.13	Postprocessing Module	157
8.1	Deformed Shape of Pressurised Cylinder	158
8.2	Deformed Shape of Pressurised Composite Cylinder	159
8.3	First Mode Shape of Cylinder	160
8.4	Second Mode Shape of Cylinder	161
8.5	Third Mode Shape of Cylinder	162
8.6	Fourth Mode Shape of Cylinder	163
8.7	Fifth Mode Shape of Cylinder	164
8.8	Cross-Section of 175 HR 14 Radial Tyre	165
8.9	Test Rig	166
8.10	Area of Contact and Pressure Distribution of Externally Loaded Radial Tyre	167
8.11a	Mesh Blocks of Radial Tyre	168
8.11b	Three Dimensional Plotting of Radial Tyre	169
8.12	Generated Elements of Radial Tyre	170
8.13	Deformed Shape of an Inflated Radial Tyre	171
8.14	The Deformed Shape o 175 Hr 14 Radial Tyre	172
8.15a	Deformed Shape of Externally Loaded Radial Tyre	173
8.15b	Radial and Axial Displacements in The Circumferential Direction of Externally Loaded Tyre	174
8.16	Load Deflection Curves of 175 HR 14 Radial Tyre	175
8.17	Stress Distribution in Section I of the Radial Tyre	176
8.18	Stress Distribution in Section II of the Radial Tyre	177
8.19	Stress Distribution in Section III of the radial Tyre	178
8.20	Stress Distribution in Section IV of the Radial Tyre	179
8.21	Stress Distribution in Section i of an Externally Loaded Radial Tyre	180
8.22	Stress Distribution in Section II of an Externally Loaded Radial Tyre	181
8.23	Stress Distribution in Section III of an Externally Loaded Radial Tyre	182
8.24	Stress Distribution in Section IV of an Externally Loaded Radial Tyre	183
8.25a	Principal Stress Distribution in a Casing Ply	

	of an Inflated Radial Tyre	184
8.25b	Principal Stress Distribution in a Casing Ply of an Externally Loaded Tyre	185
8.26a	Principal Stress Distribution in Breaker 1 of an Inflated Radial Tyre	186
8.26b	Principal Stress Distribution in Breaker 1 of an Externally Loaded Tyre	187
8.27a	Principal Stress Distribution in Breaker 2 of an Inflated Radial Tyre	188
8.27b	Principal Stress Distribution in Breaker 2 of an Externally Loaded Tyre	189
8.28a	Principal Stress Distribution in Breaker 3 of an Inflated Radial Tyre	190
8.28b	Principal Stress Distribution in Breaker 3 of an Externally Loaded Tyre	191
8.29a	Principal Strain Distribution in Casing Ply of an Inflated Radial Tyre	192
8.29b	Principal Strain Distribution in Casing Ply of an Externally Loaded Tyre	193
8.30a	Principal Strain Distribution in Breaker 1 of an Inflated Radial Tyre	194
8.30b	Principal Strain Distribution in Breaker 1 of an Externally Loaded Tyre	195
8.31a	Principal Strain Distribution in Breaker 2 of an Inflated Radial Tyre	196
8.31b	Principal Strain Distribution in Breaker 2 of an Externally Loaded Tyre	197
8.32a	Principal Strain Distribution in Breaker 3 of an Inflated Radial Tyre	198
8.32b	Principal Strain Distribution of Breaker 3 of an Externally Loaded Tyre	199
8.33a	Stress Distribution in a Casing Ply of an Inflated Radial Tyre	200
8.33b	Stress Distribution in a Casing Ply of an Externally Loaded Tyre	201
8.34a	Stress Distribution in Breaker 1	

	of an Inflated Radial Tyre	202
8.34b	Stress Distribution in Breaker 1	
	of an Externally Loaded Tyre	203
8.35a	Stress Distribution in Breaker 2	
	of an Inflated Radial Tyre	204
8.35b	Stress Distribution in Breaker 2	
	of an Externally Loaded Tyre	205
8.36a	Stress Distribution in Breaker 3	
	of an Inflated Radial Tyre	206
8.36b	Stress Distribution in Breaker 3	
	of an Externally Loaded Tyre	207
8.37	Deformed Shape of an Inflated Radial Tyre	
	with Viscous Effect	208
8.38	Principal Stress Distribution in a Casing Ply	
	Due to Inflation and Viscous Effect	209
8.39	Principal Stress Distribution in Breaker 1	
	Due to Inflation and Viscous Effect	210
8.40	Principal Stain Distribution in a Casing Ply	
	Due to Inflation and Viscous Effect	211
8.41	Principal Strain Distribution in Breaker 1	
	Due to Inflation and Viscous Effect	212
8.42	First Mode Shape of Radial Tyre	213
8.43	Second Mode Shape of Radial Tyre	214
8.44	Third Mode Shape of Radial Tyre	215
8.45	Fourth Mode Shape of Radial Tyre	216
8.46	Fifth Mode Shape of Radial Tyre	217

CHAPTER 1

INTRODUCTION

CHAPTER 1

Without the pneumatic tyre, development of motor vehicle transport would not have been possible. It plays the major role in generating vehicle stability and limiting front wheel vibration. The main functions of the tyre can be summarised as follows:

It transmits the driving and braking forces between the vehicle and the ground.

It is used for vehicle guidance through the steering mechanism

It absorbs and damps the displacements resulting from local road surface irregularities for a wide range of road materials

Therefore; the basic tyre requirements for the fulfilment of these functions are:

No appreciable change of its size with inflation.

Ability to deform from a double-curved surface to a plane surface.

Enough rigidity to develop forces in any direction.

Tyre design has progressed remarkably to today's reliable, high mileage, steel belted tubeless, radial tyre. An extensive effort is required to investigate its effects on vehicle ride and handling characteristics, as well as, tyre deflections and stresses.

The finite element technique has been chosen, as will be

explained in Chapter 2, for the static and dynamic analysis of radial tyres because of its well known versatility in handling arbitrary boundary conditions and structural vibration.

Commercially available finite element programs, have large libraries of generally-applicable elements. These packages are found to be lacking in one or other of the capabilities that are necessary to the analysis.

The main objective of this work is to design a powerful, versatile, finite element package tailored for the efficient static and dynamic analysis of radial tyres. The package will be capable of dealing with large deformation of tyre, rubber incompressibility and viscoelasticity, and composite and orthotropic laminate tyre structures. A commercially available radial tyre will be investigated using the package and the results will be compared with available analytical and/or experimental values.

The major scope of the thesis is to introduce mathematical models required for the finite element analysis of tyres and to discuss the results obtained. The thesis is divided into 9 chapters, the first of which is this introduction.

A comprehensive literature review is summarised in Chapter 2 , where classical and modern approaches for tyre analysis have been examined in order to justify the current work.

In Chapter 3 , the derivation of finite elements employed for the linear static analysis of tyres are explained, taking the following into consideration:

a- The composite nature of the reinforced layers of the tyre and the orthotropic material properties of each element.

b- The incompressibility of the rubber.

c- The type of loading, in which the tyre is inflated with or without an external radial load

In Chapter 4 , the derivation of appropriate finite elements is extended to include the nonlinearity due to the elastic properties of the material and the large deflection, using interpolative and iterative techniques. This derivation has been carried out for both the inflated and externally loaded tyre.

Another source of nonlinearity, the viscoelastic properties of the rubber, has been dealt with in Chapter 5. The derivation of the mathematical model is given as well as an interpolative technique for its solution.

It is well known that the dynamic characteristics of a structure are completly defined in terms of its natural frequency and mode shapes, as will be shown in Chapter 2. Hence, the dynamic analysis of a tyre will be directed towards the determination of the natural frequencies and the corresponding natural mode shapes. The derivation of the mathematical model, as well as the solvers used for its solution, will be given in Chapter 6.

The computer program developed in this work for the static and dynamic analysis, as well as the procedures for automating input and output for the program will be explained in Chapter 7.

In Chapter 8 , the verification of the program as well as the static and dynamic analysis of a 175 HR 14 radial tyre, will be illustrated.

The results of the package will be compared with experimental results either given by DUNLOP or carried out here at Cranfield, and some discussion will be given.

Finally, the basic conclusions and recommendations for future work will be listed in Chapter 9.

Due to the large number of formulations involved in this work, only the principal ideas and final equations are given in the main thesis, whilst the details will be described in an Appendix. A precise description of the necessary guide for the user of the programming package will be submitted in a separate report to the department.

CHAPTER 2

LITERATURE REVIEW

CHAPTER 2

LITERATURE REVIEW

The pneumatic tyre can be considered as a suspension element, and its physical models are developed for application in vehicle behaviour analysis. There are two basic types of tyre parameter which can influence its characteristics: (a) design and construction parameters, and (b) preformance parameters .

The design and construction parameters of tyres cannot be fully described without a detailed analysis of all their physical and chemical properties. The performance parameters which affect tyre characteristics are; the frequency response, the speed of travel, radial loads, the inflation pressure, road roughness, unbalance weight and out-of-roundness.

The tyre may be modelled macroscopically in terms of discrete mechanical components such as springs and dashpots[1,2]. An alternative approach to describe the tyre microscopically, in which the tyre is modelled in terms of its actual constituent components and the geometry of its structure, is also possible

The tyre modelling based upon the macroscopic analysis is reviewed very briefly here, followed by the microscopic modelling of the tyre, and finally; the development of the finite element technique suitable for the analysis of the tyre will be summarised.

2.1 MACROSCOPIC ANALYSIS OF TYRES:

For this type of analysis, the tyre may be represented by springs and dashpots, as mentioned earlier. There is a large number of publications dealing with the tyre macroscopically.

A comprehensive test programme [5] is intended to bring to light

the prevailing relations between tyre design and performance parameters. Some authors [3,7,8] treated the tyre as a stretched circular string. A simple model which represents the radial dynamic properties of pneumatic tyre is developed by Hooker [9]. His tyre model consists of a series and parallel spring-damper arrangement which fits the observed behaviour. Four different basic tyre models, suitable for dynamic vehicle simulation, are formulated by Captain et al [4].

The effect of tyre design and performance parameters on the tyre characteristics were organised in a computer program that would extract, correlate and display any data of interest by Schuring et al [5].

The selection of the appropriate tyre model for a specific analysis is a difficult task, since a wide range of model formulation exists. A comparison between model capabilities and limitations from which relative performance can be assessed is not available. Another disadvantage of the macroscopic modelling technique, is its incapablity of predicting carcass strains, cord loads, and the effect of constructional geometry and changes in constituent material properties on tyre deformation behaviour.

A brief survey of these models and their evaluation is summarised in Appendix [A].

The finite element method can be recommended as an alternative approach to microscopic analysis because it is very flexible and provides accurate results for complex structures and general loads as will be seen.

2.2 MICROSCOPIC ANALYSIS OF TYRES:

The composite nature of the tyre carcass, resulting from combinations of rubber and cord in complex geometric patterns, gives rise to a deformable body which is neither homogeneous nor isotropic.

The complex system of loads, to which the tyre is subjected, arising from rotation and road contact, causes the carcass to undergo large deformations, even though the resulting internal cord strain is small.

The basic factors which should be considered for accurate analysis of tyres are; the complex geometry of the structure, the anisotropicity of material properties, the indetermination and asymmetry of loading condition, and the large deformation for such a highly flexible body.

Hence, it is essential to find a powerful and sophisticated method of analysis which can deal with such factors. The finite element method represents a powerful numerical technique which can cope with such a problem.

The bulk of the existing literature dealt with the tyre as a purely elastic structure. Some of the previous investigators for example [11] have used a one dimensional ring model to predict its characteristics approximately. Such a model is based upon very simplified material properties.

The membrane theory is applied to calculate the stresses in the cord due to the inflation pressure [12,13]. In this model the matrix of the plies is considered as a filling material to hold the cords together, whilst the strength of the carcass is obtained from the cords.

The thin shell of revolution with membrane and bending stiffness was used by Petal, Zorowski and Dunn [14,15], to predict the deformation shape and resulting cord forces in the tyre. The material properties were assumed to be linearly orthotropic and the model was subjected to inflation pressure and rotational loading. A number of difficulties were encountered in their work, such as the high sensitivity of the iterative scheme and the large CPU time consumed in the solution.

Since the membrane theory is based upon the assumption that the thickness of the structure is very small, it will not be adequate to be employed for the analysis of tyres as has been used by [12,13] who neglect the out-of-plane-bending rigidity. On the other hand, the shell models produce a more accurate result for the actual tyre behaviour due to the inclusion of the out-of-plane-bending rigidity. None of the present models is able to account for the effect of transverse shear deformation. This effect is very significant for the case of the highly anisotropic composite materials used in tyres, since their resistance to shear is much smaller than their resistance to normal stresses.

Hence, the models mentioned earlier cannot describe accurately the deformation, stresses and strains for tyres.

The carcass is basically a composite structure consisting of layers or plies of cord reinforced rubber. The property of the individual plies themselves must be specified before calculating the load-deformation relationship for the whole tyre.

The ply properties are, in turn, functions of the constitutive equations of the component materials as well as their geometrical arrangement. The ply properties are determined from the application of micromechanic theories.

Existing micromechanic theories have been developed for materials that are homogeneous and linearly elastic [24,25,26]. The cord consists of numerous filaments of fibres twisted together to form a structure which is macroscopically heterogeneous and visco-elastic[22]. In Reference [17], the structure was considered as a two-phase material consisting of high-strength, high modulus fibres embedded in a relatively softer and lower strength matrix. The basic load carrying element is the fibre, while the matrix acts as a stress transfer medium. In reference [18], the author considered that the function of the rubber was to support the other elements in their locations adding only a relatively small amount to the overall

structural stiffness .

Watanabe and Kaldjian [17,18] used a mathematical model consisting of an aggregation of a finite number of truss elements with a three dimensional solid element, and the tread rubber has been neglected. This model was used for the analysis of the deformation of a bias-ply motorcycle tyre subjected to inflation pressure.

Trinko [21], used laminated, geometrically non-linear finite elements where the tyre was represented by one quarter model. The rubber portions were modelled using solid eight-noded hexahedra, whilst the cord-reinforced layers were modelled using four-noded quadrilateral membrane elements. The rubber was assigned a Poisson's ratio of 0.48. The footprint loading was simulated by enforcing vertical displacement at selected nodes of the model to yield a contact patch force distribution.

An axisymmetric, solid-of-revolution, element for both symmetric and asymmetric loading conditions was used for the static analysis of tyres [16,20].

Reference 16 by DeEskinaze and Ridha, used eight-noded iso-pararmetric elements for nonlinear analysis. They, discretised the tyre into bands through the thickness. The inflation pressure was applied as two equal load increments and an iterative technique was used for the solution of the equations which satisfy equilibrium at the end of each loading increment. Their analysis was used for the determination of tyre deformation and variation of cord load along the tyre profile.

Reference 20 by Kaga, Okamoto and Tozawa, used the axisymmetric solid of revolution under asymmetric loads to calculate the displacements and internal stresses and strains. They approximated tyre nonlinearities by using a sequence of linearised steps, and the final deformed shape of the tyre was determined incrementally through a sequence of equilibrium configurations, each of which was obtained

from the previous one by the application of the linear theory. Fourier series was used by Reference 20 for the representation of the external load.

In both of the models described by References 16 and 20, the warping effect due to the laminated composite structure was neglected. Hence, allowing the problem to be treated as two-dimensional. Reference 20 later goes on to consider the circumferential direction due to asymmetric loading.

An experimental investigation was carried out by Janssen and Walter[41], to measure the stresses and strains within the tyre. They used different methods for each region of the tyre. Miniature force transducers were used to measure the cord stresses arising from tyre shaping during vulcanisation, the change in cord stress patterns caused by postinflation, and the cord loads caused by tyre inflation and by cornering. Liquid metal gauges were used to measure rubber strains on tyre surfaces. A photoelastic method was used to measure the strain distribution in the interior of the tyre under simulated load.

The study of the dynamic properties of tyres is associated with difficulties, such as, the presence of large strains, anisotropicity of the material, complex shape of the tyre, and the distribution of external forces.

The simplest approach to tyre dynamics is the one-dimensional ring [11,30]. This has been found to be inaccurate for the determination of the natural frequency, the mode shapes and the tyre deformation of the stress behaviour.

In 1975, Soedal[33] presented an approach for predictng tyre response to arbitrary transient road vibrations, as well as, to arbitrary road profiles, based on the tyre natural frequency and mode shapes. It has been discovered that when the arbitrary rolling speed coincides with one of the natural frequencies divided by its circum-

ferential wave number, a standing wave will be built up to annoying and destructive levels, which results in a drastic increase in power losses and tyre temperature.

An experimental investigation was carried out by Potts[39], to display the resonant mode shapes of vibrating radial tyres with varying belt composition, using the time-avergaged holographic technique.

An analytical finite-element procedure was developed by Padovan [32], to obtain the natural frequency of rotating anisotropic shells of revolution.

The doubly-curved, axisymmetric shell finite-elements and the modal expansion approach were used for investigating the linear dynamic response of radial tyres by Chang and Yang[34,35]. This work was extended by Hunckler[36,37] to include the orthotropic material properties with first and second order nonlinear stiffness terms, but it was limited to small amplitude vibration analysis.

The standing wave which can be generated in tyres is demonstrated as a viscoelastic tyre resonance response. In 1976, Padovan[38], discussed the effect of damping on the development of the standing wave phenomenon, using the classical ring on foundation model. In 1977, the same author[40] extended his work using a rotating laminated shell model of the tyre.

The viscoelastic constitution law is treated as being of either the differential or hereditary integral type.

In the differential type the stress-strain relation may be represented by the general differential equation form[46,47,48]:

$$P_k d^k\sigma/dt^k = q_k d^k\varepsilon / dt^k \qquad \text{or}$$

$$P\,\underline{\sigma} = Q\,\underline{\varepsilon} \qquad \text{where;}$$

P & Q are differential operators:

$$P = \sum_{0}^{\infty} P_k d^k \quad / \, dt^k$$

$$Q = \sum_{0}^{\infty} q_k d^k \quad / dt^k$$

in which the mathematical model can be represented by the Kilven model, the Maxwell model or a combination of the two.

A Laplace transform can be used to solve the above equation, in which the problem of viscoelasticity will be reduced to a problem of elasticity[49,50,51]. For this case the differential equation is reduced to:

$$\underline{\sigma} = \underline{D}\,\underline{\varepsilon}$$

and the equation of equilibrium is:

$$\underline{K}\,\underline{\delta} = \underline{F} \qquad (2.1)$$

$\underline{F}$ is the Laplace transform of nodal force, and:

$$\underline{D} = \underline{D}_0 + \frac{s}{s+\bar{\gamma}_1}\underline{D}_1 + \frac{s}{s+\bar{\gamma}_2}\underline{D}_2 + \qquad + \frac{s}{s+\bar{\gamma}_n}\underline{D}_n \quad ,$$

$$\underline{K} = \underline{K}_0 + \frac{s}{s+\bar{\gamma}_1}\underline{K}_1^{s} + \frac{s}{s+\bar{\gamma}_2}\underline{K}_2 + \qquad + \frac{s}{s+\bar{\gamma}_n}\underline{K}_n$$

where ;

$$\underline{K}_i = \iiint \underline{B}^T \underline{D}_i \underline{B}\, dv \qquad i=1,2,3, \qquad n$$

Equation (2.1) can be solved using the classical finite-element technique, whilst the Laplace inversion of any particular stress component, provides the stress distribution for the original viscoelastic problem.

The Laplace transform technique is restricted to a narrow range

of problems in which it is possible to find an explicit solution to the associated equations of elasticity, and where the body and the surfaces do not change with time [52].

A step-by-step approach, using small intervals, has been proposed by Zienkeiwicz and Watson[52]. In this approach it was asumed that the stress was constant over the time interval and the finite-element method was used for the correction of the compatibility of strain at the end of each interval.

A finite-element algorithm was developed by McGens Henrikson [53], for the analysis of nonlinear viscoelastic materials. He developed a single integral constitutive law for the description of the material behaviour which can be expressed as follows:

$$\underline{\sigma}^{t} = \underline{D}\, e^{t} - \frac{1}{D_i^{t}} \{ \underline{\varepsilon} \}$$

The accuracy of the solution to this constitutive equationn is not affected by the method of derivation of the stiffness matrix but the rate of convergence of the solution may be.

In order to reduce the computational effort, a convergence-acceleration scheme as proposed by Zienkiewicz[54], is recommended.

Instead of starting with spring-dashpot analysis, some authors [46,47], employed the hypothesis that the current value of the stress tensor depends upon the complete past history of the stress and on the current value of the strain, corresponding to an instantaneous elasticity effect. The stress-strain relation based on their hypothesis may be represented by an integral form as follows:

$$\sigma_{ij}(t) = \int_0^{\infty} \varepsilon_{kl}(t-s)\, dC_{ijkl}$$

which is called, the hereditary integral. This formulation is completely equivalent to the differential formulation, and has the advantage of exhibiting greater flexibility with the measured

properties of the actual material.

2.3 FINITE ELEMENT METHODS:

Although the finite-element method did not come into use until the 1950's when it was introduced for the first time by Turner et al [55], the idea of representing a continuous medium by a set of discrete elements has been in use much longer.

In 1941, Hrennikoff[56], introduced the concept of representing arbitrary shaped plates by beams along their edges and diagonals. The displacement approach to the solution of finite-element problems, a method more widely used than the stress or hybrid, is illustrated by an axially loaded spring;

$$\underline{F} = \underline{K}\,\underline{\delta}$$

where:

$\underline{F}$ is the applied load

$\underline{K}$ is the stiffness matrix

$\underline{\delta}$ is the displacement

Contained herein, is a brief survey of some of the elements that can be used in tyre analysis.

2.3.1 Constant Strain Triangular Element:

For this element a linear displacement function is assumed, this making the task of deriving the element properties very simple. This element is limited in use, and requires considerable mesh refinement in modelling the tyre leading to increased cost and reduced numerical accuracy. The shape and orientation of the triangular element may

influence the results. It is also limited in linear analysis, and the bending stretching effect is neglected. Its application for axisymmetric loading is straightforward. However, analysis for asymmetric loading becomes cumbersome.

2.3.2 Membrane Element:

The membrane analysis is generally limited in scope and application[60], because of the following:

The abrupt changes in geometry, material properties, or loading cannot be handled.

It cannot account for the effect of transverse shear deformation in the contact area.

Local forces cannot be predicted in zones of significant curvature change or where there is a discontinuity in the orientation of the plies.

2.3.3 Thin Shell Element:

Thin, curved shell, elements extending through the tyre thickness were used by Zorowski and Dunn[61]. The main disadvantage of this element is that the convergence of the iteration process, and the accuracy of the solution, are dependent upon the size of the element and the magnitude of loading. The curved thin shell element is still limited for use due to the following:

Special care is needed in representing the finite-element grid location of the nodes or a smooth profile is necessary for accurate results.

Calculated stresses are not accurate particularly at positions

of high stress gradient and for discontinuous plies.

A plane through the thickness does not remain plane after deformation.

The transverse shear stress is neglected.

Thin shell theory can be used to obtain a more general solution of the tyre than that obtained with the membrane theory.

Most classical shell theories are not directly applicable to tyre analysis, because of complexity of geometry, variation of thickness, nonuniformity of composite properties and large deformations.

2.3.4 Axisymmetric Solid of Revoluton:

The axisymmetric element of the isoparametric family has significant advantages. It is possible to carry out a full three-dimensional analysis by using the axisymmetry of the structure. In this way the size of the mesh, and the necessary computational time, can be reduced. The element can deal with very complex structures.

There is a need for an element with which it is possible to calculate the deformation and shear stresses at the belt edge. These streses can be calculated, either by a modified two-dimensional element, or by a full three-dimensional one.

2.4 RUBBER ANALYSIS:

The pneumatic tyre contains a variety of rubber compositions, each able to contribute some particular factor to overall performance The guiding principle in the development of rubber compositions for tyres is to achieve the best balance of properties for a particular

type of tyre service.

For incompressible materials , such as rubber , for which the stress tensor can be derived from the strain energy function, and in which the deformation can occur without an appreciable change in volume, a problem arises. This problem revolves around the fact that for in-plane, or axisymmetric, situations the stress tensor cannot be determined from the deformation alone. A hydrostatic pressure which does not affect the strain tensor must be considered in the evaluation of the stress tensor[63].

There are two main types of approach used in defining the constitutive equations for describing the elastic nature of rubber. The molecular approach considers the response of the molecular network to deformation, with the elasticity parameters being calculated from the finite molecular length and molecular weight between crosslinks. The other approach is the phenomenological approach, where elasticity theory is modified, often intuitively, and a postulated form is fitted to experimental results by regression. The particular constitutive equation will contain one or more constants which must be determined.

Many forms of strain energy function have been postulated, with constants which are adjusted to fit the shape of the stress-strain curve. Experimental data from more than one type of deformation have been included in these functions, in order to make them as general as possible.

Rivlin[71], developed a finite-element approach capable of treating rubber structures, with and without cord or plate reinforcements. It was found that an expression for strain energy, suitable for describing the behaviour of rubber compounds, is:

$$W = \sum_{ij=0}^{\infty} C_{ij} (I_1 - 3)^i (I_2 - 3)^j + \sum_{n=0}^{\infty} H_n (I_3 - 1)^n$$

and; $C_{00} = H_0 = 0$

where the values and the number of constants introduced into the formula can be found through biaxial traction and hydrostatic compression.

A modified strain energy expression was defined by Takamatsu et al [63] as:

$$W = W (I_1 , I_2) + P (I_3 -1)$$

where, P is a Lagrange multiplier,

I_1 , I_2 , I_3 denote the first, second and third principal strain invariants of Green's deformation tensor.

W, is a strain energy function which is known as the Moony- Rivlin form.

Pian and Lee [64], pointed out that the incompressibility constraints, imposed upon the assumed stress hybrid elements, are much less severe than those of the displacement method.

A finite-element method for the analysis of non-linear rubber was developed by Jankovich et al [65], using a penalty function approach based on a reduced constraint concept, and with the highly non-linear equations being solved means of the Newton-Raphson method.

Thus, until a generalised molecular hypothesis is found, any phenomenologic strain energy function that is postulated is merely a convenient mathematical representation.

Having recognised this fact, the problem of finding stress-strain equations, or strain energy functions, for a particular material, is simplified to one of finding an experimental method with an associated regression equation containing sufficient terms to accurately fit the experimental results.

CHAPTER 3

LINEAR FINITE ELEMENT ANALYSIS AND MESH GENERATION FOR PNEUMATIC TYRES

CHAPTER 3

LINEAR FINITE ELEMENT ANALYSIS AND MESH GENERATION FOR PNEUMATIC TYRES

3.1 INTRODUCTION:

The pneumatic tyre can be considered as an axially symmetric composite structure, with its geometry and material properties being independent of the circumferential direction. For the case of an isotropic material; the problem which is physically three-dimensional can therefore be considered mathematically as two-dimensional.

Due to the inclination of the reinforced plies with respect to the axis of symmetry, there is a twisting (transverse) shear force acting between the various plies of the tyre, which in turn leads to a considerable displacement component, (w) in the circumferential direction,(ϑ). Although the displacement components (including the warping displacement, w) are independent of , the above stress analysis problem is a three-dimensional one, with the full six components of stress and strain taken into consideration, as will be explained later.

The axisymmetric solid of revolution element, with isoparametric transformation, can be the most efficient finite element if it is developed for a full three-dimensional analysis.

The pneumatic tyre is obviously a very complex structure. The tread region, which is made of rubber, provides a means for applying the external loads. The carcass consists of a number of rubberised layers, each consisting of either nylon, rayon or steel cords which are fabricated to form a laminated composite structure. The cord layers are surrounded by a variable thickness rubber layer, allowing the shear load to be distributed throughout the tyre and protecting the main load-carrying cord plies from damage. For the case of

radial tyres, extra layers of cords between the carcass and the tread are included to act as a reinforcing element in the circumferential direction. The carcass and the reinforcing layers will be treated here as an orthotropic composite, while the filling rubber and the tread region will be considered as isotropic material. The cord layers are anchored to a rigid steel band, the bead, which holds the tyre on to the wheel.

3.2 THE ELASTIC CONSTANTS OF A COMPOSITE LAMINATE:

The elastic constants of a ply, which consists of cord and rubber, (Figure 3.1) can be represented by an assembly of springs in different arangements in the direction of each principal axis (1,2 or 3) as will be shown. The work will be extended here to include the calculation of the secondary Young's modulus, Poisson's ratios and the shear modulus which are neglected in the previous literature.

For the reinforced layers it is convenient to employ the Young's modulus E_r and Poisson's ratio ν_r of the rubber as the two independent constants, (Section 3.1.4). Whilst the twisted, fibrous, tyre cord which contains some void contents between its fibres, should be treated as a transversely isotropic material. The tyre cord elastic constants are significantly influenced by the amount of twist employed.

$$E_c = E_f / (1 + 4 \ R^2 \ T^2) \qquad \text{(Ref. 27)}$$

where E_f is the fibre modulus,
R is the cord radius and
T is the twist.

The rubber constants for each portion of the tyre, and the cord modulus of the cords, used in the numerical example given later are taken from the data given by DUNLOP, whilst the Poisson's ratio and shear modulus are taken from References [20,27]. -

a) Determination of E_1:

The Young's modulus of the layer in the principal direction (1) can be modelled by two springs connected in parallel representing the Young's modulus of the cords E_c and the filling matrix E_r. as shown in Figure (3.2).

Assuming that the strain will be the same all over the cross-section, it can be deduced that:

$$A\,\underline{\sigma} = A_c\,\underline{\sigma}_c + A_r\,\underline{\sigma}_r$$

Using Hooke's law

$$A\,E_1\,\underline{\delta} = E_c\,\underline{\delta}\,A_c + E_r\,\underline{\delta}\,A_r$$

where A_c , A_r are the cross-sectional areas of the cord and rubber respectively.

$$E_1 = E_c\,(A_c/A) + E_r\,(A_r/A)$$

$$= E_c\,V_c + E_r\,V_r$$

where V_c , V_r are the volume fractions of cord and rubber.

b) Determination of E_2:

The secondary Young's modulus E_2 which is the elastic modulus operating in the direction 2, for the layer can be represented by an arrangement of springs in series (Figure 3.3).

Assuming the stress will be the same, using Hooke's law,

$$\underline{\sigma}_c = E_c\,\underline{\sigma}_c \quad ,$$

$$\underline{\sigma}_r = E_r \underline{\varepsilon}_r$$

For layers of constant thickness, the cross-sectional area is also constant, hence;

$$\underline{\varepsilon}_2 A L = \underline{\varepsilon}_c A L_c + \underline{\varepsilon}_r A L_r$$

$$\underline{\varepsilon}_2 = \underline{\varepsilon}_c V_c + \underline{\varepsilon}_r V_r$$

$$\underline{\sigma} / E_2 = \underline{\sigma}_c V_c / E_c + \underline{\sigma}_r V_r / E_r$$

as, $\underline{\sigma} = \underline{\sigma}_c = \underline{\sigma}_r$,

hence,

$$1 / E_2 = V_c / E_c + V_r / E_r$$

or, $E_2 = E_c E_r / (E_c V_r + E_r V_c)$

c) Determination of E_3 :

Using the same procedure as before the layer can be represented by the arrangement shown in Figure (3.4), in which V_{r2} is the volume fraction of the coated layer while V_{r1} is the volume fraction of the rubber between cords.

$$E' = E_c E_r / (E_c V_{r2} + E_r V_c)$$

$$V_c + V_{r1} + V_{r2} = 1$$

$$E' = E_c E_r / (E_c(1 - (V_{r1} + V_c)) + E_r V_c)$$

and ;

$$E_3 = E' V_2 + E_r V_{r1}$$

$$E_3 = E' (1 - V_{r1}) + E_r V_{r1}$$

$$= \frac{E_r E_c - E_c E_r V_{r1}^2 - E_c E_r V_{r1} V_c + E_r^2 V_c V_r}{E_c (1 - (V_{r1} + V_c)) + E_r V_c}$$

$$E_r E_c / (E_c (1 - (V_{r1} + V_c)) + E_r V_c)$$

If the coated layer is very thin, the equation for the Young's modulus in the direction normal to the layer can be approximated by :

$$E_3 = E_c E_r / (E_c V_r + E_r V_c)$$

d) Determination of The Shear Modulli G_{12} , G_{13} :

Assuming that the shearing stresses on the cord and on the rubber are the same as shown in Figure (3.5a).

$$\gamma_r = \tau / G_r$$

$$\gamma_c = \tau / G_c$$

On the microscopic scale, the deformation shown in Figure (3.5b) will be :

$$\Delta = \gamma W \quad ,$$

$$\Delta_r = V_r W \gamma_r$$

$$\Delta_c = V_c W \gamma_c$$

since ; $\Delta = \Delta_r + \Delta_c$,

$$\gamma = V_r \gamma_r + V_c \gamma_c$$

$$\gamma = \tau / G_{12}$$

i.e. $$\tau / G_{12} = (V_r \tau / G_r) + (V_c \tau / G_c)$$

$$G_{12} = G_c G_r / (V_r G_c + V_c G_r)$$

Similarly, it can be deduced that:

$$G_{13} = G_{12}$$

e) Determination of Poisson's Ratios :

From Figure (3. 6), the major Poisson's ratio ν_{12}, is defined as :

$$\nu_{12} = -\varepsilon_2 / \varepsilon_1$$

Assuming that $\underline{\sigma}_1 = \underline{\sigma}$, while the other components are zeros; the deformation (Δw) is determined by :

$$\Delta w = - w\underline{\varepsilon}_2 = w\nu_{12}\underline{\varepsilon}_1$$

but : $$\Delta w = \Delta_r w + \Delta_c w$$

where; $\Delta_c w, \Delta_r w$ are the deformations of the cord and rubber respectively , and can be approximated by;

$$\Delta_r w = w V_r \nu_r \underline{\varepsilon}_1 \quad ,$$

$$\Delta_c w = w V_c \nu_c \underline{\varepsilon}_1$$

Combining the above equations :

$$w V_r \nu_r \underline{\varepsilon}_1 + w V_c \nu_c \underline{\varepsilon}_1 = w \nu_{12} \underline{\varepsilon}_1$$

i.e. $$\nu_{12} = V_r \nu_r + V_c \nu_c$$

Using the following relationship ;

$$\nu_{12} / E_1 = \nu_{21} / E_2$$

it can be shown that ;

$$\nu_{21} = E_2 \nu_{12} / E_1$$

Similarly ;

$$\nu_{13} = V_r \nu_r + V_c \nu_c \quad ,$$

$$\nu_{31} = E_3 \nu_{13} / E_1$$

and ;

$$\nu_{23} = ((\nu_c / \nu_r)- 1) / (\nu_c / \nu_r) \qquad \text{Reference [29]}$$

$$\nu_{32} = E_3 \nu_{23} / E_2$$

3.3 Stress-Strain Relation for Reinforced Layers :

The reinforced layers of the pneumatic tyre will be treated as an orthotropic material. The generalised Hooke's law relating stresses to strains can be written as :

$$\sigma_i = D_{ij} \epsilon_j \qquad i,j = 1,2,.....,6$$

where σ_i are the stress components, D_{ij} is the stress-strain matrix and ϵ_j are the strain components.

For an orthotropic material, there will be nine independent components in the D_{ij} matrix thus :

$$D_{ij} = D_{ji} \quad ,$$

$$\nu_{ij} / E_i = \nu_{ji} / E_j$$

and, since the elastic constants of the layers have been determined, the matrix, D_{ij} , in terms of these constants will be[24]:

$$D_{11} = (1 - \nu_{23} \nu_{32}) / E_2 E_3 \Delta$$

$$D_{12} = (\nu_{21} + \nu_{31} \nu_{23}) / E_2 E_3 \Delta$$

$$D_{13} = (\nu_{31} + \nu_{21} \nu_{32}) / E_2 E_3 \Delta$$

$$D_{22} = (1 - \nu_{12} \nu_{31}) / E_1 E_3 \Delta$$

$$D_{23} = (\nu_{32} + \nu_{12} \nu_{31}) / E_1 E_3 \Delta$$

$$D_{33} = (1 - \nu_{12} \nu_{21}) / E_1 E_2 \Delta$$

$$D_{44} = G_{23}$$

$$D_{55} = G_{31}$$

$$D_{66} = G_{12}$$

where;

$$\Delta = (1 - \nu_{12}\nu_{21} - \nu_{23}\nu_{32} - \nu_{31}\nu_{13} - 2 \nu_{21}\nu_{32}\nu_{13}) / E_1E_2E_3$$

E_1,E_2,E_3 are the Young's modulli, ν_{12}, ν_{21}, ν_{23}, ν_{32}, ν_{31} and ν_{13} are the Poisson's ratios, G_{12}, G_{23} and G_{31} are the shear modulli along the principal axes 1,2,3 of the lamena, and the other terms of the D_{ij} are zeros.

3.4 Rubber Analysis:

The tread rubber and the filling matrix of the reinforced layers will be treated here as isotropic materials. The representation of the isotropic material properties permits large strains in the rubber

to be dealt with without having to resort to the infinite bulk modulus hypothesis, and allows it to be described according to the material's real characteristics [72].

Usually rubber is described as an incompressible material. The most common expression for the strain energy function (W), and one which is found to be very suitable for describing the behaviour of rubber is [71,72] :

$$W = \sum C_{ij} (I_1 - 3)^i (I_2 - 3)^j - \sum H_n (I_3 - 1)^n$$

and the difference between two orthogonal stresses takes the form:

$$\sigma_1 - \sigma_2 = (2/\sqrt{I_3})(\lambda_1^2 - \lambda_2^2) \left| \frac{\partial W}{\partial I_1} + \lambda_3^2 \frac{\partial W}{\partial I_2} \right|$$

where;

C_{ij} , H_n are constants and,

$$C_{00} = H_0 = 0$$

$$\lambda_1 = 1 + \varepsilon_1$$

$$\lambda_2 = 1 + \varepsilon_2$$

$$\lambda_3 = 1 + \varepsilon_3$$

ε_1 , ε_2 , ε_3 are the strains in the 1,2,3 directions, respectively, and;

$$I_1 = \lambda_1^2 + \lambda_2^2 + \lambda_3^2$$

$$I_2 = \lambda_1^2 \lambda_2^2 + \lambda_2^2 \lambda_3^2 + \lambda_3^2 \lambda_1^2$$

$$I_3 = \lambda_1^2 \lambda_2^2 \lambda_3^2$$

For an incompressible material, such as rubber; $I_3 = 1$ and for small strains the following equations can be used [71]:

$$E = 4(1 + \nu)(C_{10} + C_{01}) \quad ,$$

$$G = 2(C_{10} + C_{01})$$

in which the constants are experimentally determined. On the other hand, it was suggested by[73], that the accuracy of the solution will increase as the Poisson's ratio approaches 0.5, until it reaches a maximum value of 0.499, this value will be employed in the present work.

3.5 FINITE ELEMENT FORMULATION:

The tyre will be modelled as an axisymmetric solid of revolution based on the displacement approach where the orthotropic material properties of the reinforced layers will be considered. The analysis will be carried out for both symmetric and asymmetric loading conditions.

3.5.1 Finite Element for Tyre Under Symmetric Loading:

The strain-displacement relationship, in the linear form using cylindrical coordinates, may be written in the following form:

$$\begin{bmatrix} \varepsilon_r \\ \varepsilon_z \\ \varepsilon_\vartheta \\ \gamma_{rz} \\ \gamma_{r\vartheta} \\ \gamma_{\vartheta z} \end{bmatrix} = \begin{bmatrix} \frac{\partial u}{\partial r} \\ \frac{\partial v}{\partial z} \\ \frac{u}{r} \\ \frac{\partial u}{\partial z} + \frac{\partial v}{\partial r} \\ \frac{\partial w}{\partial r} - \frac{w}{r} \\ \frac{\partial w}{\partial z} \end{bmatrix}$$

where u,v,w are the displacements along the r,z,ϑ directions.

The necessary equilibrium equation using the virtual work principle is:

$$\Delta \chi = \Delta U - \Delta W = 0 \qquad (3.1)$$

where :

$$\Delta W = \Delta \underline{\delta}^T \underline{F} \quad , \qquad (3.2)$$

$$\Delta U = \iiint \Delta \underline{\varepsilon}^T \underline{\sigma} \, dv \qquad (3.3)$$

The stress components can be expresses in the following form:

$$\underline{\sigma} = \underline{D} \, \underline{\varepsilon} \qquad (3.4)$$

and the strain components can be expressed in terms of nodal displacements and shape functions as follows:

$$\underline{\varepsilon} = \underline{B} \, \underline{\delta} \qquad (3.5)$$

where: $\underline{\varepsilon} = \{ \varepsilon_r , \varepsilon_z , \varepsilon_\vartheta , \gamma_{rz} , \gamma_{r\vartheta} , \gamma_{z\vartheta} \}$

and,

$$\underline{B} = \begin{vmatrix} \frac{\partial N_i}{\partial r} & 0 & 0 \\ 0 & \frac{\partial N_i}{\partial z} & 0 \\ \frac{N_i}{r} & 0 & 0 \\ \frac{\partial N_i}{\partial z} & \frac{\partial N_i}{\partial r} & 0 \\ 0 & 0 & \frac{\partial N_i}{\partial r} - \frac{N_i}{r} \\ 0 & 0 & \frac{\partial N_i}{\partial z} \end{vmatrix}$$

and, N_i is the shape function of node i

Using the chain-rule of partial differentiation, it can be deduced that:

$$\begin{vmatrix} \frac{\partial N_i}{\partial \xi} \\ \frac{\partial N_i}{\partial \eta} \end{vmatrix} = J\left(\frac{r,z}{\xi,\eta}\right) \begin{vmatrix} \frac{\partial N_i}{\partial r} \\ \frac{\partial N_i}{\partial z} \end{vmatrix}$$

where J is the Jacobian defined as follows:

$$J\left(\frac{r,z}{\xi,\eta}\right) = \begin{vmatrix} \frac{\partial r}{\partial \xi} & \frac{\partial z}{\partial \xi} \\ \frac{\partial r}{\partial \eta} & \frac{\partial z}{\partial \eta} \end{vmatrix}$$

Hence,

$$\begin{vmatrix} \frac{\partial N_i}{\partial r} \\ \frac{\partial N_i}{\partial z} \end{vmatrix} = J^{-1}\left(\frac{r,z}{\xi,\eta}\right) \begin{vmatrix} \frac{\partial N_i}{\partial \xi} \\ \frac{\partial N_i}{\partial \eta} \end{vmatrix}$$

Substituting from Equation 3.4,3.5 into Equation 3.3 , it can be shown that:

$$U = \tfrac{1}{2} \left(\iiint \underline{\delta}^T \underline{B}^T \underline{D}\, \underline{B}\, \underline{\delta}\, dv \right)$$

$$= \tfrac{1}{2}\, \underline{\delta}^T \left(\iiint \underline{B}^T \underline{D}\, \underline{B}\, dv \right) \underline{\delta}$$

Using $\frac{\partial \chi}{\partial \delta} = 0$, it can be shown that:

$$\left(\iiint \underline{B}^T \underline{D}\, \underline{B}\, dv \right) \underline{\delta} - \underline{F} = 0$$

i.e. $$\underline{K}_e\, \underline{\delta} = \underline{F}$$

where: $$\underline{K}_e = \iiint \underline{B}^T \underline{D}\, \underline{B}\, dv$$

is the element stiffness matrix, and

$$dv = r\, dr\, dz\, d\vartheta$$

Since the material properties and the loading conditions are independent of ϑ , then:

$$\underline{K}_e = \iint_{area} \underline{B}^T \underline{D}\, \underline{B}\, 2\, \Pi\, r\, dr\, dz \ ,$$

also, $$dr\, dz = \left| J \left(\frac{r,z}{\xi,\eta} \right) \right| d\xi\, d\eta$$

i.e. $$\underline{K}_e = \iint B^T\, D\, B\, 2\, \pi\, r \left| J \left(\frac{r,z}{\xi,\eta} \right) \right| d\xi\, d\eta \qquad (3.6)$$

and for the isoparametric element ;

$$r = \sum_{i=1}^{n_e} r_i\, N_i$$

where n_e in the number of nodes in element e

Derivation of The Rotated Orthotropic D Matrix :

In Section (3.1.2) the elastic properties of the layers are

calculated with respect to their principal axes. In fact, these layers are oriented in the tyre structure by an angle (φ) with respect to the principal axes of the geometry.

In Figure (3.7), r, z, ϑ are the principal axes of the layer, whilst r', z', ϑ' are the principal axes of the tyre structure.

The elastic properties related to the geometrical axes can be obtained according to the following steps:

1- Transform the strain of the structure to the principal strain of the plies:

$$\underline{\varepsilon} = \underline{R}\ \underline{\varepsilon}'$$

2- Calculate the stress in the principal direction of the ply:

$$\underline{\sigma} = \underline{D}\ \underline{\varepsilon}$$

3- Transform the stress $\underline{\sigma}$ to the principal direction of the geometry according to the following:

$$\underline{\sigma} = \underline{R}\ \underline{\sigma}'$$

$$\underline{\sigma}' = \underline{R}^{-1}\ \underline{\sigma}$$

$$= \underline{R}^{-1}\ \underline{D}\ \underline{R}\ \underline{\varepsilon}$$

$$= \underline{D}'\ \underline{\varepsilon}'$$

where:

$$\underline{D}' = \underline{R}^{-1}\ \underline{D}\ \underline{R} \quad ,$$

and $\underline{R}$ is the transformation matrix [24]:

$$\underline{R} = \begin{bmatrix} 1 & 0 & 0 & 0 & 0 & 0 \\ 0 & m^2 & n^2 & 0 & 0 & 2mn \\ 0 & n^2 & m^2 & 0 & 0 & -2mn \\ 0 & 0 & 0 & m & n & 0 \\ 0 & 0 & 0 & -n & m & 0 \\ 0 & -mn & mn & 0 & 0 & m^2 - n^2 \end{bmatrix}$$

$m = \cos \varphi$

$n = \sin \varphi$

3.5.2 Finite Element for Tyre Under General Loading:

For the case of general loading in which the tyre will be subjected to an internal inflation pressure and asymmetric external loading such as; radial load traction and braking forces, and side force, the Fourier expansion is employed. With this expansion, either by Fourier series or Fourier transformation, the problem can be treated as an axisymmetric solid of revolution with a symmetric loading for each harmonic.

The displacement field is augmented and becomes:

$$u = \sum_0^\infty u_n' \cos n\vartheta + \sum_1^\infty u_n'' \sin n\vartheta$$

$$v = \sum_0^\infty v_n' \cos n\vartheta + \sum_1^\infty v_n'' \sin n\vartheta$$

$$w = \sum_0^\infty w_n' \sin n\vartheta - \sum_1^\infty w_n'' \cos n\vartheta$$

where u,v,w are the displacements along the r,z and ϑ directions.

Using the orthogonality conditions:

$$\int_{\pi}^{\pi} \cos m\vartheta \sin n\vartheta \, d\vartheta = 0 \qquad \text{for all } m \text{ and } n$$

$$\int_{\pi}^{\pi} \cos m\vartheta \cos n\vartheta \, d\vartheta = \pi \qquad \text{for } m = n = 0$$

$$= \pi \qquad \text{for } m = n \neq 0$$

$$= 0 \qquad \text{for } m \neq n$$

$$\int_{\pi}^{\pi} \sin m\vartheta \sin n\vartheta \, d = \pi \qquad \text{for } m = n \neq 0$$

$$= 0 \qquad \text{for } m \neq n \quad \text{and} \quad m = n = 0$$

The harmonics can be decoupled.

For orthotropic layered material, where the layers are oriented with the principal material direction by an angle φ ; there will be a coupling between the cosine and sine harmonics (designated by single and double bars) due to the presence of D_{16} , D_{26} , D_{36} , D_{54} , D_{45} , D_{61} , D_{62} and D_{63} .

Hence, the problem can be symbolised by the equation:

$$[\, \underline{K}_0 \, \underline{K}_1 \, \underline{K}_2 \, \cdots \underline{K}_n \,] \, \{ \, \delta_0 \, \delta_1 \, \delta_2 \, \delta_3 \cdots \delta_n \, \} = \{ \, \underline{F}_0 \, \underline{F}_1 \, \underline{F}_2 \cdots \underline{F}_n \, \}$$

where for this case K_n is a matrix of order 6M x 6M as will be explained later.

Employing the stress-strain relationships :

$$\underline{\sigma} = \underline{D} \, \underline{\varepsilon}$$

$$= \underline{D} \, (\, \underline{B}' \, \underline{\delta}' + \underline{B}'' \, \underline{\delta}'' \,) \, ,$$

the strain energy will be :

$$U = (\underline{\delta}'^{T} \underline{B}'^{T} + \delta''^{T} \underline{B}''^{T}) \underline{D} (\underline{B}' \underline{\delta}' + \underline{B}'' \underline{\delta}'')$$

$$= \underline{\delta}'^{T} (\underline{B}'^{T} \underline{D} \underline{B}') \underline{\delta}' + \underline{\delta}'^{T} (\underline{B}'^{T} \underline{D} \underline{B}'') \underline{\delta}''$$

$$+ \underline{\delta}''^{T} (\underline{B}''^{T} \underline{D} \underline{B}') \underline{\delta}' + \underline{\delta}''^{T} (\underline{B}''^{T} \underline{D} \underline{B}'') \underline{\delta}''$$

$$= \hat{\underline{\delta}}^{T} \hat{\underline{B}}^{T} \underline{D} \hat{\underline{B}} \hat{\underline{\delta}}$$

where : $\hat{\underline{B}} = [\underline{B}' \underline{B}'']$,

$\hat{\delta} = \{ \delta' \delta'' \}$

and ;

$$\underline{B}' = \begin{bmatrix} \frac{\partial N_i}{\partial r} \cos n\vartheta & 0 & 0 \\ 0 & \frac{\partial N_i}{\partial z} \cos n\vartheta & 0 \\ \frac{N_i}{r} \cos n\vartheta & 0 & \frac{nN_i}{r} \cos n\vartheta \\ \frac{\partial N_i}{\partial z} \cos n\vartheta & \frac{\partial N_i}{\partial r} \cos n\vartheta & 0 \\ -\frac{nN_i}{r} \sin n\vartheta & 0 & (\frac{\partial N_i}{\partial r} - \frac{N_i}{r}) \sin n\vartheta \\ 0 & -\frac{nN_i}{r} \sin n\vartheta & \frac{\partial N_i}{\partial z} \sin n\vartheta \end{bmatrix}$$

and;

$$\underline{B}'' = \begin{bmatrix} \frac{\partial N_i}{\partial r} \sin n\vartheta & 0 & 0 \\ 0 & \frac{\partial N_i}{\partial z} \sin n\vartheta & 0 \\ \frac{N_i}{r} \sin n\vartheta & 0 & -\frac{nN_i}{r} \sin n\vartheta \\ \frac{\partial N_i}{\partial z} \sin n\vartheta & \frac{\partial N_i}{\partial r} \sin n\vartheta & 0 \\ \frac{nN_i}{r} \cos n\vartheta & 0 & (\frac{\partial N_i}{\partial r} - \frac{N_i}{r}) \cos n\vartheta \\ 0 & \frac{nN_i}{r} \cos n\vartheta & \frac{\partial N_i}{\partial z} \cos n\vartheta \end{bmatrix}$$

The $\underline{D}$ matrix will take the form:

$$\underline{D} = \begin{vmatrix} d_{11} & d_{12} & d_{13} & 0 & 0 & d_{16} \\ d_{21} & d_{22} & d_{23} & 0 & 0 & d_{26} \\ d_{31} & d_{32} & d_{33} & 0 & 0 & d_{36} \\ 0 & 0 & 0 & d_{44} & d_{45} & 0 \\ 0 & 0 & 0 & d_{54} & d_{55} & 0 \\ d_{61} & d_{62} & d_{63} & 0 & 0 & d_{66} \end{vmatrix}$$

Hence, the element stiffness matrix can be expressed as follows:

$$\underline{K}_e = \iiint \hat{\underline{B}}^T \, \underline{D} \, \hat{\underline{B}} \, dv$$

The explicit form for the above element stiffness matrix has been derived and listed in Appendix (B).

Strain Calculation:

The strain components can be calculated using the equation:

$$\underline{\varepsilon} = \underline{B} \, \underline{\delta}$$

in which:

$$(\varepsilon_r)_i = \frac{\partial u_i}{\partial r}$$

$$= \frac{\partial N_i}{\partial r} \left[\sum_0^{\infty} u'_{im} \cos m\vartheta + \sum_1^{\infty} u''_{im} \sin m\vartheta \right]$$

$$(\varepsilon_z)_i = \frac{\partial v_i}{\partial z}$$

$$= \frac{\partial N_i}{\partial z}\left[\sum_0^\infty v'_{im}\cos m\vartheta + \sum_1^\infty v''_{im}\sin m\vartheta\right]$$

$$(\varepsilon_\vartheta)_i = \frac{u_i}{r} + \frac{1}{r}\frac{\partial w_i}{\partial \vartheta}$$

$$= \frac{N_i}{r}\left[\sum_0^\infty u'_{im}\cos m\vartheta + \sum_1^\infty u''_{im}\sin m\vartheta\right.$$

$$\left. + \sum_0^\infty - m\, w'_{im}\sin m\vartheta + \sum_1^\infty w''_{im}\cos m\vartheta\right]$$

$$(\gamma_{rz})_i = \frac{\partial u_i}{\partial z} + \frac{\partial v_i}{\partial r}$$

$$= \frac{\partial N_i}{\partial z}\left[\sum_0^\infty u'_{im}\cos m\vartheta + \sum_1^\infty u''_{im}\sin m\vartheta\right]$$

$$+ \frac{\partial N_i}{\partial r}\left[\sum_1^\infty v'_{im}\cos m\vartheta + \sum_1^\infty v''_{im}\sin m\vartheta\right]$$

$$(\gamma_{z\vartheta})_i = \frac{1}{r}\frac{\partial v}{\partial \vartheta} + \frac{\partial w}{\partial z}$$

$$= \frac{N_i}{r}\left[\sum_0^\infty - m\, v'_{im}\sin m\vartheta + \sum_1^\infty m\, v''_{im}\cos m\vartheta\right]$$

$$+ \frac{\partial N_i}{\partial z}\left[\sum_0^\infty w'_{im}\cos m\vartheta + \sum_1^\infty w''_{im}\sin m\vartheta\right]$$

$$(\gamma_{\vartheta r})_i = \frac{1}{r}\frac{\partial u_i}{\partial \vartheta} + \frac{\partial w_i}{\partial r} - \frac{w_i}{r}$$

$$= \frac{N_i}{r}\left[\sum_0^\infty - m\, u'_{im}\sin m\vartheta + \sum_1^\infty m\, u''_{im}\cos m\vartheta\right]$$

$$+ \left(\frac{\partial N_i}{\partial r} - \frac{N_i}{r}\right)\left[\sum_0^\infty w'_{im}\cos m\vartheta + \sum_i^\infty w''_{im}\sin m\vartheta\right]$$

Stress Calculation:

By substituting the above strain equations into the following stress-strain relationship:

$$\underline{\sigma} = \underline{D}\,\underline{\varepsilon}$$

the stress components can be found as:

$$\{ \sigma_r \quad \sigma_z \quad \sigma_\vartheta \quad \tau_{rz} \} = \sum_{\bullet}^{\infty} \{ \sigma_{rm} \quad \sigma_{zm} \quad \sigma_{\vartheta m} \quad \tau_{rzm} \} \cos m\vartheta$$

$$\{ \tau_{r\vartheta} \quad \tau_{\vartheta z} \} = \sum_{\bullet}^{\infty} \{ \tau_{r\vartheta m} \quad \tau_{\vartheta zm} \} \sin m\vartheta$$

where the barred quantities are functions of r,z and m but not of ϑ .

N.B. If the tyre is subjected to an external radial load which is symmetric along the plane ($\vartheta = 0$), the second part of the Fourier series will vanish, reducing the stiffness matrix to 3Mx3M .

The explicit form of the stiffness matrix for this case is given in Appendix (C).

3.6 LOADING ANALYSIS:

There are two basic types of loading conditions for the static analysis of pneumatic tyres. They can be summarised as follows:

3.6.1 Inflation Prassure:

For this case the tyre is loaded by an internal pressure (p), which is assumed to be uniformly distributed . Consider an infinitesimal part of the internal surface of the tyre as shown in Figure (3.8). It can be deduced that:

$$d\underline{F} = - p \hat{n} \, t \, ds \qquad (3.7)$$

where t is the thickness.

$$ds \, \hat{n} = dy \, \hat{i} - dx \, \hat{j} \qquad (3.8)$$

$$- \hat{n} = -\left(\frac{dy}{ds}\right) \hat{i} + \left(\frac{dx}{ds}\right) \hat{j} \qquad (3.9)$$

i.e. $$d\underline{F} = - p\ t \frac{dy}{ds}\ ds\ \hat{i} + p\ t \frac{dx}{ds}\ ds\ \hat{j} \qquad (3.10)$$

$$= - t\ p\ dy\ \hat{i} + t\ p\ dx\ \hat{j}$$

$$= dF_x\ \hat{i} + dF_y\ \hat{j}$$

where:

$$dF_x = - t\ p\ dy$$

$$dF_y = \quad t\ p\ dx \qquad (3.11)$$

and the work done (W) will be:

$$dW = dF_x\ u + dF_y\ v \qquad (3.12)$$

Defining an axisymmetric surface element as shown in Figure (3. 8), it can be deduced that:

$$u = \sum u_i\ N_i\ (\ \xi\ )$$

$$v = \sum v_i\ N_i\ (\ \xi\ ) \qquad (3.13)$$

Hence ;

$$dW = dF_x \sum u_i\ N_i + dF_y \sum v_i\ N_i \qquad (3.14)$$

$$= \underline{\delta}^T\ dF$$

i.e. $$\underline{\delta}^T\ \underline{F} = \sum u_i\ (\ dF_x\ )_i + \sum v_i\ (\ dF_y\ )_i \qquad (3.15)$$

From 3.14 , 3.15

$$(\ dF_x\ )_i = N_i\ dF_x \qquad (3.16)$$

$$(\ dF_y\ )_i = N_i\ dF_y \qquad (3.17)$$

From the isoparametric transformation of the surface element:

$$x(\xi) = \sum x_i N_i(\xi) \qquad (3.18)$$

$$y(\xi) = \sum y_i N_i(\xi)$$

$$dx = \left(\sum x_i \frac{dN_i}{d\xi}\right) d\xi = J_x \, d\xi \qquad (3.19)$$

$$dy = \left(\sum y_i \frac{dN_i}{d\xi}\right) d\xi = J_y \, d\xi \qquad (3.20)$$

where ; J_x , J_y are the x-Jacobian and y-Jacobian respectively.

Substituting Equations 3.11 , 3.19 into 3.16 :

$$(dF_x)_i = -N_i(\xi)\,(-t\,p\,dy)$$

$$= -N_i(\xi)\,t\,p\,J_y\,d\xi$$

similarly ;

$$(dF_y)_i = N_i(\xi)\,t\,p\,J_x\,d\xi$$

Hence, the equivalent nodal forces can be expressed as follows:

$$(F_x)_i = -\int_0^1 t\,p\,N_i(\xi)\,J_y(\xi)\,d\xi \quad ,$$

$$(F_y)_i = \int_0^1 t\,p\,N_i(\xi)\,J_x(\xi)\,d\xi$$

3.6.2 General Loading:

For the case of externally loaded tyres, the pressure distributon on the surface of contact will be assumed constant in the present work, similarly the contact surface will be considered to be flat. This external pressure is calculated from the external load, and the area of contact.

Using Fourier series; for each harmonic (n), the pressure will be :

$$P = \sum_{0}^{\infty} P' \ (r,z) \cos n\vartheta + \sum_{1}^{\infty} P'' \ (r,z) \sin n\vartheta$$

and ;

$$P' \ (r,z) = \frac{1}{\pi} \int_{0}^{2\pi} P \cos n\vartheta \ d\vartheta$$

$$P'' \ (r,z) = \frac{1}{\pi_0} \int_{0}^{2\pi} P \sin n\vartheta \ d\vartheta$$

The cyclic loading is represented as shown in Figure (3.9) by the load ($P/2\varphi$); where (2φ) is the angle of the arc of contact.

i.e. $$P' = \frac{2}{\pi_0} \int^{\pi} \left(\frac{P}{2\varphi} \right) \cos n\vartheta \ d\vartheta$$

$$= \frac{2}{\pi} \ {}_0\int^{\varphi} \left(\frac{P}{2\varphi} \right) \cos n\vartheta \ d\vartheta$$

$$= \left(\frac{P}{n\varphi\pi} \right) \sin n\varphi$$

while, $P'' = 0$

3.7 BOUNDARY CONDITIONS:

The tyre will be treated as a three-dimensional axisymmetric structure with the following assumptions:

a- The nodes in contact with the rim will be totally fixed.

b- The nodes along the r-axis will be free in the radial and circumferential directions, fixed in the tangential direction.

c- There will be no deformation in the foundation plate under the area of contact.

d- The pressure acting in the area of contact will be uniformly distributed.

3.8 MESH GENERATION :

The pneumatic tyre, as previously stated, is a very complex layered composite structure, and the first step of the finite element analysis is to discretise the structure into finite elements connected by nodes. For a strcture, such as a tyre, it is necessary to discretise it into a sufficient number of elements in order to obtain a reasonable accuracy. On the other hand, the more elements that are used, the more costly will be the analysis. Therefore, it becomes very desirable to incorporate an automatic mesh generator into the finite element analysis in order to alleviate this difficulty. This technique has been employed by many investigators [75,76,77].

The recursive approach, which was originated by Zienkiewicz and Philips [66], and developed by EL-Zafrany [59], is adopted for the present finite element program.

The mesh generator developed for this work has the following facilities:

i- The use of arbitrary elements for the discretised block.

ii- The inclusion of some efficient transition elements.

iii- A facility for modifying the generated mesh.

iv- The ability to specify the element type and material within the mesh.

v- An interactive mesh generation facility, with which each step can be displayed and checked.

vi- A facility for renumbering the generated elements in order to obtain the minimum front width and hence an efficient

frontal solution.

3.8.1 Mesh Generation Steps:

The mesh generation procedure can be formulated so as to be applicable to any two-dimensional structure. The basic steps can be summarised as follows:

a) Block Modelling:

In this step the true complex geometry will be approximated by a number of blocks, each block being represented by one of standard finite elements as shown in Figure (3.10a).

b- Block Transformation:

Each block will be transformed into a uniform one in the local intrinsic space, using the isoparametric transformation and shape functions. For example, any quadrilateral block can be transformed to a uniform square in the (ξ - η) plane as shown in figure (3.10b) using the following equations:

$$x = \sum x_i N_i (\xi, \eta)$$

$$y = \sum y_i N_i (\xi, \eta)$$

where; x_i, y_i are the cartesian coordinates, and N_i is the shape function of the i th node.

c) Block Discretisation:

The block will be discretised into the required elements in intrinsic space Figure (3.10b,c). The compatibility between blocks

should be maintained, using the same division at the common boundary. For the example of a uniform quadrilateral block, with m divisions along the ξ-axis and n divisions along the η-axis, α_1 , α_2 , ... , α_m are the division ratios along the ξ-axis, β_1 , β_2 , ... , β_n are the division ratios along the η-axis , and $\xi_1 = \eta_1 = 0$

$$\text{i.e. } \xi_{r+1} = \sum_{i=1}^{r} \alpha_i \Big/ \sum_{j=1}^{m} \alpha_j \qquad , \; r = 1,2, \; \ldots\ldots\ldots , \; m$$

$$\eta_{s+1} = \sum_{i=1}^{s} \beta_i \Big/ \sum_{j=1}^{n} \beta_j \qquad , \; s = 1,2, \; \ldots\ldots\ldots , \; n$$

d- Transformation of A Block to The Global Space:

Each generated node is to be transformed back to the original global space using the isoparametric transformation. For the above example, any general n-node quadrilateral element can be fitted in the domain of the generated 4-node simple element. Each fitted element can be described as a square of unit side length in its local intrinsic space (ξ- η), as shown in Figure (3.10d). The intrinsic coordinates of the element nodes, with respect to the block (ξ- η), will be:

$$\xi_i = \sum_{k=1}^{n_c} N_k (\xi'_i , \eta'_i) \xi_k$$

$$\eta_i = \sum_{k=1}^{n_c} N_k (\xi'_i , \eta'_i) \eta_k$$

where n_c is the number of simple element nodes.

The mathematical derivation for other types of blocks and elements wil be given in Appendix (D).

3.9 MESH PLOTTING:

The plotting facility is important for any finite element package as it can be used in the folowing ways:

1- To check the mesh generation of the structure.

2- To display the results of the analysis.

The mesh plotter uses the basic GINO-F subroutines only for pen movement and character plotting, whilst all other subroutines have been generated in this work.

The Facilities of The Mesh Plotter:

1- Plotting two and three dimensional structures.

2- Plotting of rotated structure.

3- Plotting of nodal numbers if required.

4- Arbitrary magnification of the structure and/or deformation.

5- Plotting of deformed structure and deformed surfaces in two or three dimensions and in different colours.

6- Plotting of any title.

7- Plotting of the stress and strain distribution along any arbitrary layer of the structure.

8- Plotting of the cord-load variation in the meridional direction.

9- Plotting of principal stresses and principal srains.

10- Plotting of the stress variation along the principal axes of the geometry.

11- Plotting the stress distribution within any portion of the cross-section by arrows facility.

12- Arbitrary selection of device.

Construction of Plotting Program:

This is divided into four main sections:

1- Device nomination; in which the device will be nominated.

2- Device qualification; which contains the plotting units and the paper-dimension subroutines.

3- Plotting procedure; which contains the subroutines necessary for plotting of the required data and results.

4- Device end; in order to end the plotting.

The mathematical theory and the program will be given in Appendix (E).

CHAPTER 4

NONLINEAR FINITE ELEMENT ANALYSIS OF A RADIAL TYRE

CHAPTER 4

NONLINEAR FINITE ELEMENT ANALYSIS OF A RADIAL TYRE

4.1 INTRODUCTION:

The pneumatic tyre is considered as a highly nonlinear composite structure. The main sources of nonlinearity are:

1- Material properties.

2- Large deflection of the tyre.

The equilibrium equations governing the tyre take the form of six, second order, partial differential equations. These equations can be solved numerically by the Newton-Raphson iteration technique.

The large deflection and material nonlinearity, will be treated, here, for both symmetric and asymmetric loading.

4.2 ANALYSIS OF MATERIAL NONLINEARITY:

The stress-strain relationship of the rubber is not linear. From the minimum total potential energy theorem:

$$\Delta \chi = \Delta U - \Delta W = 0$$

it can be deduced that:

$$\iiint \underline{B}^T \underline{\sigma} \, dv - \underline{F} = 0$$

which is valid for any material. For a nonlinear material, the stress vector $\underline{\sigma}$ is a nonlinear function of the nodal displacement $\underline{\delta}$,

i.e. $\underline{\sigma} = \underline{\sigma} (\underline{\delta})$

Hence, if the value of $\underline{\delta}_0$ is taken to be linear as a first approximation, there will then be a residual force $\underline{R}_o$:

$$\underline{R}_o = \iiint \underline{B}^T \underline{\sigma} (\underline{\delta}_0) \, dv - \underline{F}$$

The corresponding displacement ($\Delta\underline{\delta}_0$) is due to the residual $\underline{R}_o$.

and,

$$\underline{\delta}_1 = \underline{\delta}_0 + \Delta\underline{\delta}_1$$

From the Taylor series:

$$\underline{\sigma} (\underline{\delta}_o + \Delta \underline{\delta}_o) = \underline{\sigma} (\underline{\delta}_o) + \frac{\partial \sigma}{\partial \delta} \Delta\underline{\delta}$$

it can be proved that :

$$\iiint \underline{B}^T (\frac{\partial \sigma}{\partial \delta}) \, dv \; \Delta\underline{\delta} \simeq \underline{F} - \iiint \underline{B}^T \underline{\sigma} (\underline{\delta}_0) \, dv$$

The Newton-Raphson, or the modified Newton-Raphson, Figure 4.1(a,b) can be used as follows:

1- Solve the equation:

$$\underline{K} \, \underline{\delta}_o = \underline{F}_o$$

linearly to obtain $\underline{\delta}_o$.

2- From $\underline{\delta}_o$, the residual $\underline{R}_o$ can be calculated.

3- Solve the equation:

$$\underline{K}^{-1} \underline{R}_o = \Delta \underline{\delta}_o$$

to obtain the increment displacement corresponding to $\underline{R}_o$

4- Update the stresses and strains as follows:

$$\Delta \underline{\varepsilon} = \underline{B}\, \Delta\underline{\delta}$$

$$\varepsilon_{i+1} = \varepsilon_i + \Delta\, \varepsilon_i$$

$$\Delta\, \sigma_i = \underline{D}\, \Delta\varepsilon_i$$

$$\sigma_{i+1} = \sigma_i + \Delta\, \sigma_i$$

5- The residual forces at the end of each step i may be calculated as follows:

a- From the stresses and strains at this step, the equivalent stress and strain (σ' , ε') will be calculated as [59]:

$$\sigma' = \frac{1}{\sqrt{2}}\Big[(\sigma_x - \sigma_y)^2 + (\sigma_y - \sigma_z)^2 + (\sigma_z - \sigma_x)^2 + 6 (\tau_{xy}^2 + \tau_{yz}^2 + \tau_{zx}^2) \Big]^{\frac{1}{2}}$$

$$\varepsilon' = \frac{1}{\sqrt{2(1+\nu)}}\Big[(\varepsilon_x - \varepsilon_y)^2 + (\varepsilon_y - \varepsilon_z)^2 + (\varepsilon_z - \varepsilon_x)^2 + \frac{3}{2} (\gamma_{xy}^2 + \gamma_{yz}^2 + \gamma_{zx}^2) \Big]^{\frac{1}{2}}$$

b- From the uniaxial stress-strain curve, find σ_1 corresponding to ε'

c- Calculate : $\Delta\, \underline{\sigma} = \sigma' - \sigma_1$

d- The residual $\underline{R}$ will be :

$$\underline{R} = \sum_{\text{element}} \iiint \underline{B}^T \Delta\, \underline{\sigma}\, dv$$

6- The above sequence is repeated from step 3 until a reasonable

error is achieved , where ;

$$\text{Error} = \underline{R}^T \underline{R} \; / \; \underline{F}^T \underline{F}$$

4.3 ANALYSIS OF LARGE DEFORMATION FOR AXISYMMETRIC LOADING:

For the case of pneumatic tyres, the assumption that both displacement and strains are small, together with the associated assumptions that the geometry of the element remains unchanged during the loading process, and that only the first order linear terms of strains need be considered, is found to be incorrect even though the real strains may be small and elastic limits not exceeded.

For accurate determination of displacements, stresses and strains, the geometrical nonlinearity should be considered.

A Lagrangian approach [74], in which displacements are referred to the original configuration is adopted throughout this work. This approach is accurate only for the case of deflectIons which are not very large. To improve upon the above limitation, the incremental value of the inflation pressure is used, and the coordinates of the nodes will be updated after each pressure increment. An alternative approach would be to use the Eulerian.

Finite Element Formulation:

The strain-displacement relationships have been derived as explained in Appendix (G), and the final equations can be represented by the following formulae:

$$\varepsilon_r = \frac{\partial u}{\partial r} + \frac{1}{2}\left[\left(\frac{\partial u}{\partial r}\right)^2 + \left(\frac{\partial v}{\partial r}\right)^2 + \left(\frac{\partial w}{\partial r} - \frac{w}{r}\right)^2 \right]$$

$$\varepsilon_z = \frac{\partial v}{\partial z} + \frac{1}{2}\left[\left(\frac{\partial u}{\partial z}\right)^2 + \left(\frac{\partial v}{\partial z}\right)^2 + \left(\frac{\partial w}{\partial z}\right)^2 \right]$$

$$\varepsilon_\theta = \frac{u}{r} + \frac{1}{2}\left[\left(\frac{u}{r}\right)^2 \right]$$

$$\gamma_{rz} = \frac{\partial u}{\partial z} + \frac{\partial v}{\partial r} + \left[\frac{\partial u}{\partial z}\frac{\partial u}{\partial r} + \frac{\partial v}{\partial z}\frac{\partial v}{\partial r} + \frac{\partial w}{\partial z}\left(\frac{\partial w}{\partial r} - \frac{w}{r}\right) \right]$$

$$\gamma_{r\theta} = \frac{\partial w}{\partial r} - \frac{w}{r} + \left[\frac{u}{r}\left(\frac{\partial w}{\partial r} - \frac{w}{r}\right) \right]$$

$$\gamma_{\theta z} = \frac{\partial w}{\partial z} + \left[\frac{u}{r}\frac{\partial w}{\partial z} \right]$$

which include both linear and nonlinear terms.

Whether the displacements are large or small, the equilibrium conditions between the internal and external forces must be satisfied The necessary equilibrium equation, using the virtual work principle, is :

$$\Delta \chi = \Delta U - \Delta W = 0$$

in which,

$$\Delta W = \Delta \underline{\delta}^T \underline{F}$$

$$\Delta U = \iiint \Delta \underline{\varepsilon}^T \sigma \, dv$$

and the strain vector $\underline{\varepsilon}$ may be partitioned as follows:

$\underline{\varepsilon} = \underline{\varepsilon}_L + \underline{\varepsilon}_{NL}$ where;

$\underline{\varepsilon}_L$ = strains due to linear terms .

$\underline{\varepsilon}_{NL}$ = strains due to nonlinear terms.

using the strain-displacement relationships; it can be deduced that:

$$\Delta \underline{\varepsilon} = \underline{B}\ \Delta\underline{\delta}$$

$$\Delta\ \varepsilon = (\ \underline{B}_L + \underline{B}_{NL}\ )\Delta\ \underline{\delta}$$

where :

$$\Delta\ \underline{\varepsilon}_L = \underline{B}_L \Delta\delta \qquad \text{, and}$$

$$\Delta\ \underline{\varepsilon}_{NL} = \underline{B}_{NL} \Delta\delta$$

Hence, it can be shown in a similar way to that explained in Section (4.2), that the general equilibrium equation will be:

$$\sum \iiint \underline{B}^T\ \underline{\sigma}\ dv - \underline{F} = 0$$

or; $$\sum \iiint (\ \underline{B}_L + \underline{B}_{NL}\ )^T\ \underline{\sigma}\ dv - \underline{F} = 0$$

If $\underline{B}$ is increased to $(\ \underline{B} + \Delta\ \underline{B}\ )$

and, $\underline{\sigma}$ to $\underline{\sigma} + \Delta\ \underline{\sigma}$

Substituting in the above equilibrium equation and then in the minimum potential energy equation we obtain:

$$\iiint (\ \underline{B} + \Delta\underline{B}\ )^T\ (\ \underline{\sigma} + \Delta\underline{\sigma}\ )\ dv - \underline{F} = 0$$

i.e. $$\iiint (\ \underline{B}^T\ \underline{\sigma} + \Delta\ \underline{B}^T\ \underline{\sigma} + \underline{B}^T\ \Delta\underline{\sigma} + \Delta\underline{B}^T\Delta\underline{\sigma}\ )\ dv - \underline{F} = 0$$

Neglecting the second order term ($\Delta\underline{B}\ \Delta\underline{\sigma}$), it can be proved that:

$$\underline{B}^T\ \Delta\underline{\sigma} = \Delta\underline{B}^T\ \underline{\sigma}$$

Hence, the equilibrium equation will be :

$$\iiint (\ \underline{B}^T\ \underline{\sigma} + 2\ \Delta\underline{B}^T\ \underline{\sigma}\ )dv - \underline{F} = 0$$

$$\iiint\ \ \underline{B}^T\ \underline{\sigma}\ dv = \iiint\ \underline{B}^T\ \underline{D}\ \underline{B}\ dv$$

$$= \iiint \left(\underline{B}_L + \underline{B}_{NL} \right)^T \underline{D} \left(\underline{B}_L + \underline{B}_{NL} \right) dv$$

$$= \iiint \left(\underline{B}_L^T \underline{D} \underline{B}_L + \underline{B}_L^T \underline{D} \underline{B}_{NL} + \underline{B}_{NL}^T \underline{D} \underline{B}_L \right.$$

$$\left. + \underline{B}_{NL}^T \underline{D} \underline{B}_{NL} \right) dv$$

$$= \underline{K}_L + \underline{K}_{NL}$$

and, $$\iiint 2 \, \Delta \underline{B}^T \underline{\sigma} \, dv = \underline{K}_\sigma$$

i.e. $$\left(\underline{K}_L + \underline{K}_{NL} + \underline{K}_\sigma \right) \underline{\delta} - \underline{F} = 0$$

where;

$$\underline{K}_L = \iiint \underline{B}_L^T \underline{D} \underline{B}_L \, dv$$

is the linear stiffness matrix.

$$\underline{K}_{NL} = \iiint \left(\underline{B}_L^T \underline{D} \underline{B}_{NL} + \underline{B}_{NL}^T \underline{D} \underline{B}_L + \underline{B}_{NL}^T \underline{D} \underline{B}_{NL} \right) dv$$

is the nonlinear stiffness matrix

$$\underline{K}_\sigma = \iiint \underline{G}^T \underline{M} \underline{G} \, dv$$

is the stress matrix.

and,

$$\underline{K}_T = \underline{K}_L + \underline{K}_{NL} + \underline{K}_\sigma$$

is the total stiffness matrix.

The $\underline{B}_L$ matrix, is the linear part of the strain-displacement relationships as was explained in Section (3.2).

The nonlinear part of the strain vector $\underline{\varepsilon}_{NL}$ can be expressed in terms of displacement components as follows:

$$\underline{\varepsilon}_{NL} = \tfrac{1}{2} \begin{vmatrix} (\frac{\partial u}{\partial r})^2 + (\frac{\partial v}{\partial r})^2 + (\frac{\partial w}{\partial r} - \frac{w}{r})^2 \\ (\frac{\partial u}{\partial z})^2 + (\frac{\partial v}{\partial z})^2 + (\frac{\partial w}{\partial z})^2 \\ (\frac{u}{r})^2 \\ 2\ \frac{\partial u}{\partial z}\ \frac{\partial u}{\partial r} + 2\ \frac{\partial v}{\partial z}\ \frac{\partial v}{\partial r} + 2\ \frac{\partial w}{\partial z}\ (\frac{\partial w}{\partial r} - \frac{w}{r}) \\ 2\ \frac{u}{r}\ (\frac{\partial w}{\partial r} - \frac{w}{r}) \\ 2\ \frac{u}{r}\ \frac{\partial w}{\partial z} \end{vmatrix}$$

which can be written in the following form:

$$\underline{\varepsilon}_{NL} = \tfrac{1}{2}\ \underline{A}\ \Theta$$

where;

$$\underline{A} = \begin{vmatrix} \frac{\partial u}{\partial r} & \frac{\partial v}{\partial r} & (\frac{\partial w}{\partial r} - \frac{w}{r}) & 0 & 0 & 0 \\ 0 & 0 & 0 & \frac{\partial u}{\partial z} & \frac{\partial v}{\partial z} & \frac{\partial w}{\partial z} \\ 0 & 0 & 0 & 0 & 0 & \frac{u}{r} \\ \frac{\partial u}{\partial z} & \frac{\partial v}{\partial z} & \frac{\partial w}{\partial z} & \frac{\partial u}{\partial r} & \frac{\partial v}{\partial r} & (\frac{\partial w}{\partial r} - \frac{w}{r}) \\ 0 & 0 & \frac{u}{r} & 0 & 0 & 0 \\ 0 & 0 & 0 & 0 & 0 & \frac{u}{r} \end{vmatrix} \quad \begin{vmatrix} 0 \\ 0 \\ (\frac{\partial w}{\partial r} - \frac{w}{r}) \\ 0 \\ \frac{\partial w}{\partial z} \end{vmatrix}$$

and,

$$\Theta = \{\ \frac{\partial u}{\partial r}\ \ \frac{\partial v}{\partial r}\ \ (\frac{\partial w}{\partial r} - \frac{w}{r})\ \ \frac{\partial u}{\partial z}\ \ \frac{\partial v}{\partial z}\ \ \frac{\partial w}{\partial z}\ \ \frac{u}{r}\ \}$$

using the following expressions:

$$u = \sum u_i\ N_i$$

$$v = \sum v_i N_i$$

$$w = \sum w_i N_i$$

It can be proved that:

$$\underline{\theta} = \underline{G}\ \underline{\delta}$$

wher;

$$\underline{G} = \begin{bmatrix} \frac{\partial N_i}{\partial r} & 0 & 0 \\ 0 & \frac{\partial N_i}{\partial r} & 0 \\ 0 & 0 & \frac{\partial N_i}{\partial r} - \frac{N_i}{r} \\ \frac{\partial N_i}{\partial z} & 0 & 0 \\ 0 & \frac{\partial N_i}{\partial z} & 0 \\ 0 & 0 & \frac{\partial N_i}{\partial z} \\ 0 & 0 & \frac{N_i}{r} \end{bmatrix}$$

and, $\delta = \{ u , v , w \}$

Hence, it can be shown that:

$$\underline{\varepsilon}_{NL} = \tfrac{1}{2}\,\underline{A}\,\underline{\theta}$$

$$= \tfrac{1}{2}\,A\,G\,\delta$$

$$= \underline{B}_{NL}\,\underline{\delta}$$

where;

$$\underline{B}_{NL} = \tfrac{1}{2}\,\underline{A}\,\underline{G}$$

Derivation of The Stress Stiffness Matrix:

From the previous analysis, the stress stiffness matrix is defined as follows:

$$\underline{K}_{\sigma} = \int\int\int \Delta \underline{B}^{T} \underline{\sigma} \, dv$$

From the partitioning of the $\underline{B}$ matrix as follows:

$$\underline{B} = \underline{B}_{L} + \underline{B}_{NL}$$

it can be deduced that:

$$\Delta \underline{B} = \Delta (\underline{B}_{L} + \underline{B}_{NL})$$

$$= \Delta \underline{B}_{NL}$$

Since, $\underline{B}_{NL} = \underline{A}\,\underline{G}$

Then, $\Delta \underline{B}^{T} = \underline{G}^{T} \Delta \underline{A}^{T}$

Hence, it can be shown that:

$$\underline{K}_{\sigma} = \int\int\int \underline{G}^{T} \Delta \underline{A}^{T} \underline{\sigma} \, dv$$

From the definition of $\underline{A}$,then:

$$\underline{A}^T \underline{\sigma} = \begin{bmatrix} \sigma_r \frac{\partial u}{\partial r} + \tau_{rz} \frac{\partial u}{\partial z} - \tau_{r\theta} \frac{w}{r} \\ \sigma_r \frac{\partial v}{\partial r} + \tau_{rz} \frac{\partial v}{\partial z} \\ \sigma_r (\frac{\partial w}{\partial r} - \frac{w}{r}) + \tau_{rz} \frac{\partial w}{\partial z} + \tau_{r\theta} \frac{u}{r} \\ \sigma_z \frac{\partial u}{\partial z} + \tau_{rz} \frac{\partial u}{\partial r} - \tau_{\theta z} \frac{w}{r} \\ \sigma_z \frac{\partial v}{\partial z} + \tau_{rz} \frac{\partial v}{\partial r} \\ \sigma_z \frac{\partial w}{\partial z} + \tau_{rz} (\frac{\partial w}{\partial r} - \frac{w}{r}) + \tau_{\theta z} \frac{u}{r} \\ \sigma_\theta \frac{u}{r} + \tau_{r\theta} (\frac{\partial w}{\partial r} - \frac{w}{r}) + \tau_{\theta z} \frac{\partial w}{\partial z} \end{bmatrix}$$

This vector can be written in the form:

$$\underline{A}^T \underline{\sigma} = \underline{M} \underline{\Theta} = \underline{M} \underline{G} \underline{\delta}$$

where;

$$\underline{M} = \begin{bmatrix} \sigma_r & 0 & 0 & \tau_{rz} & 0 & 0 & 0 \\ 0 & \sigma_r & 0 & 0 & \tau_{rz} & 0 & 0 \\ 0 & 0 & \sigma_r & 0 & 0 & \tau_{rz} & \tau_{r\vartheta} \\ \tau_{rz} & 0 & 0 & \sigma_z & 0 & 0 & 0 \\ 0 & \tau_{rz} & 0 & 0 & \sigma_z & 0 & 0 \\ 0 & 0 & \tau_{rz} & 0 & 0 & \sigma_z & \tau_{\vartheta z} \\ 0 & 0 & \tau_{r\vartheta} & 0 & 0 & \tau_{\vartheta z} & \sigma_\vartheta \end{bmatrix}$$

Hence,

$$\underline{K}_\sigma = \iiint \underline{G}^T \underline{M} \underline{G} \, dv$$

To generate the nonlinear solution using the Lagrangian algorithm, the following steps may be followed:

1- A linear solution is employed as the first step of the approximation to obtain the initial deformation $\underline{\delta}_o$, strain $\underline{\varepsilon}_o$ and stress $\underline{\sigma}_o$, as follows:

$$\iiint \underline{B}_L \underline{D} \underline{B}_L \, dv \, \underline{\delta}_o = \underline{F}$$

$$\underline{\varepsilon}_o = \underline{B}_L \underline{\delta}_o$$

$$\underline{\sigma}_o = \underline{D} \underline{\varepsilon}_o$$

2- Calculate the residual forces $\underline{R}_o$:

$$\underline{R}_o = \underline{F} - \iiint \left(\underline{B}_L + \underline{B}_{NL} \right)^T \underline{\sigma}_o \, dv$$

3- Establish the total stiffness matrix $\underline{K}_T$

$$\underline{K}_T = \underline{K}_L + \underline{K}_{NL} + \underline{K}_\sigma$$

4- Calculate the second approximation:

$$\underline{K}_T \Delta \underline{\delta} = \underline{R}_o$$

$$\Delta \underline{\varepsilon} = \underline{B} \Delta \underline{\delta}$$

$$\Delta \underline{\sigma} = \underline{D} \Delta \underline{\varepsilon}$$

5- Update the results as follows:

$$\underline{\delta}_1 = \underline{\delta}_o + \Delta \underline{\delta}$$

$$\underline{\varepsilon}_1 = \underline{\varepsilon}_o + \Delta \underline{\varepsilon}$$

$$\underline{\sigma}_1 = \underline{\sigma}_o + \Delta \underline{\sigma}$$

6- Repeat the steps from 2 to 5 until the error is found to be within some appropriate range, where:

$$\text{Error} = \underline{R}^T \underline{R} \,/\underline{F}^T \underline{F}$$

4.4 ANALYSIS OF LARGE DEFORMATION WITH GENERAL LOADING:

The analysis here will be an extension to that of Section (3.2.2), to include the nonlinear terms of the strain-displacement relationships. The component of the nonlinear strain vector ($\underline{\varepsilon}_{NL}$), which is derived in Appendix (G), can be defined as:

$$\varepsilon_r = \frac{1}{2}\left[\left(\frac{\partial u}{\partial r}\right)^2 + \left(\frac{\partial v}{\partial r}\right)^2 + \left(\frac{\partial w}{\partial r} - \frac{w}{r}\right)^2 \right]$$

$$\varepsilon_z = \frac{1}{2}\left[\left(\frac{\partial u}{\partial z}\right)^2 + \left(\frac{\partial v}{\partial z}\right)^2 + \left(\frac{\partial w}{\partial z}\right)^2 \right]$$

$$\varepsilon_\theta = \frac{1}{2}\left[\left(\frac{1}{r}\frac{\partial u}{\partial \theta}\right)^2 + \left(\frac{1}{r}\frac{\partial v}{\partial \theta}\right)^2 + \left(\frac{1}{r}\frac{\partial w}{\partial \theta} + \frac{u}{r}\right)^2 \right]$$

$$\gamma_{zr} = \frac{\partial u}{\partial z}\frac{\partial u}{\partial r} + \frac{\partial v}{\partial z}\frac{\partial v}{\partial r} + \frac{\partial w}{\partial z}\left(\frac{\partial w}{\partial r} - \frac{w}{r}\right)$$

$$\gamma_{r\theta} = \frac{\partial u}{\partial r}\frac{1}{r}\frac{\partial u}{\partial \theta} + \frac{\partial v}{\partial r}\frac{1}{r}\frac{\partial v}{\partial \theta} + \left(\frac{\partial w}{\partial r} - \frac{w}{r}\right)\left(\frac{1}{r}\frac{\partial w}{\partial \theta} + \frac{u}{r}\right)$$

$$\gamma_{\theta z} = \left(\frac{1}{r}\frac{\partial u}{\partial \theta}\right)\frac{\partial u}{\partial z} + \frac{1}{r}\frac{\partial v}{\partial \theta}\frac{\partial v}{\partial z} + \left(\frac{1}{r}\frac{\partial w}{\partial \theta} + \frac{u}{r}\right)\frac{\partial w}{\partial z}$$

using a Fourier series expansion:

$$u = u' \cos n\vartheta + u'' \sin n\vartheta$$

$$v = v' \cos n\vartheta + v'' \sin n\vartheta$$

$$w = w' \sin n\vartheta - w'' \cos n\vartheta$$

and the strain-displacement relationships following the same procedure as that employed in (4.3):

$$\underline{\varepsilon}_{NL} = \tfrac{1}{2}\,\underline{A}\,\underline{\theta}$$

$$= \tfrac{1}{2}\,(\,\underline{A}' + \underline{A}''\,)(\,\underline{\theta}' + \underline{\theta}''\,)$$

$$\underline{K}_T = \underline{K}_L + \underline{K}_{NL} + \underline{K}_\sigma$$

where;

$$\underline{K}_{NL} = \iiint [\ \underline{B}_L^{\,T}\,\underline{D}\,\underline{B}_{NL} + \underline{B}_{NL}^{\,T}\,\underline{D}\,\underline{B}_L + \underline{B}_{NL}^{\,T}\,\underline{D}\,\underline{B}_{NL}\ ]\ dv$$

$$= \iiint [\ \underline{B}_L^{\,T}\,\underline{D}\,\underline{A}\,\underline{G} + \underline{G}^T\,\underline{A}^T\,\underline{D}\,\underline{B}_L + \underline{G}^T\,\underline{A}^T\,\underline{D}\,\underline{A}\,\underline{G}\ ]\ dv$$

$$= \underline{K}_{NL}^{\,1} + \underline{K}_{NL}^{\,2} + \underline{K}_{NL}^{\,3}$$

where;

$$\underline{K}_{NL}^{\,1} = \iiint \underline{B}_L^{\,T}\,\underline{D}\,\underline{A}\,\underline{G}\ dv$$

$$= \iiint\ (\,\underline{B}_L' + \underline{B}_L''\,)^T\,\underline{D}\,(\,\underline{A}' + \underline{A}''\,)(\,\underline{G}' + \underline{G}''\,)\ dv$$

$$= \iiint\ (\,\underline{B}_L' + \underline{B}_L''\,)^T\,\underline{D}\,(\,\underline{A}'\,\underline{G}' + \underline{A}'\,\underline{G}'' + \underline{A}''\,\underline{G}'$$

$$+ \underline{A}''\,\underline{G}''\,)\ dv$$

$$= \iiint\ (\,\underline{B}_L'^T + \underline{B}_L''^T\,)(\,\underline{D}\,\underline{A}'\,\underline{G}' + \underline{D}\,\underline{A}'\,\underline{G}''$$

$$+ \underline{D}\,\underline{A}''\,\underline{G}' + \underline{D}\,\underline{A}''\,\underline{G}''\,)\ dv$$

$$= \iiint\ (\,\underline{B}_L'^T\,\underline{D}\,\underline{A}'\,\underline{G}' + \underline{B}_L'^T\,\underline{D}\,\underline{A}'\,\underline{G}'' + \underline{B}_L'^T\,\underline{D}\,\underline{A}''\,\underline{G}'$$

$$+ \underline{B}_L'^T\,\underline{D}\,\underline{A}''\,\underline{G}'' + \underline{B}_L''^T\,\underline{D}\,\underline{A}'\,\underline{G}' + \underline{B}_L''^T\,\underline{D}\,\underline{A}'\,\underline{G}''$$

$$+ \underline{B}_L''^T\,\underline{D}\,\underline{A}''\,\underline{G}' + \underline{B}_L''^T\,\underline{D}\,\underline{A}''\,\underline{G}''\,)\ dv$$

$$= 0$$

Similarly;

$$\underline{K}_{NL}^{\,2} = 0$$

and ;

$$\underline{K}_{NL}^{\,3} = \iiint [\, \underline{G}'^{T} + \underline{G}''^{T} \,][\, \underline{A}'^{T} + \underline{A}''^{T} \,]\, \underline{D}\, [\, \underline{A}' + \underline{A}'' \,]$$

$$[\, \underline{G}' + \underline{G}'' \,]\, dv$$

$$= \iiint [\, \underline{G}'^{T} + \underline{G}''^{T} \,][\, \underline{A}'^{T} + \underline{A}''^{T} \,]\, \underline{D}\, [\, \underline{A}'\, \underline{G}' + \underline{A}'\, \underline{G}''$$

$$+ \underline{A}''\, \underline{G}' + \underline{A}''\, \underline{G}'' \,]\, dv$$

$$= \iiint [\, \underline{G}'^{T} + \underline{G}''^{T} \,][\, \underline{A}'^{T} + \underline{A}''^{T} \,][\, \underline{D}\, \underline{A}'\, \underline{G}' + \underline{D}\, \underline{A}'\, \underline{G}''$$

$$+ \underline{D}\, \underline{A}''\, \underline{G}' + \underline{D}\, \underline{A}''\, \underline{G}'' \,]\, dv$$

$$= \iiint [\, \underline{G}'^{T} + \underline{G}''^{T} \,][\, \underline{A}'^{T}\, \underline{D}\, \underline{A}'\, \underline{G}' + \underline{A}'^{T}\, \underline{D}\, \underline{A}'\, \underline{G}''$$

$$+ \underline{A}'^{T}\, \underline{D}\, \underline{A}''\, \underline{G}' + \underline{A}'^{T}\, \underline{D}\, \underline{A}''\, \underline{G}''$$

$$+ \underline{A}''^{T}\, \underline{D}\, \underline{A}'\, \underline{G}' + \underline{A}''^{T}\, \underline{D}\, \underline{A}'\, \underline{G}' + \underline{A}''^{T}\, \underline{D}\, \underline{A}'\, \underline{G}''$$

$$+ \underline{A}''^{T}\, \underline{D}\, \underline{A}''\, \underline{G}'' \,]\, dv$$

$$= \iiint [\, \underline{G}'^{T}\, \underline{A}'^{T}\, \underline{D}\, \underline{A}'\, \underline{G}' + \underline{G}'^{T}\, \underline{A}'^{T}\, \underline{D}\, \underline{A}'\, \underline{G}''$$

$$+ \underline{G}'^{T}\, \underline{A}'^{T}\, \underline{D}\, \underline{A}''\, \underline{G}' + \underline{G}'^{T}\, \underline{A}'^{T}\, \underline{D}\, \underline{A}''\, \underline{G}''$$

$$+ \underline{G}'^{T}\, \underline{A}''^{T}\, \underline{D}\, \underline{A}'\, \underline{G}' + \underline{G}'^{T}\, \underline{A}''^{T}\, \underline{D}\, \underline{A}'\, \underline{G}''$$

$$+ \underline{G}'^{T}\, \underline{A}''^{T}\, \underline{D}\, \underline{A}''\, \underline{G}' + \underline{G}'^{T}\, \underline{A}''^{T}\, \underline{D}\, \underline{A}''\, \underline{G}''$$

$$+ \underline{G}''^{T}\, \underline{A}'^{T}\, \underline{D}\, \underline{A}'\, \underline{G}' + \underline{G}''^{T}\, \underline{A}'^{T}\, \underline{D}\, \underline{A}'\, \underline{G}''$$

$$+ \underline{G}''^{T}\, \underline{A}'^{T}\, \underline{D}\, \underline{A}''\, \underline{G}' + \underline{G}''^{T}\, \underline{A}'^{T}\, \underline{D}\, \underline{A}''\, \underline{G}''$$

$$+ \underline{G}^{''T}\,\underline{A}^{'T}\,\underline{D}\,\underline{A}^{''}\,\underline{G}' + \underline{G}^{''T}\,\underline{A}^{'T}\,\underline{D}\,\underline{A}^{''}\,\underline{G}''$$

$$+ \underline{G}^{''T}\,\underline{A}^{''T}\,\underline{D}\,\underline{A}'\,\underline{G}' + \underline{G}^{''T}\,\underline{A}^{''T}\,\underline{D}\,\underline{A}'\,\underline{G}''$$

$$+ \underline{G}^{''T}\,\underline{A}^{''T}\,\underline{D}\,\underline{A}^{''}\,\underline{G}' + \underline{G}^{''T}\,\underline{A}^{''T}\,\underline{D}\,\underline{A}''\,\underline{G}''\ ]\ dv$$

$$= \iiint [\ \underline{G}^{'T}\,\underline{A}^{'T}\,\underline{D}\,\underline{A}'\,\underline{G}' + \underline{G}^{''T}\,\underline{A}^{''T}\,\underline{D}\,\underline{A}^{''}\,\underline{G}''\ ]\ dv$$

$$= \underline{K}_{NL\ sy} + \underline{K}_{NL\ asy}$$

where:

$$\underline{K}_{NL\ sym} = \iiint \underline{G}^{'T}\,\underline{A}^{'T}\,\underline{D}\,\underline{A}'\,\underline{G}'\ dv$$

is the nonlinear stiffness matrix corresponding to the first part of the Fourier expansion.

Due to the symmetry of the external load along the plane($\varphi = 0$), as explained previously, the asymmetric part of the Fourier expansion will vanish [57].

The derivation of the stiffness matrices and the explicit form of the stiffness matrices, will be given in Appendix (F).

4.5 APPLICATION TO NONLINEAR ANALYSIS OF TYRE:

For the case of pneumatic tyres, the nonlinear solution can be obtained by a combination of the analysis of nonlinear material and the analysis of large deformations.

Nonlinear iterations can be achieved by employing any one of the following procedures:

a- The Newton-Raphson iteration scheme which requires the updating of the stiffness matrix at each iteration. This

scheme may converge within a small number of iterations.

b- The modified Newton-Raphson scheme, which keeps the same stiffness matrix throughout the iterations but may require more iterations for convergence than would the basic Newton-Raphson scheme.

c- A slight modification to the Newton-Raphson iteration procdure by taking:

$$\underline{K}_T = \underline{K}_L + \underline{K}_\sigma$$

was tested in the present work and was proved to give results of the same order of accuracy as those obtained by using the Newton-Raphson scheme, as will be shown later. It has also been found that this modified approach has saved computer CPU time for the same accuracy as compared with approaches (a) and (b). It was also found to produce convergence whenever the Newton-Raphson procedure failed.

An illustration of the above three methods is shown in Figures 4.1, a,b,c respectively.

CHAPTER 5

VISCOELASTIC STRESS ANALYSIS

CHAPTER 5

VISCOELASTIC STRESS ANALYSIS

5.1 INTRODUCTION:

For a long time the mechanics of deformable bodies has been based upon Hooke's law. Most non-metallic engineering materials, such as rubber , are not linearly elastic. For the case of elastic materials, elastic strains are generated instantaneously for any applied load, and fully recovered upon the removal of the load. For most non-metallic materials, the stress-strain behaviour is time dependent, and is influenced by the so-called viscous effect.

Some Observed Phenomena:

1- Creep: this is the change of strain with time as the stress is kept constant.

2- Recovery: this is the reduction of strain with time as the stress is reduced (either partially or completely).

3- Relaxation: the decrease of stress with time as the strain is kept constant.

4- Rate effect: the stress-strain response as the stress rate or strain rate is increased.

These phenomena are demonstrated in Figure(5.1).

5.2 MECHANICAL REPRESENTATION OF VISCOELASTIC BEHAVIOUR:

In the pneumatic tyre the use of a time dependent material, such as rubber, will add another variable, i.e. time, to the conventional

elastic solution. Viscous behaviour can be described by a dashpot which contains a perfectly viscous fluid. For such a case, the extension ($\underline{\delta}$) is described as proportional to the applied load($\underline{F}$) by the equation:

$$\underline{F} = \eta \dot{\underline{\delta}}$$

where;

$\dot{\underline{\delta}}$ is the rate of extension ($\frac{\partial \delta}{\partial t}$),

and, η is the damping coefficient.

A particular behaviour can be represented by a spring which is governed by the equation:

$$\underline{F} = \underline{K}\,\underline{\delta}$$

where; $\underline{K}$ is the spring stiffness.

In general, a viscoelastic material can be represented by springs and dashpots arranged in different forms, using the generalised Maxwell model, the generalised Kelvin model or a combination of both [46] as shown in Figure (5.2). In this case, if the total stress and strain history is known at an instant of time (t), then it is possible to proceed by an infinitesimal increment(Δt) to a new state of stress and strain as will be explained in Section (5.3).

5.3 VISCOELASTIC STRESS ANALYSIS:

The static analysis of the viscoelastic behaviour of a pneumatic tyre will be carried out based on the hereditary integral form. This approach is very accurate, and the stress can be determined as a function of the strain and the past history of the stress as explained in Chapter 3.

The stress-strain constitutive equation, in the hereditary integral form, may be represented by the following equation [46]:

$$\sigma_{ij}(t) = \int_0^{\infty} \varepsilon_{kl}(t-s)\, dC_{ijkl}(s) \qquad (5.1)$$

where:

$\sigma_{ij}(t)$, $\varepsilon_{kl}(t)$ are the stress and strain tensors at a time (t),
C_{ijkl} is the elastic properties during the time interval (s).

Equation (5.1) can be rewritten in the following form :

$$\sigma_{ij}(t) = C_{ijkl}(0)\ \varepsilon_{kl}(t) + \int_0^t \varepsilon_{kl}(t-s)\ \frac{dC_{ijkl}}{ds}\, ds \qquad (5.2)$$

Assuming $\tau = t-s$, and integrating (5.2) by parts, the above integral equation will be :

$$\sigma_{ij}(\tau) = C_{ijkl}(t)\ \varepsilon_{kl}(0) + \int_0^t C_{ijkl}(t-\tau)\ \frac{d\varepsilon(\tau)}{d\tau}\, d\tau \qquad (5.3)$$

In this equation, the current stress is determined by the superposition of the responses to the complete spectrum of increments of strain.

The elastic properties of the material can be expressed in an exponential form, using any of the models mentioned in Section(5.2).

For the analysis of relaxation, the tyre will be represented by springs and dashpots, as shown in Figure (5.3), and the elastic properties will be :

$$C_{ijkl} = C^{0}_{ijkl} + \sum_{n=1}^{N} C^{n}_{ijkl}\ e^{-t/\lambda^{n}} \qquad (5.4)$$

in which λ^{n} is a positive time constant and is equal to:

$$\lambda^{n} = \eta_{n} / E_{n}$$

where :

η_n is the damping coefficient and ,

E_n is Young's modulus.

From Equation (5.4), it can be deduced that:

$$\frac{dC_{ijkl}(t)}{dt} = -\sum_{n=1}^{N} \frac{C^n_{ijkl}}{\lambda^n} e^{-t/\lambda^n} \qquad (5.5)$$

Substituting Equations 5.4,5.5, into 5.2, it can be shown that:

$$\sigma_{ij}(t) = \left[C^0_{ijkl} + \sum_{n=1}^{N} C^n_{ijkl} \right] \epsilon_{kl}(t) - \sum_{n=1}^{N} \frac{C^n_{ijkl}}{\lambda^n} \int_0^t \epsilon_{kl}(\tau)\, e^{-(t-\tau)/\lambda^n} \qquad (5.6)$$

Changing the time by an increment Δt, then the corresponding stress $\Delta \sigma_{ij}$ will be :

$$\Delta\sigma_{ij}(t) = \sigma_{ij}(t) - \sigma_{ij}(t - \Delta t)$$

where:

$$\sigma_{ij}(t - \Delta t) = \sigma^{0}_{ij}(t - \Delta t) + \sum_{n=1}^{N} \sigma^{n}_{ij}(t - \Delta t), \qquad \text{and}$$

$$\sigma^{0}_{ij}(t - \Delta t) = C^{0}_{ijkl}\, \epsilon_{kl}(t - \Delta t) ,$$

$$\sigma^{n}_{ij}(t - \Delta t) = C^{n}_{ijkl}\, \epsilon_{kl}(t - \Delta t) + \frac{-C^{n}_{ijkl}}{\lambda^{n}} \int_0^{t-\Delta t} \epsilon_{kl(\tau)}\, e^{-(\tau - \Delta t - \tau)/\lambda^{n}}\, d\tau$$

From Equation (5.6):

$$\sigma^{n}_{ij}(t) = C^{n}_{ijkl}\, \epsilon_{kl}(t) + \frac{-C^{n}_{ijkl}}{\lambda^{n}} \int_0^t \epsilon_{kl}(\tau)\, e^{-(t-\tau)/\lambda^{n}}\, d\tau$$

$$= C^{n}_{ijkl}\, \epsilon_{kl}(t) + \frac{-C^{n}_{ijkl}}{\lambda^{n}} \int_0^{t-\Delta t} \epsilon_{kl}(\tau)\, e^{-(t-\tau)/\lambda^{n}}\, d\tau$$

$$+ \frac{-C^n_{ijkl}}{\lambda^n} \int_{t-\Delta t}^{t} \varepsilon_{kl}(\tau)\ e^{-(t-\tau)/\lambda^n}\, d\tau$$

Hence, it can be shown that;

$$\sigma^n_{ij}(t) = C^n_{ijkl}\,\varepsilon_{kl}(t) + \frac{C^n_{ijkl}}{\lambda^n}\, e^{-\Delta t/\lambda^n} \int_0^{t-\Delta t} \varepsilon_{kl}(\tau)\ e^{(t-\Delta t-\tau)/\lambda^n}\, d\tau + \frac{-C^n_{ijkl}}{\lambda^n} \int_{t-\Delta t}^{t} \varepsilon_{kl}(\tau)\ e^{-(t-\tau)/\lambda^n}\, d\tau \qquad (5.7)$$

Defining the strain increment $\Delta\varepsilon$, such that:

$$\varepsilon_{kl}(t) = \varepsilon_{kl}(t-\Delta t) + \Delta\varepsilon(t) \qquad (5.8)$$

and substituting into (5.7), then:

$$\sigma^n_{ij}(t) = C^n_{ijkl}\,\varepsilon_{kl}(t-\Delta t) + C^n_{ijkl}\,\Delta\varepsilon_{kl}(t) - e^{-\Delta t/\lambda^n} * \frac{C^n_{ijkl}}{\lambda^n} \int_0^{t-\Delta t} \varepsilon_{kl}(\tau)\ e^{-(t-\tau)/\lambda^n}\, d\tau - \frac{C^n_{ijkl}}{\lambda^n} \int_{t-\Delta t}^{t} \varepsilon_{kl}(\tau)\ e^{-(t-\tau)/\lambda^n}\, d\tau$$

$$= e^{-\Delta t/\lambda^n} C^n_{ijkl}\,\varepsilon_{kl}(t-\Delta t) - e^{-\Delta t/\lambda^n} C^n_{ijkl}\,\varepsilon_{kl}(t-\Delta t) + C^n_{ijkl}\,\varepsilon_{kl}(t-\Delta t) + C^n_{ijkl}\,\Delta\varepsilon_{kl}(t) - \frac{C^n_{ijkl}}{\lambda^n}\, e^{-\Delta t/\lambda^n} \int_0^{t-\Delta t} e^{-(t-\tau)}\, d\tau - \frac{C^n_{ijkl}}{\lambda^n} \int_{t-\Delta t}^{t} \varepsilon_{kl}(\tau)\ e^{-(t-\tau)/\lambda^n}\, d\tau$$

$$= e^{-\Delta t/\lambda^n} \sigma^n_{ij}(t-\Delta t) + C^n_{ijkl}\,\varepsilon_{kl}(t-\Delta t)\left[1 - e^{-\Delta t/\lambda^n}\right] + C^n_{ijkl}\,\Delta\varepsilon_{kl}(t)$$

$$- \frac{C^n_{ijkl}}{\lambda^n} \int_{t-\Delta t}^{t} \varepsilon_{kl}(\tau) e^{-(t-\tau)/\lambda^n} d\tau \qquad (5.9)$$

Assuming a linear variation of strain during the time interval Δt, it can be shown that:

$$\varepsilon_{kl}(t) = \varepsilon_{kl}(t - \Delta t) + \frac{t-(t-\Delta t)}{\Delta t} \varepsilon_{kl}(t) \qquad (5.10)$$

The integration of each part of Equation (5.9) using equation (5.10) can be carried out as follows:

$$a- \int_{t-\Delta t}^{t} \varepsilon_{kl}(\tau)\ e^{-(t-\tau)/\lambda^n}\ d\tau = \int_{t-\Delta t}^{t} [\varepsilon_{kl}(t-\Delta t) + \frac{t+\Delta t}{\Delta t} \varepsilon_{kl}(t)\, e^{-(t-\tau)/\lambda^n}\ ]\ d\tau$$

$$= \int_{t-\Delta t}^{t} \varepsilon_{kl}(t-\Delta t) e^{-(t-\tau)/\lambda^n} d\tau + \int_{t-\Delta t}^{t} \frac{\tau - t + \Delta t}{\Delta t} \Delta\varepsilon_{kl} e^{-(t-\tau)/\lambda^n} d\tau \qquad (5.11)$$

and;

$$b- \int_{t-\Delta t}^{t} \varepsilon_{kl}(t-\Delta t)\, e^{-(t-\Delta t)/\lambda^n}\ d\tau = \varepsilon_{kl}(t-\Delta t)\ \lambda^n \Big| \bar{e}^{(t-\tau)/\lambda^n} \Big|_{t-\Delta t}^{t}$$

$$= \varepsilon_{kl}(t-\Delta t)\ \lambda^n\ [1 - \bar{e}^{\Delta t/\lambda^n}] \qquad (5.12)$$

$$c- \int_{t-\Delta t}^{t} (\frac{\tau - t + \Delta t}{\Delta t})\Delta\ \varepsilon_{kl}(t)\ e^{-(t-\tau)/\lambda^n}\ d\tau$$

$$= \Delta\varepsilon_{kl}(t) \int_{t-\Delta t}^{t} (\frac{\tau - t + \Delta t}{\Delta t})\ e^{-(t-\tau)/\lambda^n}\ d(\tau - t) \qquad (5.13)$$

Defining: $s = \frac{\tau - t}{\lambda^n}$

$$ds = \frac{1}{\lambda^n} d\tau$$

i.e. $$\int_{t-\Delta t}^{t} (\frac{\tau - t \pm \Delta t}{\Delta t})\Delta\varepsilon_{kl}(t)\ e^{-(t-\tau)/\lambda^n} d\tau = \Delta\varepsilon_{kl}(t) \lambda^n \int_{-\Delta t/\lambda^n}^{0} (s \frac{\lambda^n}{\Delta t} + 1) e^s\, ds$$

$$= \Delta\varepsilon_{kl}(t)\lambda^n \left[\int_{-\Delta t/\lambda^n}^{0} \frac{\lambda^n}{\Delta t} s\, e^s\, ds + \int_{-\Delta t/\lambda^n}^{0} e^s\, ds \right]$$

$$= \Delta\varepsilon_{kl}(t)\lambda^n \left[\left| \frac{\lambda^n}{\Delta t}(s-1)e^s + e^s \right|_{-\Delta t/\lambda^n}^{0} \right]$$

$$= \Delta\varepsilon_{kl}(t)\lambda^n \left[\left(1 - \frac{\lambda^n}{\Delta t}\right) - \left(\frac{\lambda^n}{\Delta t}\left(\frac{-\Delta t}{\lambda^n} - 1\right) + e^{-\Delta t/\lambda^n}\right)\right]$$

$$= \Delta\varepsilon_{kl}(t)\lambda^n \left[1 - \frac{\lambda^n}{\Delta t} - \left(\left(-1 - \frac{\lambda^n}{\Delta t}\right)e^{-\Delta t/\lambda^n} + e^{-\Delta t/\lambda^n}\right)\right]$$

$$= \Delta\varepsilon_{kl}(t)\lambda^n \left[1 - \frac{\lambda^n}{\Delta t}\left(1 - e^{-\Delta t/\lambda^n}\right)\right]$$

(5.14)

Substitute 5.12,5.14 into 5.11 to obtain:

$$\int_{t-\Delta t}^{t} \varepsilon_{kl}(\tau) e^{-(t-\tau)/\lambda^n} d\tau = \varepsilon_{kl}(t-\Delta t)\lambda^n \left[1 - e^{-\Delta t/\lambda^n} \right] + \Delta\varepsilon_{kl}(t)\lambda^n \left[1 - \frac{\lambda^n}{\Delta t}\left(1 - e^{-\Delta t/\lambda^n}\right)\right]$$

(5.15)

Also, the stress increment $\Delta\sigma_{ij}(t)$ can be determined from the following:

$$\Delta\sigma_{ij}(t) = \sigma^0_{ij}(t) - \sigma^0_{ij}(t-\Delta t) + \sum_{n=1}^{N} \left[\sigma^n_{ij}(t) - \sigma^n_{ij}(t-\Delta t) \right]$$

$$= C^0_{ijkl}\Delta\varepsilon_{kl}(t) + \sum_{n=1}^{N} \Delta\sigma^n_{ij}(t) \qquad (5.16)$$

where :

$$\Delta\sigma^n_{ij}(t) = \sigma^n_{ij}(t) - \sigma^n_{ij}(t-\Delta t) \qquad (5.17)$$

Substituting Equations 5.9,5.15 into 5.17, the stress increment $\Delta\sigma^n_{ij}(t)$ will be:

$$\Delta\sigma^n_{ij}(t) = -(1 - e^{-\Delta t/\lambda^n})\sigma^n_{ij}(t - \Delta t)$$

$$+ C^n_{ijkl}\epsilon_{kl}(t - \Delta t)[1 - e^{-\Delta t/\lambda^n}]$$

$$+ C^n_{ijkl}\Delta\epsilon_{kl}(t)$$

$$- \frac{C^n_{ijkl}}{\lambda^n}\int_{t-\Delta t}^{t}\epsilon_{kl}\tau\ e^{-(t-\tau)/\lambda^n}\,d\tau$$

$$= -(1 - e^{-\Delta t/\lambda^n})\sigma^n_{ij}(t - \Delta t)$$

$$+ C^n_{ijkl}\epsilon_{kl}(t-\Delta t)[1 - e^{-\Delta t/\lambda^n}]$$

$$+ C^n_{ijkl}\Delta\epsilon(t)$$

$$- \frac{-C_{ijkl}}{\lambda^n}\epsilon_{kl}(t-\Delta t)\lambda^n(1 - e^{-\Delta t/\lambda^n})$$

$$- \frac{C_{ijkl}}{\lambda^n}\Delta\epsilon_{kl}(t)\lambda^n[1 - \frac{\lambda^n}{\Delta t}(1 - e^{-\Delta t/\lambda^n})]$$

$$= -(1 - e^{-\Delta t/\lambda^n})\sigma^n_{ij}(t - \Delta t)$$

$$+ C^n_{ijkl}\epsilon_{kl}(t - \Delta t)[1 - e^{-\Delta t/\lambda^n}]$$

$$+ C^n_{ijkl}\Delta\epsilon(t)$$

$$- C^n_{ijkl}\epsilon_{kl}(t - \Delta t)(1 - e^{-\Delta t/\lambda^n})$$

$$- C^n_{ijkl}\Delta\epsilon(t)[1 - \frac{\lambda^n}{\Delta t}(1 - e^{-\Delta t/\lambda^n})]$$

$$= -(1 - e^{-\Delta t/\lambda^n})\sigma^n_{ij}(t-\Delta t)$$

$$+ C^n_{ijkl}\Delta\epsilon(t)\frac{\lambda^n}{\Delta t}(1 - e^{-\Delta t/\lambda^n}) \qquad (5.18)$$

Substituting 5.18 into 5.16 ;

$$\Delta\sigma_{ij}(t) = C^0_{ijkl}\Delta\epsilon(t) + \sum_{n=1}^{N} C^n_{ijkl}\Delta\epsilon_{kl}(t)\frac{\lambda^n}{\Delta t}(1 - e^{-\Delta t/\lambda^n})$$

$$- \sum_{n=1}^{N} \left(1 - e^{-\Delta t/\lambda^n} \right) \sigma^n_{ij(t-\Delta t)}$$

$$= \left[C^0_{ijkl} + \sum_{n=1}^{N} C^n_{ijkl} \frac{\lambda^n}{\Delta t} \left(1 - e^{-\Delta t/\lambda^n} \right) \right] \Delta \cdot \varepsilon(t)$$

$$- \sum_{n=1}^{N} \left(1 - e^{-\Delta t/\lambda^n} \right) \sigma^n_{ij} (t-\Delta t) \qquad (5.19)$$

From Equation 5.19 , the stress increment $\Delta\sigma_{ij}$ at any time (t) can be determined from the strain increment $\Delta\dot{\varepsilon}_{kl}$ at this time and the stress at the previous time $(t - \Delta t)$.

5.4 SOLUTION ALGORITHM:

Using the principle of virtual work, the equilibrium equation (4.2) at any time (t) can be written in the following form:

$$\sum_{\text{element}} \iiint B^T \sigma\,(t)\, dv - F_{ext}\,(t) = R(t) \qquad (5.20)$$

where the stress $\sigma\,(t)$, is the stress at any time (t) which can be calculated from Equation (5.19).

As the stress is time dependent, it will change during the time interval (Δt). The new stress will not satisfy the complete equilibrium of forces, which must vanish at the end of the time increment.

Using the finite element procedure, the change of stress wil be converted to nodal forces, in which the residual forces R(t) can be obtained, using Equation (5.20).

The material properties considered are those at the instant at which the analysis is to be carried out. The analysis is purely elastic, the resulting stresses are superimposed upon the residual distribution that existed at the time of this relaxation. A new stress state will be used for the next interval of time.

Algorithm Iteration Steps:

The modified Newton-Raphson technique will be used as an iterative approach as follows :

1- The relaxation time will be divided into time increments(Δt).

2- For each time interval, solve the linear equation:

$$\underline{K}_o(t)\ \underline{\delta}_o(t) = \underline{F}_{ext}(t)$$

where:

$\underline{K}_o(t)$ is the stiffness matrix at time (t).

$\underline{F}_{ext}(t)$ is the external applied load.

For the i th time increment:

3- Calculate the residual force $\underline{R}_i(t)$ using Equation (5,20).

4- For iteration (r+1), the residual force can be calculated using the equation:

$$\underline{R}_i^{r+1} = \underline{R}_i^r + \underline{K}_i\ \delta_i^r$$

5- Update the displacement, strain and stress for each step of the iteration.

6- Repeat the iteration steps (3-5), until the ratio $\left(\frac{\Delta\delta_i^T\ \Delta\delta_i}{\delta_i^T\ \delta_i}\right)$ is equal to, or less than, a permissible error.

7- Repeat the steps (1-6) until the ratio $\frac{\Delta\sigma\ (i+1)}{\sigma\ (i)}$ is within a certain accuracy.

CHAPTER 6

LINEAR AND NONLINEAR DYNAMIC ANALYSIS OF RADIAL TYRES

CHAPTER 6

LINEAR AND NONLINEAR DYNAMIC ANALYSIS OF RADIAL TYRES

6.1 INTRODUCTION:

The dynamic analysis will be based upon the energy approach. In this approach, it is assumed that the total energy, which includes; the strain energy U, the kinetic energy KE, dissipation energy DE, and the potential energy V, is kept constant.

According to the above principle :

$$U + KE + DE + V = \text{constant} \qquad (6.1)$$

a- The strain energy U is defined as:

$$U = \tfrac{1}{2}\, \underline{\delta}^T\, \underline{K}\, \underline{\delta} \qquad (6.2)$$

where $\underline{K}$ is the stiffness matrix, explained in detail for both linear and nonlinear analysis in Chapters 3,4.

b- The kinetic energy KE, is defined as :

$$KE = \tfrac{1}{2}\, \dot{\underline{\delta}}^T\, \underline{M}\, \dot{\underline{\delta}} \qquad (6.3)$$

where:

$$\dot{\delta} = \frac{\partial}{\partial t}(\delta)$$

$\underline{M}$ is the mass matrix.

c- The dissipation energy DE is equal to :

$$DE = \tfrac{1}{2}\ \delta^T \underline{C}\ \dot{\delta} \qquad (6.4)$$

where:

$\underline{C}$ is the damping matrix.

d- The potential energy V is defined as:

$$V = -\underline{\delta}^T\ \underline{F} \qquad (6.5)$$

From Equations (6.2 - 6.5) it can be seen that these types of energy, are functions of the displacement (δ).

Hence; according to the energy approach :

$$\frac{\partial}{\partial \dot{\delta}}\frac{U}{\delta} + \frac{\partial}{\partial \dot{\delta}}\frac{KE}{\delta} + \frac{\partial}{\partial}\frac{DE}{\delta} + \frac{\partial}{\partial}\frac{V}{\delta} = 0$$

i.e. $$\underline{K}\ \delta + \underline{M}\ \ddot{\delta} + \underline{C}\ \dot{\delta} - \underline{F} = 0$$

or $$\underline{M}\ \ddot{\delta} + \underline{C}\ \dot{\delta} + \underline{K}\ \delta - \underline{F} = 0 \qquad (6.6)$$

The derivation of KE, DE and V is explained in detail in Reference [59].

If the external forces $\underline{F}$ and the damping, are neglected, Equation (6.6) will become:

$$\underline{M}\ \underline{\ddot{\delta}} + \underline{K}\ \underline{\delta} = 0 \qquad (6.7)$$

in which the characteristics of the structure represented by the vibration of natural modes can be determined.

In a natural mode, each point of the structure excutes harmonic motions about the position of static equilibrium at the same frequency. Hence, the vector of nodal displacement $\delta(t)$ can be represented by :

$$\delta(t) = \delta \cos \omega t \qquad (6.8)$$

Substituting Equation (6.8) into Equation (6.7):

$$(-\underline{M}\ \omega^2 + \underline{K})\,\delta = 0$$

or;
$$(\underline{K} - \lambda\ \underline{M})\,\delta = 0 \qquad (6.9)$$

where;
$$\lambda = \omega^2$$

Equation (6.9) has a nontrivial solution if:

$$\left| \underline{K} - \lambda\ \underline{M} \right| = 0$$

The roots of λ are called the eigenvalues, and for each λ_i, there will be a corresponding vector δ_i such that :

$$(\underline{K} - \lambda_i\ \underline{M})\,\delta_i = 0 \qquad (6.10)$$

and δ_i is known as the eigenvector.

As was mentioned in Chapter 2, the tyre response can be predicted, if the natural frequency and mode shape are defined [33].

In this chapter, the analysis of natural frequency and mode shapes will be carried out as a first step for the analysis of the steady state and transient response.

6.2 DERIVATION OF STIFFNESS AND MASS MATRICES:

It is clear from Equation (6.10) that the first step of the analysis is to derive the stiffness matrix $\underline{K}$ and the mass matrix $\underline{M}$.

The stiffness matrix used in the analysis can be either that derived for the linear solution in Chapter 3, or that for the

nonlinear analysis given in Chapter 4.

The consistent mass matrix $\underline{M}$ for the three-dimensional axisymmetric element, used in this analysis, can be derived as follows:

a- Define the nodal displacement and nodal velocities as:

$$\delta = \{ \; u_i \quad v_i \quad w_i \; \}$$

$$\dot{\delta} = \{ \; \dot{u}_i \quad \dot{v}_i \quad \dot{w}_i \; \}$$

b- Express the velocity vector at any point in terms of nodal velocities and shape functions:

$$\dot{u} = \Sigma \, \dot{u}_i \, N_i$$

$$\dot{v} = \Sigma \, \dot{v}_i \, N_i$$

$$\dot{w} = \Sigma \, \dot{w}_i \, N_i$$

where; N_i is the shape function.

Defining the velocity q at any point as:

$$\dot{q} = \{ \; \dot{u} \quad \dot{v} \quad \dot{w} \; \} \quad ,$$

it can be deduced that :

$$\dot{q} = \underline{N} \, \underline{\dot{\delta}}$$

where:

$$\underline{N} = \begin{vmatrix} N_i & 0 & 0 \\ 0 & N_i & 0 \\ 0 & 0 & N_i \end{vmatrix}$$

c- The kinetic energy of the element can be expressed as follows:

$$KE_{element} = \int \dot{q}^T \dot{q} \, dm$$

$$= \iiint \rho \, \dot{\varsigma}^T \dot{q} \, dv$$

where, ρ is the mass density.

d- From the definition of the element mass matrix $\underline{M}_e$;

$$(KE)_{element} = \dot{\underline{\delta}}^T \underline{M}_e \dot{\underline{\delta}}$$

it can be proved that the element mass matrix is as follows:

$$\underline{M}_e = \iiint \rho \, \underline{N}^T \underline{N} \, dv$$

The consistent mass matrix for the whole structure can be assembled from element mass matrices in a way similar to that employed for the structure stiffness matrix.

6.3 DYNAMIC EIGENVALUE PROBLEM:

The dynamic eigenvalue problem can be solved by means of different algorithms. The simple iteration solver, the most popular technique, is developed here. The basic disadvantage of the simple iteration solver is the large CPU time consumed, particularly when used for large structures such as tyres. For this reason, some of the economical solvers such as dynamic condensation, subspace iteration and the double economiser are derived here using a frontal solver.

6.3.1 Simple Iteration Algorithm :

Equation (6.9) can be written in the form:

$$\underline{M}\ \underline{\delta} = \frac{1}{\lambda}\ \underline{K}\ \underline{\delta}$$

Multiplying both sides by $\underline{K}^{-1}$, the equation can be expressed as:

$$\underline{Q}\,\underline{\delta} = \frac{1}{\lambda}\ \underline{I}\ \underline{\delta} \qquad (6.11)$$

where;

$$\underline{Q} = \underline{K}^{-1}\ \underline{M}$$

To solve equation (6.11) for the eigenvalues and the corresponding eigenvectors, the following steps may be taken:

i) Iteration for the lowest eigenvalue:

The following steps will be carried out to determine the lowest eigenvalue:

a- Assume an eigenvector

b- Calculate the vector $\underline{Y}$ such that:

$$\underline{Y} = \underline{Q}\ \underline{\delta}$$

c- Calculate the eigenvalue λ and the corresponding eigenvector using the equations:

$$\lambda = \underline{Y}^T\ \underline{Y} \,/\, \underline{Y}^T\ \underline{Q}\ \underline{Y}\ ,$$

$$\delta = \underline{Y} \,/\, \sqrt{\underline{Y}^T\ \underline{M}\ \underline{Y}}$$

d- If ($\lambda_{new} - \lambda_{old}$) > a permissible error, the steps (b-d) will be repeated.

ii) Sweeping for λ_j:

From the orthogonality of eigenvectors, it can be proved that:

$$\underline{Q}_{j+1}\,\underline{\delta} = \frac{1}{\lambda}\,\underline{I}\,\underline{\delta}$$

will converge to λ_{j+1} Reference [59], where;

$$\underline{Q}_{j+1} = \underline{Q}_j - \frac{1}{\lambda_j}\,\delta_j\,\delta_j^T\,\underline{M} \quad ,$$

$$\lambda_1 < \lambda_2 < \lambda_3 \ldots\ldots$$

6.3.2 Dynamic Condensation:

The idea of dynamic condensation is based upon dividing the nodal displacements into two groups:

a- The first group is known as the Master group and will be denoted by δ_m.

b- The second group is known as the Slave group, and is dnoted by δ_s.

It is assumed that the Slaves minimise the strain energy regardless of the effect on the kinetic energy, and hence that they can be eliminated from the equations as shown below.

Partitioning the nodal displacement vector;

$$\delta = \{\, \delta_m \quad \delta_s \,\}$$

the corresponding partitioned stiffness and mass matrices will be as

follows:

$$\underline{K} = \begin{bmatrix} \underline{K}_{mm} & \underline{K}_{ms} \\ \\ \underline{K}_{sm} & \underline{K}_{ss} \end{bmatrix} ,$$

$$\underline{M} = \begin{bmatrix} \underline{M}_{mm} & \underline{M}_{ms} \\ \\ \underline{M}_{sm} & \underline{M}_{ss} \end{bmatrix}$$

Hence, the strain energy will be:

$$U = \tfrac{1}{2} \{ \delta_m \quad \delta_s \} \begin{bmatrix} \underline{K}_{mm} & \underline{K}_{ms} \\ \\ \underline{K}_{sm} & \underline{K}_{mm} \end{bmatrix} \begin{bmatrix} \delta_m \\ \\ \delta_s \end{bmatrix}$$

$$= \tfrac{1}{2} \{ \delta_m \quad \delta_s \} \begin{bmatrix} \underline{K}_{mm}\delta_m + \underline{K}_{ms}\delta_s \\ \\ \underline{K}_{sm}\delta_m + \underline{K}_{ss}\delta_s \end{bmatrix}$$

$$= \tfrac{1}{2} [\delta_m^T \underline{K}_{mm}\delta_m + \delta_m^T \underline{K}_{ms}\delta_s + \delta_s^T \underline{K}_{sm}\delta_m + \delta_s^T \underline{K}_{ss}\delta_s]$$

Similarly; the kinetic energy is:

$$KE = \tfrac{1}{2} [\delta_m^T \underline{M}_{mm}\delta_m + \delta_m^T \underline{M}_{ms}\delta_s + \delta_s^T \underline{M}_{sm}\delta_m + \delta_s^T \underline{M}_{ss}\delta_s]$$

Since the slaves minimise the strain energy;

then; $$\frac{\partial u}{\partial s} = 0 \quad ,$$

and; $$\delta^T_m \underline{K}_{ms} \delta_s = \delta^T_s \underline{K}_{sm} \delta_m$$

Hence:

$$\tfrac{1}{2} \left[\underline{K}_{sm} \delta_m + \underline{K}_{sm} \delta_m + 2 \underline{K}_{ss} \delta_s \right] = 0$$

i.e. $$\underline{K}_{ss} \delta_s = - \underline{K}_{sm} \delta_m \quad ,$$

$$\delta_s = - \underline{K}^{-1}_{ss} \underline{K}_{sm} \delta_m$$

Differentiating with respect to time,

$$\dot{\delta}_s = - \underline{K}^{-1}_{ss} \underline{K}_{sm} \dot{\delta}_m$$

eliminating $\dot{\delta}_s$, δ_s from U , KE equations;

$$U = \tfrac{1}{2} \left[\delta^T_m \underline{K}_{mm} \delta_m - \delta^T_m \underline{K}_{ms} \underline{K}^{-1}_{ss} \underline{K}_{sm} \delta_m - \delta^T_m \underline{K}_{ms} \underline{K}^{-1}_{ss} \underline{K}_{sm} \delta_m \right.$$

$$\left. + \delta^T_m \underline{K}_{ms} \underline{K}^{-1}_{ss} \underline{K}_{sm} \delta_m \right]$$

$$= \tfrac{1}{2} \delta^T_m \underline{\overset{*}{K}} \delta_m$$

where;

$$\underline{\overset{*}{K}} = \underline{K}_{mm} - \underline{K}_{ms} \underline{K}^{-1}_{ss} \underline{K}_{sm} \quad ,$$

Similarly; the kinetic energy:

$$KE = \tfrac{1}{2} \dot{\delta}_m \underline{\overset{*}{M}} \dot{\delta}_m$$

where;

$$\underline{\overset{*}{M}} = \underline{M}_{mm} - \underline{M}_{ms} \underline{K}^{-1}_{ss} \underline{K}_{sm} - \underline{K}_{ms} \underline{K}^{-1}_{ss} \underline{M}_{sm} + \underline{K}_{ms} \underline{K}^{-1}_{ss} \underline{M}_{ss} \underline{K}^{-1}_{ss} \underline{K}_{sm}$$

$\underline{K}^*$, $\underline{M}^*$ are the condensed stiffness and mass matrices, which can be solved by the simple iteration algorithm.

6.3.3 Subspace Iteration:

Subspace iteration is a very accurate and economical tool for determining the eignvalues of a structure such as a tyre where the stiffness and mass matrices are of a large order, and when only a few eigenvalues are required.

The idea behind subspace iteration is that the stiffness and mass matrices can be reduced whilst keeping the lowest eigenvalue. The subspace iteration algorithm may be carried out as follows:

a- Assume a set of loading vectors $\underline{Y}_i$, i = 1,2,....,p
where; p is the required number of eigenvalues.

b- Solve the equation:

$$\underline{K}\ \delta_r = \underline{Y}_r \qquad , r = 1,2,.....,p$$

The solution of the above system of equations can be carried out efficiently by employing a frontal solver.

c- Form the following matrix:

$$\underline{Q} = [\ \delta_1\ \ \delta_2\ \ .....\ \delta_p\ ]$$

d- The reduced stiffness and mass matrices $\underline{K}_s$, $\underline{M}_s$ can be obtained as follows:

$$\underline{K}_s = \underline{Q}^T\ \underline{K}\ \underline{Q}\ ,$$

$$\underline{M}_s = \underline{Q}^T\ \underline{M}\ \underline{Q}$$

e- Using the simple iteration solver, the subspace eigenvalues

can be obtained.

$$\underline{K}_s \ \delta_s = \lambda \underline{M}_s \ \delta_s$$

f- Form the matrix $\underline{Q}_s$ such that:

$$\underline{Q}_s = [\ \delta_1 \quad \delta_2 \quad \cdots \quad \delta_p\ ]_s$$

g- Transform back to the original space, using the relationship:

$$\underline{Q}_{new} = \underline{Q}_{old} * \underline{Q}_s$$

and the corresponding new load vector:

$$\underline{Y}_{new} = \underline{M}\ \underline{Q}_{new}$$

h- Calculate the maximum error;

$$\text{Error} = \max\ (\ |\ \lambda_{inew} - \lambda_{iold}\ |\ )\ ,\ i = 1,2,\ldots\ldots,p$$

If the maximum error is greater than a given permissible error, then steps (b-h) will be repeated until it is smaller.

6.3.4 Double Economiser:

The principle of the double economizer is to combine the improvement given by the two previous economical solvers as follows:

a- As the lowest eigenvalue will correspond to the minimum value of (K_{ii} / M_{ii}), then dynamic condensation will be used to reduce the stiffness and mass matrices to $\underline{K}_c$, $\underline{M}_c$ as explained in Section (6.3.2).

b- The subspace iteration technique will be used to solve for the eigenvalues using $\underline{K}_c$, $\underline{M}_c$ instead of the total stiffness and mass matrices ($\underline{K}$, $\underline{M}$) as explained in Section(6.3.3).

CHAPTER 7

FINITE ELEMENT PROGRAMMING

CHAPTER 7

FINITE ELEMENT PROGRAMMING

7.1 INTRODUCTION:

The finite element package developed for the static and dynamic analysis of radial tyres, is reviewed here. The basic facilities of the package are summarised as follows:

1- A full three-dimensional, linear and nonlinear static analysis of radial tyres, using the axisymmetric-solid-of-revolution element.

2- A nonlinear static analysis which takes the material non-linearity and large deflection into consideration.

3- A nonlinear analysis based on the viscoelastic behaviour of rubber.

4- Linear and nonlinear dynamic analysis of radial tyres for calculation of the eigenvalues and the corresponding natural mode shapes.

5- A powerful mesh generator used for the automatic discretisation of the cross-section.

6- A plotter for graphical output results.

7- In addition to the axisymmetric-solid-of-revolution elements the package contains other types of elements; viz. two-dimensional plane stress/strain elements, Ahmad's element and facet shell elements, that can be employed for different modelling of structures.

The iteration procedures employed for the nonlinear analysis can

be any of the following approaches:

1- The incremental approach.

2- The Newton-Raphson technique (NR).

3- The modified Newton-Raphson technique (MNR).

4- Another approach, which is developed in this work, under the name of developed Newton-Raphson technique (DNR).

This fourth approach was tested and although the given results were the same as those given by the (NR) technique, the new technique may be more suitable for a complex composite structure, such as a tyre, where the Newton-Raphson solution may diverge.

In all of the above types of iterative technique, the analysis is based upon the Lagrangian approach, with increment load and updating of the coordinates after each load increment.

For the viscoelastic behaviour, the analysis is carried out based upon the relaxation phenomenon, using the modified Newton-Raphson iteration technique.

A schematic drawing of the package structure is shown in Figure (7.1).

7.2 PREPROCESSING MODULES:

This part of the package is used for the preparation of the data necessary for the analysis to be carried out. It can be divided into two parts, as shown in Figure (7.2).

7.2.1 The Data Module:

The data module reads the necessary data required to define the problem. It includes:

a) Geometrical Data:

These are the minimum data by which the geometry of the structure can be specified for the automatic mesh generator to be used .

The geometry of the structure can be completely defined by the following three sets of information:

(i) Specification of The Coordinates of Each Nodal Point:

The total number of the nodal points, the number of degrees of freedom for each node and the coordinates of each nodal point with reference to a global coordinate system must be specified.

(ii) Specification of Block Connections:

The structure is discretised into blocks, the number of blocks and type and topology array of each block must be defined.

(iii) Specification of Block Divisions:

The number of divisions for each block in two different directions and the type of the required elements must be specified for each block.

b) Material Properties:

Each different material should be allocated an identification number and the properties related to this material will be stored in an array. Each block is associated with a particular material type

(1 for isotropic , 2 for orthotropic). Each layer of the reinforced composite structure is specified by a certain number within the orthotropic section.

The properties of each material are completely defined in terms of the Young's modulus, the shear modulus and Poisson's ratio in the principal directions of each reinforced layer, as well as by the mass density of the material, the angle of inclination of the reinforced cords with respect to the axes of the geometry of the structure, and the damping coefficient of the material.

c) Boundary Conditions:

Having defined the geometry of the structure, it is necessary to specify the boundary conditions. For the displacement approach, the boundary conditions are specified in terms of some prescribed values of the relevant degrees of freedom at some nodes. For an axisymmetric solid of revolution, the following values may be prescribed:

Displacement in the r-direction.

Displacement in the z-direction.

Displacement in the θ-direction.

In the boundary condition subroutine, the number of quadrature points for the axisymmetric element, and for the one-dimensional element for the loading analysis, should be defined.

d) Loading Conditions:

These include the inflation pressure, the value of the external loads, the area of contact, the number of loaded elements, the number of nodes and topology array for each loaded element.

e) Control Data:

The control parameters required as input in order to complete the analysis are listed as follows:

(i) The number of increments of load.

(ii) The number of harmonics for external loads.

(iii) The maximum permissible error for the iteration.

(iv) The time step increment for the viscoelastic analysis.

(v) The number of eigenvalues required.

In addition to the above control data, there are some control parameters related to the output which must be decided upon:

(i) Whether the viscoelastic analysis is required or not, and

(ii) Whether the principal stresses/strains are required or not.

f) Data Checking and Error Diagnostics:

It is important to inform the user if anything is wrong with his data and to provide him with a useful printed message if the program is aborted.

For each of the sections (a-d), there are basic steps for error diagnosis followed by printed messages for each supposed error.

g) Gauss Quadrature:

The function of this subroutine is to set up the sampling point positions and weighting factors for numerical integration. This subroutine is valid up to 16 quadrature points (in one-direction)

with single and double precision.

The data employed by this subroutine are listed in Table(7.1).

7.2.2 Mesh Generator Module:

The input data explained in Section (7.2.1), will be given to the mesh generator in which the structure will be discretised into the required elements according to the theory with the merits and facilities given in Chapter 3 . A schematic diagram for this module is given in Figure (7.3).

7.3 ANALYSIS MODULES:

7.3.1 Equivalent Nodal Loading Module:

In the finite element analysis using the displacement approach, the only permissible form of loading, is by the specification of concentrated loads at the nodal points. Therefore, the inflation pressure and the external load, must be replaced by equivalent nodal forces.

For any finite element program based upon the isoparametric transformation, the calculation of equivalent nodal forces is difficult to perform manually, since surface integration over arbitrarily shaped regions is generally involved. Hence, it is necessary to include some subroutines with which to perform this task.

As explained in Section (3.6), the one-dimensional element can be used to evaluate the equivalent nodal forces. The required subroutines and the sequence of calculation are illustrated in Figure (7.4).

7.3.2 Element Matrix Generator Module:

In this module, the element stiffness matrix ($\underline{K}_e$) and the element mass matrix ($\underline{M}_e$) will be generated as follows:

a) Tyre Subjected to Inflation Pressure:

The element stiffness matrix is to be determined according to Equation (3.1) as follows:

$$\underline{K}_e = \int_0^1 \int_0^1 \underline{B}^T \underline{D} \underline{B} (2 \pi r) \left| J \left(\frac{r,z}{\xi, \eta} \right) \right| d\xi \, d\eta$$

A numerical integration scheme is used to evaluate this integral, and Gaussian quadrature has proved to be an efficient method which can be adopted as follows:

$$\underline{K}_e = \sum_{r=1}^{NQ} \sum_{s=1}^{NQ} W_{r,s} \, 2 \pi r \, \underline{B}^T \underline{D} \underline{B} (\xi_r , \eta_s) \left| J \left(\frac{r,z}{\xi, \eta} \right) \right|$$

The element mass matrix, as defined by Equation (6.11), can be calculated as follows:

$$\underline{M}_e = \int\int\int \rho \, \underline{N}^T \underline{N} \, dv$$

$$= \int_0^1 \int_0^1 2 \pi r \, \rho \, \underline{N}^T \underline{N} (\xi, \eta) \left| J \left(\frac{r,z}{\xi, \eta} \right) \right| d\xi \, d\eta$$

$$= \sum_{r=1}^{NQ} \sum_{s=1}^{NQ} \rho \, W_{r,s} (2 \pi r) \underline{N}^T \underline{N} (\xi_r , \eta_s) \left| J \left(\frac{r,z}{\xi, \eta} \right) \right|$$

where:

$W_{r,s} = W_r \, W_s$ for quadrilateral elements and,

$W_{r,s} = W_r \, W_s \, (1 - \eta_s)$ for triangular elements ,

$$r = \sum_{i=1}^{N_e} r_i \, N_i$$

r,s are the Gauss quadrature points,

W_r , W_s are Gaussian quadrature parameters, and the other terms are defined in Sections (3.5.1),(6.2).

The required subroutines and the sequence of calculation are given in Figure (7.4).

b) Tyre Subjected to External Load:

For the case of a tyre externally loaded, the element stiffness matrix for each harmonic must be calculated using the explicit form shown in Appendix (B) for linear analysis, and the explicit form mentioned in Appendix (F) for the nonlinear analysis.

7.3.3 Linear Static Analysis of Radial Tyre:

The objective of this section is to formulate, and solve, the equilibrium equations:

$$\underline{K}\ \underline{\delta} = \underline{F}$$

The method adopted for the solution of the above equations is a major factor influencing the efficiency of the finite element program.

Several options for the solution of such equations are available in the present package ranging from direct Gauss-elimination, and Choleski factorisation solvers, to a sophisticated asymmetric frontal solver with dynamic front width. The above solvers can be summarised as follows:

a) Ordinary Solvers:

The steps shown in Figure (7.5) for the formulation and solution of the above equations using ordinary solvers are summarised as follows:

(i) Assembler Module:

In this module the stiffness and mass matrices of the whole structure are formulated. The concept of topology array can be employed for this formulation as follows:

$$\underline{K}_G (I_G , J_G) = \sum_{\text{elements}} \underline{K}_e (I_L , J_L)$$

$$\underline{M}_G (I_G , J_G) = \sum_{\text{elements}} \underline{M}_e (I_L , J_L)$$

where:

$\underline{K}_G$,$\underline{M}_G$ are the stiffness and mass matrices of the whole structure.

$\underline{K}_e$, $\underline{M}_e$ are the element stiffness and mass matrices of the element.

$$I_G = Dof * [TA (e,i) - 1] + r$$

$$J_G = Dof * [TA (e,i) -1] + s$$

$$i,j = 1,2,.... \quad ,n$$

$$r,s = 1,2,.... \quad ,Dof$$

n = number of element nodes.

(ii) Reducer Module:

In this module, the equations of the prescribed displacement will be eliminated from the equilibrium equations of the structure.

If some values of the displacement vector are prescribed, the displacement vector $\underline{\delta}$ can rearranged as:

$$\underline{\delta} = \{ \underline{\delta}_u \quad \underline{\delta}_p \}$$

where:

$\underline{\delta}_u$ is the unknown nodal displacement.

$\underline{\delta}_p$ is the prescribed nodal displacement, and the corresponding matrix equations can be partitioned as follows:

$$\begin{bmatrix} \underline{K}_{uu} & \underline{K}_{up} \\ \underline{K}_{pu} & \underline{K}_{pp} \end{bmatrix} \begin{bmatrix} \delta_u \\ \underline{\delta}_p \end{bmatrix} = \begin{bmatrix} \underline{F}_u \\ \underline{F}_p \end{bmatrix}$$

i.e. $$\underline{K}_{uu}\,\underline{\delta}_u + \underline{K}_{up}\,\underline{\delta}_p = \underline{F}_u$$

$$\underline{K}_{pu}\,\underline{\delta}_u + \underline{K}_{pp}\,\underline{\delta}_p = \underline{F}_p$$

Hence;

$$\underline{K}_{uu}\,\underline{\delta}_u = \underline{F}_u - \underline{K}_{up}\,\underline{\delta}_p$$

represents the reduced system of equations, and

$$\underline{F}_p = \underline{K}_{pu}\,\underline{\delta}_u + \underline{K}_{pp}\,\underline{\delta}_p$$

is the vector of reaction forces.

(iii) Equation Solver:

After formulating the reduced stiffness matrix ($\underline{K}_R$), one of the following solvers can be employed:

Gauss Elimination Solver:

In this solver, the matrix $\underline{K}_R$ is eliminated to an upper triangular matrix, and the resulting equations can be solved by backward substitution, as shown in Appendix (H).

Choleski Factorisation Solver:

This solver is more efficient than the Gauss elimination solver particularly for the case of multiple loading systems, and can be reviewed in Appendix (H).

b- Economical Solver:

The time spent on the solution of the stiffness equations of the structure, represents a large percentage of the total computation time. Therefore the method of solving these equations is very crucial. The optimal approach for the solution may produce considerable savings in both the computer core storage and the CPU time.

The frontal solver is the most efficient for a complex structure such as a tyre, and for use a computer with a virtual memory such as the VAX. It was originated by Irons [67], and developed by El-Zafrany and Cookson [68], to be suitable for asymmetric matrices.

The main structure of the frontal solver consists of the three parts:

(i) Initiation:

In which the element nodes can be eliminated and labelled after assembly of their elements. Also, the maximum front width is calculated at this stage, and additional boundary condition arrays prepared.

(ii) Assembly and Elimination:

In which the finite element equations are assembled, reduced and eliminated whenever possible. As soon as an equation is eliminated it will be stored in the back-up storage and deleted

from the dynamic memory matrix (the frontal matrix).

(iii) Solution:

In this section the finite element equations are solved using backward substitution to obtain the nodal displacements. Each equation (begining with the last) is recalled from the back-up storage and only one equation at a time appears in the direct access memory.

Concerning The Frontal Solver:

The ordering of elements is crucial while the ordering of nodal numbering is irrelevant. This is a completely opposite condition to that required for the banded solution, and one that is easier to satisfy.

Because of the compact nature of the front and because variables are eliminated as soon as possible, the total arithmetic operations are fewer than for other methods.

An elaborate housekeeping system is required for the frontal solution. However, since it is performed with integer variables, little storage or computer time is used.

It is efficient for asymmetric matrices.

There is no storing or manipulation of intermediate gaps or zeros

It is quicker than other solvers.

It has a variable front width with random orders.

7.3.4 Nonlinear Static Analysis of Radial Tyres:

A nonlinear solution for the static analysis of a radial tyre can be carried out, depending upon the type of nonlinearity, through one of the following approaches:

a) Material Nonlinearity:

(i) Newton-Raphson technique, where the tangent stiffness matrix to the material curve will be considered.

(ii) Modified Newton-Raphson technique, in which the stiffness matrix is kept constant.

The theoretical analysis for these approaches is explained in Chapter 3, and a flow chart for this procedure is shown in Figure(7.6).

b) Large Deflection:

For large deflections one of the following approaches can be used:

i) The incremental approach, where the inflation pressure is divided into small increments and a linear solution, with coordinate updating, carried out for each load increment. A flow chart for this procedure is shown in Figure (7.7).

ii) Iterative approaches; which contain:

1- The Newton-Raphson technique; where the total stiffness matrix will be:

$$\underline{K}_T = \underline{K}_L + \underline{K}_{NL} + \underline{K}_\sigma$$

as explained in Chapter 4 .

2- The modified Newton-Raphson technique; where the stiffness matrix will be:

$$\underline{K}_T = \underline{K}_L$$

3- The developed Newton-Raphson technique; where the stiffness matrix will be:

$$\underline{K}_T = \underline{K}_L + \underline{K}_\sigma$$

Schematic flow chart for the above iterative solutions are given in Figure (7.8) for each of these approaches.

c) Viscoelastic Analysis:

The present package contains a facility for viscoelastic analysis based on the theory explained in Chapter 5. The modified Newton-Raphson technique is used for the iteration procedure as shown in Figure (7.9).

7.3.5 Dynamic Analysis:

A linear or nonlinear dynamic analysis can be carried out for calculating the required eigenvalues, and the corresponding natural mode shapes, using the equation:

$$\underline{K} - \lambda \underline{M} = 0$$

This equation can be solved with the aid of any of the solvers explained in Section (6.3), which include:

a) The simple iteration technique.

b) The dynamic condensation technique.

c) The subspace iteration technique.

d) The double economiser technique.

The steps of the above solvers are shown in Figures (7.10 , 7.11 and 7.12) for the simple iteration, dynamic condensation and subspace iteration respectively.

7.4 POSTPROCESSING MODULES:

With regard to the output results, the nodal displacements, the reaction, and the stresses and strains are all calculated for the static and viscoelastic analysis. the eigenvalues and the natural mode shapes are calculated for the dynamic analysis. The output results can be presented in any of the following forms:

a) Tabulated Form:

In which the output can be given in tables.

b) Graphical Form:

Useful graphics can be produced as follows:

i) After mesh generation, it is worthwhile plotting the mesh before any finite element analysis is carried out, in order to check nodal coordinate locations, and the aspect ratio of the elements which may affect the accuracy of the results.

ii) Plotting the deformed shape of the structure.

iii) Displaying the stress distribution or principal stress

vectors. Such plots indicate to the engineer the areas where a close examination of the stresses may be necessary.

The basic output modules can be summarised as follows:

7.4.1 Reaction Module:

The reaction at the fixed nodes can be calculated using the equations:

$$\underline{K}_{pu} \ \underline{\delta}_u + \underline{K}_{pp} \ \underline{\delta}_p = \underline{F}_p$$

as explained in Section (7.3.3).

7.4.2 Stress and Strain Module:

Once the nodal displacements have been found, the incremental values of the stress and strain can be determined at any point (either at the quadrature points or the nodal points) in the tyre, using the equations explained in Section (3.5).

Since the six components of stress and strain are defined, other forms of stress and strain can be obtained as follows:

a) Principal Stress/Strain Module:

For a set of six components of stress ($\underline{\sigma}$), the corresponding principal stress components (σ_1 , σ_2 , σ_3) and their direction cosines can be calculated as follows:

The equation :

$$\begin{vmatrix} \sigma_{xx} - \sigma_p & \sigma_{xy} & \sigma_{xz} \\ \sigma_{yx} & \sigma_{yy} - \sigma_p & \sigma_{yz} \\ \sigma_{zx} & \sigma_{zy} & \sigma_{zz} - \sigma_p \end{vmatrix} = 0$$

represents a cubic equation in $\underline{\sigma}_p$, and from its solution, the principal stress values can be determined where:

$$\sigma_1 \geq \sigma_2 \geq \sigma_3$$

The maximum shear is defined as :

$$\tau_{max.} = (\sigma_1 - \sigma_3)/2$$

Having determined the three principal stress values, a complete solution of the problem generally requires the determination of the directions in which the principal stresses act. These directions can be determined by the direction cosines of the normals as follows:

If the direction cosines for $\underline{\sigma}_p$ are l_p , m_p , n_p ; then:

$$(\sigma_{xx} - \sigma_p) l_p + \tau_{xy} m_p + \tau_{xz} n_p = 0$$

$$\tau_{xy} l_p + (\sigma_{yy} - \sigma_p) m_p + \tau_{yz} n_p = 0$$

$$\tau_{xz} l_p + \tau_{yz} m_p + (\sigma_{zz} - \sigma_p) n_p = 0$$

the above equations can be written in the following form:

$$\begin{bmatrix} \sigma_{xx} - \sigma_p & \tau_{xy} & \tau_{xz} \\ \tau_{xy} & \sigma_{yy} - \sigma_p & \tau_{yz} \\ \tau_{xz} & \tau_{yz} & \sigma_{zz} - \sigma_p \end{bmatrix} \begin{bmatrix} l_p \\ m_p \\ n_p \end{bmatrix} = 0$$

the cofactors of the determination of the above matrix will be:

$$a = \begin{bmatrix} \sigma_{yy} - \sigma_p & \tau_{yz} \\ \tau_{yz} & \sigma_{zz} - \sigma_p \end{bmatrix}$$

$$b = \begin{bmatrix} \tau_{xy} & \tau_{yz} \\ \tau_{xz} & \sigma_{zz} - \sigma_p \end{bmatrix}$$

$$c = \begin{bmatrix} \tau_{xy} & \sigma_{yy} - \sigma_p \\ \tau_{xz} & \tau_{yz} \end{bmatrix}$$

and the direction cosines will be given by:

$$l = a\,k \quad , \; m = b\,k \quad , \; n = c\,k$$

where:

$$k = 1/\sqrt{a^2 + b^2 + c^2}$$

For the principal strains, the same steps can be followed.

b) Cord Load Module:

The load in a single cord can be derived by considering the stress acting in the direction of the cord in each reinforced layer.

Applying the transformation equation:

$$\underline{\sigma}' = \underline{R}\,\underline{\sigma} \quad ,$$

where $\underline{R}$ is the transformation matrix given in Chapter 3.

The load $\underline{P}_c$ in a single cord of area A_c is: $\underline{P}_c = A_c\,\underline{\sigma}'$

CHAPTER 8

RESULTS AND DISCUSSION

CHAPTER 8

RESULTS AND DISCUSSION

8.1 PACKAGE VERIFICATION:

A necessary step to be taken before the present package is used for the analysis of radial tyres, is to verify the reliability and soundness of each part of the package. This verification has been carried out by comparing the results obtained from the present package with those obtained from analytical solutions and/or with those obtained from other finite element packages. Some of the various axisymmetric structural examples, so treated, are described below.

8.1.1 Static Analysis of An Isotropic Structure:

The static analysis of an isotropic pressurised cylinder, carried out with the aid of the the present package, is compared with an analytical solution using the following equations [59]:

$$\sigma_r = \frac{p_i}{\lambda^2 - 1}\left[\, 1 - \left(\frac{r_o}{r}\right)^2 \,\right]$$

$$\sigma_\vartheta = \frac{p_i}{\lambda^2 - 1}\left[\, 1 + \left(\frac{r_o}{r}\right)^2 \,\right]$$

$$u_r = \frac{r p_i}{E(\lambda^2 - 1)}\left[\, (1 - \nu) + (1 + \nu)\left(\frac{r_o}{r}\right)^2 \,\right]$$

with the following hypothetical material properties:

Young's modulus (E) = 1×10^4 Kgf / mm^2

Poissons's ratio υ = 0.3

r_o = 50 mm

r_i = 2 0 mm

$\lambda = r_0 / r_i$

and with internal pressure (P_i) = 10 Kgf / mm2

The initial, as well as the deformed shape, of the cylinder are shown in Figure (8.1).

The results of the analytical solution and those obtained from the package are given in Table (8.1).

It is clear that the results obtained with the aid of the package correlate well with the analytical solution and that the difference between them is within an accepted tolerance.

8.1.2 Static Analysis of a Composite Structure:

The static analysis of a composite pressurised cylinder, as shown in Figure (8.2), has been carried out. The outer layer of the cylinder is made of a compressible metal with the following material properties:

Young's modulus (E) = 1×10^4 Kgf / mm^2

Poisson's ratio = 0.3

Whilst the inner layer is mΔade of rubber with the following material properties:

Young's modulus (E) = 0.8 Kgf / mm^2

Poisson's ratio = 0.4995

Rubber thickness = 15 mm

Mooney-Rivlin constants:

C_{10} = 0.10667 Kgf / mm^2

C_{01} = 0.02666 Kgf / mm^2

With internal pressure (P_i) = 0.1 Kgf / mm^2

Outer diameter = 100 mm

The results obtained with the aid of the present package were compared with the results obtained from the finite element package MARC and which are shown in Table (8.2). The deformed shape for the composite cylinder is shown in Figure (8.2).

The MARC package has three different approaches for the analysis of a structure constructed from an incompressible material, and it is clear from Table (8.2), that the results obtained from the present package are close to the most accurate results (those obtained from the Mooney-Rivlin approach) from the MARC package.

8.1.3 Dynamic Analysis:

The natural frequency and natural mode shapes of a vibrating isotropic cylinder were calculated and compared with the corresponding results obtained from avaliable codes; PAFEC and ABSEA.

The natural frequencies are listed in Table (8.3), while the mode shapes are shown in Figures (8.3 - 8.7).

For all of the calculated modes of vibration, the results of our package were nearly identical with those obtained by both of the other packages.

8.2 THE CASE STUDY OF THE RADIAL TYRE:

a) Tyre Specification:

A 175 HR 14 radial tyre with two steel belt breakers (1,2), and one Nylon breaker was employed as a case study. The following types of analysis have been carried out:

i) The deformed shape for the inflated and externally loaded tyre.

ii) The stresses and strains for the different cases of loading.

iii) The cord loads.

iv) The viscoelastic effect.

v) The natural frequency and the corresponding natural mode shape.

Most of the material properties used in this analysis, as well as the tyre design, were kindly made available by DUNLOP. The data not available from DUNLOP were taken from earlier References [20,27].

The tyre structure is shown in Figure (8.8), while the material properties are given in Table (8.4).

b) Experimental Work:

An experimental investigation was carried out, using the test rig shown in Figure (8.9), in order to measure the initial and inflated shape of the 175 HR 14 radial tyre.

The basic component of the test rig are:

1- 175 HR 14 radial tyre.

2- D.C. displacement transducer.

3- Amplifier.

4- D.C. power supply.

5- Voltmeter.

Two displacement transducers of type D2/500A were used to measure the deformation in the radial and axial directions. An amplifier was used with the transducers as their signals were not strong enough to be measured by the voltmeter.

It was necessary to calibrate both the displacement transducers and the voltmeter before carrying out tests. The calibration procedure and the instrumentation specifications are given in Appendix (I).

The results of the initial and inflated shape will be shown in Figure (8.14).

c) Numerical Work:

Before using the package, the orthotropic constants of the reinforced laminate were calculated manually according to the analysis given in Section (3.3.2). The elastic properties of the rubber were given by the well-known Mooney-Rivlin equation as explained in Section (3.3.4). The Poisson's ratio was taken as 0.499

The following boundary conditions and assumptions were employed:

In the equatorial plane, displacements in the axial direction are zero.

Displacements of the tyre surface in the region of the rim are zero in all directions.

For the static analysis, it was assumed that the external load was uniformly distributed in the region of the area of contact and the Fourier series expansion was used.

The external load was transformed into a uniform pressure distribution (P), using the following equation:

$$P = F / A$$

where;

F is the external radial load.
A is the area of contact shown in Figure (8.10).

The axisymmetric-solid-of-revolution element derived in Chapters (3,4), for the static analysis, and in Chapter 6 , for the dynamic analysis, was employed.

The structure of the tyre was discretised into 75 blocks as shown in Figures 8.11(a,b) , and using the package automatic mesh generator these blocks were discretised into 648 four-noded elements connected by 738 nodes as shown in Figure (8.12).

8.3 STATIC ANALYSIS OF THE TYRE:

8.3.1 Tyre Deformed Shape:

The deformed shape was calculated and plotted for the inflated tyre with inflation pressure = 2.0 bar, as shown in Figure (8.13), while a comparison with the shape obtained from the test rig results is shown in Figure (8.14). From this figure, it can be seen that the calculated deflected shape is quite close to that obtained experimentally.

The deformed shape for an externally loaded tyre with radial load of 500 Kgf as well as an inflation pressure of 2.0 bar is shown in Figure 8.15 (a), and the displacement along the circumferential direction is given in Figure 8.15(b).

The finite element model of the tyre was subjected to a total of 30 different loading conditions. The external load was chosen to be 100, 200, 300, 400 and 500 Kgf, each with a range of inflation pressures of 1.2, 1.4, 1.6, 1.8, 2.0 and 2.2 bar.

A comparison between the deformed shape calculated with the aid of the present package and the measured load-deflection curves given by DUNLOP, is shown in Figure (8.16). It is clear from the curves illustrated in Figure (8.16) for the previous 30 cases, that a good agreement between the calculated and measured results has been achieved.

8.3.2 Stresses and Strains:

Having obtained the six components of stress and strain at each quadrature point, using the equations given in Chapter 3 , the following results were found:

a) Principal Stresses:

The principal stresses and their direction cosines, were calculated following the analysis given in Section (7.4.3), and plotted in the vector form shown in Figures (8.17 - 8.20) for inflated tyre and and Figures (8.21 - 8.24) for externally loaded tyres. From these figures, it can be seen that there are two positions of stress concentration; one of them is in the belt edge area, which is the least durable portion, because of fatigue loading, and it must be carefully considered by the designers. The other stress concentration is in a position near to the bead, which may be due to the bending around the rim or possibly due to a numerical instability resulting from the big difference in material properties of the bead and the adjacent layers.

The principal stresses were also plotted for the casing ply, breakers 1, 2 and 3 as shown in Figures 8.25(a,b) - 8.28(a,b), in which Figures (a) are assigned to the inflated tyre results, while Figures (b) are for externally loaded tyre results. These figures show that the maximum principal stresses are near the belt edge for the breakers and that there are two peaks of stress concentration near to the belt edge and the side wall for the casing ply.

b) Principal Strains:

The principal strains and the maximum shear strain were also calculated following the same procedure explained in Section(7.4.3)

These strains were plotted for the breakers and the casing ply as shown in Figures 8.29(a,b) - 8.32(a,b) for the casing ply and breakers 1,2,3 respectively.

It can be seen from these figures that the maximum strains occur at the belt edge for the breakers. This strain concentration at the belt edge might cause separation of the cord-rubber interface.

For the casing ply, the maximum strain occurs at the side wall. This strain is responsible for approximatly 60 - 70 % of the heat generation in the radial tyre, as explained by Reference [41], and govern the number of cycles required to produce fatigue failure of rubber.

8.3.3 Cord Load:

The six stress components of each layer were computed relative to the principal axes of geometry of the tyre. These stresses were rotated using the equation:

$$\underline{\sigma}' = \underline{R}\,\underline{\sigma}$$

to obtain the stress components ($\underline{\sigma}$) with respect to the axes of the laminate. The rotated stress components are shown in Figures 8.33(a,b) - 8.36(a,b), where σ_z' represents the stress component in the cord direction. Figures (a,b) represent the stress components for the inflated and externally loaded tyres respectively.

The average stress of the cord can be calculated from Equation[20]:

$$\sigma_c = \sigma_z' V_c$$

where, V_c is the volume fraction of the cord.

Since the value of σ_z can be obtained from the above figures, the average stress in the cord can be estimated.

8.4 VISCOELASTIC ANALYSIS OF THE TYRE:

The viscoelastic effect, based on the relaxation approach explained in chapter 5 , has been determined. The static analysis with viscoelastic effect has been carried out using a damping coofficient = 0.2, and inflation pressure of 2.0 bar.

8.4.1 Tyre Deformed Shape:

The deformed shape for the inflated tyre is shown in Figure (8.37). The given deformation is higher by about 69% in some areas than that illustrated in Figure (8.13). This increase in the deformation is due to the viscoelastic effect of the rubber. The rubber will relax in time if the pressure is kept constant, as explained in Chapter 5.

8.4.2 Principal Stresses:

Following the same procedure given in Section (8.3.2), the principal stresses are calculated and plotted. Some samples of these results are illustrated in Figures 8.38 , 8.39 , in which the principal stress distribution for casing ply and breaker 1 are demonstrated.

From these figures, it can be deduced that these principal stresses are lower than those obtained for the elastic material although they have a more or less similar general distribution. The decrease of viscoelastic stresses is , of course, due to the relaxation of the rubber.

8.4.2 Principal Strains:

The principal strains were calculatd and some samples of the

results for the casing ply and breaker 1 are shown in Figures 8.40 , 8.41 respectively.

It can also be seen that the maximum strains are at the belt edge for breaker 1 and at the side wall for the casing ply. This result is similar to that observed for the elastic analysis.

However, due to the relaxation of the rubber, the resulting strains were higher than those evaluated for an elastic material, as mentioned before.

This increase in the strain will cause an increase in the generated heat, an increase in the hysteresis losses and a decrease in the transmitted power.

8.5 DYNAMIC ANALYSIS OF THE TYRE;

The modes of vibration for the tyre 175 HR 14 were obtained using the analysis given in Chapter 6. The finite element model was the same as that used for the static analysis.

The first twenty natural frequencies of the tyre are listed in ascending order in Table (8.5). The vibration mode shapes for the first five natural frequencies are represented graphically in Figures 8.42 - 8.46 .

Since the natural frequencies and mode shapes are defined, the tyre response to an arbitrary road vibration or to an arbitrary road profile, can be obtained as explained in Reference [33]. Having this information the tyre manufacturer can take steps to modify this response in order to improve vehicle ride and handling characteristics.

8.6 GENERAL DISCUSSION:

The accuracy of a finite element solution is a function of many parameters, for example:

Grid size or number of elements in the mesh.

Element type: triangular or quadrilateral.

Element order or number of element nodes.

Quadrature order or number of quadrature points.

Measured or known properties of the material; such as Young's modulus, shear modulus,Poisson's ratio, mass density and damping coefficient.

Effective non-linear modelling or iterative schemes, etc.

Analysis of a complex structure, such as a radial tyre, using one fixed set of parameters is not recommended. The investigator should test a reasonable number of sets of parameters until convergence of the results has been achieved.

The present package contains its own mesh generator which has proved to be a useful tool for modifying the generated mesh and one which allows the user to employ different meshes with a minimum amount of data and effort. The package mesh plotter can provide a facility for an immediate check of the generated mesh which minimises the human effort and errors.

Although the optimum number of Gauss quadrature points for each type of element has been published [58], and used successfully in linear analysis, it has been proved, during the course of this work, that nonlinear analysis does not usually obey such rules. When using 4-noded quadrilateral elements with 3 quadrature points for nonlinear

analysis of radial tyres, the results were worse than those obtained with 2 quadrature points !. The optimum number of quadrature points for such a case has been proved in this work to be 4.

Package economisers have been tried and shown to be indispensable. When attempting to carry out the dynamic analysis for a complete radial tyre, using the accurate finite element mesh, it was brought to our attention by the C.I.T. Computer-Centre Staff, that there was no computer available in the U.K. which could accept such large matrices and run the ordinary eigenvalue solver. Without the frontal solver developed specifically for this type of structure (with asymmetric matrices), the problem could not have been solved at the present time. The surprising fact is that not only does the frontal solver reduce the direct access memory drastically, but it also reduces the CPU time by an enormous amount particularly for computers such as the VAX, which have virtual memory and a pagination system, as the one used for this analysis.

For the case of an externally loaded tyre, it was observed that when the inflation pressure was 1.2 bar, the finite element analysis required 6 harmonics, in order to yield results close to those obtained experimentally. However, when the inflation pressure was increasd to 2.2 bars, the number of harmonics required for an accurate finite element solution reduced to 4, i.e. a lower number of harmonics is required for a higher loading. In general, the previous order of harmonics matches those (from 3 to 6) recommended in the literature for an economical Fourier series analysis as compared with a fully 3-dimensional analysis.

It should perhaps be pointed out at this stage, that the results obtained with the aid of the present package for the 175 HR 14 radial tyre were based upon some simplifications and assumptions, which can be summarised as follows:

The moulding stress has been neglected.

Some of the material properties were unavailable and their values have been taken from previous literature.

It was assumed that, there is no viscous effect on Poisson's ratio.

The thermo-viscoelastic effect on the static and dynamic analysis has been neglected.

Centrifugal stiffening was not considered.

The lack of material properties appears to be general in the field of pneumatic tyres. This package would certainly be capable of accepting more realistic values if, and when, they are available.

CHAPTER 9

CONCLUSIONS

CHAPTER 9

CONCLUSIONS

The major objective of designing a versatile finite element package, which is tailored for the static and dynamic analysis of radial tyres, and with facilities not available in most commercial packages, has been achieved.

A generalised axisymmetric-solid-of-revolution element has been developed and used in the present static and dynamic analysis of radial tyres. With the aid of this new element it is possible to consider the effects of large deformation, the influence of composite orthotropic materials, and the viscoelasticity and the nonlinearity of the material properties. The present finite element package has proved to be capable of evaluating the deformation, stresses, strains, cord loads and natural frequencies of radial tyres using such a sophisticated element.

The orthotropic material properties have been derived, for composite laminate structures, in three-dimensional space so as to be applicable for a generalised axisymmetric-solid-of-revolution element. Using such an element, it also becomes possible to include the transverse shear due to the inclination of the reinforced layers.

A feasible method for carrying out time-dependent analysis, where the viscoelastc effect is expressed in the hereditary integral form, has been successfully attempted. This analysis is based upon the relaxation phenomenon using an interpolative scheme.

It has been proved that the semi-analytical, finite element non-linear algorithms (using a Fourier expansion) developed in this work, can produce accurate answers with a reasonable number of harmonics resulting in a considerable computer economy when compared with the fully three-dimensional analysis.

The developed Newton-Raphson scheme derived in this work, has proved to be more stable than the standard Newton-Raphson iteration scheme, and to produce more rapid convergence than the modified Newton-Raphson scheme.

Other conclusions related to the characteristics and merits of the package can be summarised as follows:

Reliability and accuracy of the package have been confirmed through the painstaking comparison of results obtained with its aid with available analytical and/or experimental results.

Package economisers have proved to be indispensable for the static and dynamic analysis of radial tyres using an accurate mesh and with the generalised, axisymmetric-solid-of-revolution element produced in this study.

Different solvers and interpolative, iterative, and increment schemes included in the package should help the user to overcome numerical instability problems encountered with a sspecific algorithm, and make the package very flexible.

Since different finite element meshes should be employed in order to confirm the convergence of results, the package's own mesh generator will provide the user with an efficient facility for so doing, with the generation of less data and with minimum effort.

The extensive error diagnostic facility of the package has proved to be helpful when modelling a complex structure.

Control parameters in the data modules proved to be an efficient facility for the selection of the relevant type of solver, nonlinear scheme, type of analysis, type of results, etc. and economises the computer resources.

The package post-processor, while being relatively simple, can

provide the designer with many useful plots by which he or she could, for example, immediately find the stess-strain concentration zones within the tyre and consequently allow him to improve the design of the tyre by suitable modification.

RECOMMENDATIONS FOR FUTURE WORK:

This work can be extended to investigate the following:

1- Steady state and transient response under general loading condition [loading - traction - braking force and road roughness].

2- The viscoelastic effect on the natural frequency and mode shapes.

3- The thermoviscoelastic effect on the static and dynamic analysis.

4- The camber angle effect on the dynamic response.

5- The effect of centrifugal stiffening.

6- General contour plotting.

REFERENCES

REFERENCES

1. RICHARD, N. and DODGE — The Dynamic Stiffness of A Pneumatic Tyre Model. SAE Paper 650491.

2. TIELKING, J. T. — Plane Vibration Characteristics of A Pneumatic Tyre model. SAE Paper 650492.

3. PACEJKA, H. B. — Tyre Factors and Front Wheel Vibrations. Int. J. of Vehicle Design, Vol. 1 No. 2, 1982.

4. KAPTAIN, K. M., BOGHANI, A. B. and WORMLEY, D. N. — Analytical Tyre Models for Dynamic Vehicle Simulation. Vehicle System Dynamics. Vol. 8, 1979, pp 1 - 32.

5. SCHURING, D. J., TAPIA, G. A. and GUSAKOV, I. — Influence of Tyre Design Parameters on Tyre Force and Moment Characteristics. SAE Paper 760732.

6. PACEJKA, H.B. — The Wheel Shimmy Phenomenon. PH.D. Thesis Delft University of Technology.1966

7. PACEJKA, H. B. — Analysis of The Dynamic Response of A Rolling String Type Tyre Model to Lateral Wheel-Plane Vibrations. Vehicle System Dynamics. V. 1, 1972

8. GORAJ, Z. J. — Selfexcited vibrations of The Tyre. Vehicle System Dynamics. V. 11, 1982

9. HOOKER, R. J. — A Model for The Radical Dynamic Behaviour of Pneumatic Tyres. Int. J. of Vehicle Design. V. 1, N. 4, 1980, pp 361 - 372.

10. CLARK, S. K. — Measuring Tyre Carcass Elastic Characteristics. SAE 667C.

11. POTTS,G.R.,CHAREK,L.T. BELL,C.A.,and ROY,T.K. — Vibrations of a Radial Tyre-Analytical Model and Experimental Results. ASTM Symposium on Tyre Noise and Vibration, Cleveland, Ohio, May,1977.

12. LAUTERBACH, H. G. and AMES, W. F. — Cord Stresses in Inflated Tyres. Textile Research International, Vol. 35, pp 890 - 900.

13. MILLER, C., POPPER,P., GILMOUR, P. W. and SCHAFFERS, W. J. — Textile Mechanics Model of A Pneumatic Tyre. Tyre Science and Technology, v. 13, N. 4, 1985 pp 187

14. PATEL, H. P. and ZOROWSKI, C. F. — Deformation of The Pneumatic Tyre. Tyre Science and Technology, V. 6, N. 4, 1978, pp 233 - 247.

15. ZOROWSKI, C. F., DUNN, S. E. and SHAH, N. M. — The influence of Geometric and Cord-Load Design Parameters on The Profile Shape and Cord Tensions in Inflated Pneumatic Tyres. Textile Research International. V. 41, 1971. pp 501 - 509.

16. DeESKINAZI, J. and REDHA — Finite Element Analysis of Giant Earth-mover Tyres. Rubber Chemistry and Technology. V. 55, 1982, pp 1044 - 1054.

17. WATANABE, Y. and KALDJIAN, M. — Modeling and Analysis of Bias-Ply Motor-cycle Tyres. Computers & Structures, V. 17, N. 5-6, 1983, pp 653 - 658.

18. WATANABE, Y. — A Finite Element Model for Analysis of Deformations of Bias-Ply Motorcycle Tyres

Subjected to Inflation Pressure. Vehicle System Dynamics. V. 13, 1984, pp 113 .

19. REDHA, R. A. — Computation of Stresses, Strains and Deformations of Tyres. Rubber Chemistry and Technology. V. 53, N. 4, 1980.

20. KAGA, OKAMOTO, K. and TOZAWA, Y. — Stress Analysis of A Tyre Under Vertical Load by A Finite Element Method. Tyre Science and Technology. V. 5, N. 2, 1977.

21. TRINKO, M. J. — Ply and Rubber Stresses and Contact Forces for A Loaded Radial Tyre. Tyre Science and Technology. V. 11, N. 1-4, 1984, pp 20-38

22. CLARK,S.K. — Mechanics of Pneumatic Tyres. National Bareau of Standard Monographes.(122)1971.

23. FRATER, J. LESTING, J. and PADOVAN, J. — Complex Stiffness Formulation for The Δ Finite Element Analysis of Anisotropic Axisymmetric Solids Subjected to Non-symmetric Loads. Tyre Science and Technology. V. 11, 1983, pp 20 - 37.

24. JONES, R. M. — Mechanics of Composite Materials McGraw-Hill , 1975.

25. CALCOTE, L. R. — The Analysis of Laminated Composite Structure. 1969.

26. TSAI, S. W. and HAHN, H. T. — Introduction to Composite Materials. Technomic, 1980.

27. WALTER, J. D. , AVGEOPOULOS, G. N. and JANSSEN,M.L. — Advances in Tyre Composite Theory. Tyre Science and Technology. V. 1, N. 2, 1973, pp 210 - 250.

28. PATEL, H. P. , TURNER, J. L. and WALTER, J. D. — Radial Tyre Cord-Rubber Composites. Rubber Chemistry and Technology. V. 49, N. 4, 1976, pp 1095 - 1110.

29. BREWER, H. K. — Tyre Stress and Deformation from Composite Theory. Tyre Science and Technology. V. 1, N. 1, 1973, pp 47 - 76.

30. KUNG, L. E. and SOEDEL, W. — Free Vibration of A Pneumatic Tyre-Wheel Unit Using A Ring on An Elastic Foundation and A Finite Element Model. Journal of Sound and Vibration. 1986, 107 (2), 181 - 194.

31. BREWER, H. K. — Stresses and Deformation in Multi-Ply Aircraft Tyres Subjected to Inflation Pressure Loading. AFFDL-TR-70-62 , 1970.

32. PADOVAN, J. — Traveling Waves Vibrations and Buckling of Rotating Anisotropic Shells of Revolution by Finite Elements. Int. J. Solid Structures. V.11, 1975, pp 1376-1380

33. SOEDEL, W. — On The Dynamic Response of Rolling Tyres According to Thin Shell Approximations. J. of Sound and Vibration. V. 41 (2),1975.

34. CHANG, Y. B., YANG, T. Y. and SOEDAL — Dynamic Analysis of A Radial Tyre by Finite Elements and Modal Expansion. J. of Sound and Vibration. 69 (1), 1984.

35. CHANG, Y. B. YANG, T. Y. and SOEDAL — Linear Dynamic Analysis of Revolutional Shells Using Finite Elements and Modal Expansion. J. of Sound and Vibration. 86 (4), 1983, pp 523 - 538.

36. HUNCKLER, C. J. — The Dynamic Behaviour of An Automobile Tyre. Ph. D. Thesis, Purdue University, 1979.

37. HUNCKLER, C. J., YANG, T. Y. and SOEDEL. — A Geometrically Nonlinear Shell Finite Element for Tyre Vibration Analysis. Computers & Structures. V. 17, N. 2, 1983, pp 217 - 225.

38. PADOVAN, J. — On Viscoelasticity and Standing Waves in Tyres. Tyre Science and Technology. V. 4, N. 4, 1976, pp 233 - 246.

39. POTTS, G. R. — The Application of Holography to The Visualization of Tyre Vibrations. Paper Presented at SESA Meeting, Cleveland, Ohaio, 1972.

40. PADOVAN, J. — On Standing Waves in Tyres. Tyre Science and Technology. V. 5, N. 2, 1977, p 498.

41. JANSSEN, M. L. and WALTER, J. D. — Stresses and Strains in Tyres. Tyre Science and Technology. V. 3, N. 2, 1975.

42. KNOWN, Y. D. and PREVORSEK, D. C. — Formation of Standing Waves in Radial Tyres. Tyre Science and Technology. V. 12, N. 1-4, 1984, pp 44-63.

43. TABADDOR, F. , CLARK, S. K. , DODGE, R. N. and PERRAUT, J. M. — Viscoelastic Loss Characteristics of Cord-Rubber Composites. Tyre Science and Technology. V. 14, N. 2, 1986, pp 75-101.

44. WALTER, J. D. and CONANT, F. S. — Energy Losses in Tyres. Tyre Science and Technology. V. 2, N. 4, 1974, pp 2355-260.

45. AMES, W. F. — Waves in Tyres. Textile Research Journal V. 14, N. 6, 1970, pp 498- 507.

46. FLUGGE, W. — Viscoelasticity. Second Edition. 1975, Springer-Verlag.

47. CRISTESCU, N. and SULICIA, I. — Viscoelasticity. 1982 Martinus Nijhoff Publishers.

48. FERRY, J. D. — Viscoelastic Properties of Polymers. John-Willey. Sons Third Edition, 1982.

49. LEE, H. E., RADOK,J.R. and WOODWARD, W. B. — Stress Analysis for Linear Viscoelastic Materials. Transactions of The Society of Rheology III, 1959, 41-59.

50. BOOKER, J. R. and SMALL, J. C. — An Investigation of The Stability of Numerical Solutions of The Equations of Viscoelasticity. Int. J. for Num. Meth. in Eng. V.11, 1977, pp 1819-1830.

51. ADEY, R. A. and BREBBIA, C. A. — Efficient Method for Solution of Viscoelastic Problems. Journal of Eng. Mech. Division. V.99, 1973.

52. ZIENKIEWICZ, O. C., WATSON, M. and KING,I. — A Numerical Method of Viscoelastic Stress Analysis. Int. J. Mech. Sci. V. 10, 1965.

53. HENRIKSEN, M. — Nonlinear Viscoelastic Stress Analysis- A Finite Element Analysis Approach. Computer & Structures V.18, N. 1, 1984.

54. ZIENKIEWICZ, O. C., and Lohner — Accelerated Relaxation or Direct Solution? Future Prospects for FEM. Int. J. for Num. Meth. in Eng. V. 21, 1-11, 1985.

55. TURNER, M. J., COLOUGH, R. W. J. Aeronaut. Sci. 23, 805,1956.
MARTIN, H. C. and TOPP,I.J.

56. HRENNIKOFF, A. J. Appl. Mech. ASME, 1941, pp 160-175

57. COOK, R.D. Concepts and Application of Finite Element Analysis. Second Edition. John Willey & Sons. 1981.

58. ZIENKIEWICZ,O.C. The Finite Element Method. Third Edition McGraw-Hill Book Comppany, 1983.

59. EL-ZAFRANY, A. An Advanced Finite Element System for Engineering Analysis. Ph.D. Thesis, 1983.

60. RIDHA, R.A. Computation of Stresses, Strains and Deformation of Tyres. Rubber Chemistry and Technology. V. 53, N. 4, 1980.

61. ZOROWSKI, C.E. , and DUNN, S. E. A Mathematical Model for The Pneumatic Tyre . North Carolina State University. Raleigh June, 1970.

62. JAMES, A. G., GREEN,A. and SIMPSON,G.M. Strain Energy Functions of Rubber.I. Characterisation of Gum Vulcanizates. Journal of Applied Polymer Science V. 19, 1975, pp 2033-2058.

63. TAKAMATSU,T. , STRICKLIN, J.A. and KEY,J. Symmetric Stiffness Matrix for Incompressible Hyperelastic Materials. AIAA Journal V. 14, N. 3, pp 414-416.

64. PIAN, T.H. and LEE,S.W. Notes on Finite Elements for Nearly Incompressible Materials. AIAA Journal, V. 14, N. 6, 1976, pp 824-826.

65. JANKOVICH,E. , LEBLANC,F. and DURAND, M. — A Finite Element Method for The Analysis of Rubber Parts, Experimental and Analytical Assessment. Computers & Structures V. 14, N.5-6, 1981, pp 385-391.

66. ZIENKIEWICZ,O.C. and PHILIPS, D.V. — An Automatic Mesh Generation Scheme for Plane and Curved Surfaces by Isoparameric Coordinates. Int. J. Math. Eng. V. 3, 1971

67. IRONS, B. M. — A Frontal Solution Program. Int. J. Num. Meth. Eng. V. 2, 1970, pp 5-32.

68. EL-ZAFRANY,A. and COOKSON, R. A. — ABSEA Finite Element System. Presented at the Mechanical Engineering Conference MTC, EGYPT, May, 1984.

70. HEARN, E. J. — Mechanics of Materials. Second Edition. Pergamon Press. 1985.

71. BARSON, C. W., OSBORNE, D. J. and STANOJEVIC, M. — Relationship Between Rivlin Constants and Classical Elastic Constants. Report No. TD 1294. May, 1982.

72. TAVAZZA, G. and REMONDI, G. — Stress and Strain Calculation of Rubber International Rubber Conference. Kieve, 1978.

73. BERCOVIER, M. and LIUNE, E. — A 4CST Quadrilateral Element for Incompressible Materials and Nearly Incompressible Materials. CALCOLD. V. 14, 1979, pp 1-15.

74. WOOD, R. D. and ZIENKIEWICZ, O. C. — Geometrically Nonlinear Finite Element of Beams, Frames, Arches and Axisymmetric Shells. Computers & Structures. V. 7, 1977, pp 725-735.

75. FREDERICK, C. O., EDGE, F. W. and WONG, Y. C. — Two Dimensional Automatic Mesh Generation for Structural Analysis. Int. J. Num. Eng. V. 2 , 1970 pp 133 - 144.

76. SADEK, E. A. — A Scheme for the Automatic Generation of Triangular Finite Elements. Int. Num. Meth. Eng. V. 15 1980. pp 1813-1822

77. IMAFUKU, I. , KODERA, Y. and SAYAWAKI,M. — A Generalized Automatic Mesh Generation Scheme for Finite Element Method. Int. J. Num. Meth. Eng., V. 15 1980, pp 713-731.

TABLES

16,1 GAUSSIAN QUADRATURE PARAMETERS

1	1
1.000000000000000	0.500000000000000

2	2
0.500000000000000	0.211324865405187
0.500000000000000	0.788675134594813

3	3
0.277777777777780	0.112701665379258
0.444444444444445	0.500000000000000
0.277777777777780	0.887298334620742

4	4
0.173927422568727	6.943184420297349E-02
0.326072577431273	0.330009478207572
0.326072577431273	0.669990521792428
0.173927422568727	0.930568155797026

5	5
0.118463442528094	4.691007703066799E-02
0.239314335249683	0.230765344947158
0.284444444444445	0.500000000000000
0.239314335249683	0.769234655052841
0.118463442528094	0.953089922969332

6	6
8.566224618958500E-02	3.376524289842403E-02
0.180380786524069	0.169395306766867
0.233956967286345	0.380690406958402
0.233956967286345	0.619309593041598
0.180380786524069	0.830604693233132
8.566224618958500E-02	0.966234757101576

7	7
6.474248308443500E-02	2.544604382862050E-02
0.139852695744639	0.129234407200303
0.190915025252559	0.297077424311302
0.208979591836734	0.500000000000000
0.190915025252559	0.702922575688698
0.139852695744639	0.870765592799697
6.474248308443500E-02	0.974553956171379

8	8
5.061426814518800E-02	1.985507175123200E-02
0.111190517226687	0.101666761293186
0.156853322938943	0.237233795041835
0.181341891689181	0.408282678752175
0.181341891689181	0.591717321247825
0.156853322938943	0.762766204958164

CON'D

0.1111905172266870	0.8983332387068135
5.0614268145188000E-02	0.9801449282487680

9	9
4.0637194180787000E-02	1.5919880246186999E-02
9.0324080347428500E-02	8.1984446336681997E-02
0.1303053482014675	0.1933142836497050
0.1561735385200015	0.3378732882980955
0.1651196775006300	0.5000000000000000
0.1561735385200015	0.6621267117019045
0.1303053482014675	0.8066857163502950
9.0324080347428500E-02	0.9180155536633180
4.0637194180787000E-02	0.9840801197538130

10	10
3.3335672154344000E-02	1.3046735741414003E-02
7.4725674575290500E-02	6.7468316655507503E-02
0.1095431812579910	0.1602952158504880
0.1346333596549980	0.2833023029353765
0.1477621123573765	0.4255628305091845
0.1477621123573765	0.5744371694908155
0.1346333596549980	0.7166976970646235
0.1095431812579910	0.8397047841495120
7.4725674575290500E-02	0.9325316833444925
3.3335672154344000E-02	0.9869532642585860

11	11
2.7834283558087000E-02	1.0885670926971500E-02
6.2790184732452500E-02	5.6468700115952501E-02
9.3145105463866999E-02	0.1349239972129755
0.1165968822959950	0.2404519354446595
0.1314022722551235	0.3652284220238275
0.1364625433889505	0.5000000000000000
0.1314022722551235	0.6347715779761725
0.1165968822959950	0.7595480645553405
9.3145105463866999E-02	0.8650760027870245
6.2790184732452500E-02	0.9435312998840475
2.7834283558087000E-02	0.9891143290730285

12	12
2.3587668193256000E-02	9.2196828766405031E-03
5.3469662997659000E-02	4.7941371814762497E-02
8.0039164271673000E-02	0.1150486629028475
0.1015837133615330	0.2063410228566915
0.1167462682691775	0.3160842505409100
0.1245735229067015	0.4373332957442655
0.1245735229067015	0.5626667042557345
0.1167462682691775	0.6839157494590900
0.1015837133615330	0.7936589771433085
8.0039164271673000E-02	0.8849513370971525

CON'D

5.3469662997659000E-02	0.9520586281852375
2.3587668193256000E-02	0.9907803171233595

13	13
2.0242002382658000E-02	7.9084726407060019E-03
4.6060749918864000E-02	4.1200800388510997E-02
6.9436755109893500E-02	9.9210954633344998E-02
8.9072990380972999E-02	0.1788253302798300
0.1039080237684445	0.2757536244817765
0.1131415901314485	0.3847708420224325
0.1162757766154370	0.5000000000000000
0.1131415901314485	0.6152291579775675
0.1039080237684445	0.7242463755182235
8.9072990380972999E-02	0.8211746697201700
6.9436755109893500E-02	0.9007890453666550
4.6060749918864000E-02	0.9587991996114890
2.0242002382658000E-02	0.9920915273592940

14	14
1.7559730165876000E-02	6.8580956515940025E-03
4.0079043579880000E-02	3.5782558168212998E-02
6.0759285343951500E-02	8.6399342465117497E-02
7.8601583579097000E-02	0.1563535475941575
9.2769198738968999E-02	0.2423756818209230
0.1025992318606480	0.3404438155360550
0.1076319267315790	0.4459725256463280
0.1076319267315790	0.5540274743536720
0.1025992318606480	0.6595561844639450
9.2769198738968999E-02	0.7576243181790770
7.8601583579097000E-02	0.8436464524058425
6.0759285343951500E-02	0.9136006575348825
4.0079043579880000E-02	0.9642174418317870
1.7559730165876000E-02	0.9931419043484060

15	15
1.5376620998058500E-02	6.0037409897574986E-03
3.5183023744054000E-02	3.1363303799646997E-02
5.3579610233586000E-02	7.5896708294786501E-02
6.9785338963077001E-02	0.1377911343199150
8.3134602908497000E-02	0.2145139136957305
9.3080500007781000E-02	0.3029243264612185
9.9215742663555500E-02	0.3994029530012825
0.1012891209627805	0.5000000000000000
9.9215742663555500E-02	0.6005970469987175
9.3080500007781000E-02	0.6970756735387815
8.3134602908497000E-02	0.7854860863042695
6.9785338963077001E-02	0.8622088656800850
5.3579610233586000E-02	0.9241032917052135
3.5183023744054000E-02	0.9686366962003530

1.537662099805850E-02	0.993996259010242 5
16	16
1.357622970587700E-02	5.299532504175003E-03
3.112676196932400E-02	2.771248846338349E-02
4.757925584124650E-02	6.718439880608399E-02
6.231448562776700E-02	0.122297795822498 5
7.479799440828850E-02	0.191061877798678 0
8.457825969750150E-02	0.270991611171386 5
9.130170752246200E-02	0.359198224610370 5
9.472530522753449E-02	0.452493745081181 5
9.472530522753449E-02	0.547506254918818 5
9.130170752246200E-02	0.640801775389629 5
8.457825969750150E-02	0.729008388828613 5
7.479799440828850E-02	0.808938122201322 0
6.231448562776700E-02	0.877702204177501 5
4.757925584124650E-02	0.932815601193916 0
3.112676196932400E-02	0.972287511536616 5
1.357622970587700E-02	0.994700467495825 0

Table (7.1) GAUSSIAN QUADRATURE PARAMETERS

Node Numb.	Displacement (u)			Radial Stress (σ_r)			Tangential Stress (σ_θ)		
	Anal.	4-Node	8-Node	Anal.	4-Node	8-Node	Anal.	4-Node	8-Node
1	.380E-2	.372E-2	.380E-2	0.0	-1.18	0.2514	3.8	3.341	3.915
2	.447E-2	.437E-2	.446E-2	-1.98	-3.074	-1.139	5.79	5.154	6.142
3	.447E-2	.431E-2	.446E-2	-1.98	-1.155	-1.155	5.79	5.092	6.131
4	.380E-2	.365E-2	.380E-2	0.0	-1.304	-.22	3.8	3.195	3.895
5	.672E-2	.639E-2	.670E-2	-10.	-9.439	-7.421	13.8	13.55	14.87
6	.672E-2	.635E-2	.671E-2	-10.0	-9.46	-7.503	13.8	13.30	14.81
7	.447E-2	.409E-2	.445E-2	-1.98	-2.853	-1.109	-5.97	4.905	6.131
8	.380E-2	.350E-2	.380E-2	0.0	-1.151	.2368	3.8	3.075	3.897
9	.672E-2	.603E-2	.666E-2	-10.	-12.33	-7.392	13.8	13.35	14.69

Table (8.1) Comparison Between the Computed and Analytical Solution for Pressurised Cylinder.

Stress/Disp. Component	MARC			Present Package
	Mooney	Classical	Mooney-Rivlin	
σ_z	0.23783	0.23729	0.23792	0.23771
σ_r	0.067897	0.06775	0.067942	0.067991
σ_θ	0.38209	0.37324	0.38134	0.38254
τ_{rz}	0.10925	0.10896	0.10929	0.10955
u_z	2.0	2.5967	1.8072	1.822
u_r	1.3314	2.0624	1.2044	1.261

Table (8.2) Comparison of the Results Between the Package and the MARC Package for A Composite Pressurised Cylinder

Freq. No.	PAFEC	ABSEA	THE PRESENT PACKAGE
1	0.7511	0.75102	0.7512
2	1.170	0.170	0.169
3	1.444	1.444	1.444
4	2.663	2.662	2.662
5	2.968	2.968	2.968

Table (8.3) The Natural frequencies of A Cylinder

Component	K Kgf/mm2	C10	C01	C11	C20	C02
Tread	245.8	.0533	.00129	.00025	-.00248	.00036
Side Wall	254.4	.04252	.00284	-.000384	-.002288	.000403
Apex	315.5	.1324	.0155	-.0056	-.0315	.0108
Clinch Strip	As Apex	.....	.....	.....	.....	.....
Liner	137.8	.03726	.01539	-.002656	-.001043	.000637

Component	Cord Modulus	Ends/mm	Bias Angle
Casing Plies	119	1.12	88
Chafer	51	0.75	25
Breakers 1,2	394	0.8	+21
Breaker 3	46	1.0	0

The properties of the bead are defined by the constants D_{ij} in the equation:

$$\begin{bmatrix} D_{11} & D_{12} & D_{13} & 0 \\ D_{21} & D_{22} & D_{23} & 0 \\ D_{31} & D_{32} & D_{33} & 0 \\ 0 & 0 & 0 & D_{66} \end{bmatrix}$$

Where the axes shown in Sketch (8.1).

The D_{ij} constants (in Kgf/mm2), are defined in the following matrix:

$$\begin{bmatrix} 168.9 & 84.9 & 84.3 & 0 \\ 84.9 & 168.9 & 84.3 & 0 \\ 84.3 & 84.3 & 7648 & 0 \\ 0 & 0 & 0 & 44.8 \end{bmatrix}$$

Table (8.4) Material Properties of 175 HR 14 Radial Tyre

MODE	EIGENVALUE (rad./sec)**2	NATURAL FREQUENCY HZ
1	144.94	1.916
2	262.99	2.581
3	426.4902	3.2869
4	572.3285	3.807
5	894.2413	4.7594
6	1973.962	7.061
7	2644.431	8.18
8	3162.938	8.95
9	3686.060	9.66
10	4000.344	10.060
11	4231.578	10.35
12	4948.721	11.196
13	5111.634	11.379
14	6163.882	12.459
15	6455.897	12.802
16	7143.532	13.45
17	7877.157	14.1259
18	8762.090	14.898
19	9041.094	15.133
20	10475.52	16.2899

Table (8.5), The Eigenvalue and Natural Frequencies of The 175 HR 14 Radial Tyre

Node	N-R		M-N-R		D-N-R	
No	u	v	u	v	u	v
1	0.3327E-02	0.0000E+00	0.3353E-02	0.0000E+00	0.3326E-02	0.0000
2	0.3914E-02	0.0000E+00	0.3935E-02	0.0000E+00	0.3913E-02	0.0000
3	0.3875E-02	-0.3330E-03	0.3885E-02	-0.3186E-03	0.3875E-02	-0.3331
4	0.3275E-02	-0.1630E-03	0.3292E-02	-0.2031E-03	0.3275E-02	-0.1628
5	0.5739E-02	0.0000E+00	0.5764E-02	0.0000E+00	0.5739E-02	0.0000
6	0.5714E-02	-0.4908E-03	0.5728E-02	-0.4970E-03	0.5714E-02	-0.4907
7	0.3703E-02	-0.5872E-03	0.3699E-02	-0.5701E-03	0.3703E-02	-0.5874
8	0.3129E-02	-0.3222E-03	0.3159E-02	-0.4361E-03	0.3129E-02	-0.3220
9	0.5459E-02	-0.1063E-02	0.5452E-02	-0.1069E-02	0.5459E-02	-0.1062

Table(8.6) Radial(u) and Axial(v) Displacements of Pressurised Cylinder Using N-R, M-N-R and D-N-R

FIGURES

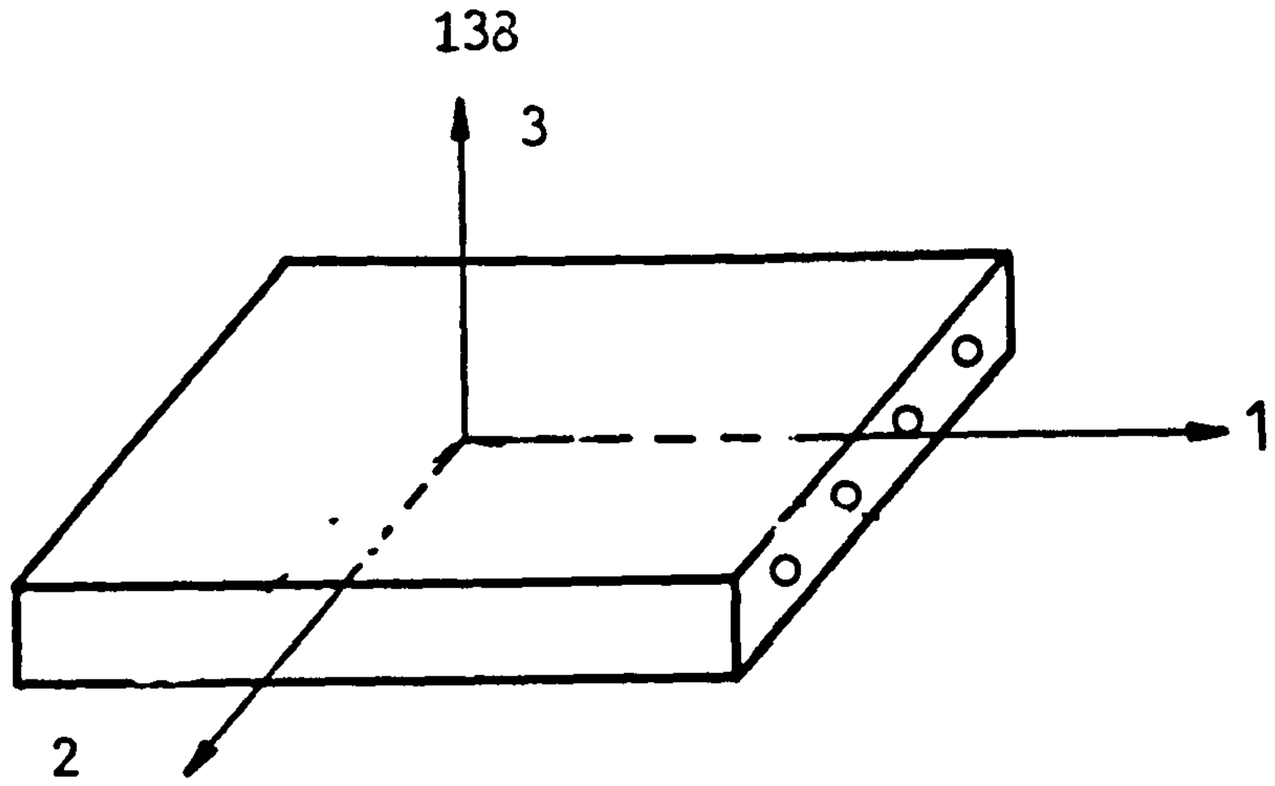


FIG. 3.1. CORD AND RUBBER PLY LAMINATE

FIG.3.2. ELASTIC MODULUS
REPRESENTATION IN DIRECTION1

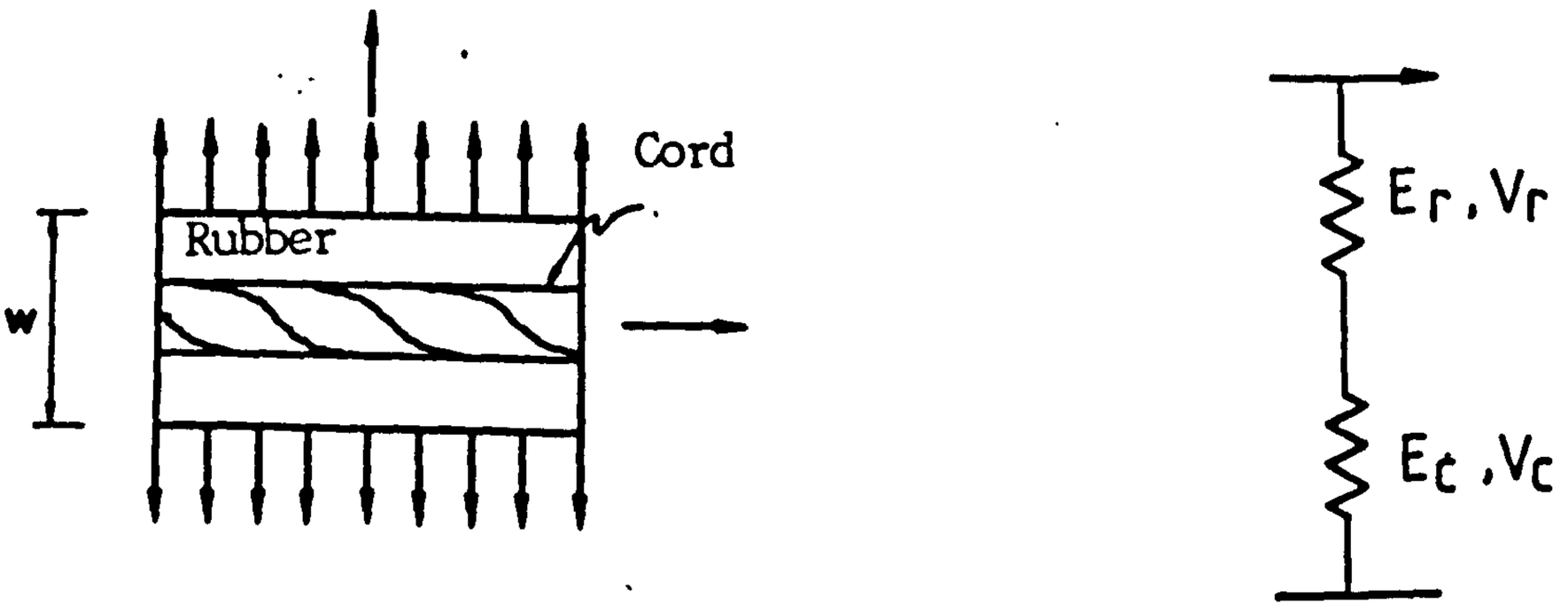


FIG.3.3. ELASTIC MODULUS
REPRESENTATION IN DIRECTION2

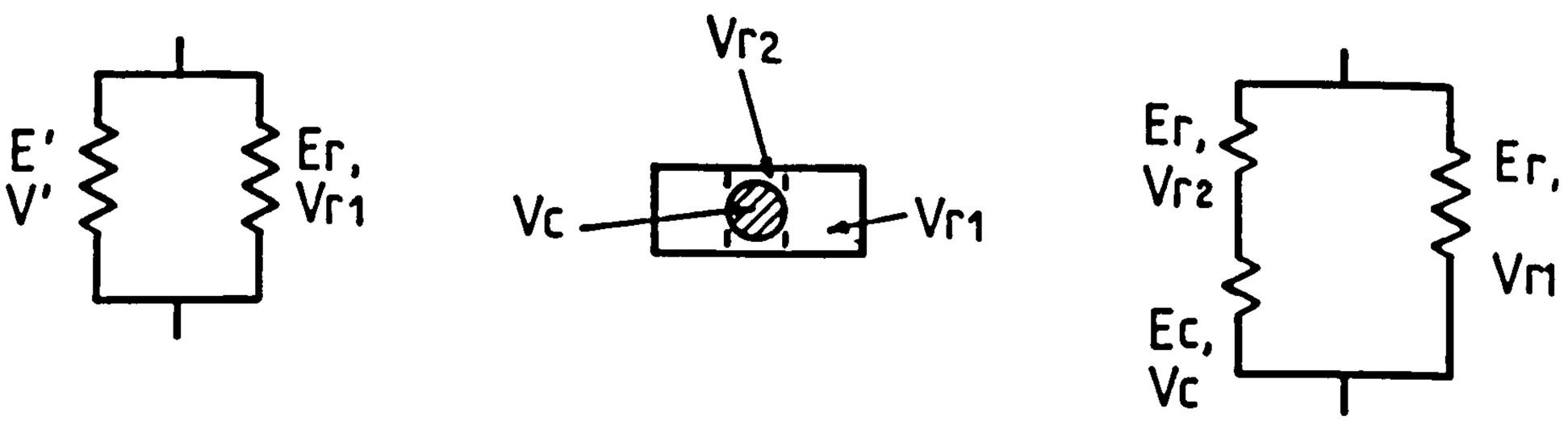


FIG. 3.4. ELASTIC MODULUS REPRESENTATION IN DIRECTION 3



a) Loaded Lamena b) Deformed Lamena

Fig.(3.5) LAMINA UNDER SHEARING LOAD

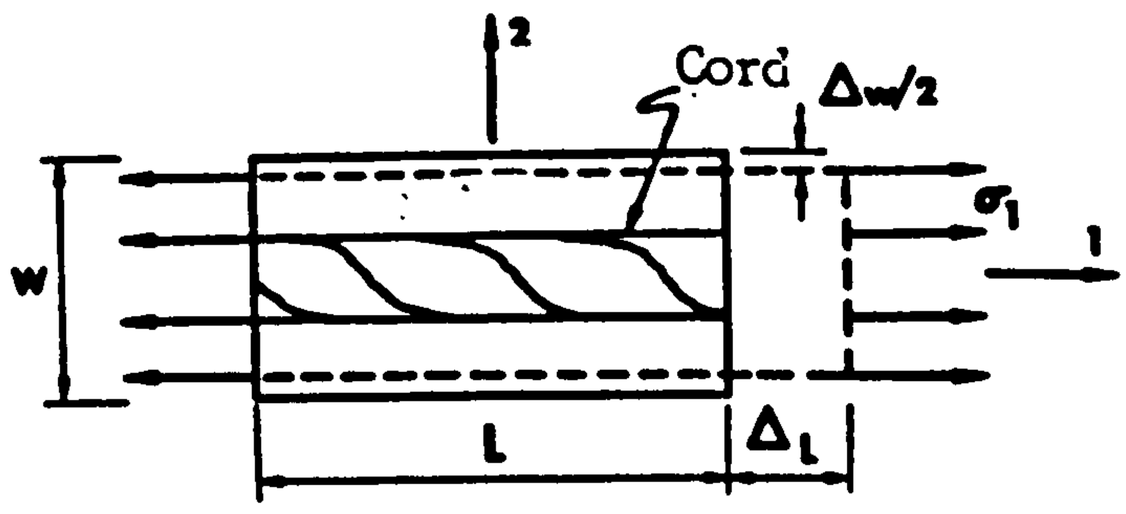


Fig.(3.6) LOADED LAMINA UNDER UNIDIRECTIONAL LOAD

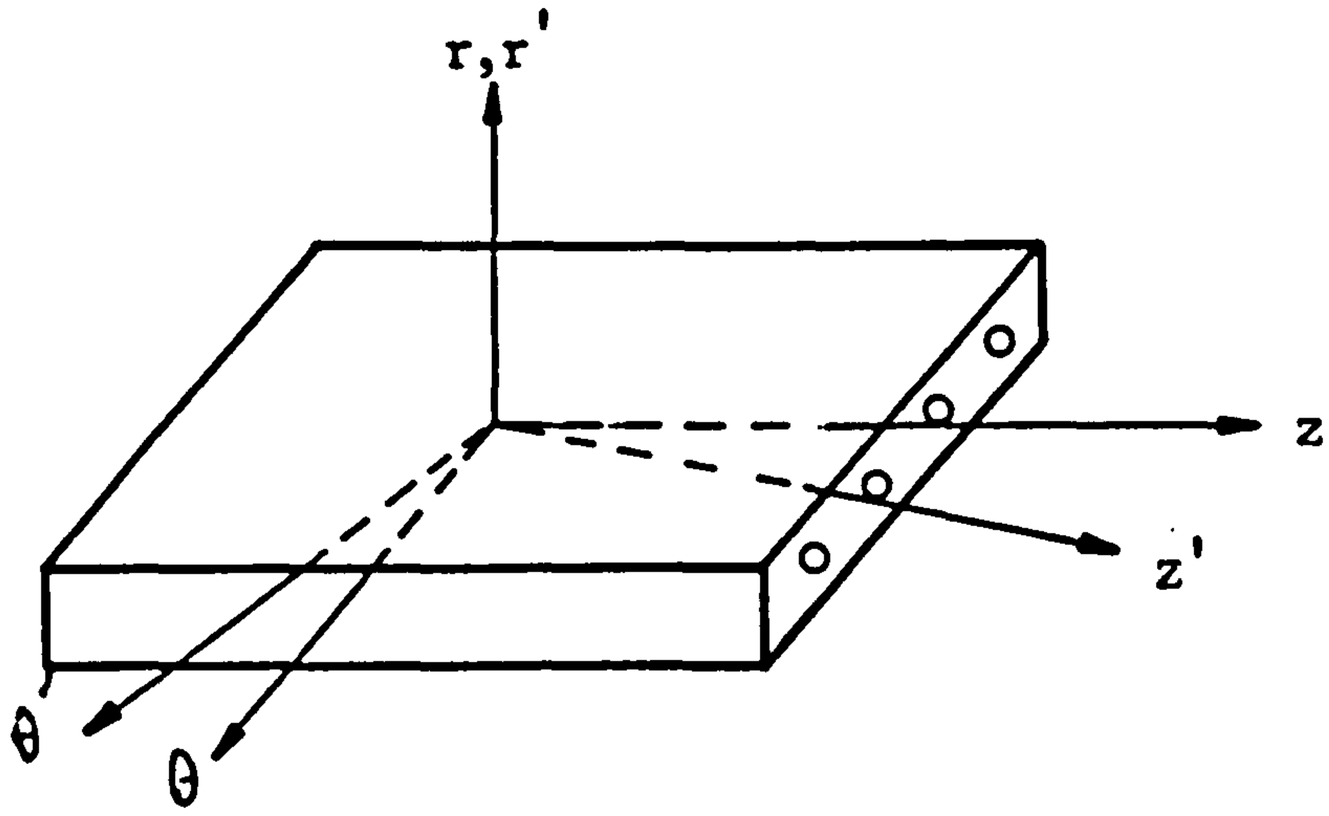


Fig.(3.7) ROTATION OF COORDINATE IN z,θ PLANE

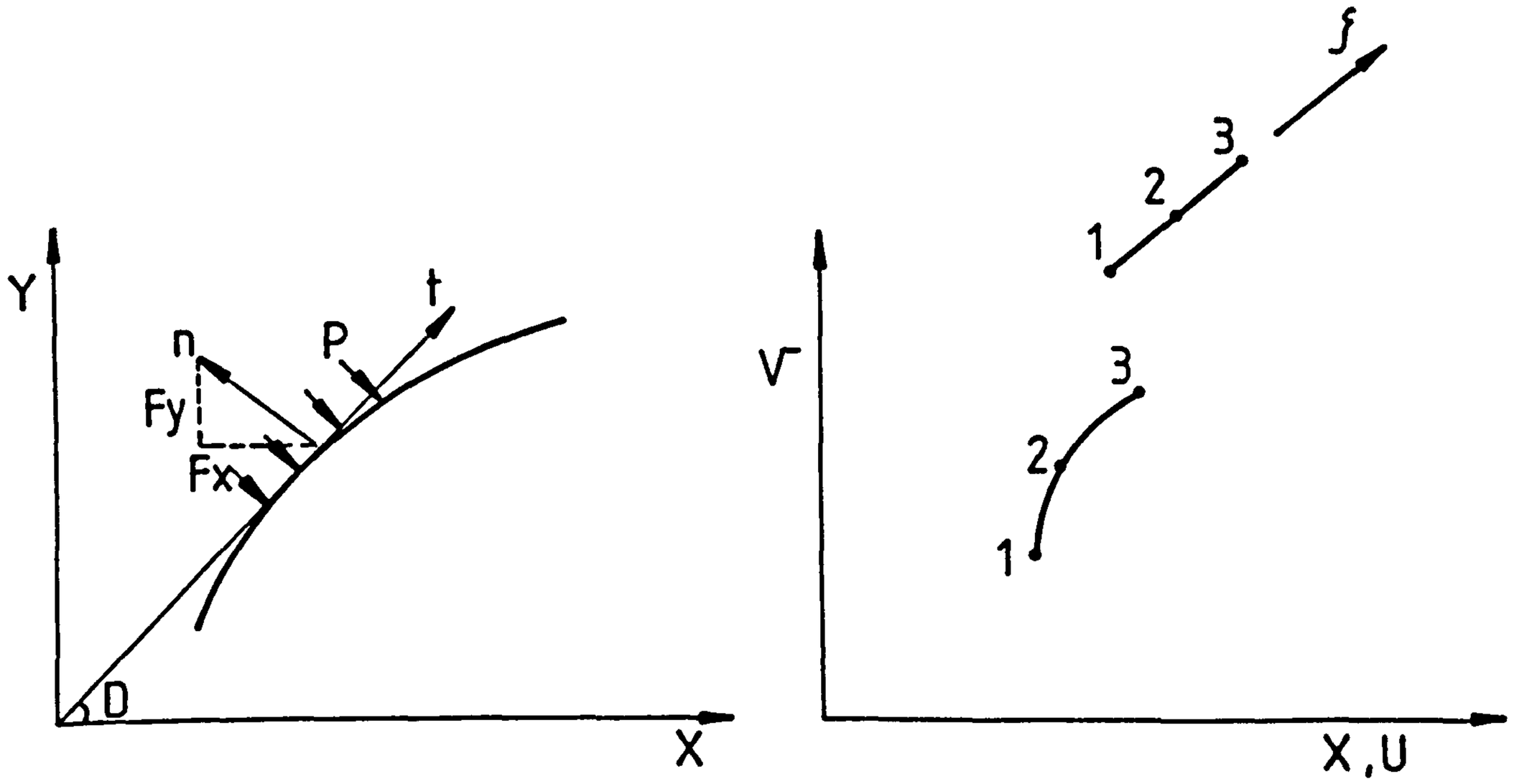


FIG. 3.8. USE OF ONE-D ELEMENT FOR EQUIVALENT NODAL FORCE OF A UNIFORMLY - DISTRIBUTED PRESSURE

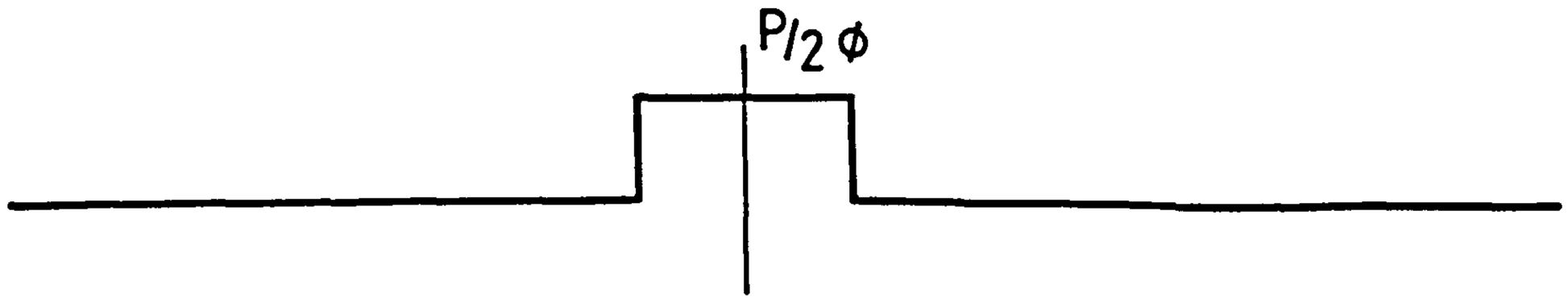
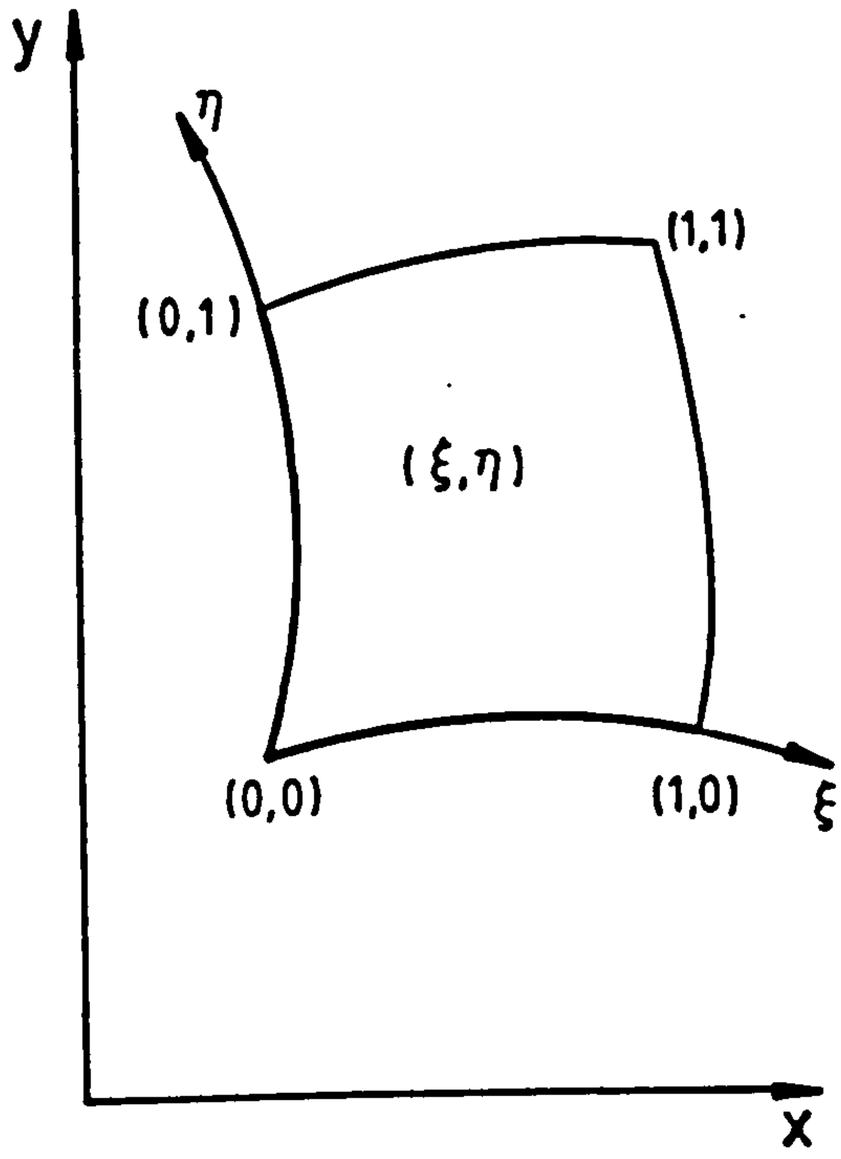
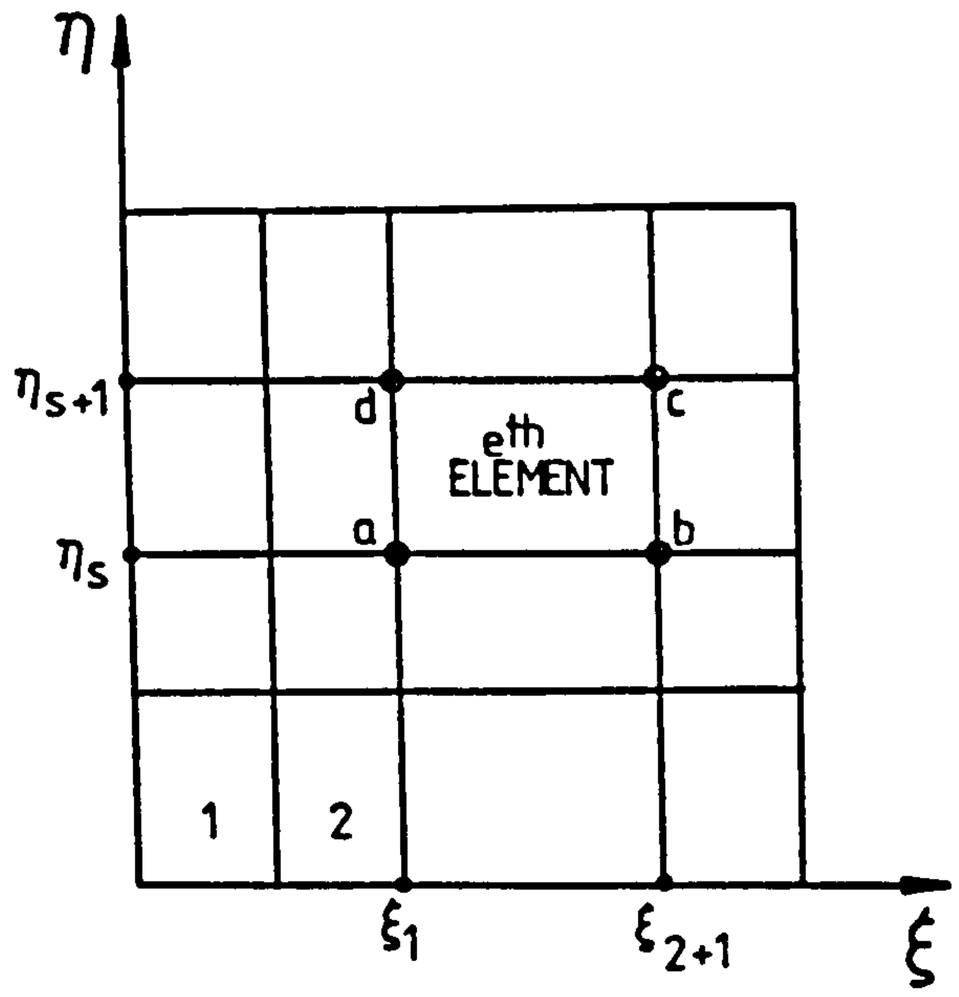


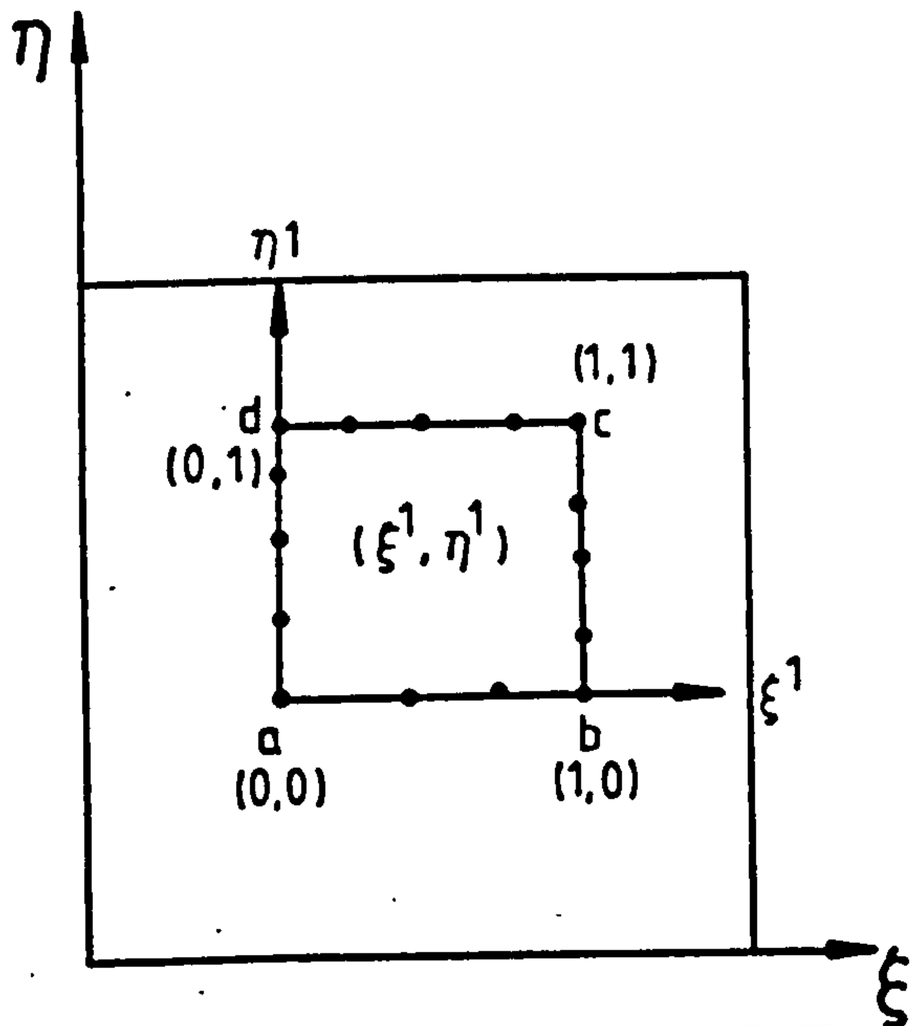
FIG. 3.9. REPRESENTATION OF PRESSURE DISTRIBUTION FOR, AN EXTERNALLY LOADED TYRE



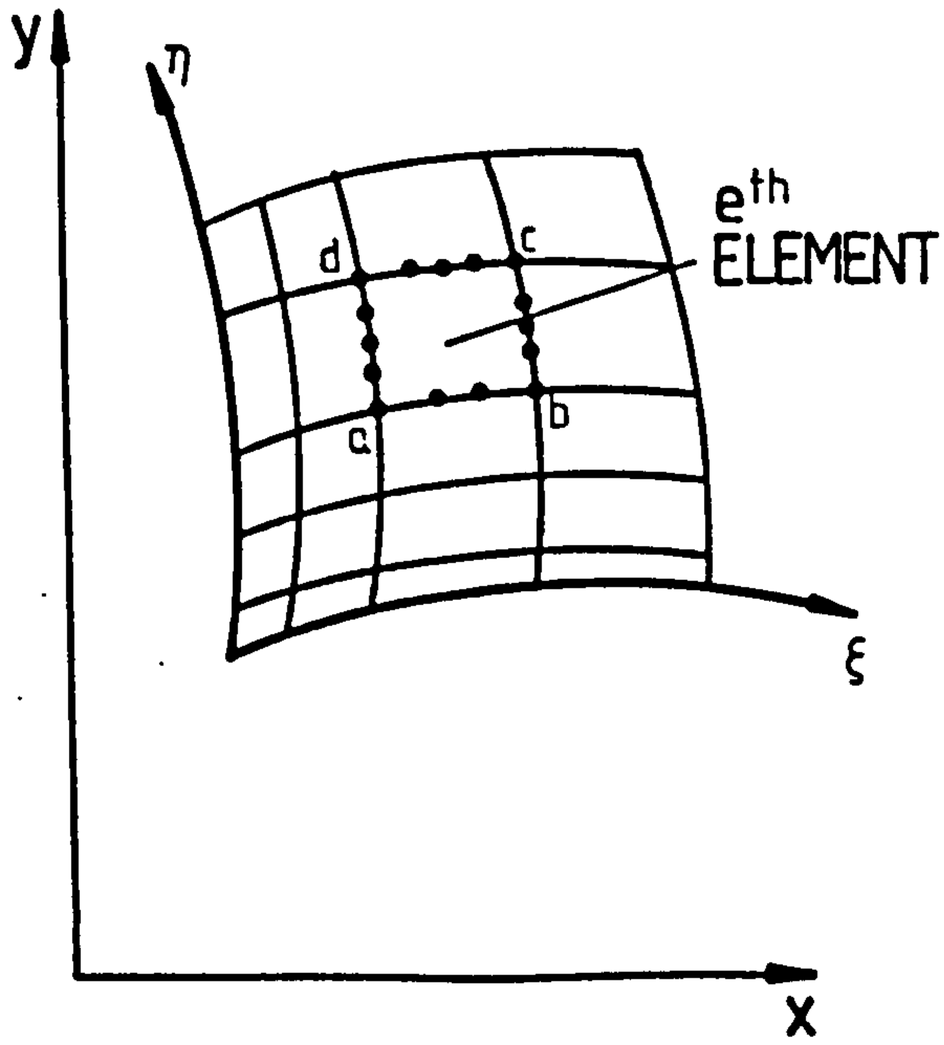
a - BLOCK IN CARTESIAN SPACE



b - DIVISION INTO ELEMENTS IN ξ-η SPACE

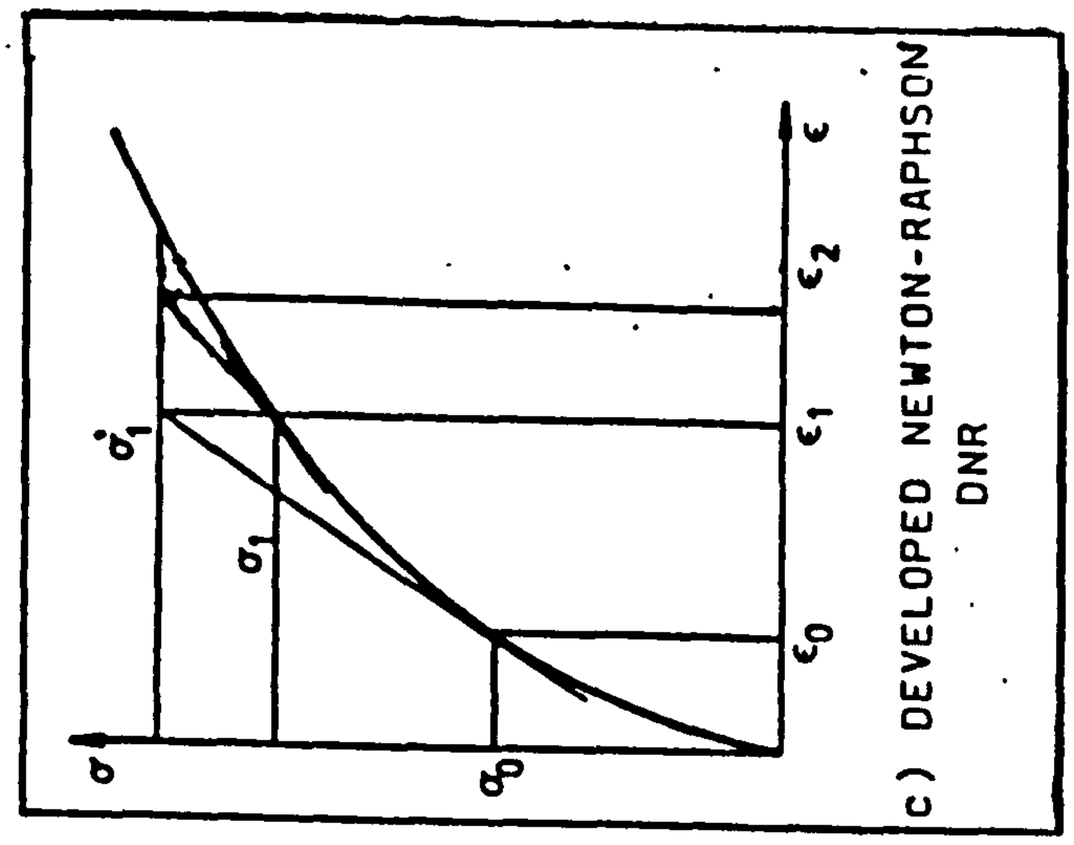


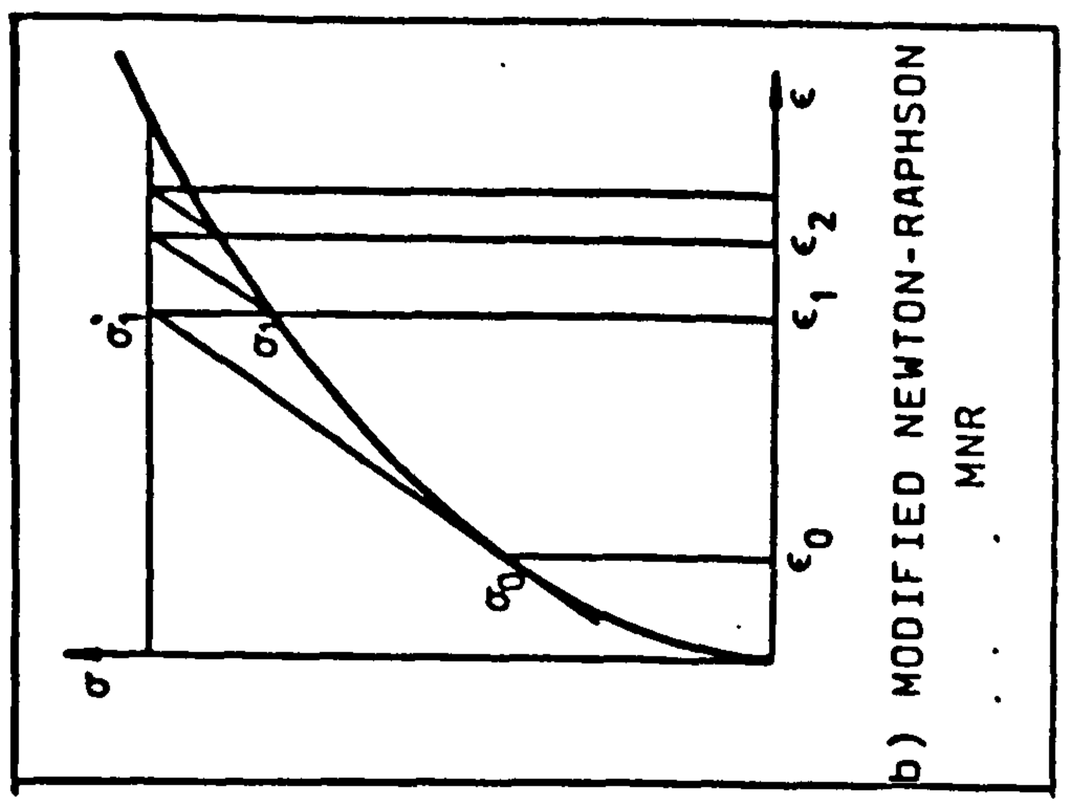
c - DESCRIPTION OF ELEMENT IN ITS LOCAL ξ^1 η^1 SPACE



d - RETURN TO THE CARTESIAN SPACE

FIGURE 3.10 GENERATION OF QUADRILATERAL ELEMENTS IN A QUADRILATERAL BLOCK.





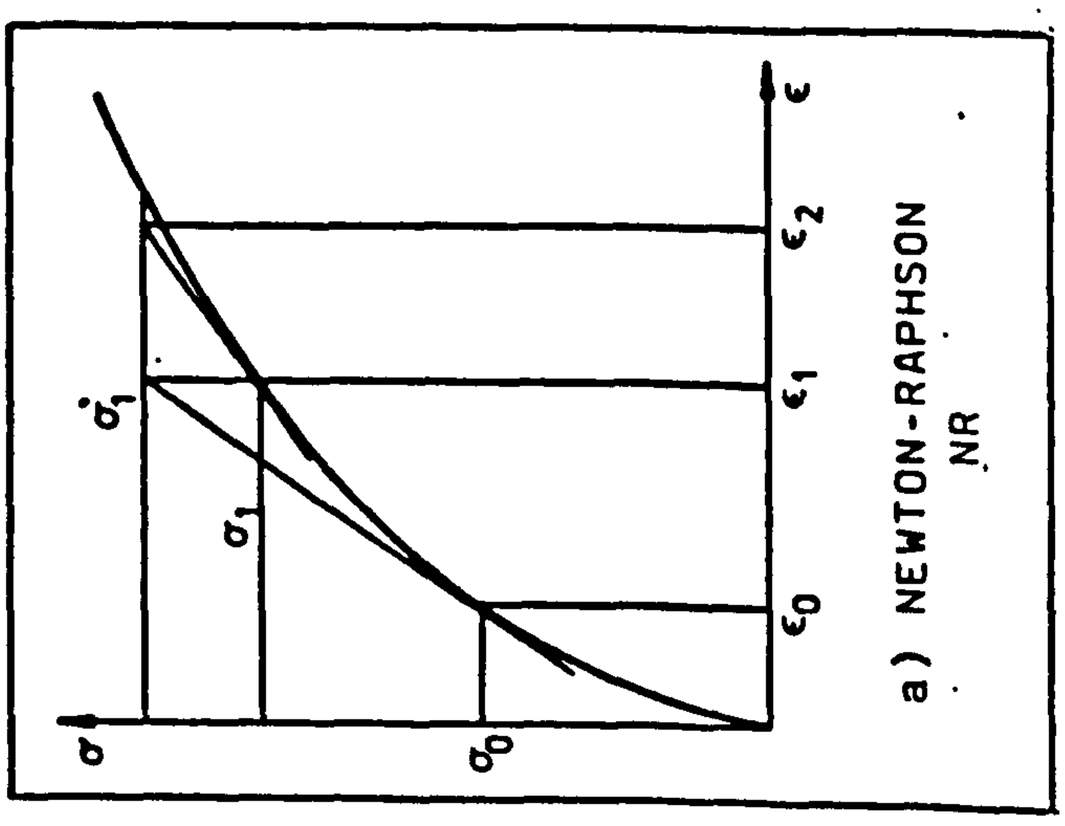


Fig..(4.1) ITERATIVE PROCEDURE

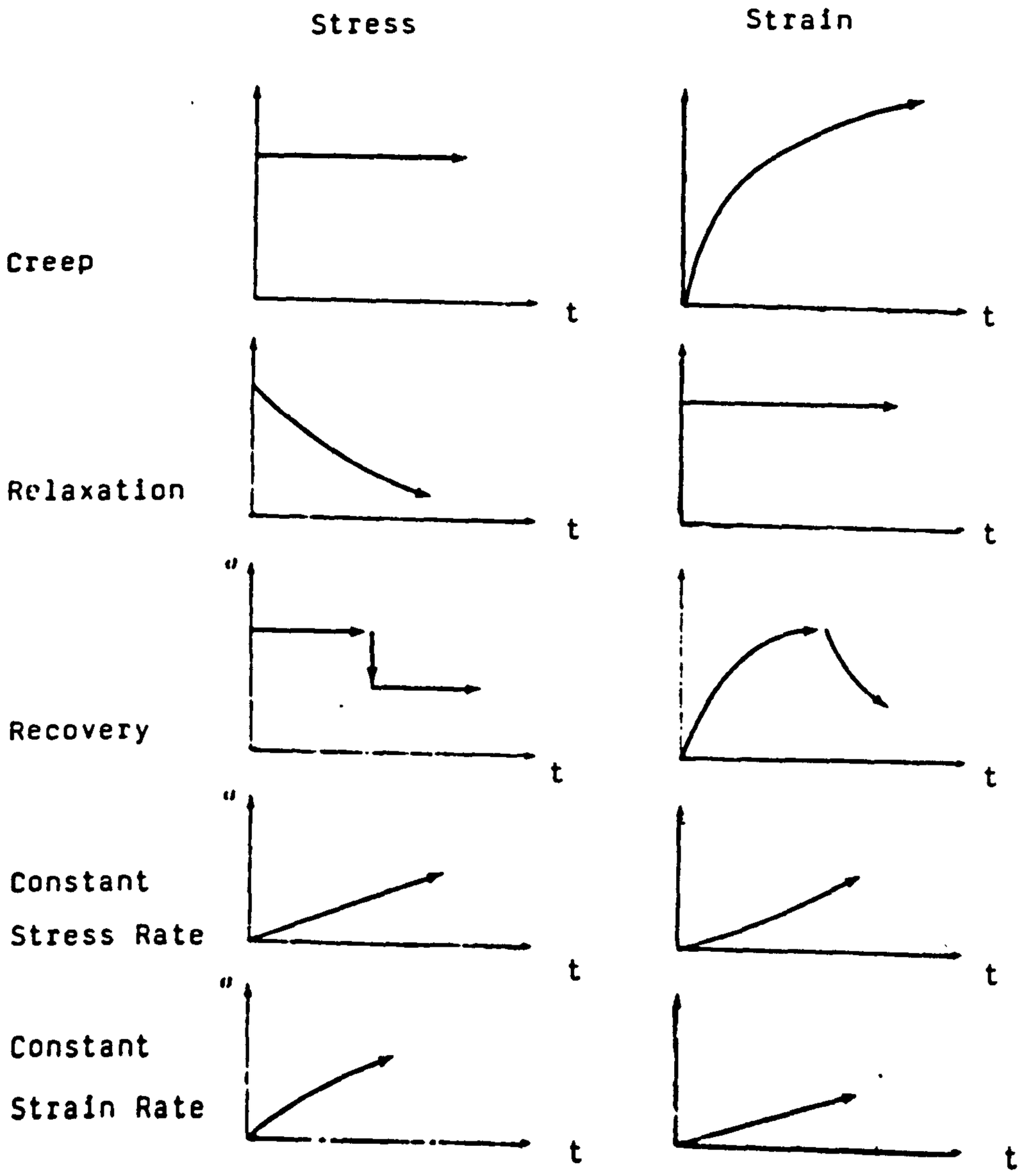
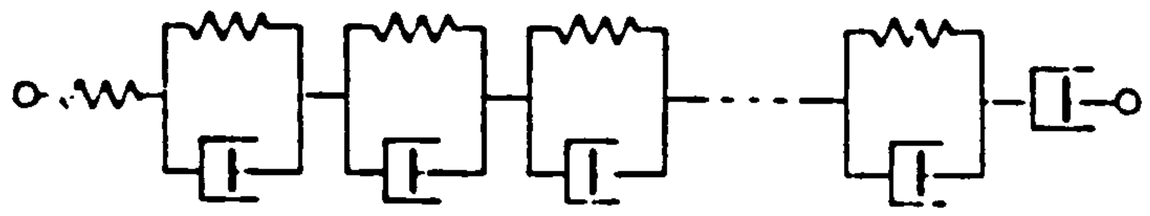
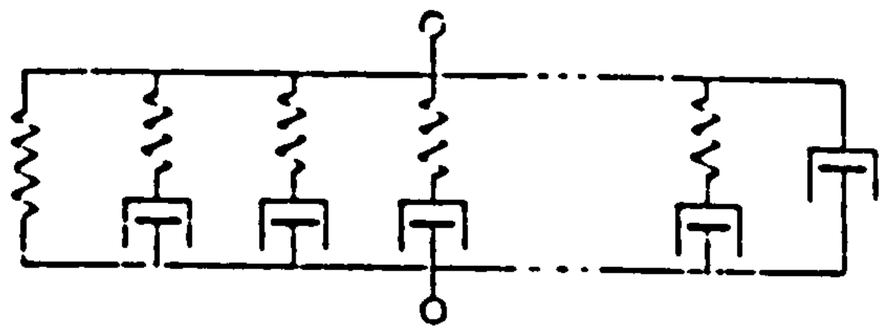


Fig.(5.1) TIME DEPENDENT BEHAVIOUR OF STRESS AND STRAIN



a- General KELVIN



b- GENERAL MAXWELL

Fig.(5,2) SPRING-DASHPOT MODELS

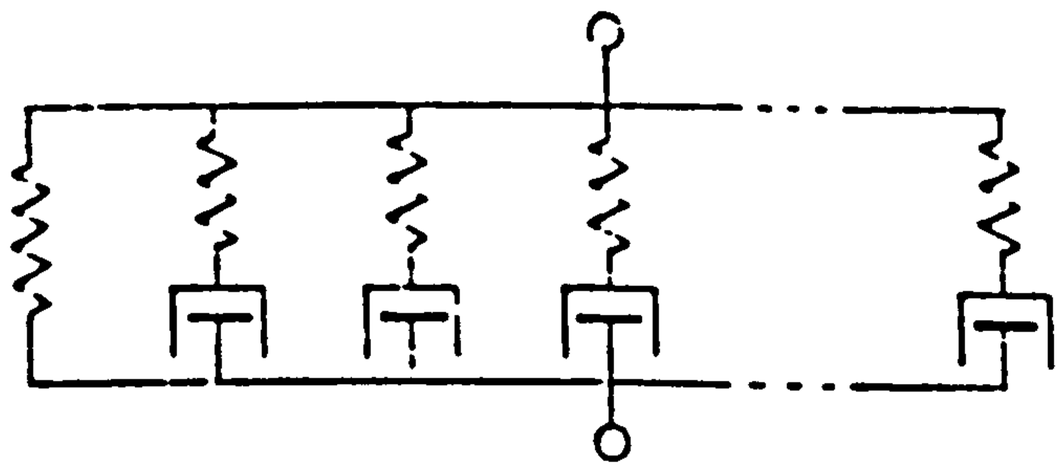


Fig.(5.3) TYRE-TIME DEPENDENT MODEL

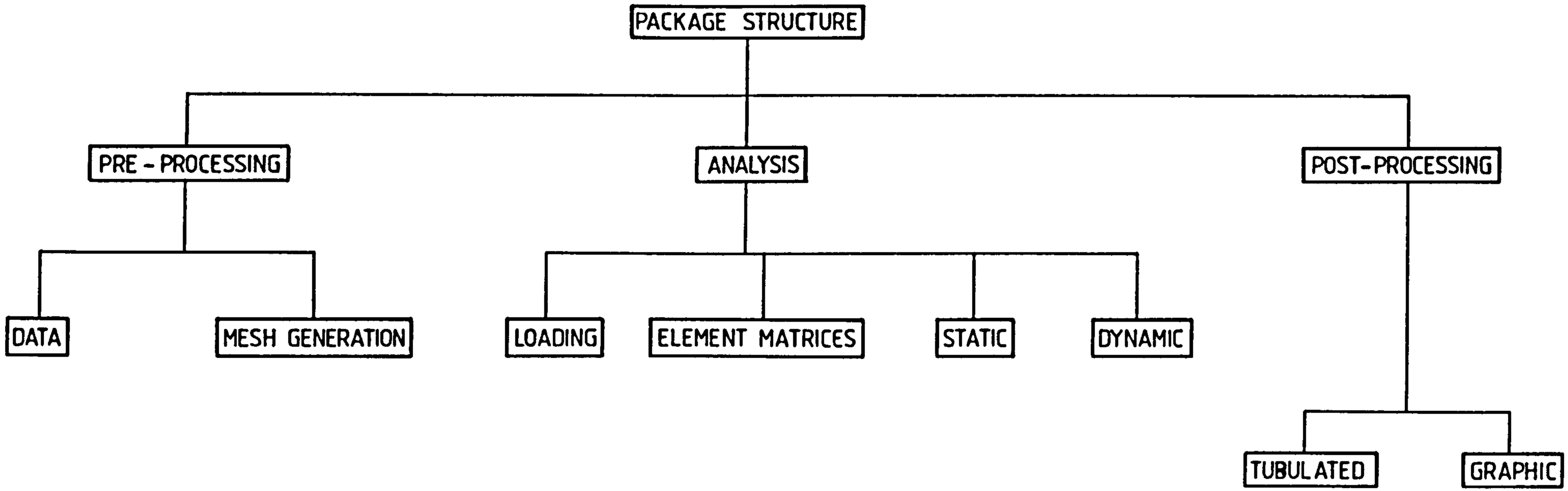


FIG. 7. 1. PACKAGE STRUCTURE

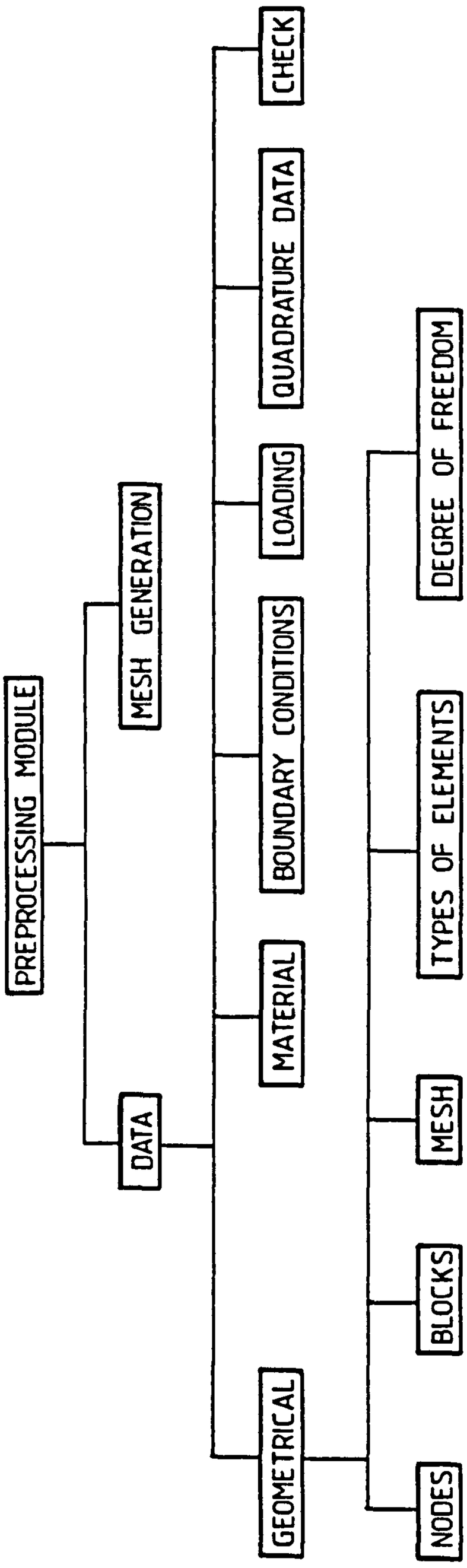


FIG. 7. 2. SCHEMATIC DIAGRAM OF THE PREPROCESSING MODULE

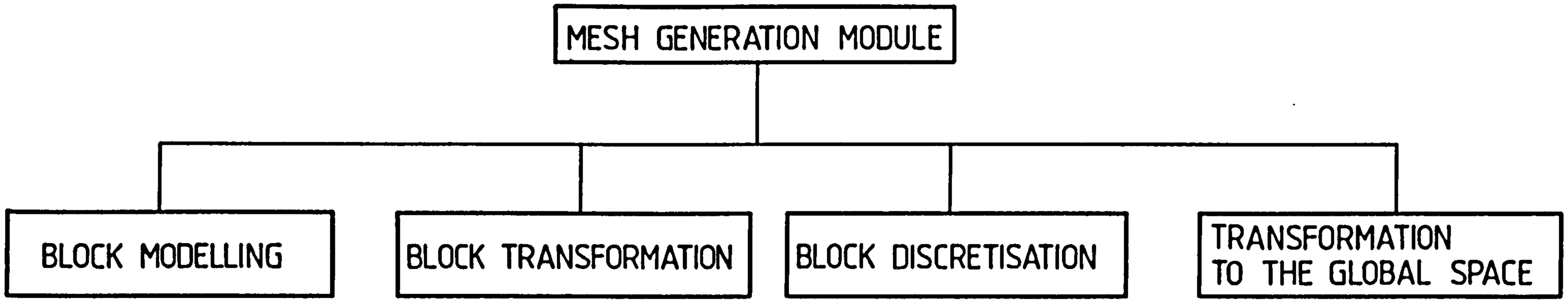


FIG. 7. 3. SCHEMATIC DIAGRAM OF THE MESH GENERATION MODULE

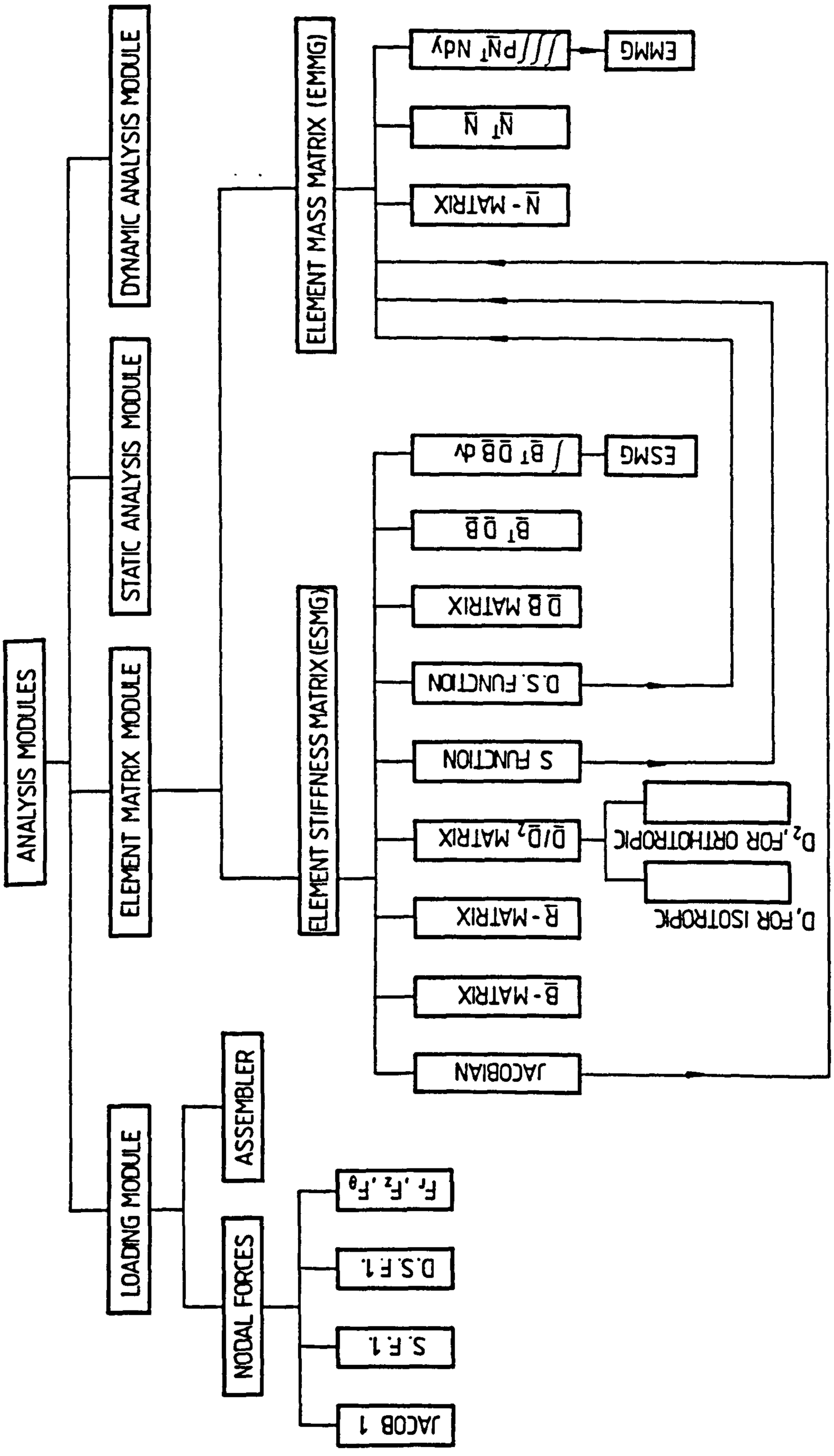


FIG.(7·4) SCHEMATIC DIAGRAM OF THE ANALYSIS MODULE

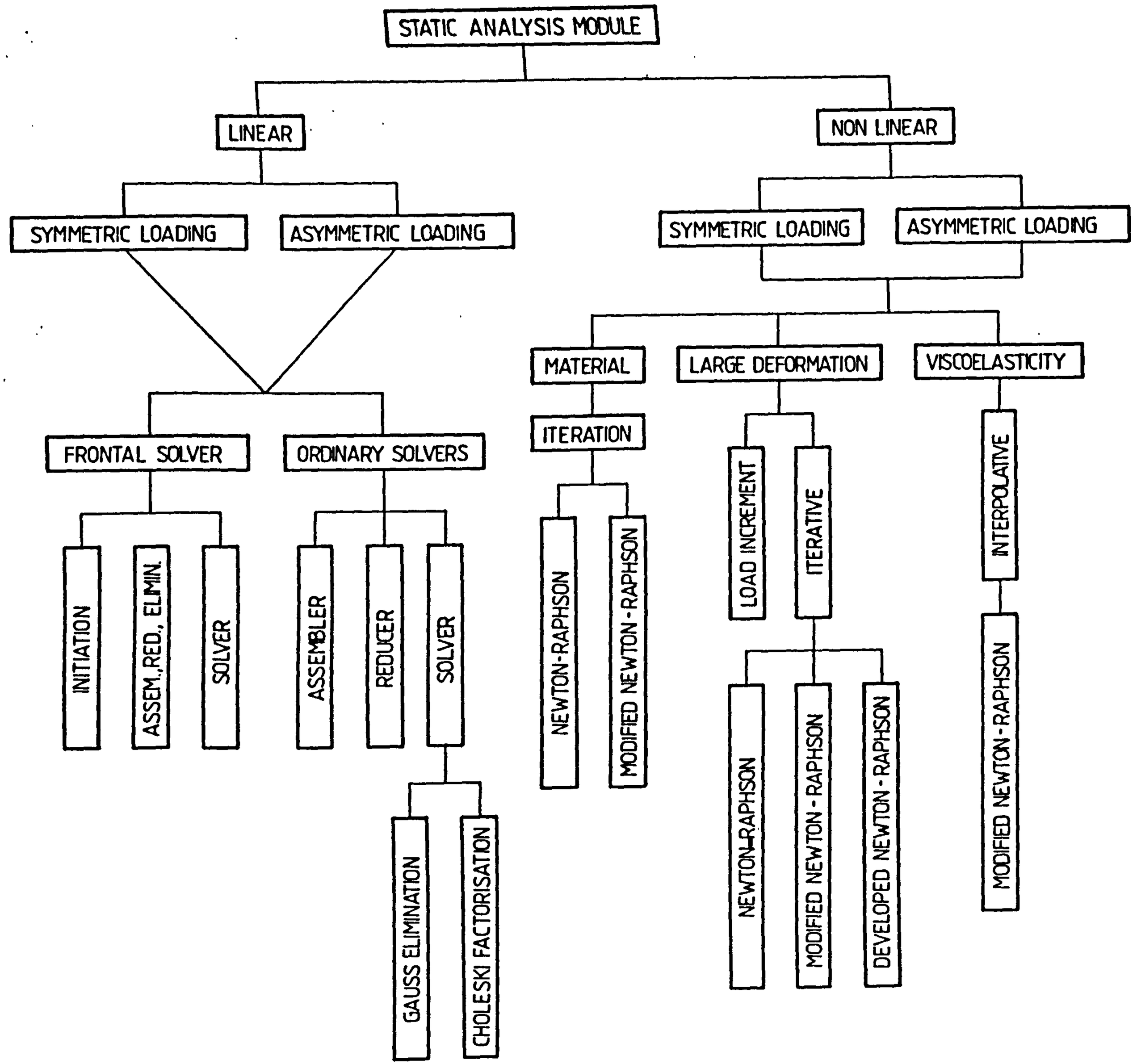


FIG.(7·5) STATIC ANALYSIS MODULE

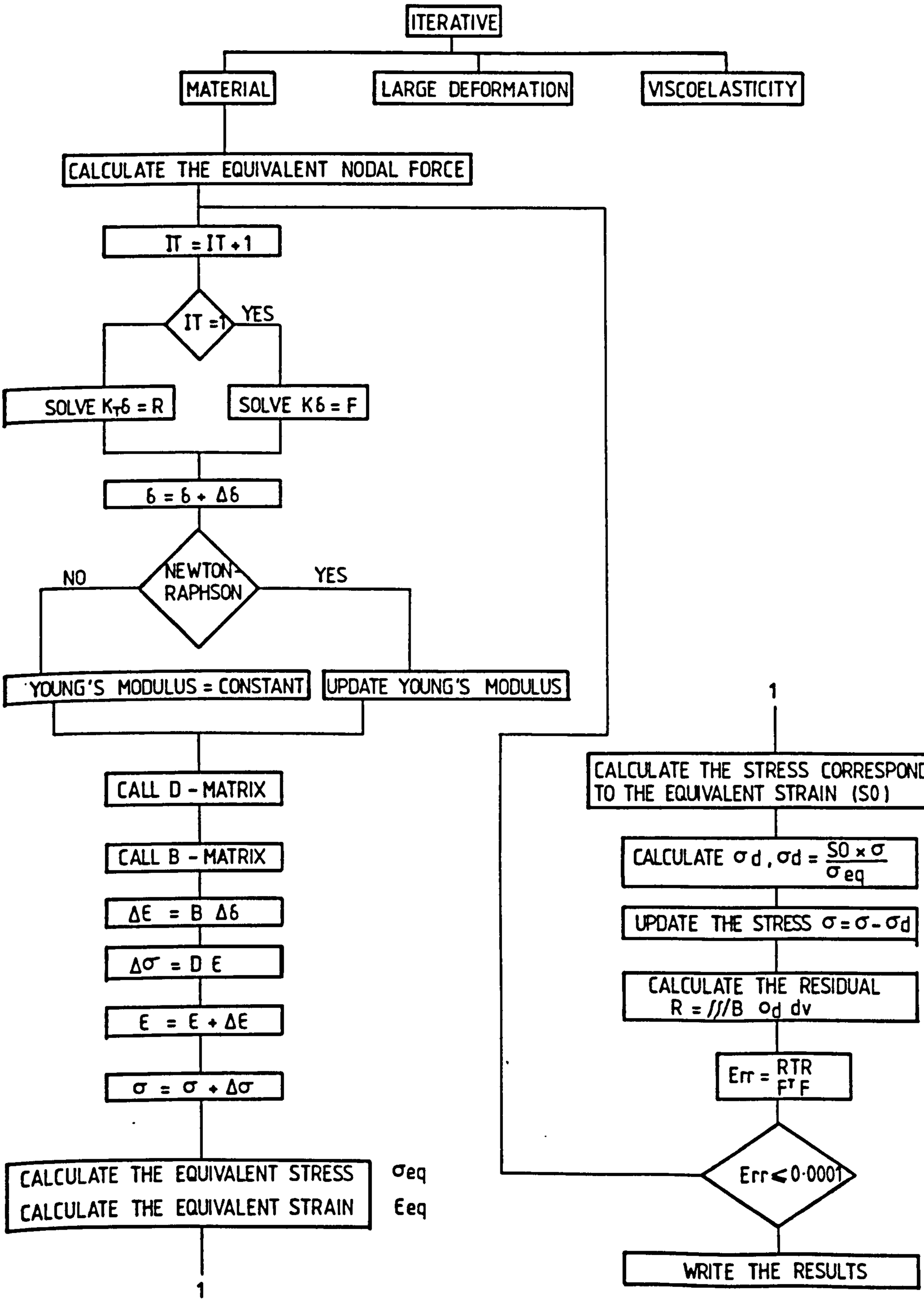
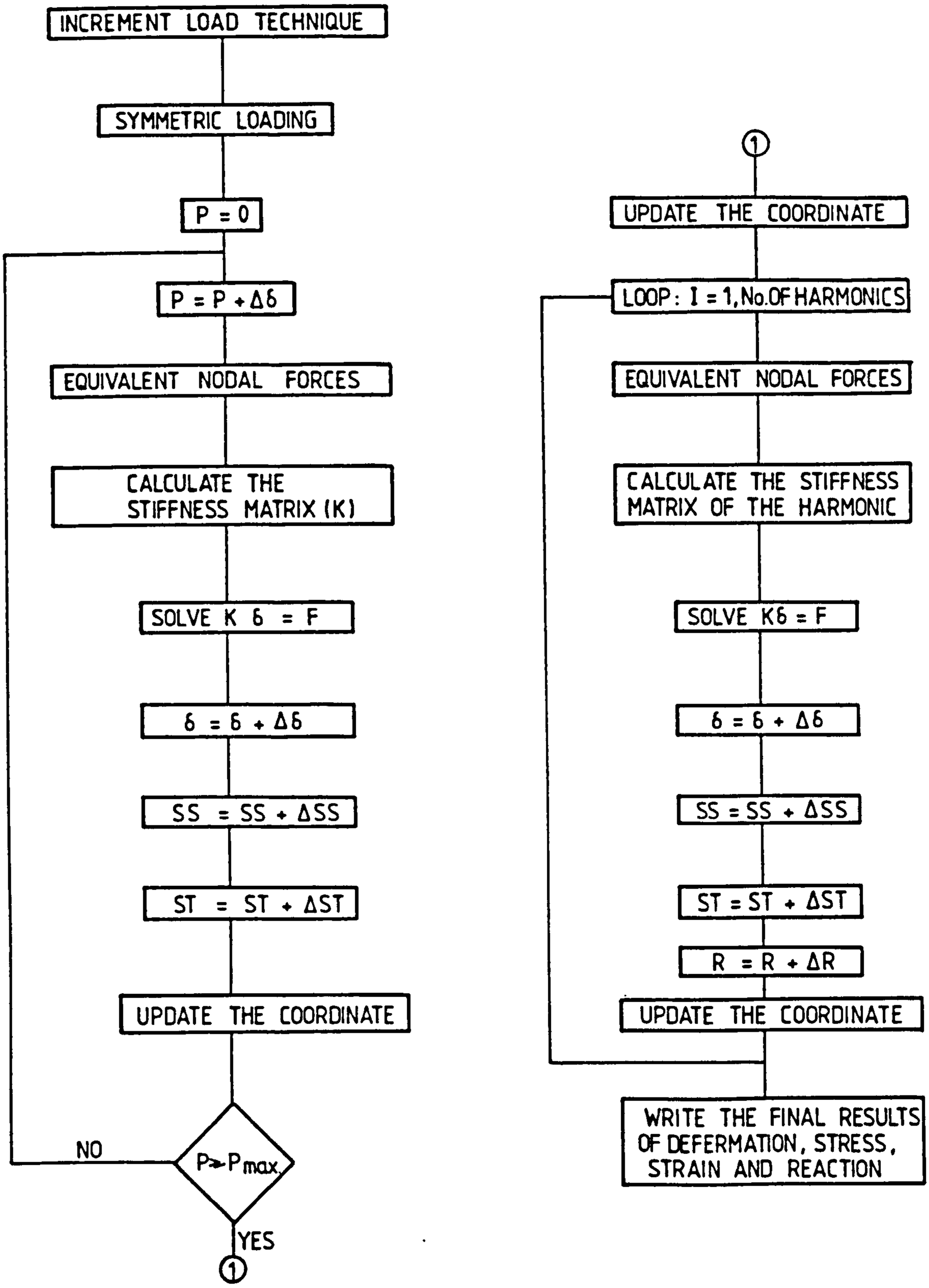


FIG. 7.6. ITERATIVE PROCEDURE FOR MATERIAL NONLINEARITY



δ = DEFORMATION
SS = STRESS
ST = STRAIN
R = REACTION

FIG. 7.7. INCREMENT LOAD PROCEDURE AND FOURIER SERIES EXPANSION

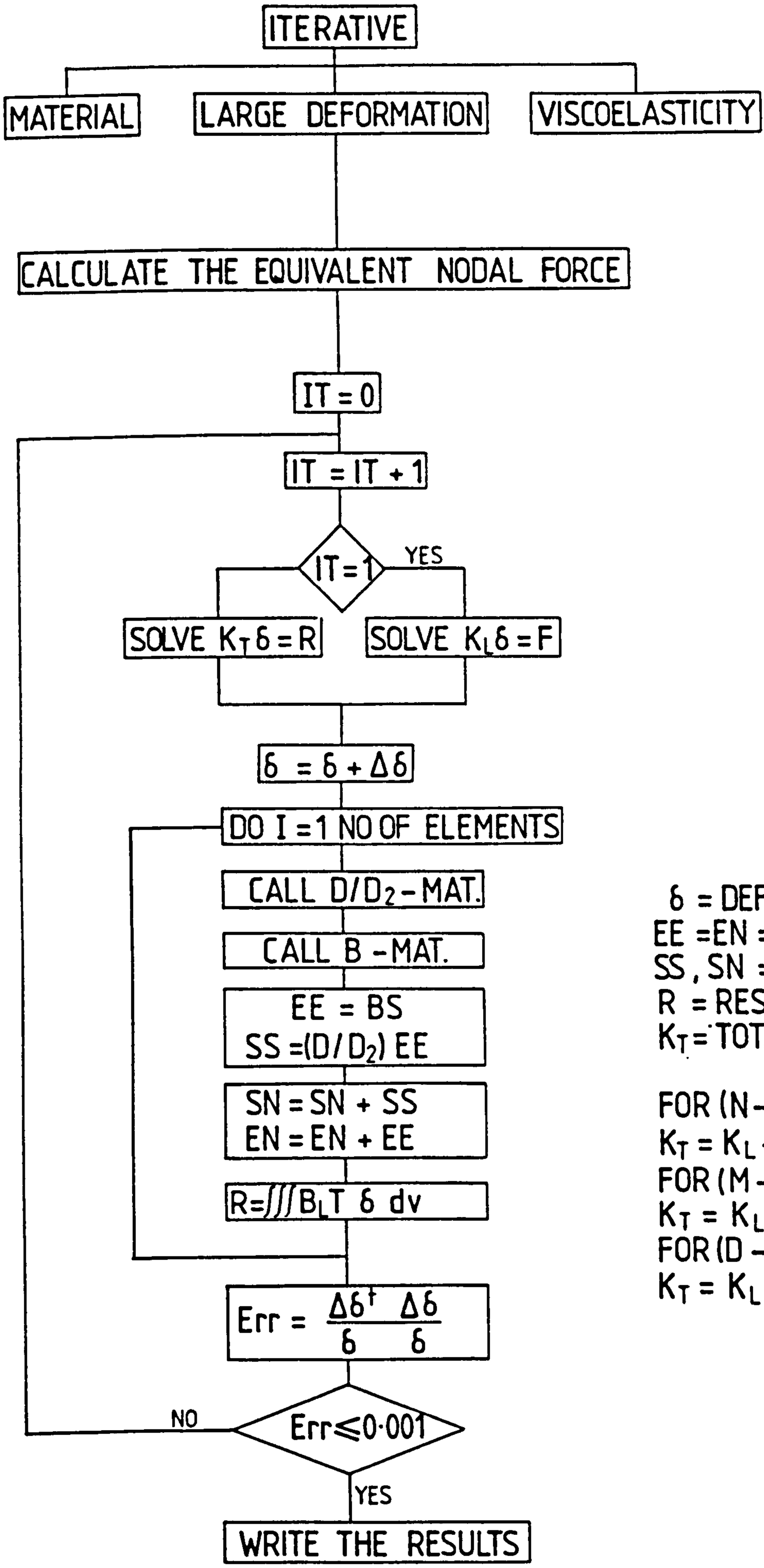


FIG. 7.8. ITERATIVE PROCEDURE FOR LARGE DEFORMATION ANALYSIS

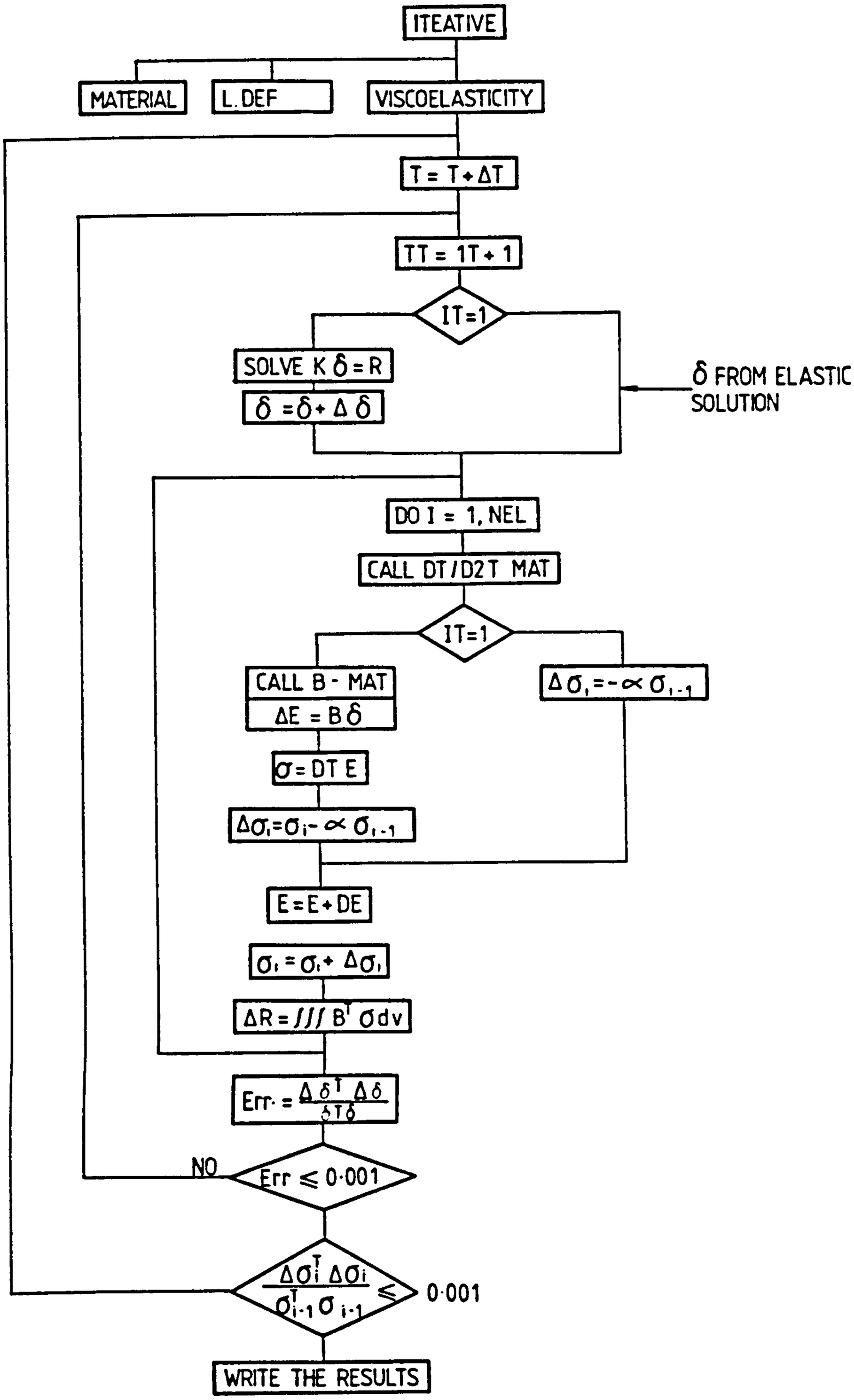
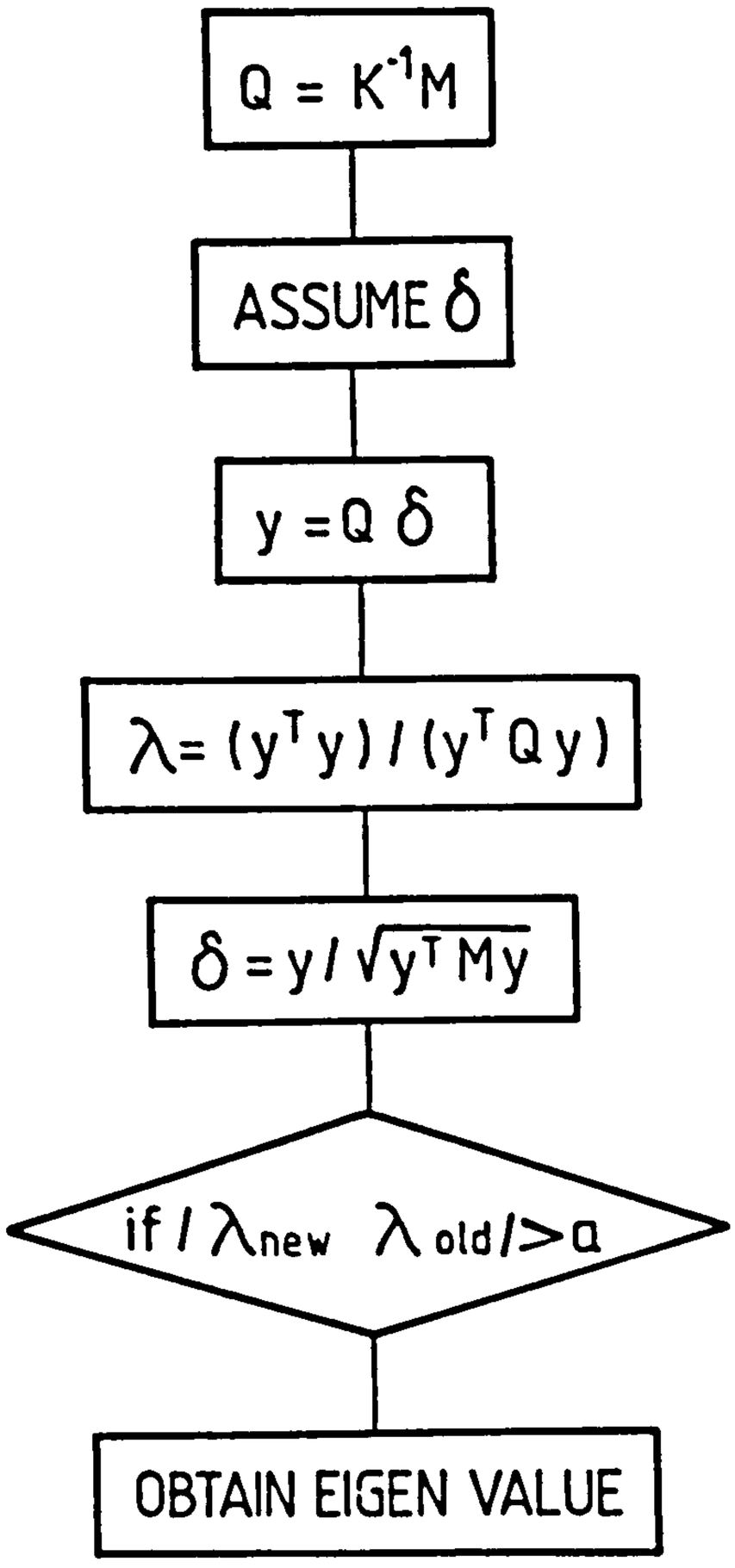


FIGURE 7·9 INTERPOLATIVE PROCEDURES OF VISCOELASTIC ANALYSIS

LOWEST EIGEN VALUE :



b - SWEEPING FOR λ_j

WE HAVE : $a, \delta, = \frac{1}{\lambda} I\,\delta$

WILL CONVERGE TO $\lambda,$

FROM THE ORTHOGONALITY OF EIGEN VECTORS :

$$Q_{j+1}\,\delta = \frac{1}{\lambda} I\,\delta$$

$$Q_{j+1} = Q_j - \frac{1}{\lambda_j}\,\delta_j\,\delta_j^T M$$

$$\lambda_1 \leqslant \lambda_2 \leqslant \lambda_3$$

FIG.(7·10). SIMPLE ITERATION TECHNIQUE.

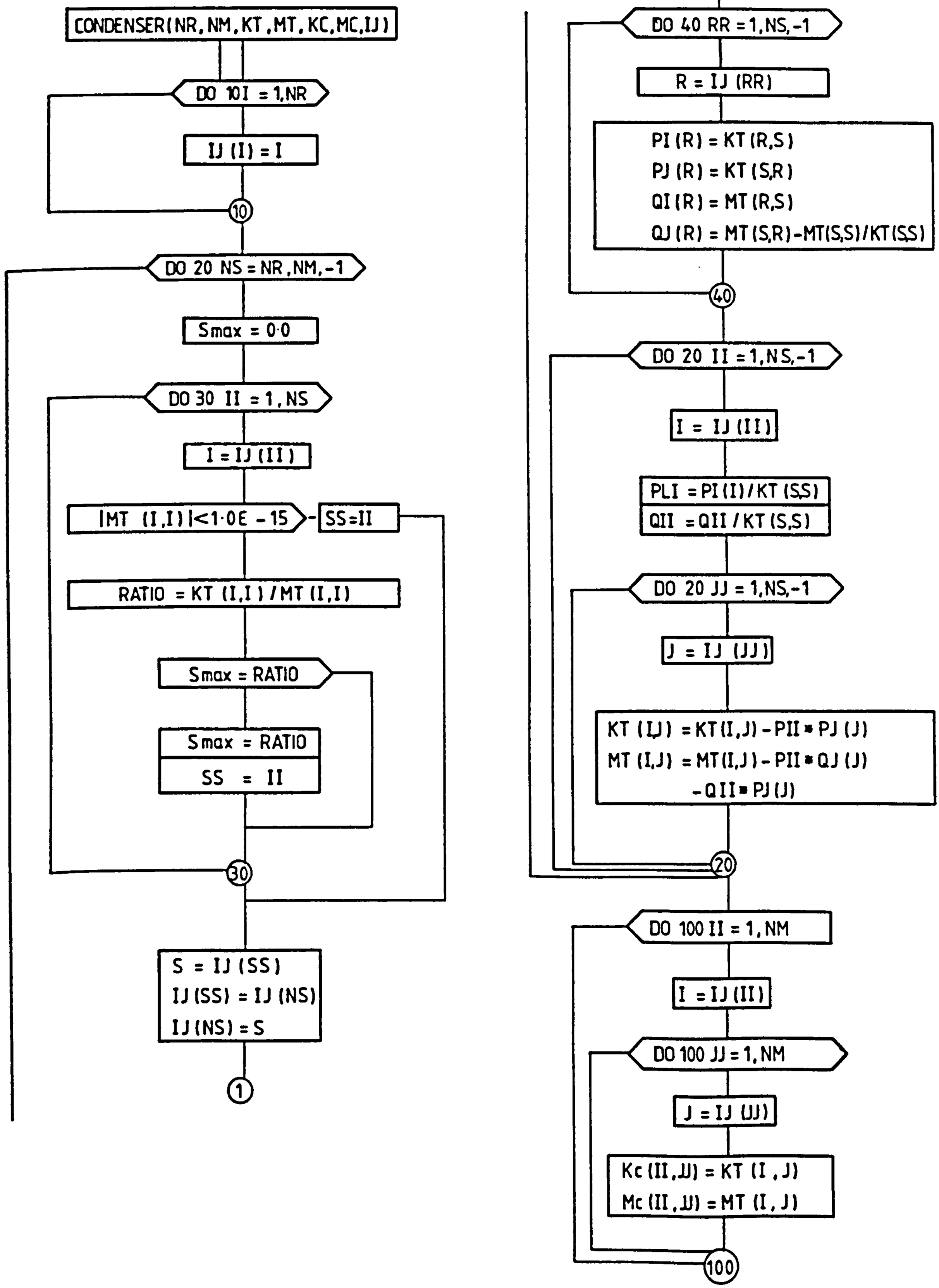


FIG. 7.11. FLOW CHART OF DYNAMIC CONDENSATION

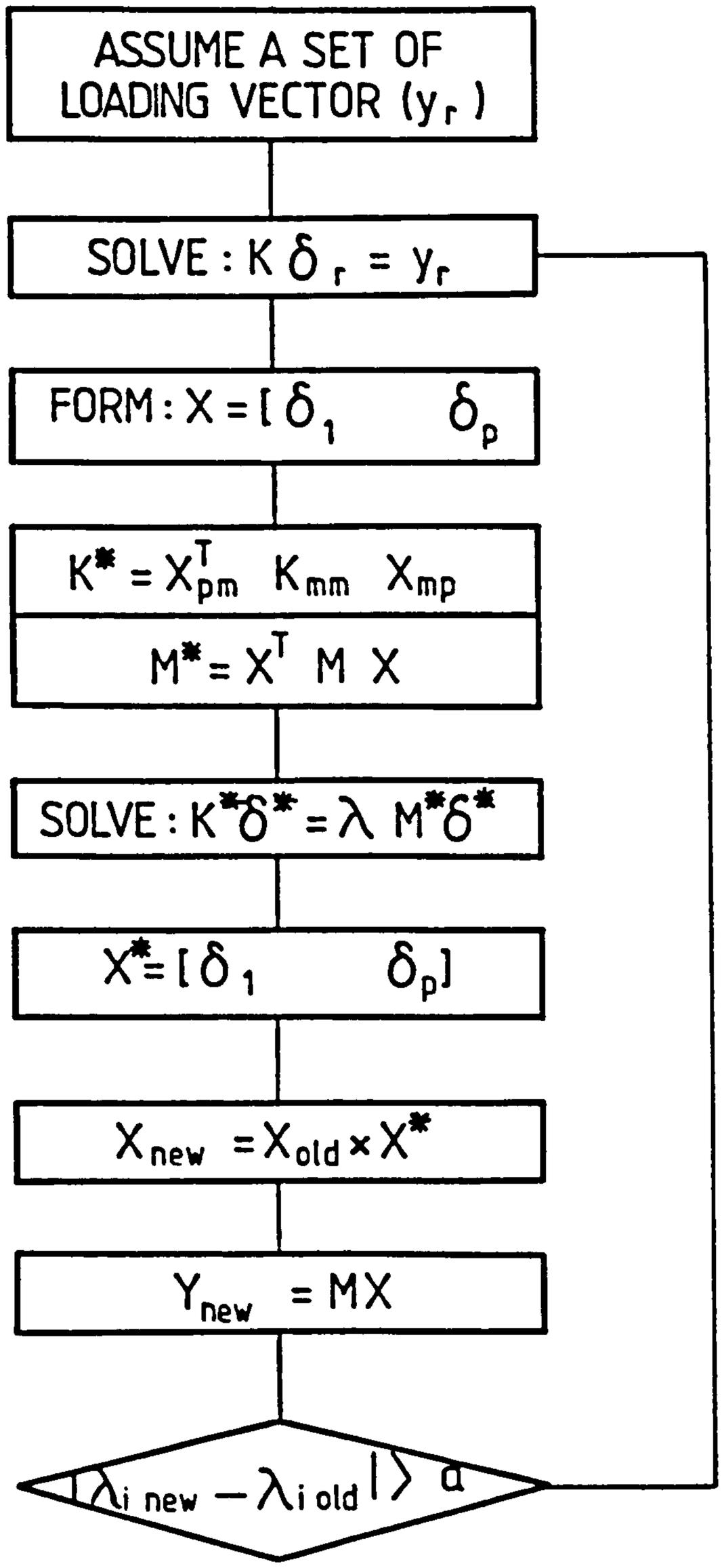


FIG. (7·12) SUBSPACE ITERATION TECHNIQUE

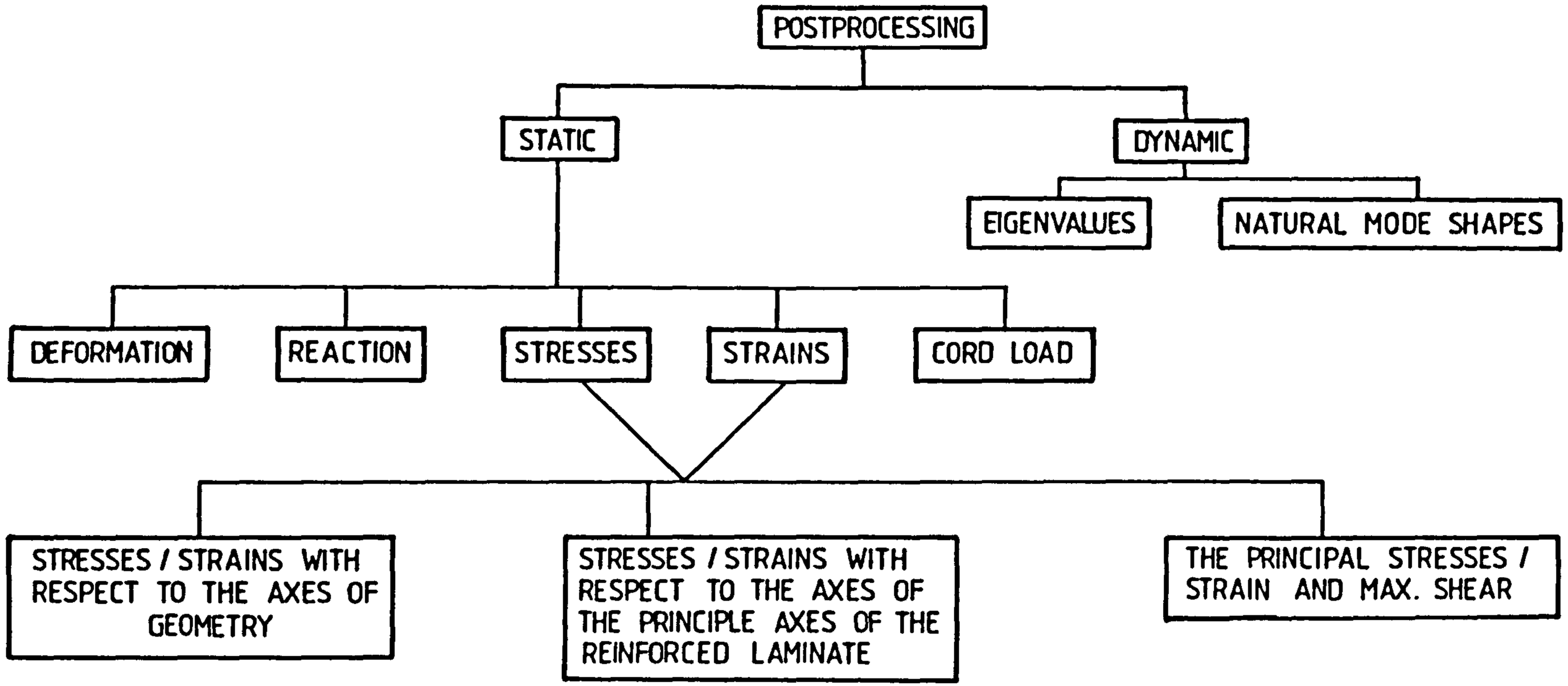
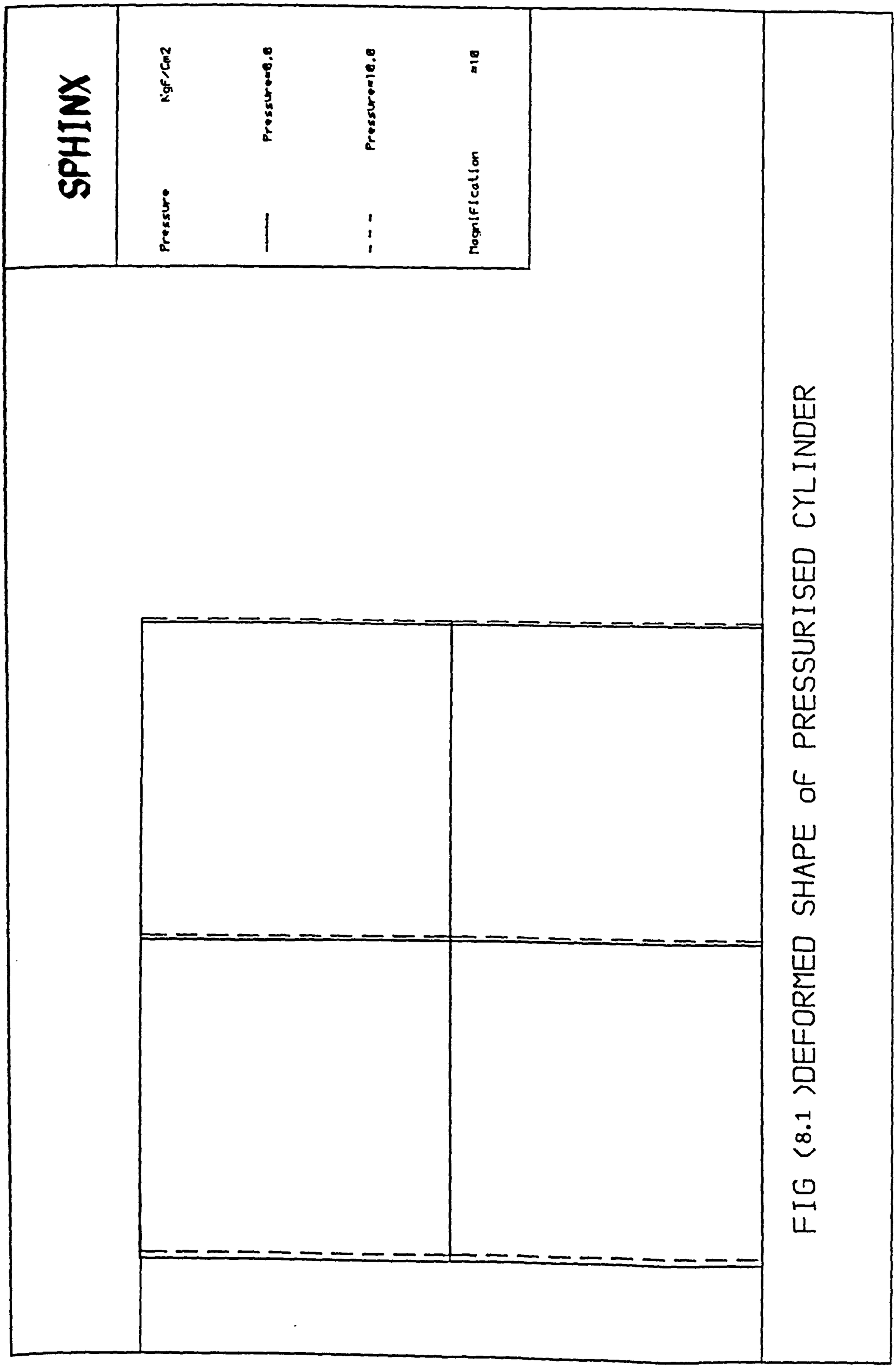


FIG. 7. 13. POSTPROCESSING MODULE


SPHINX
Pressure KgF/Cm2
Pressure=8.8
Pressure=10.8
Magnification =10
FIG (8.1)DEFORMED SHAPE of PRESSURISED CYLINDER

SPHINX

Tyre Size 175HR14

Made DUNLOP

Internal Pressure Kgf/mm2

_____ I.P.=0.0

- - - - I.P.=0.1

Magnification =5

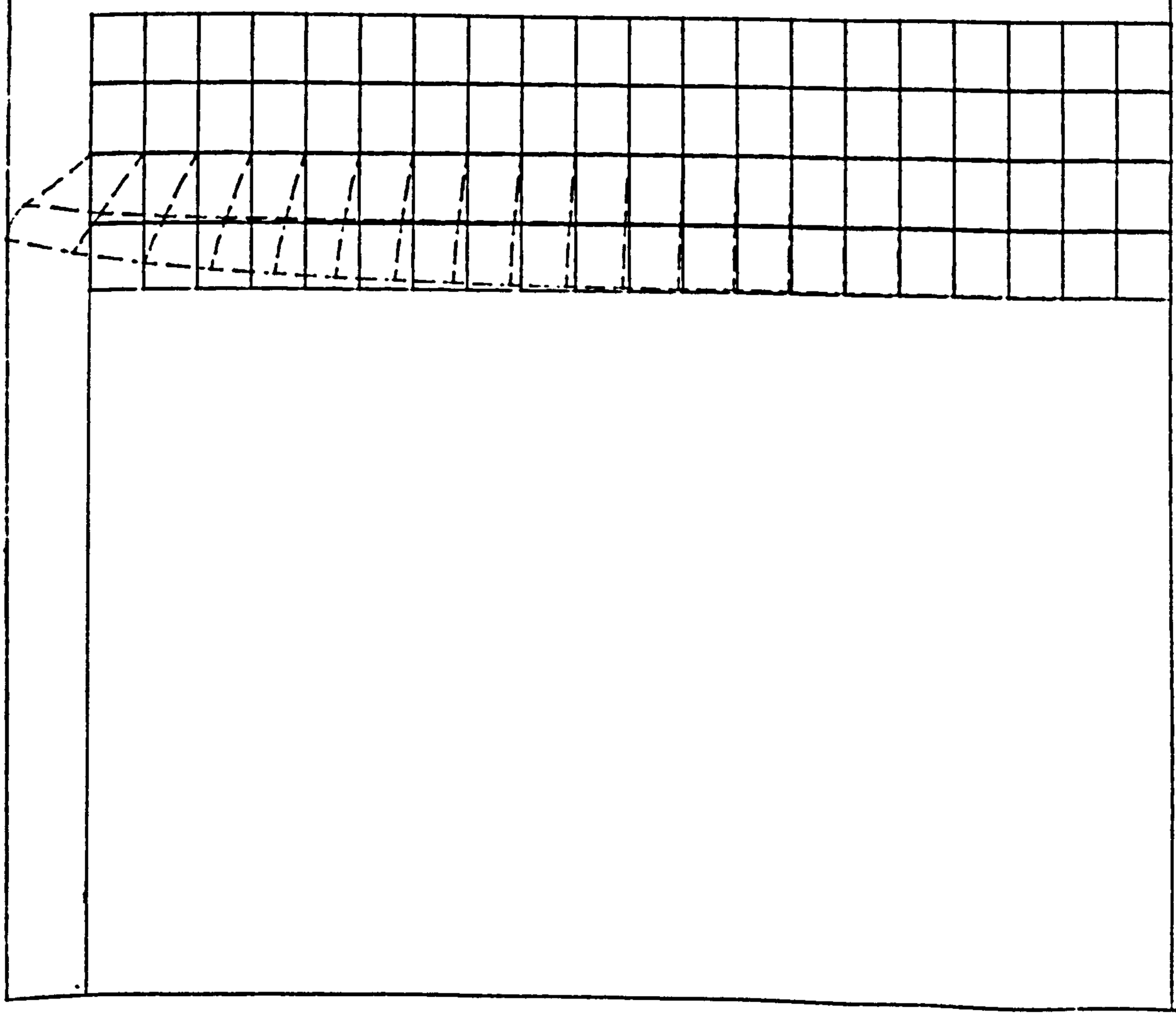
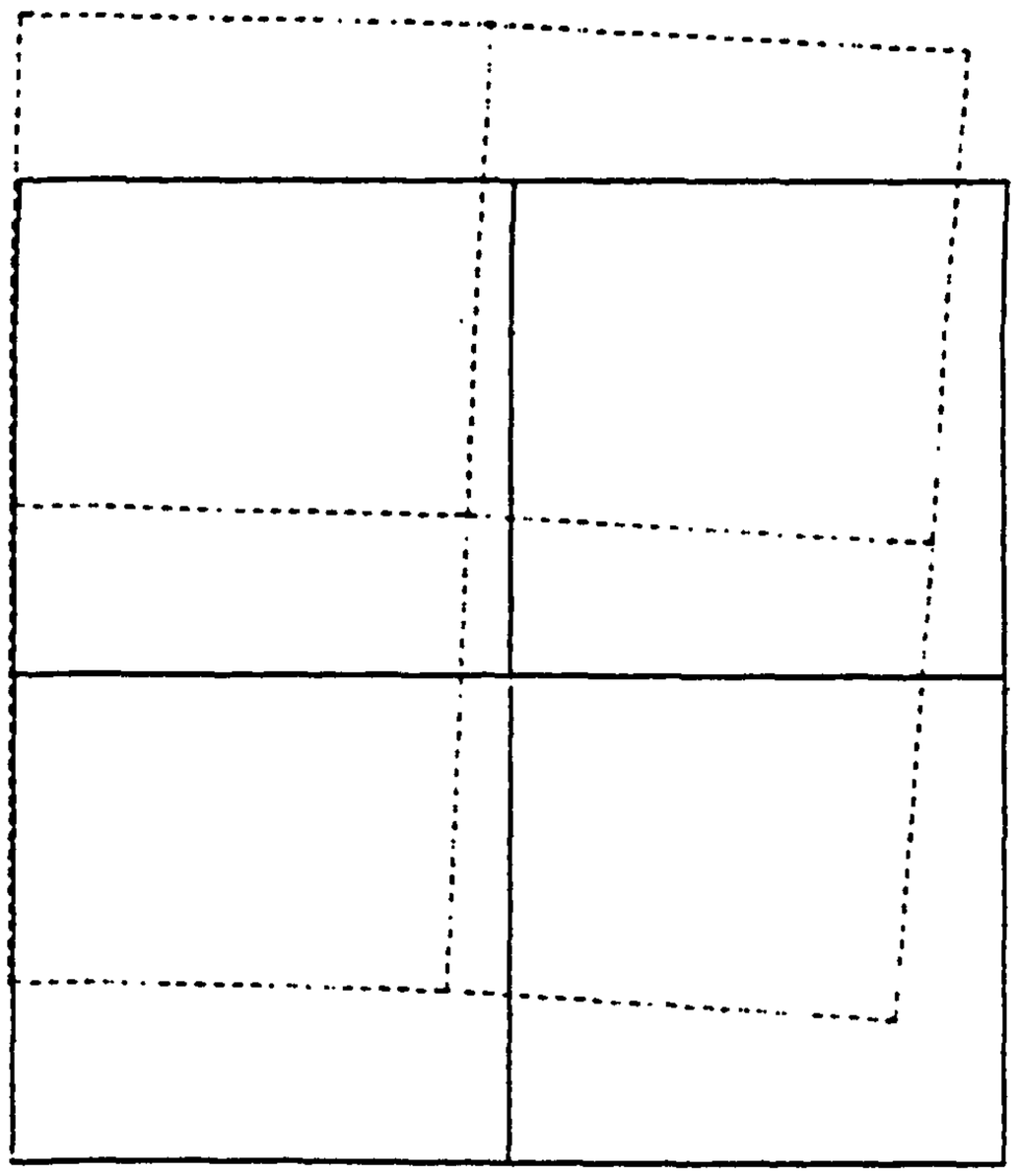
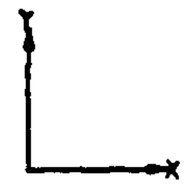


FIG (8.2) DEFORMED SHAPE of PRESSURISED COMPOSITE CYLINDER



PAFEC

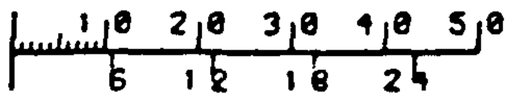
VIEW FROM X = .0000
Y = .0000
Z = 1.000



Z TOWARDS VIEWER

MODE SHAPE NUMBER 1
FREQUENCY = 0.7511 HERTZ

WHOLE STRUCTURE DRAWN
AS DEFINED IN FRONT. ORDER



mm.
STRUCTURAL UNITS

DRAWING NO. 1
SCALE = 0.1000E-1 :1
DRAWING TYPE= 1

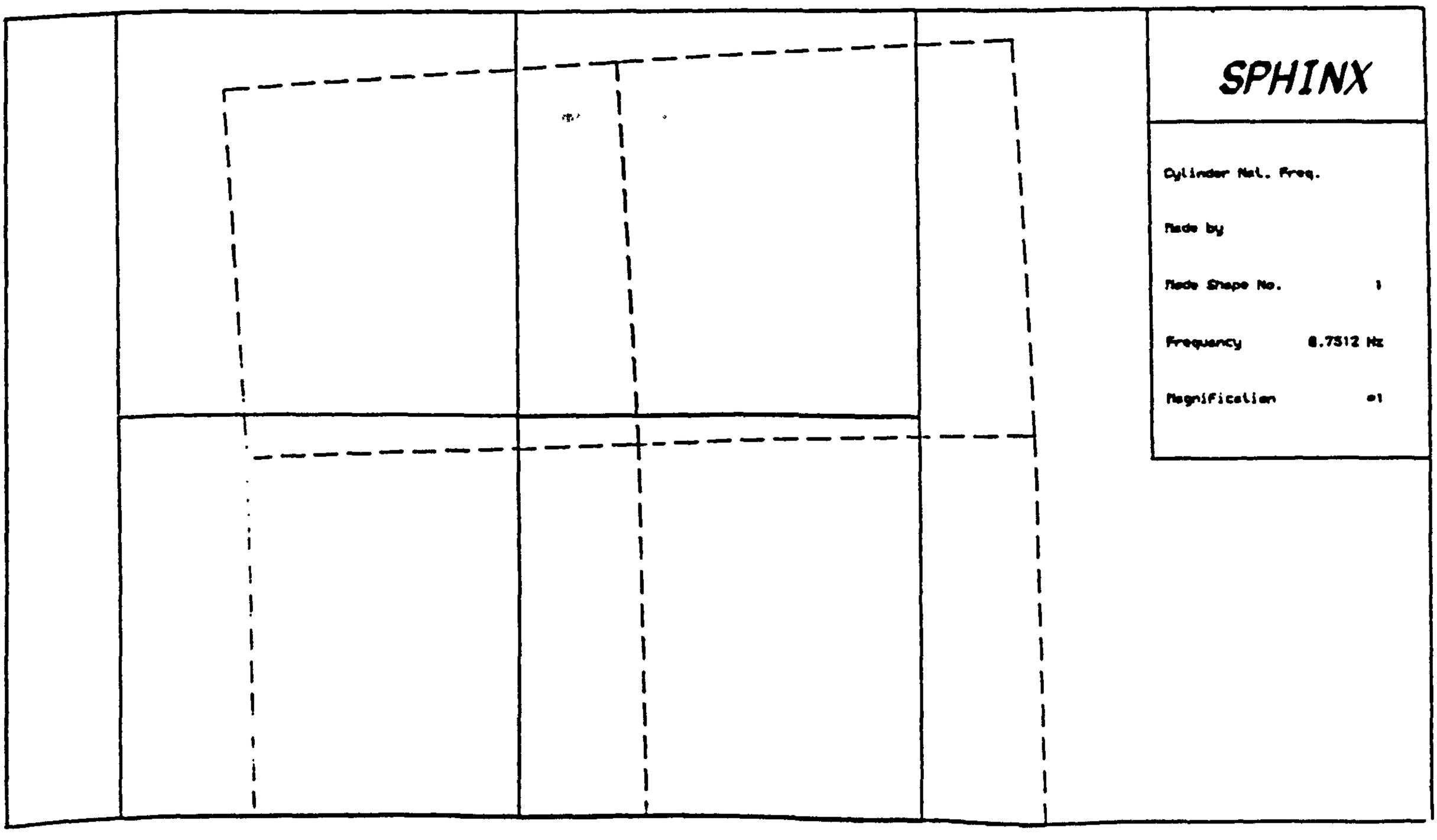
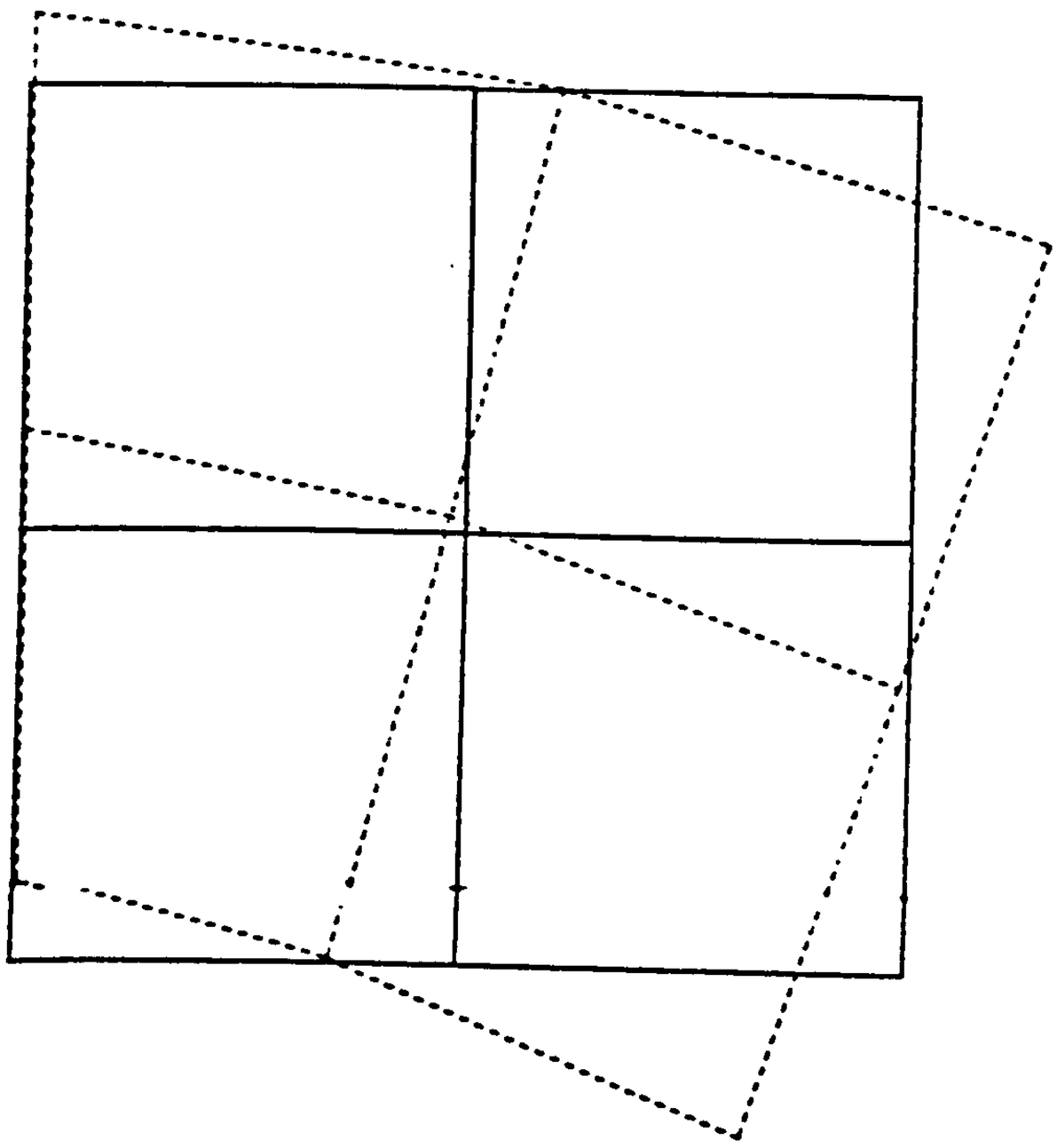


FIG.(8.3)FIRST MODE SHAPE oF CYLINDER



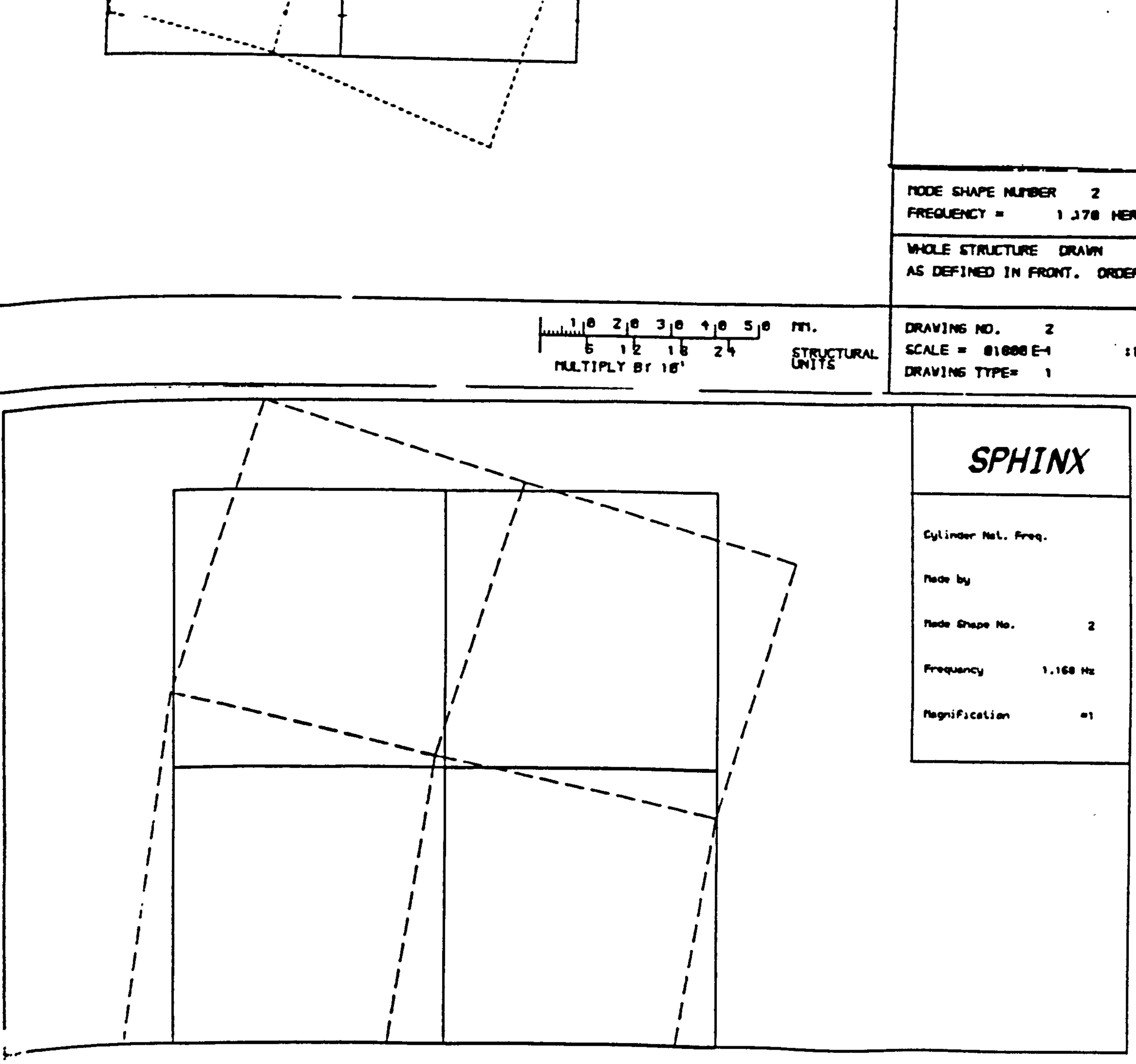
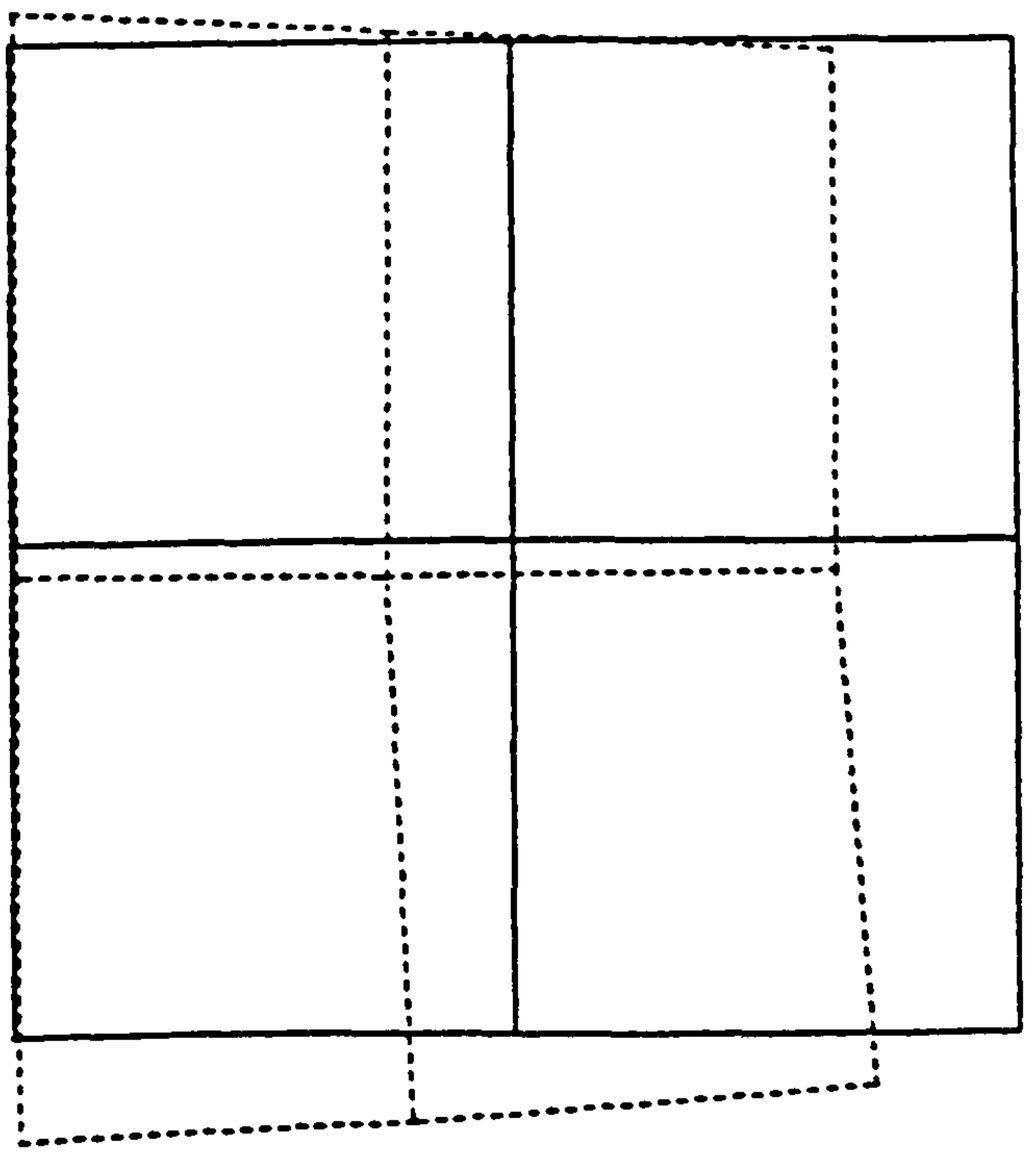


FIG.(8.4)SECOND MODE SHAPE oF CYLINDER



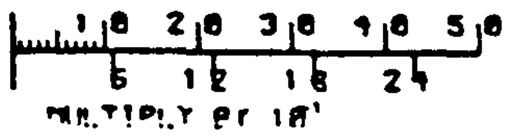
PAFEC

VIEW FROM X = .0000
Y = .0000
Z = 1.000

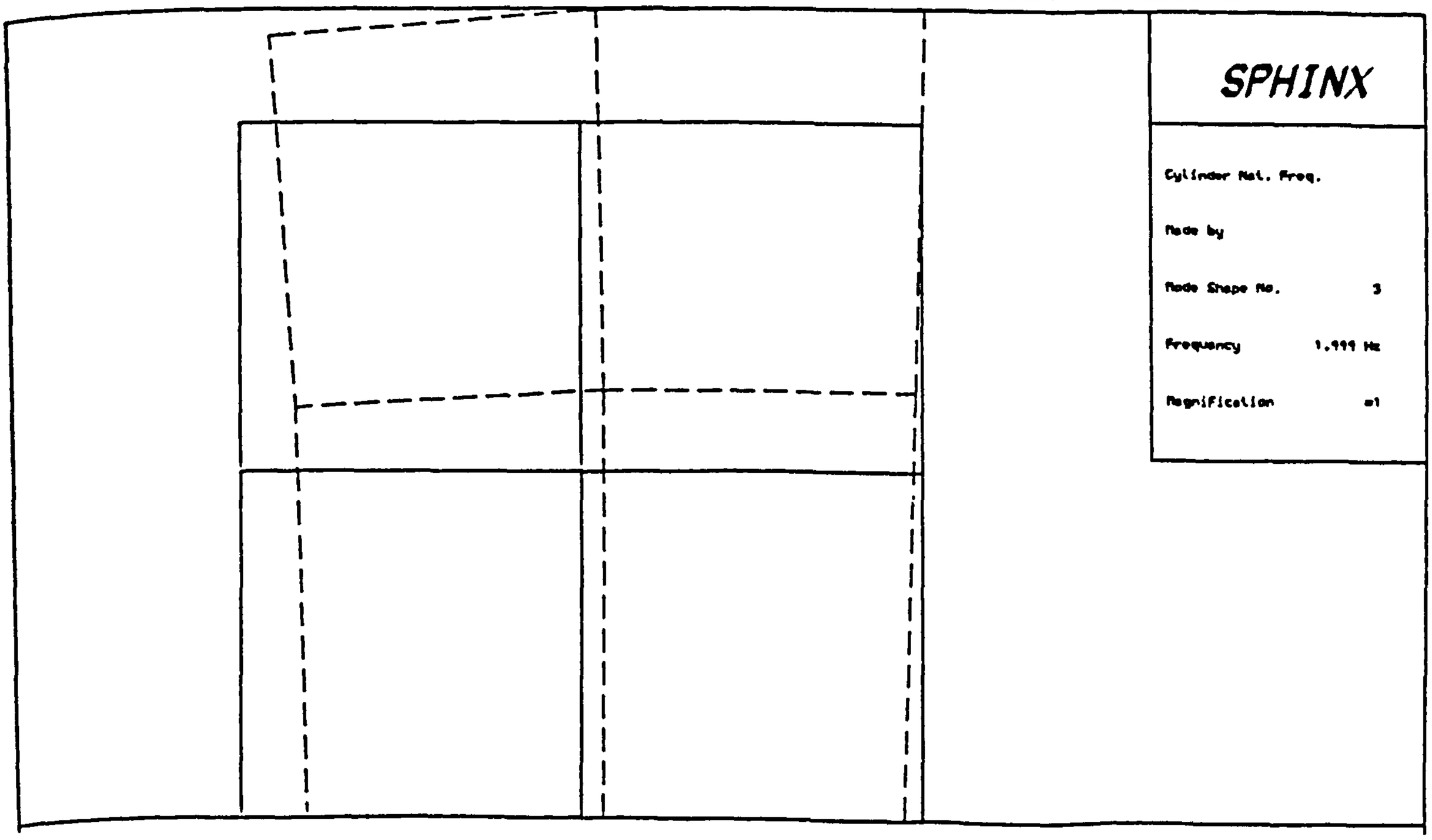
Z TOWARDS VIEWER

MODE SHAPE NUMBER 3
FREQUENCY = 1.995 HERTZ

WHOLE STRUCTURE DRAWN
AS DEFINED IN FRONT. ORDER



DRAWING NO. 3
SCALE = 0.1000E-1 :1
DRAWING TYPE= 1



SPHINX

Cylinder Nat. Freq.

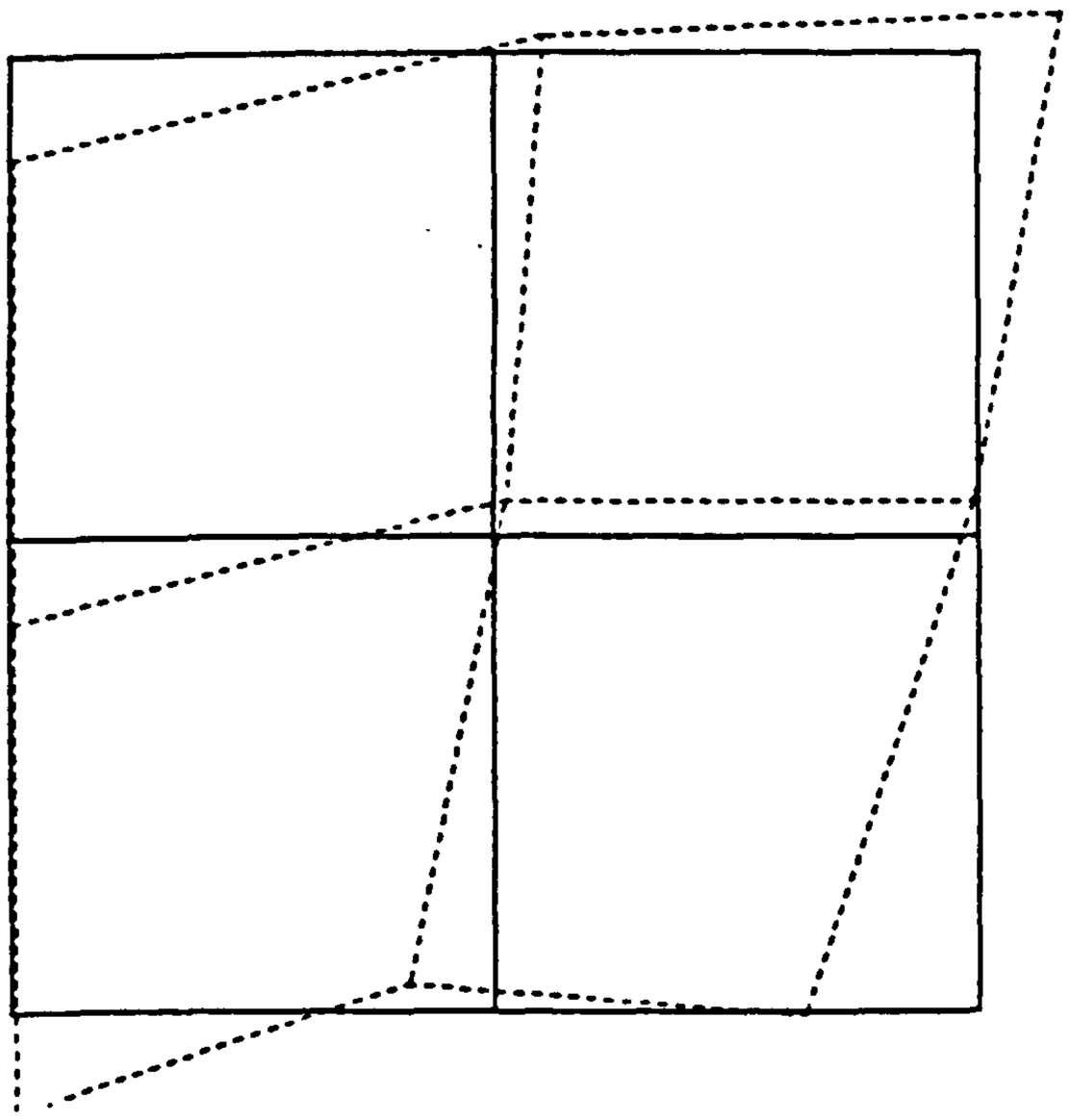
Mode by

Mode Shape No. 3

Frequency 1.999 Hz

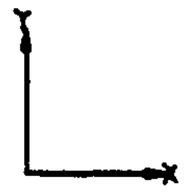
Magnification =1

FIG.(8,5)THIRD MODE SHAPE oF CYLINDER



PAFEC

VIEW FROM X = .0000
Y = .0000
Z = 1.000



Z TOWARDS VIEWER

MODE SHAPE NUMBER 4
FREQUENCY = 2.663 HERTZ

WHOLE STRUCTURE DRAWN
AS DEFINED IN FRONT. ORDER



DRAWING NO. 4
SCALE = .01000 E+4 :1
DRAWING TYPE= 1

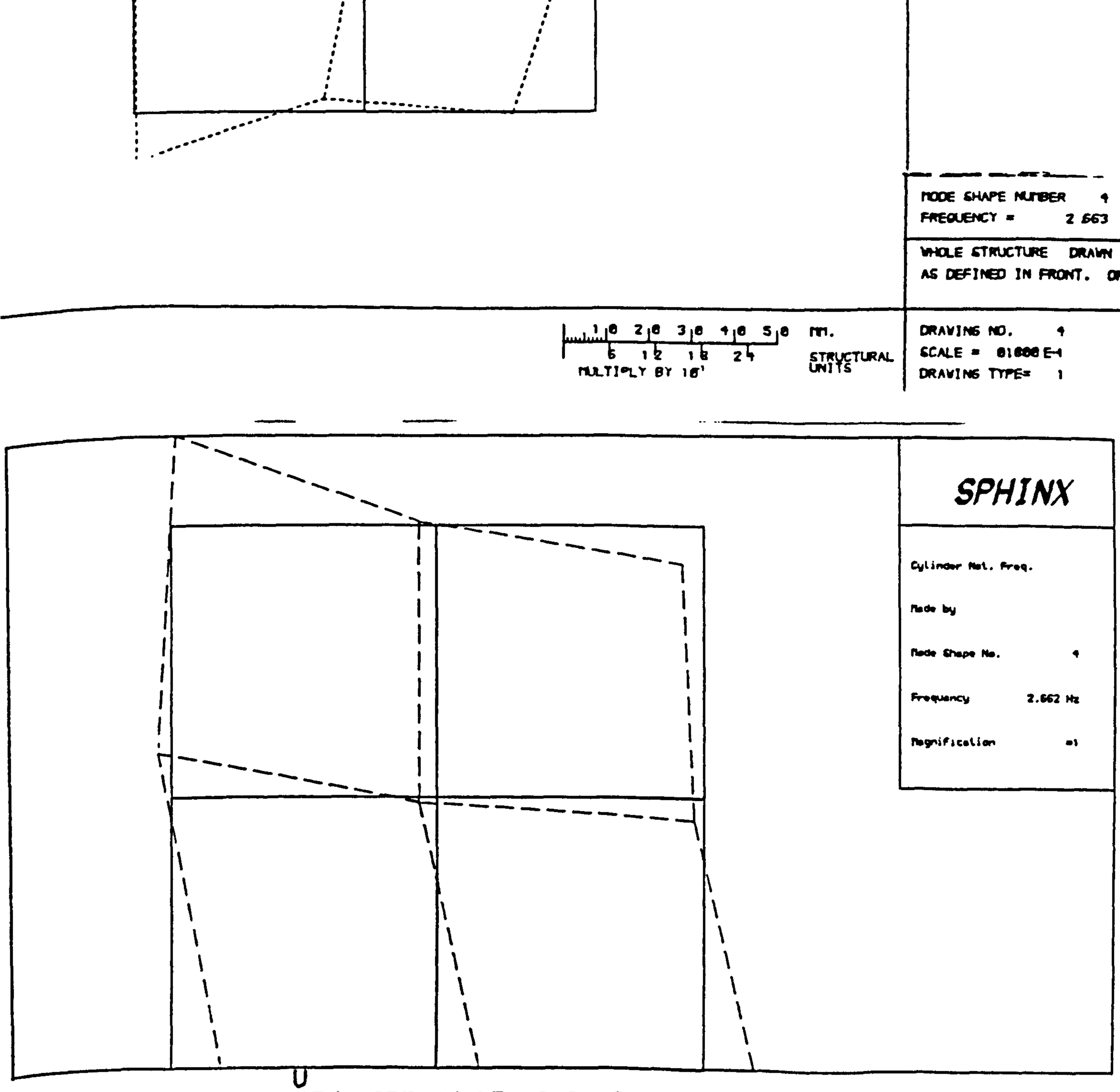
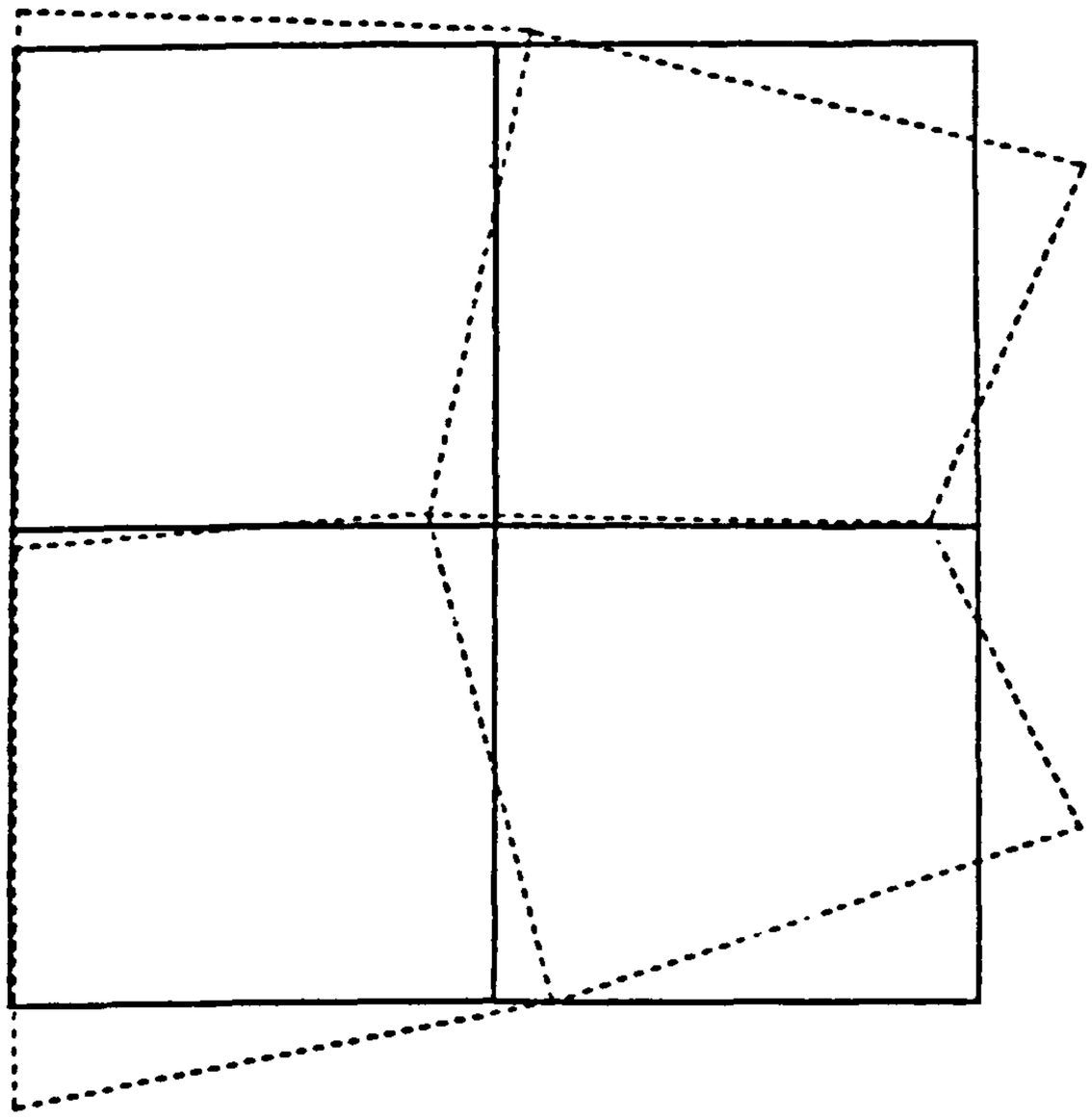
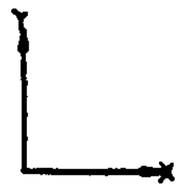


FIG.(8.6)FOURTH MODE SHAPE OF CYLINDER



PAFEC

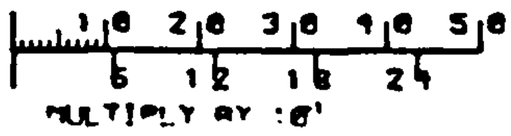
VIEW FROM X = .0000
Y = .0000
Z = 1.000



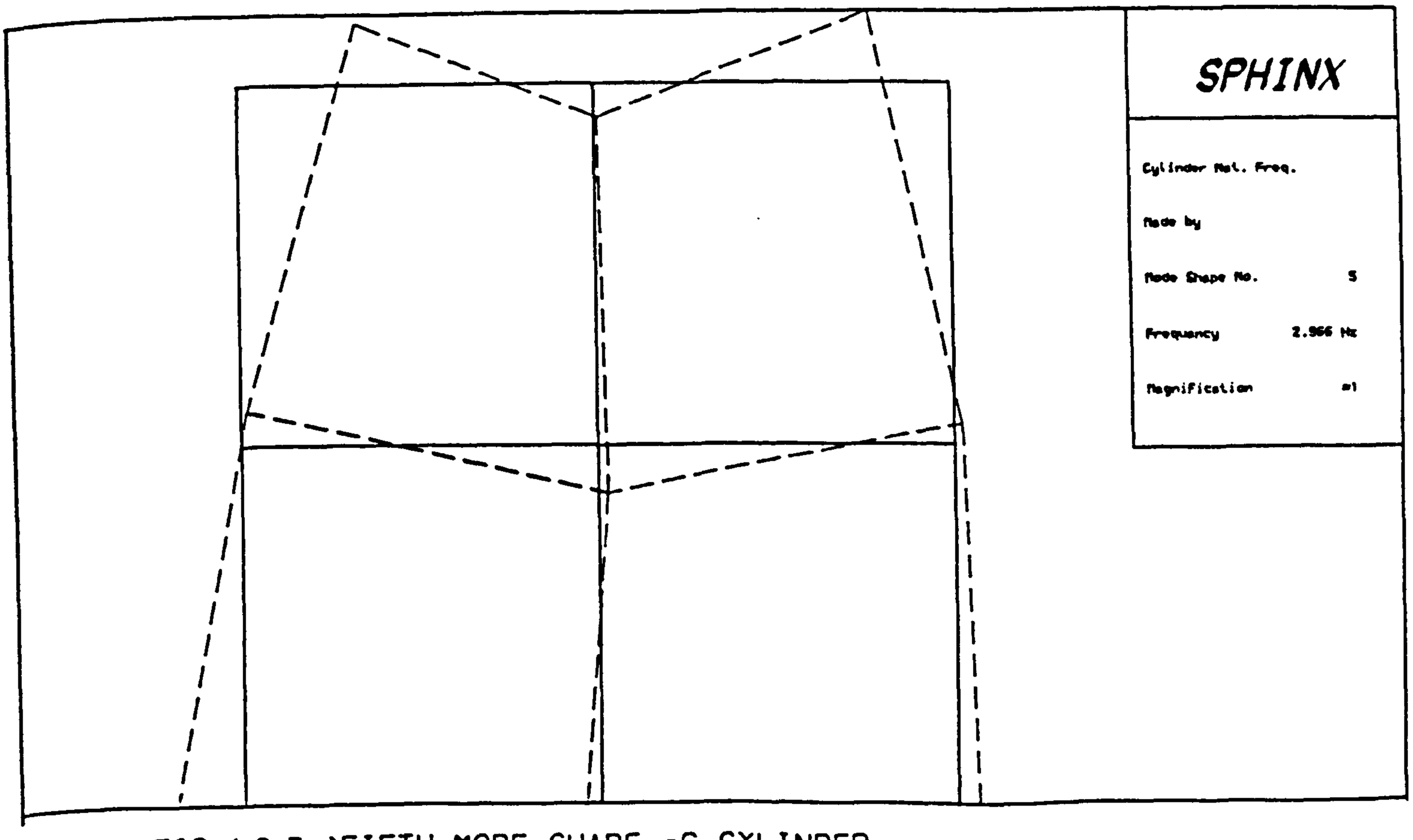
Z TOWARDS VIEWER

MODE SHAPE NUMBER 5
FREQUENCY = 2.966 HERTZ

WHOLE STRUCTURE DRAWN
AS DEFINED IN FRONT. ORDER



DRAWING NO. 5
SCALE = 0.1000E-1
DRAWING TYPE= 1



SPHINX

Cylinder Nat. Freq.

Mode by

Mode Shape No. 5

Frequency 2.966 Hz

Magnification =1

FIG.(8.7)FIFTH MODE SHAPE oF CYLINDER

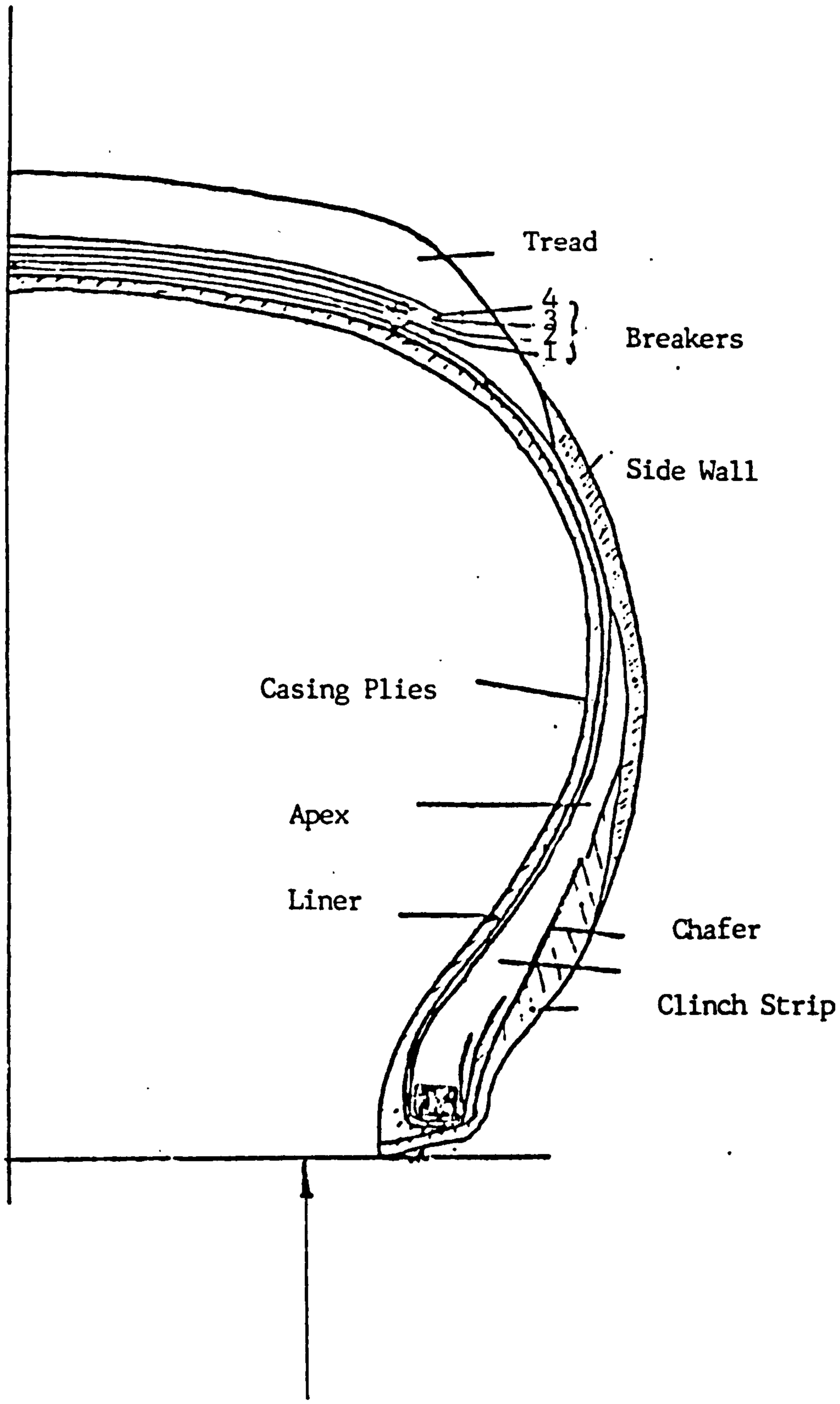


Fig.(8.8) CROSS SECTION OF 175-HR-14 RADIAL TYRE

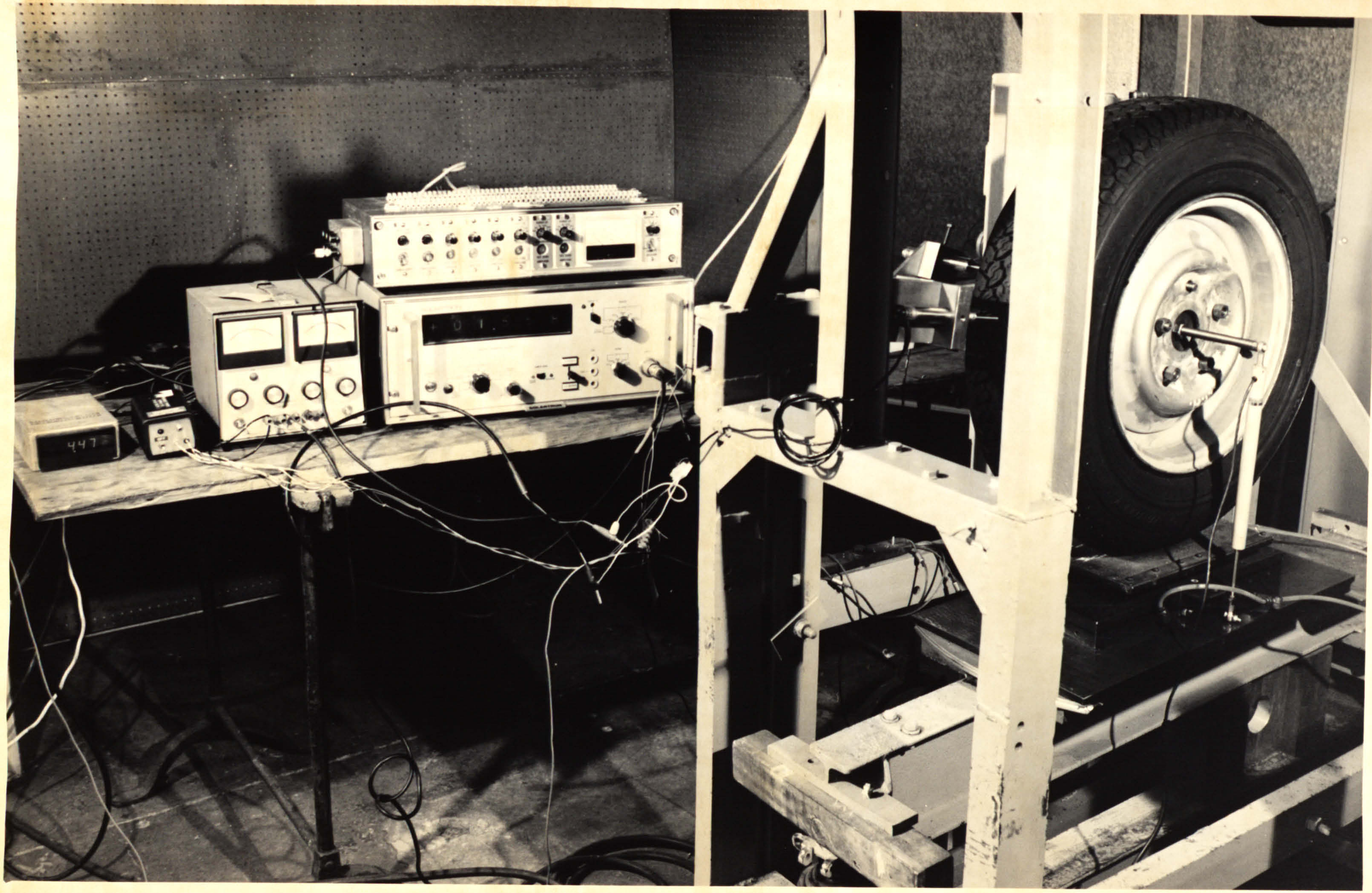


Fig. (8,9) TEST RIG

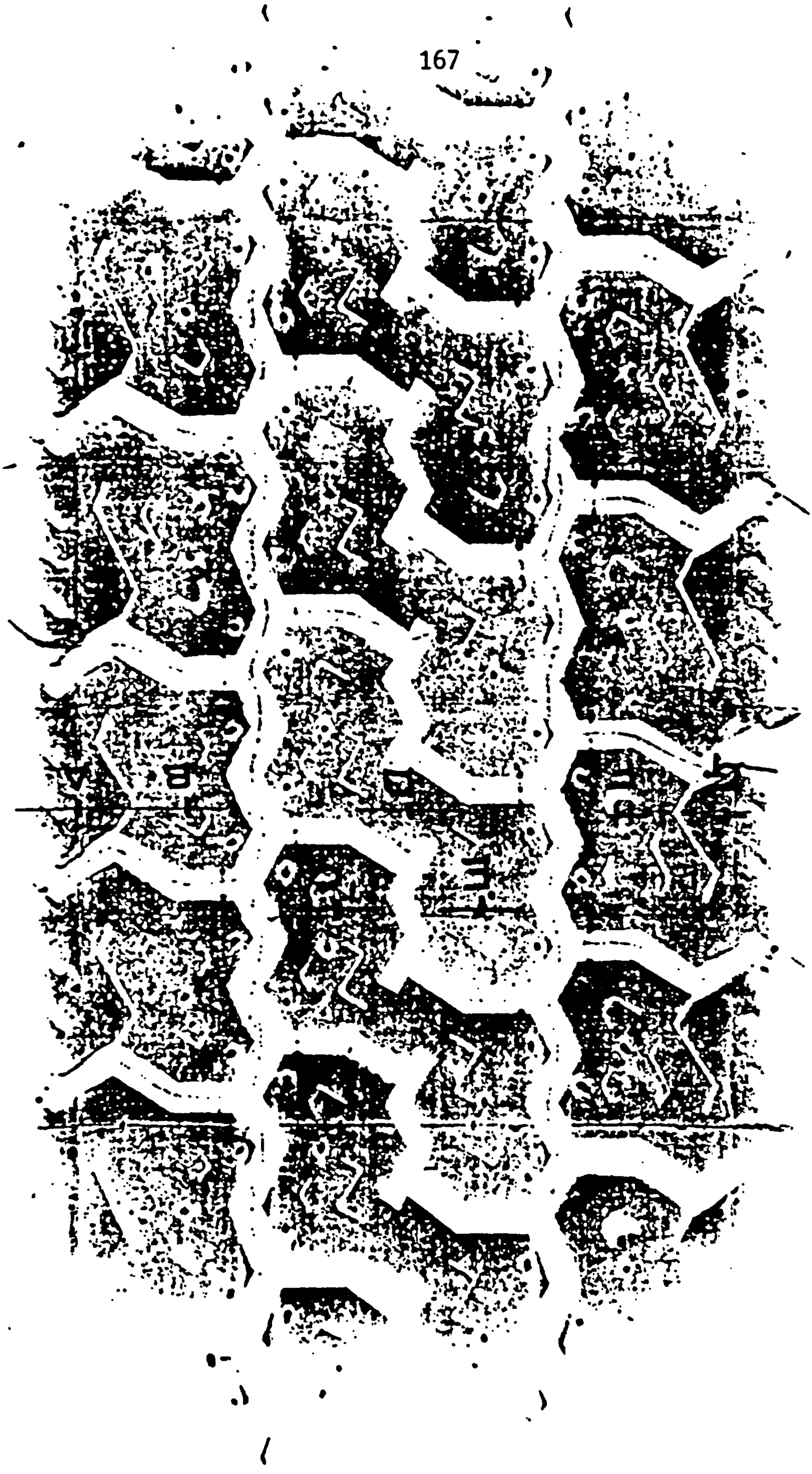
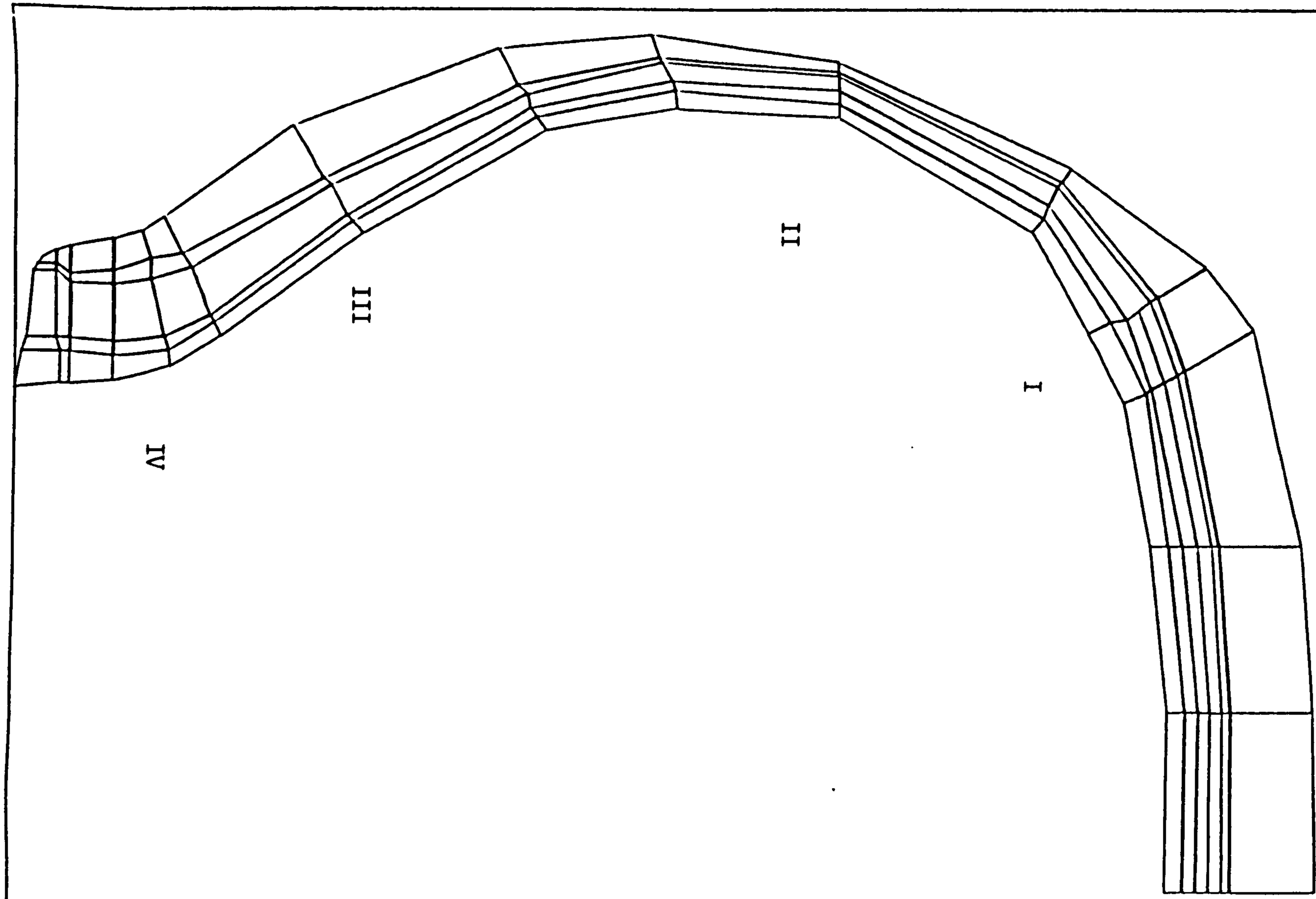


Fig.(8.10) AREA OF CONTACT AND PRESSURE DISTRIBUTION
FOR EXTERNALLY LOADED RADIAL TYRE



SPHINX	
Tyre Size	175HR14
Made	DUNLOP
Inflation Pressure	bar
------	I.P.=0.0
Radial Load	=0.0 Kg
Damp.Co.	=0.0

FIG (8.11a) MESH BLOCKS of RADIAL TYRE

SPHINX

Tyre Size 175HR14

Make DUNLOP

Inflation Pressure bar

..... 1.0.-0.8

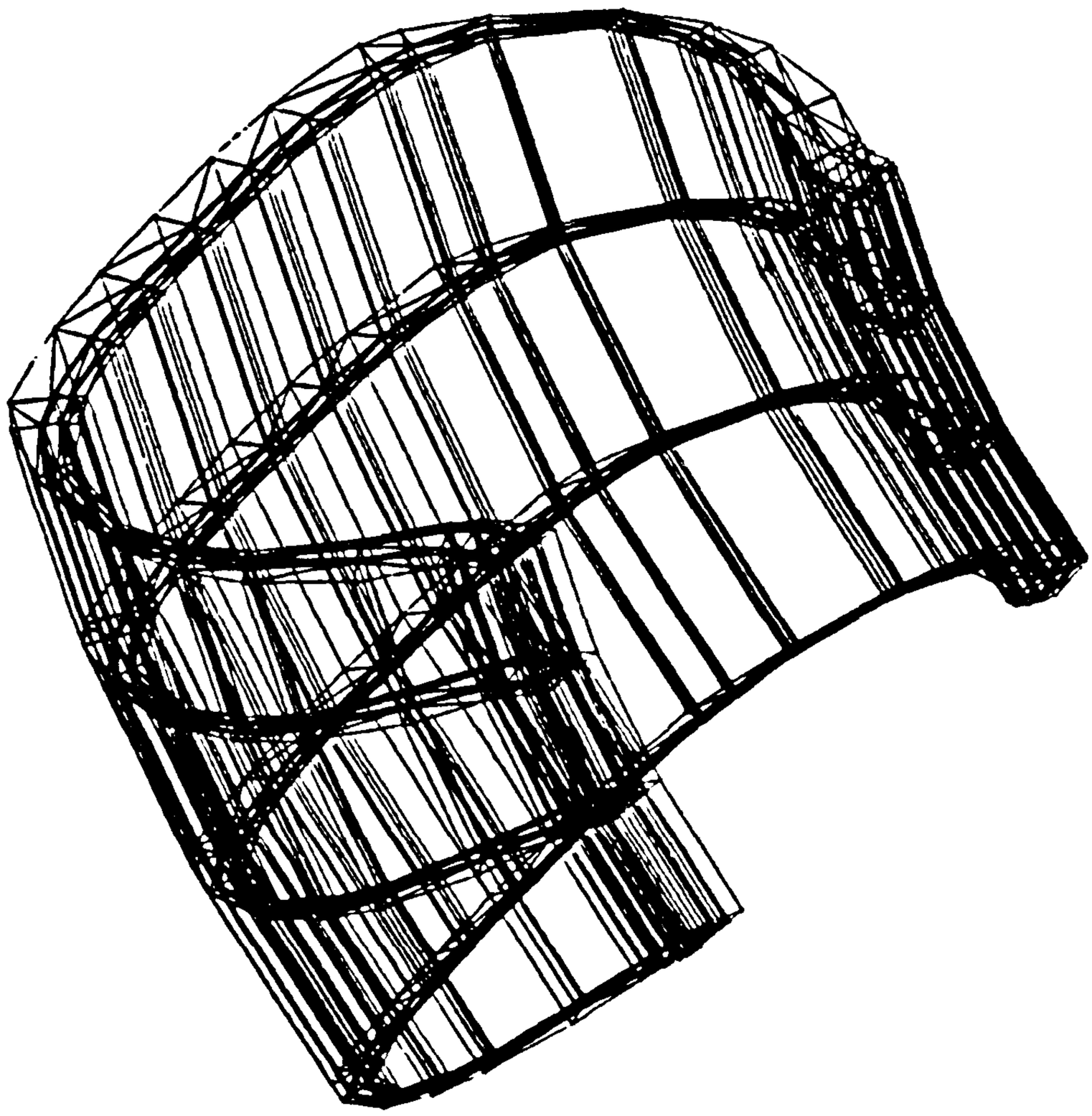


Fig. (8.11b) THREE DIMENSIONAL PLOTTING OF RADIAL TYRE

SPHINX

Tyre Size 175HR14

Made DUNLOP

Inflation Pressure bar

---- I.P.=0.0

Radial Load =0.0 Kg

Damp.Co. =0.0

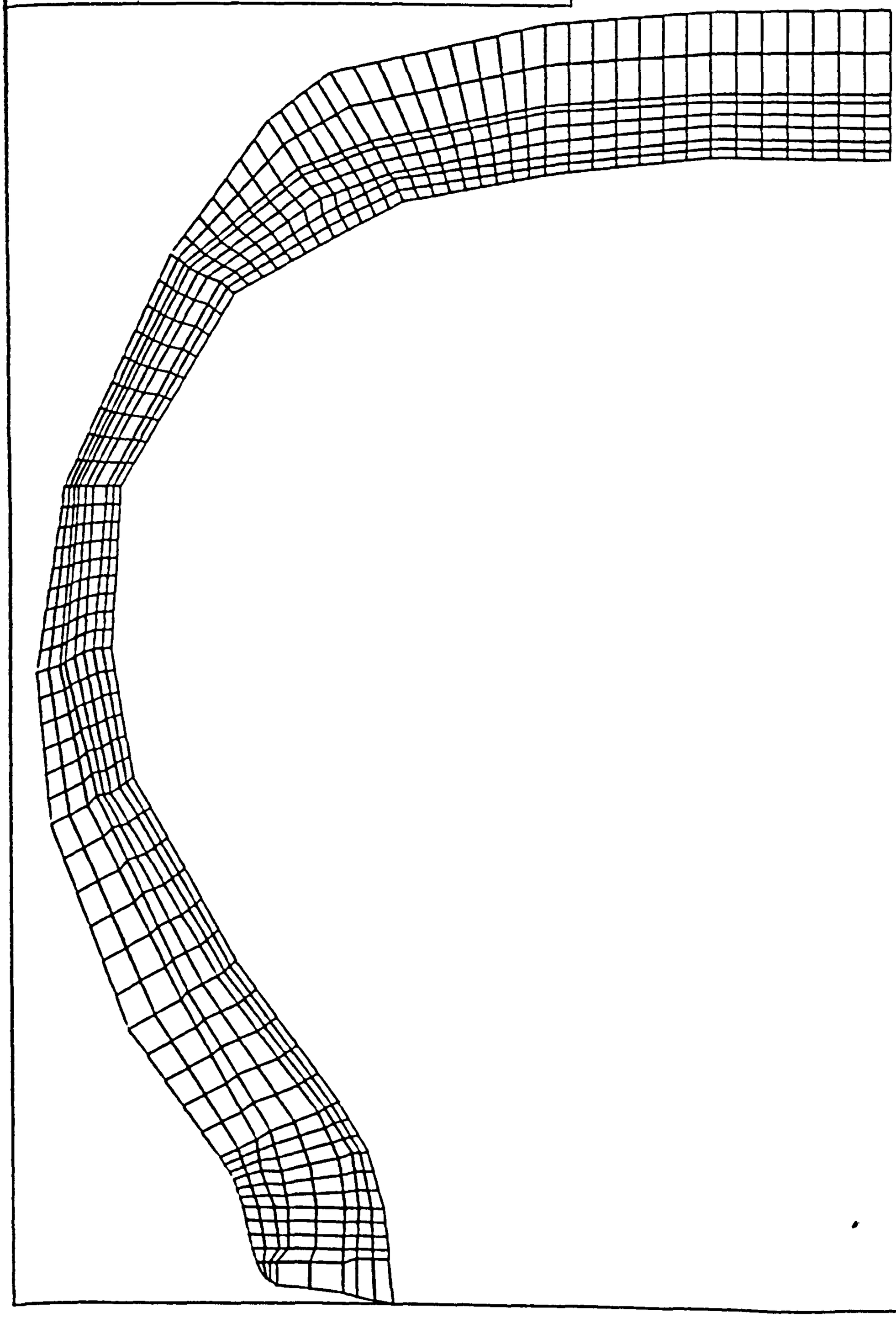


FIG (8.12)3-D RADIAL TYRE

SPHINX

Tyre Size 175HR14

Made by DUNLOP

Inflation Pressure bar

----- I.P.=0.0

- - - - I.P.=2.0

Radial Load =0.0 Kg

Damp.Coef. =0.0

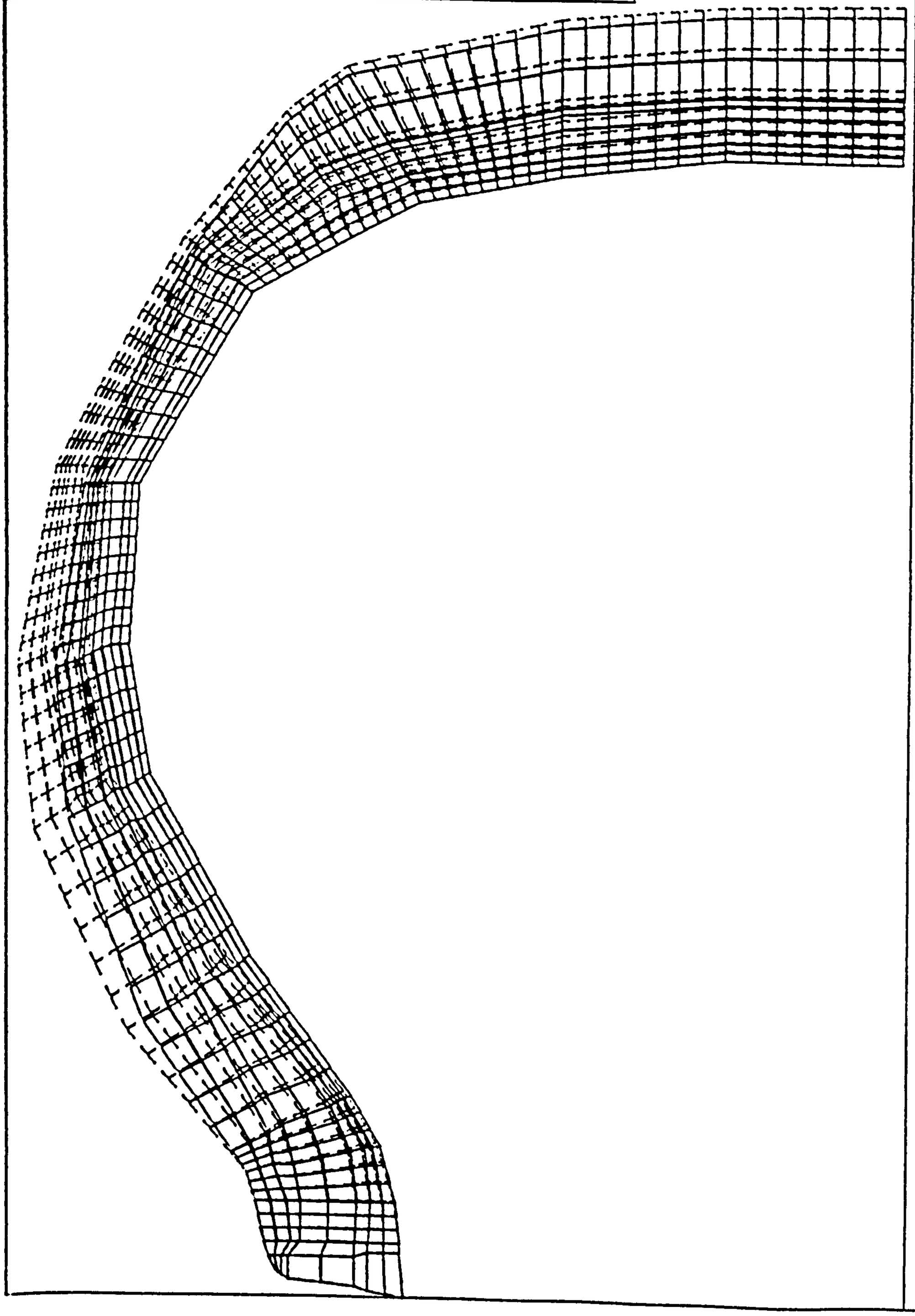


Fig.(8.13) Deformed Shape of An Inflated Radial Tyre

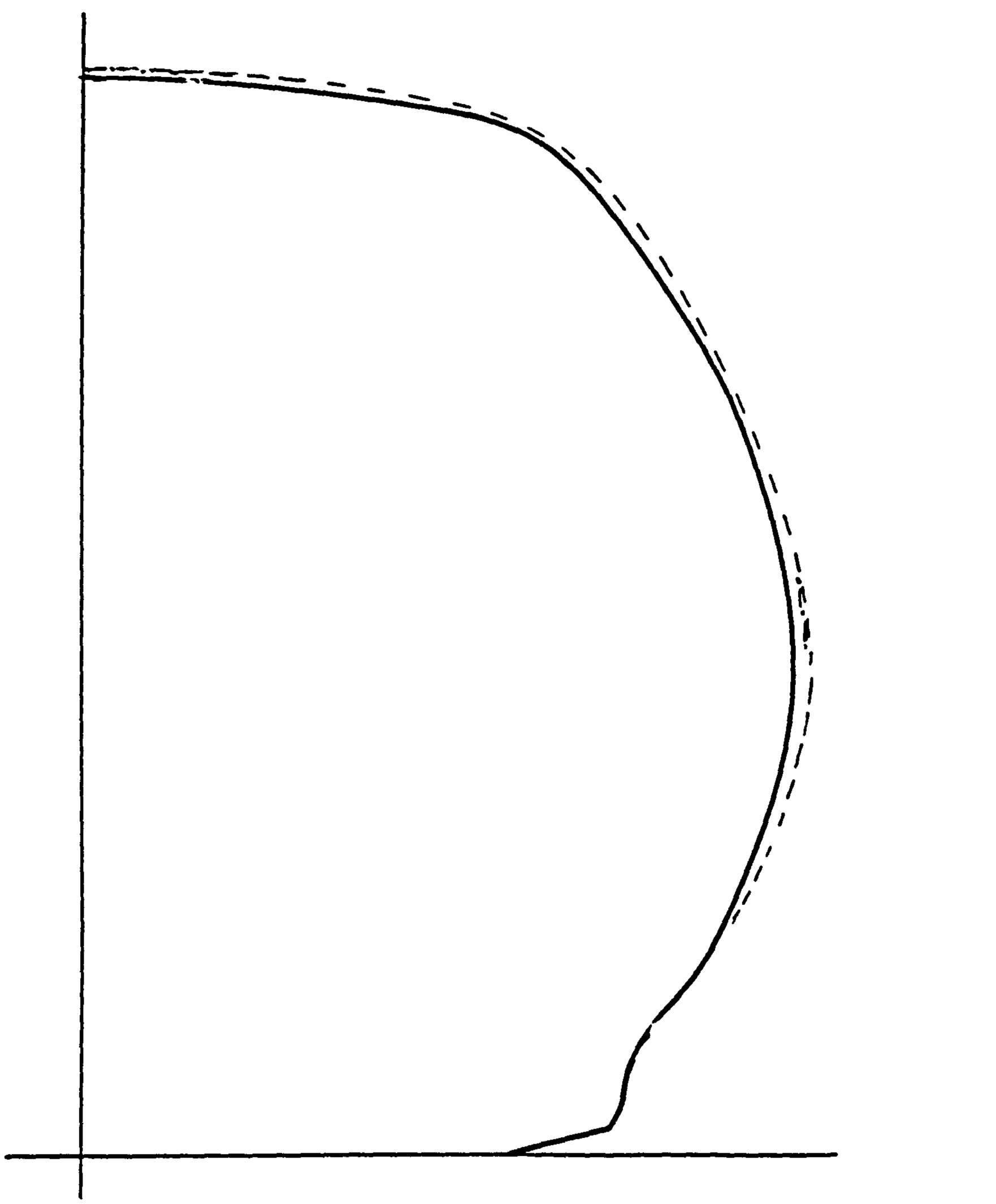


FIG. (8.14) THE DEFORMED SHAPE OF 175 HR 14 (EXP. - ANALYTICAL)

SPHINX

Tyre Size 175HR14

Made by DUNLOP

Inflation Pressure bar

_____ I.P.=0.0

- - - - I.P.=2.0

Radial Load =500.0 Kg

Damp.Coef. =0.0

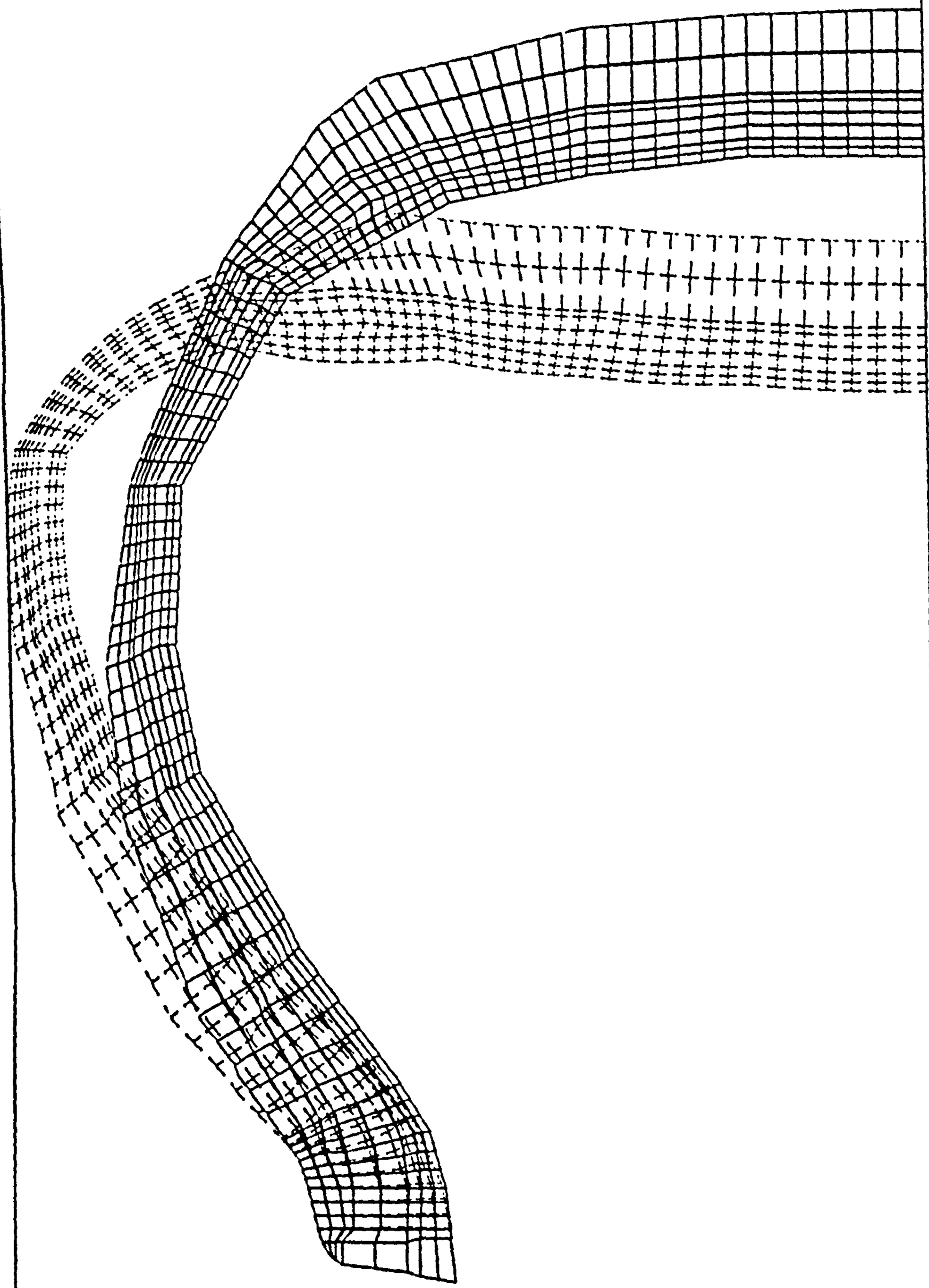


Fig.(:8.15a) Deformed Shape of External Radially Loaded Radial Tyre

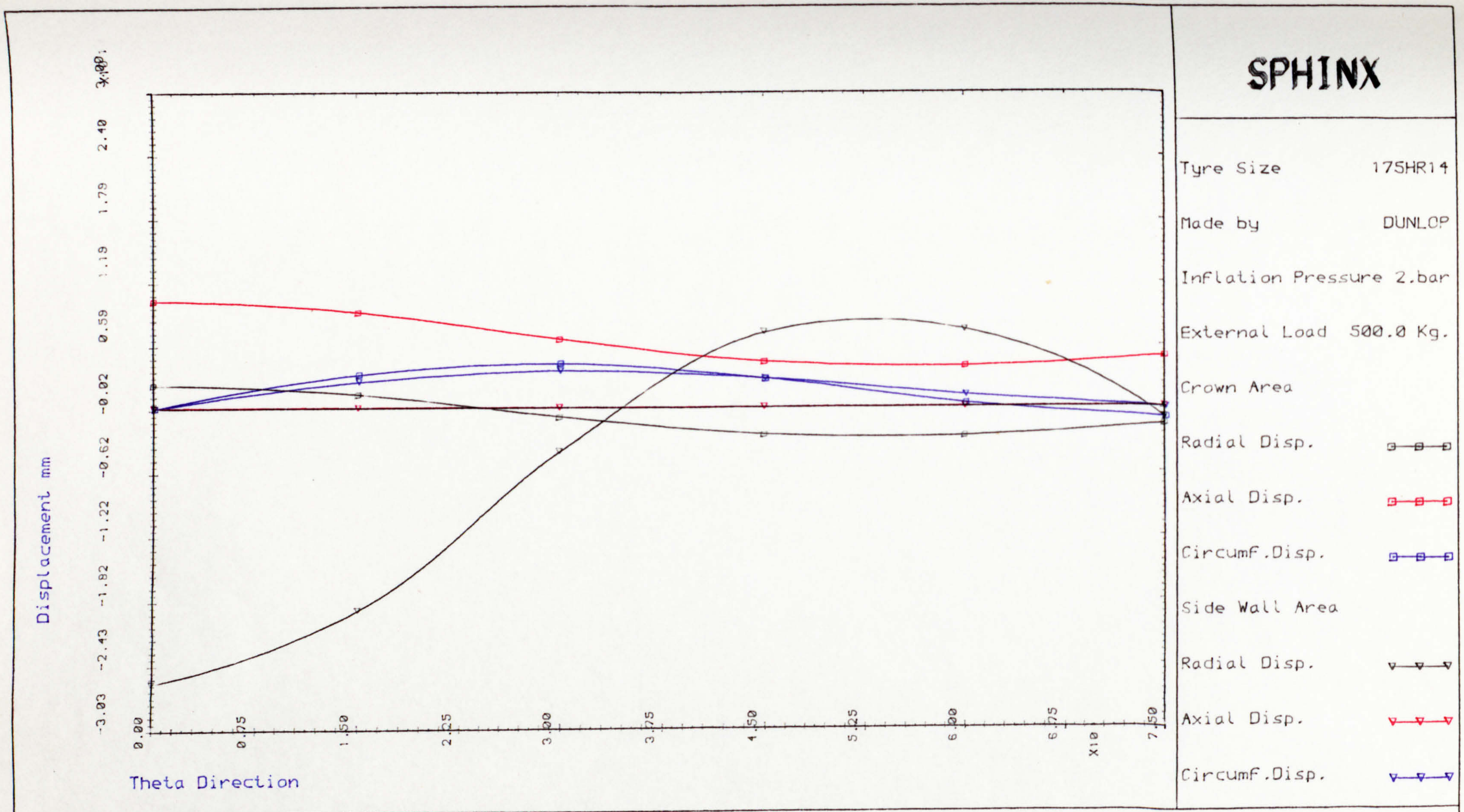


Fig.(8.15 b)Radial and Axial Displacements in The Circumferential Direction for Externally Loaded Tyre

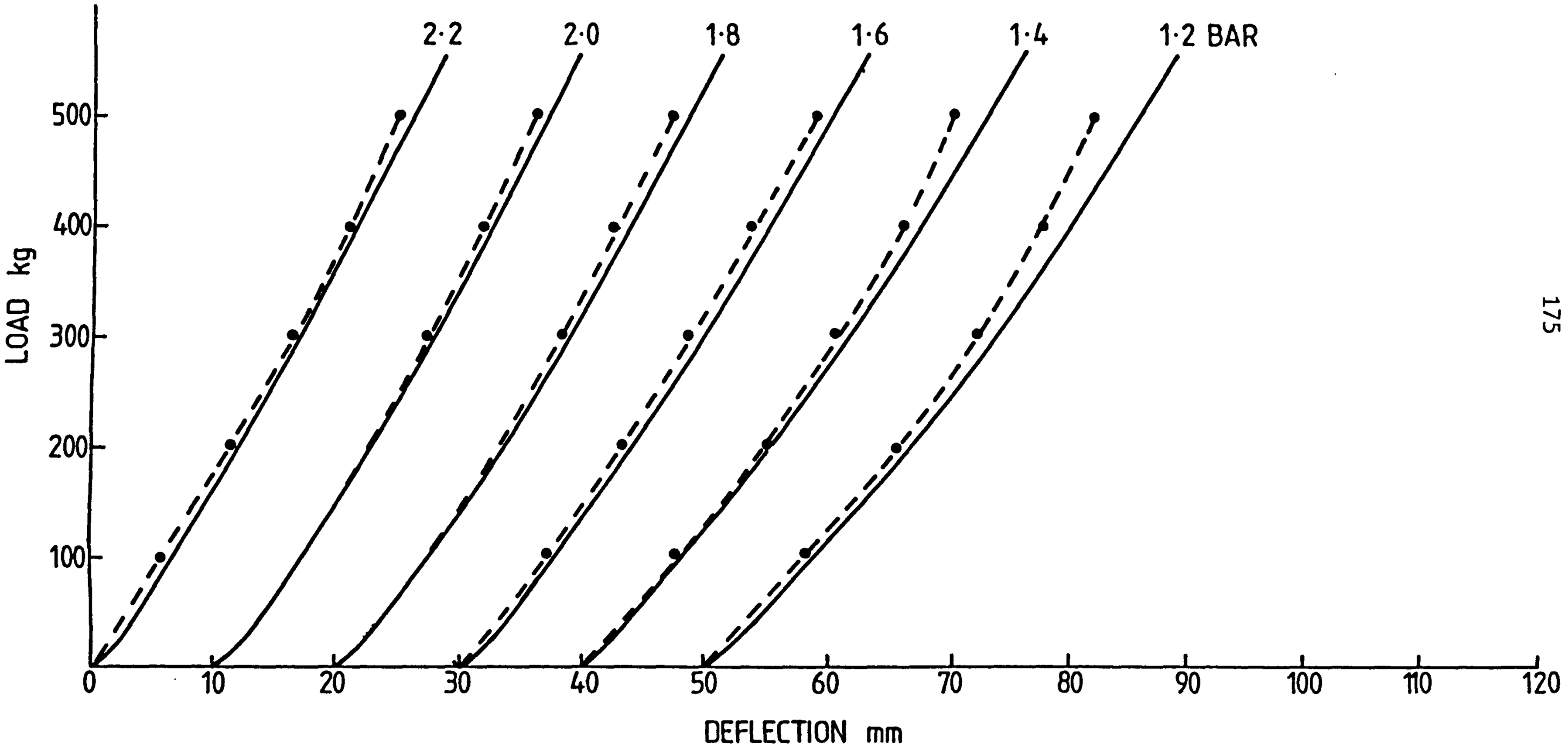


FIG.(8.16) LOAD DEFLECTION CURVES of 175 HR 14 RADIAL TYPE

SPHINX

Tyre Size 175HR14

Made by DUNLOP

Inflation Pressure bar

Inflation Pressure =2.0

External Load 0.0Kg.

Damping Co. 0.0

Scale 1 mm=1.0 Kgf/mm2

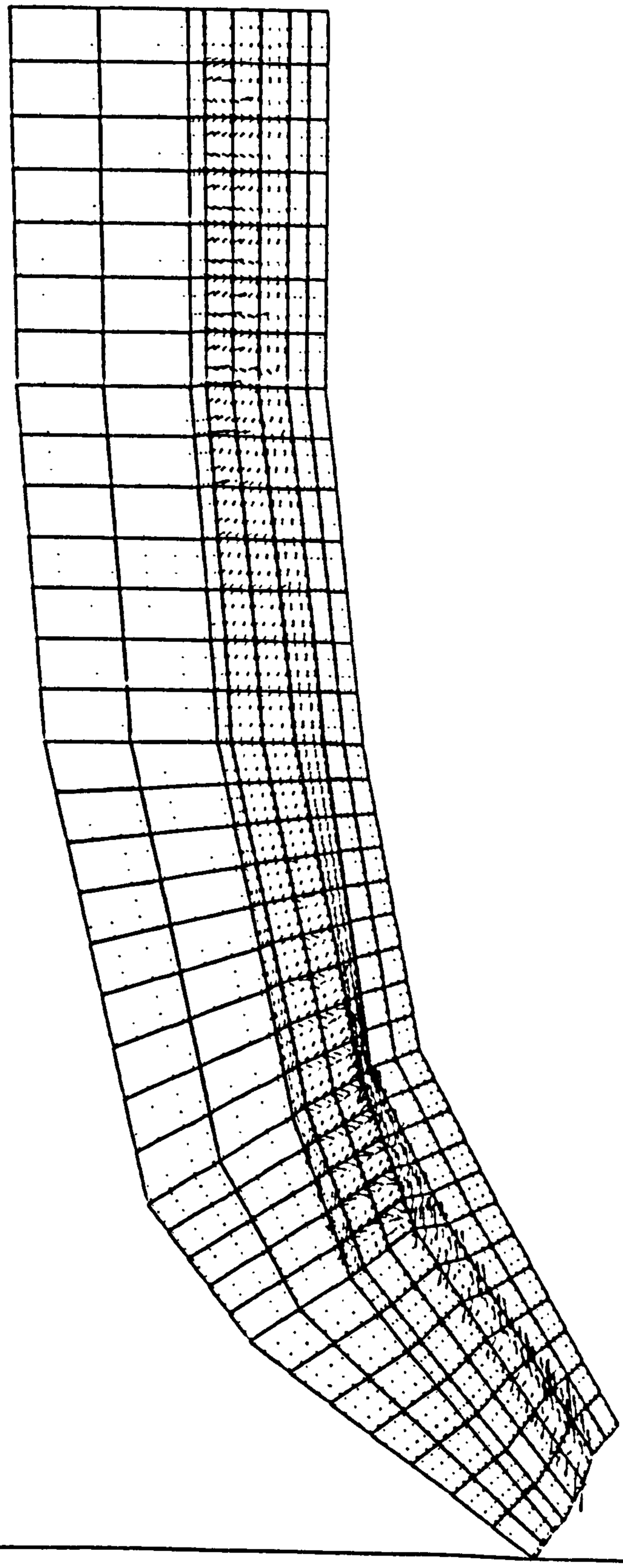
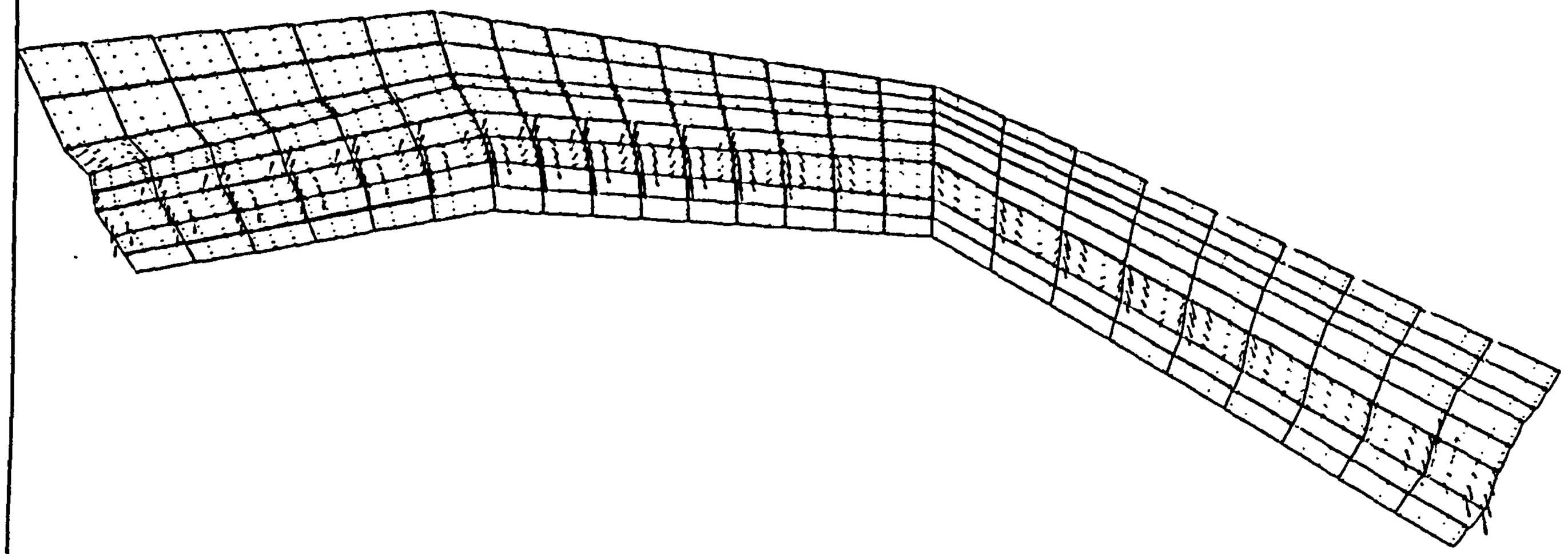


FIG (8.17) Stress Destribution in Section I
OF The Radial Tyre



SPHINX

Tyre Size	175HR14
Made by	DUNLOP
Inflation Pressure	bar
Inflation Pressure	=2.0
External Load	0.0Kg.
Damping Co.	0.0
Scale	1 mm=1.0 KgF/mm2

FIG (8.18) Stress Destribution in Section II
Of The Radial Tyre

SPHINX

Tyre Size 175HR14

Made by DUNLOP

Inflation Pressure bar

Inflation Pressure =2.0

External Load 0.0Kg.

Damping Co. 0.0

Scale 1 mm=1.0 Kgf/mm2

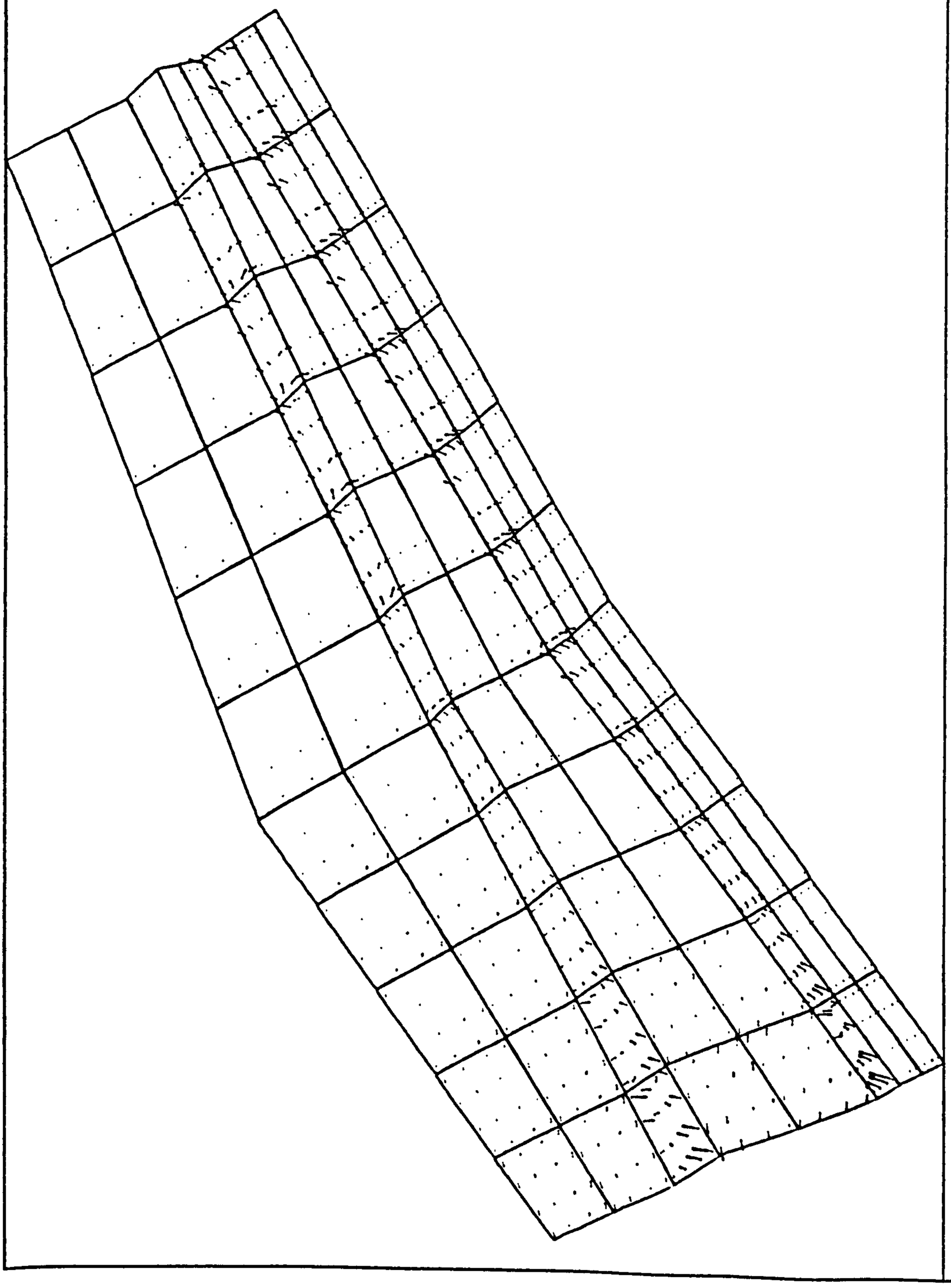


FIG (8.19) Stress Destribution in Section III Of The Radial Tyre

SPHINX

Tyre Size 175HR14

Made by DUNLOP

Inflation Pressure bar

Inflation Pressure =2.0

External Load 0.0Kg.

Damping Co. 0.0

Scale 1 mm=1.0 Kgf/mm2

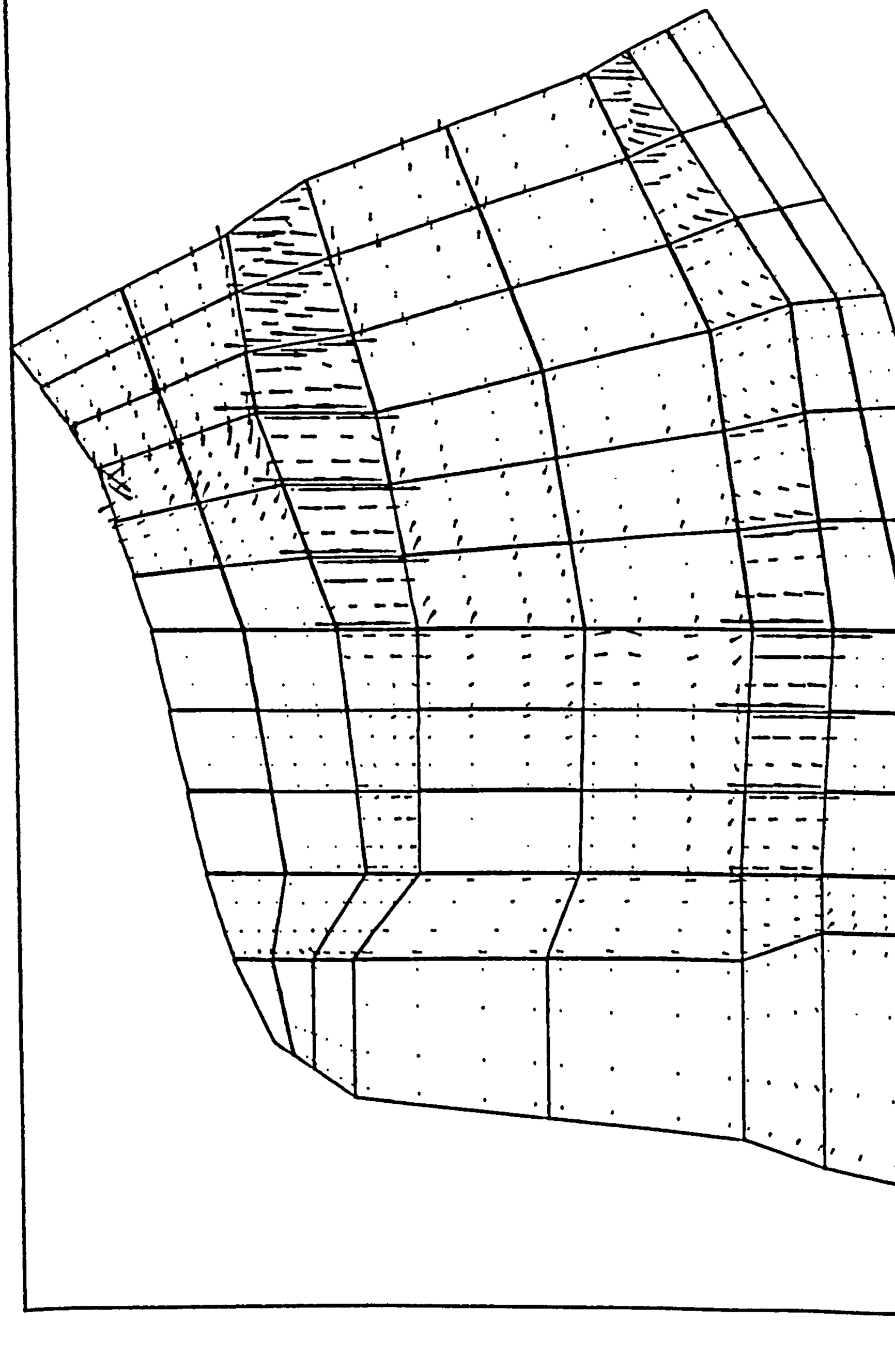


FIG (8.20) Stress Destribution in Section IV
OF The Radial Tyre

SPHINX

Tyre Size 175HR14

Made by DUNLOP

Inflation Pressure bar

Inflation Pressure =2.0

External Load 500.0Kg.

Damping Coef. 0.0

Scale 1 mm=0.25 Kgf/mm2

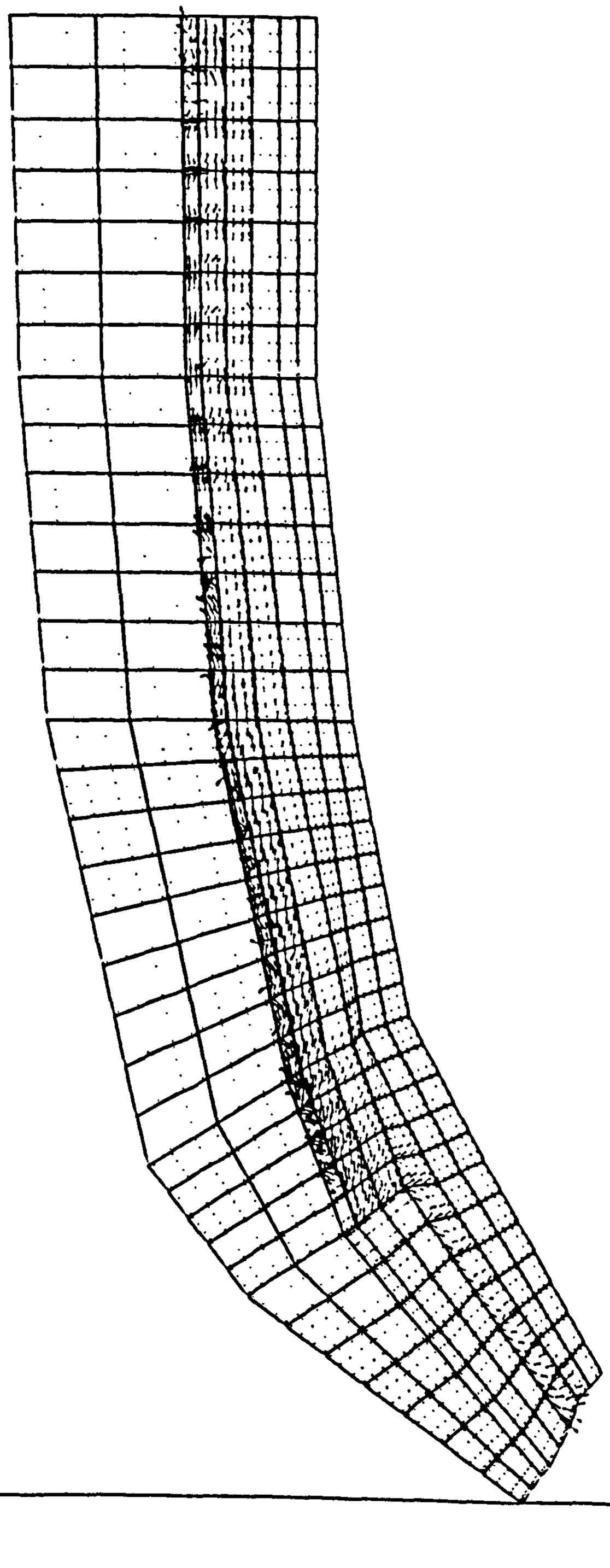
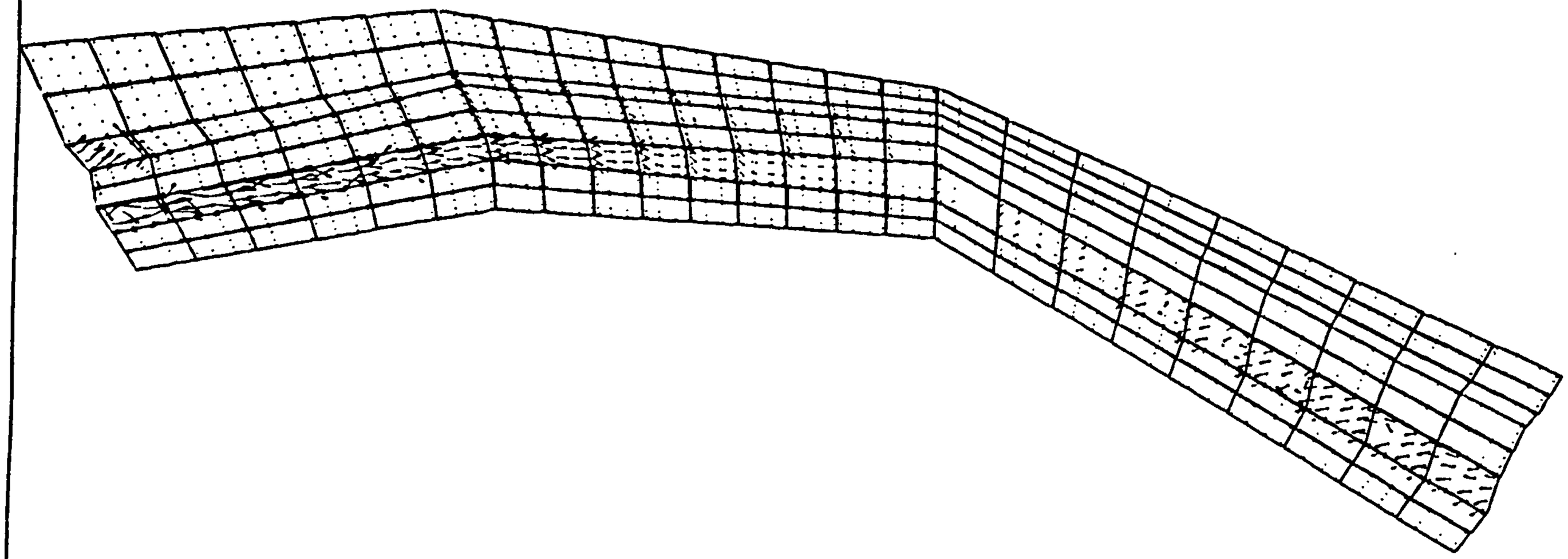


FIG (8.21) Stress Destribution in Section I
OF An Externally Loaded Radial Tyre



SPHINX

Tyre Size	175HR14
Made by	DUNLOP
Inflation Pressure	bar
Inflation Pressure	=2.0
External Load	500.0Kg.
Damping Coof.	0.0
Scale	1 mm=0.25 KgF/mm2

FIG (8.22) Stress Destribution in Section II
OF An Externally Loaded Radial Tyre

SPHINX

Tyre Size	175HR14
Made by	DUNLOP
Inflation Pressure	bar
Inflation Pressure	=2.0
External Load	500.0Kg.
Damping Coof.	0.0
Scale	1 mm=0.25 Kgf/mm2

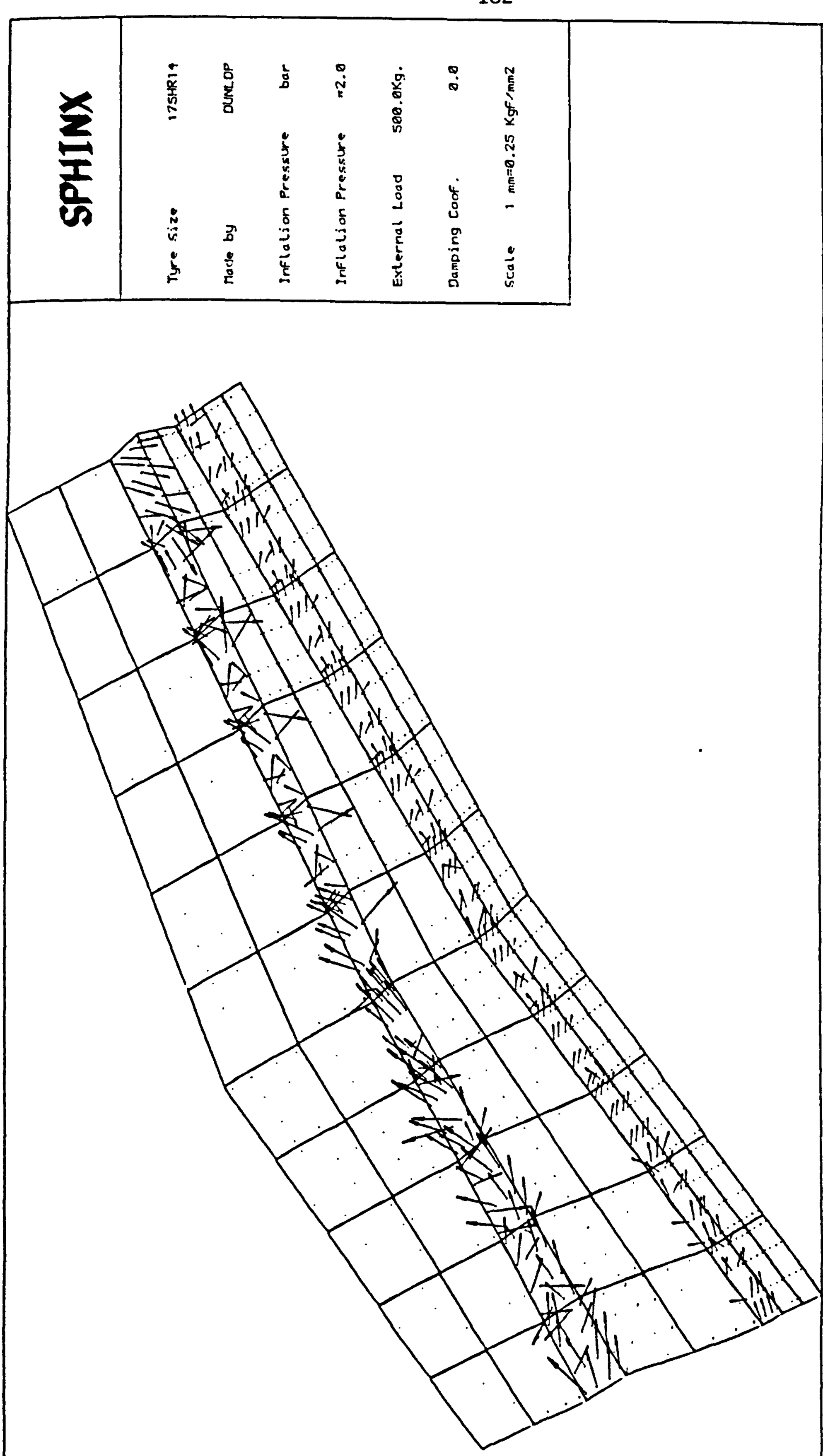


FIG (8.23) Stress Destribution in Section III
OF An Externally Loaded Radial Tyre

SPHINX

Tyre Size 175HR14

Made by DUNLOP

Inflation Pressure bar

Inflation Pressure =2.0

External Load 500.0Kg.

Damping Coof. 0.0

Scale 1 mm=0.25 Kgf/mm2

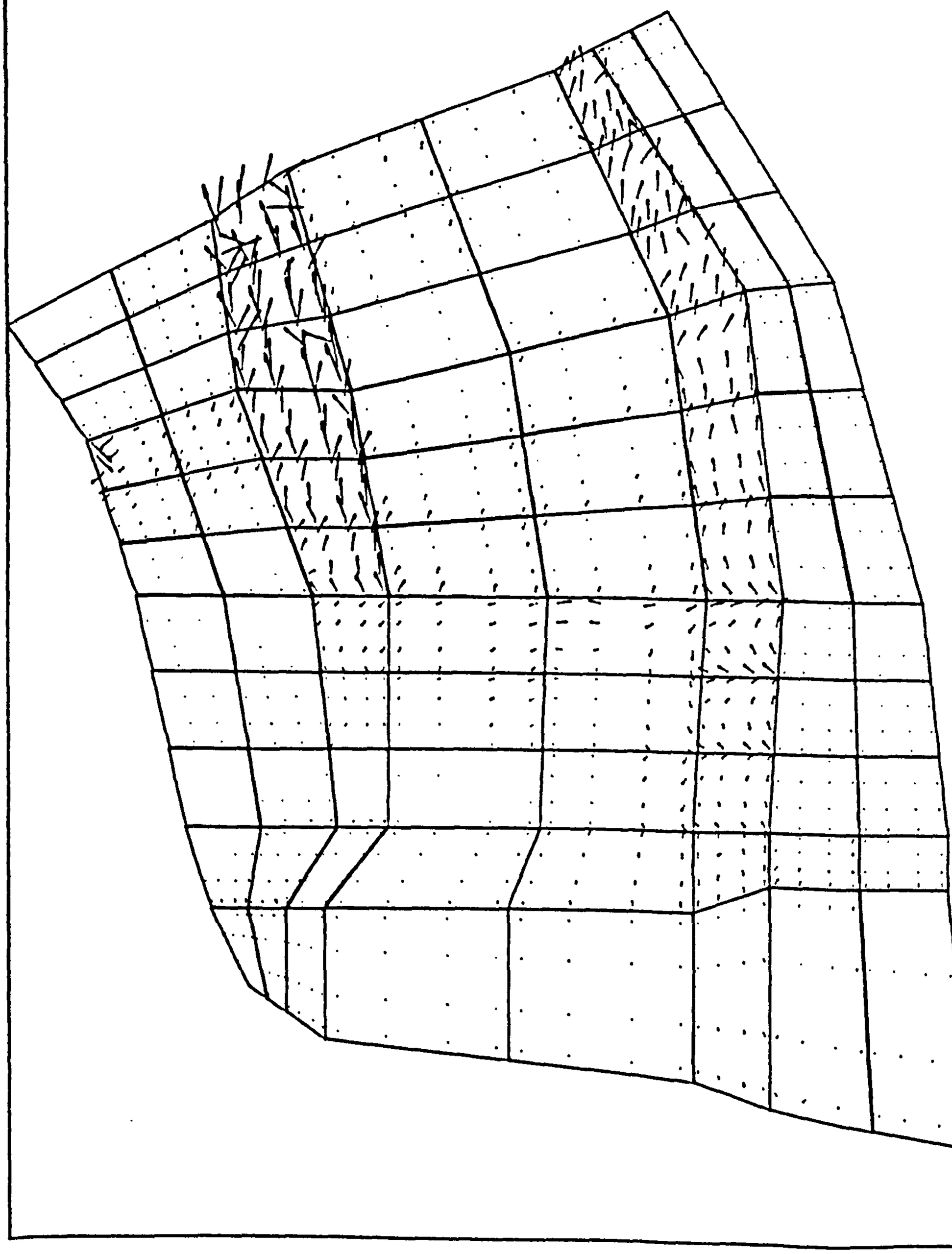


FIG (8.24) Stress Destribution in Section IV
OF An Externally Loaded Radial Tyre

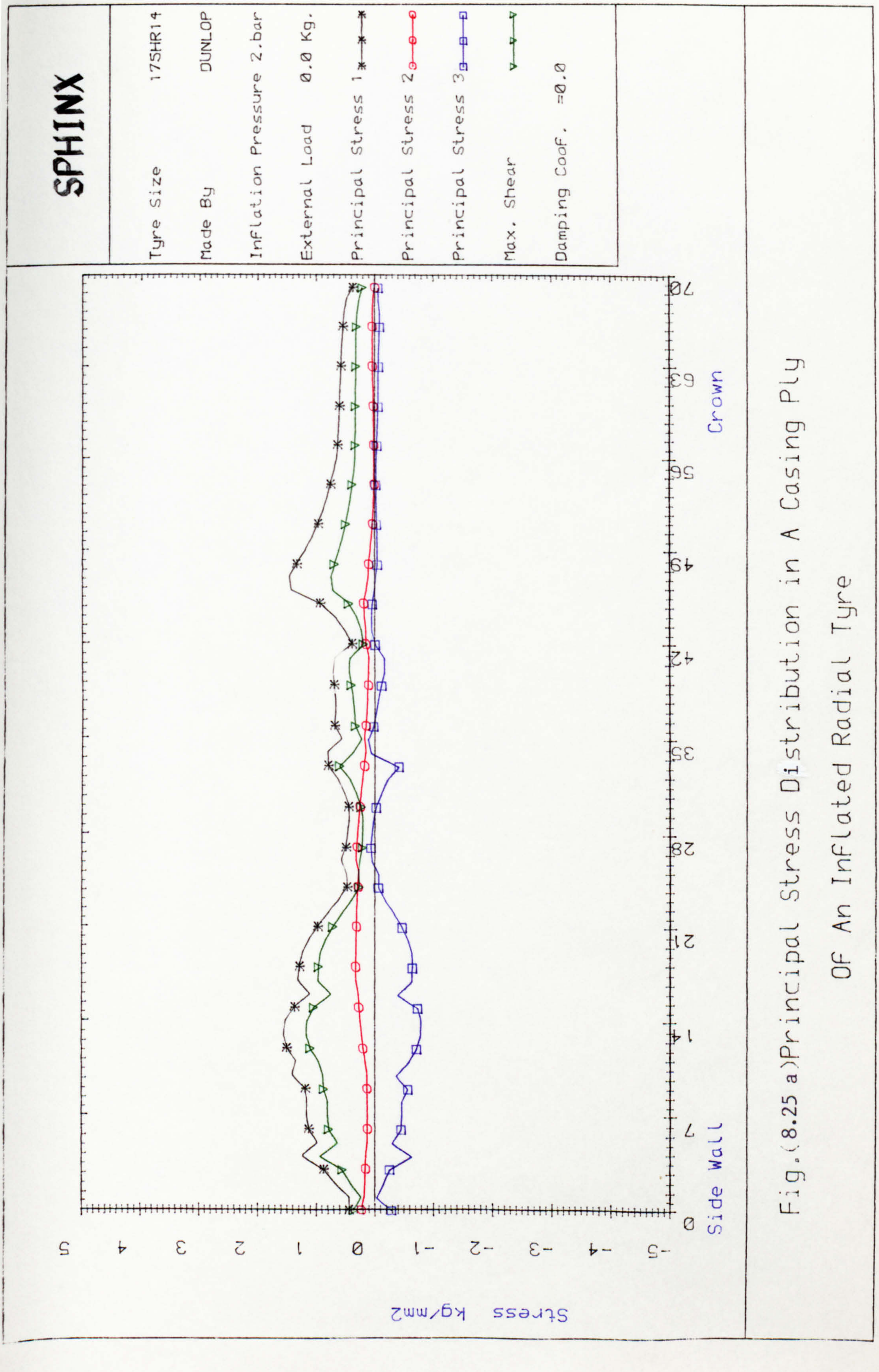


Fig.(8.25 a)Principal Stress Distribution in A Casing Ply Of An Inflated Radial Tyre

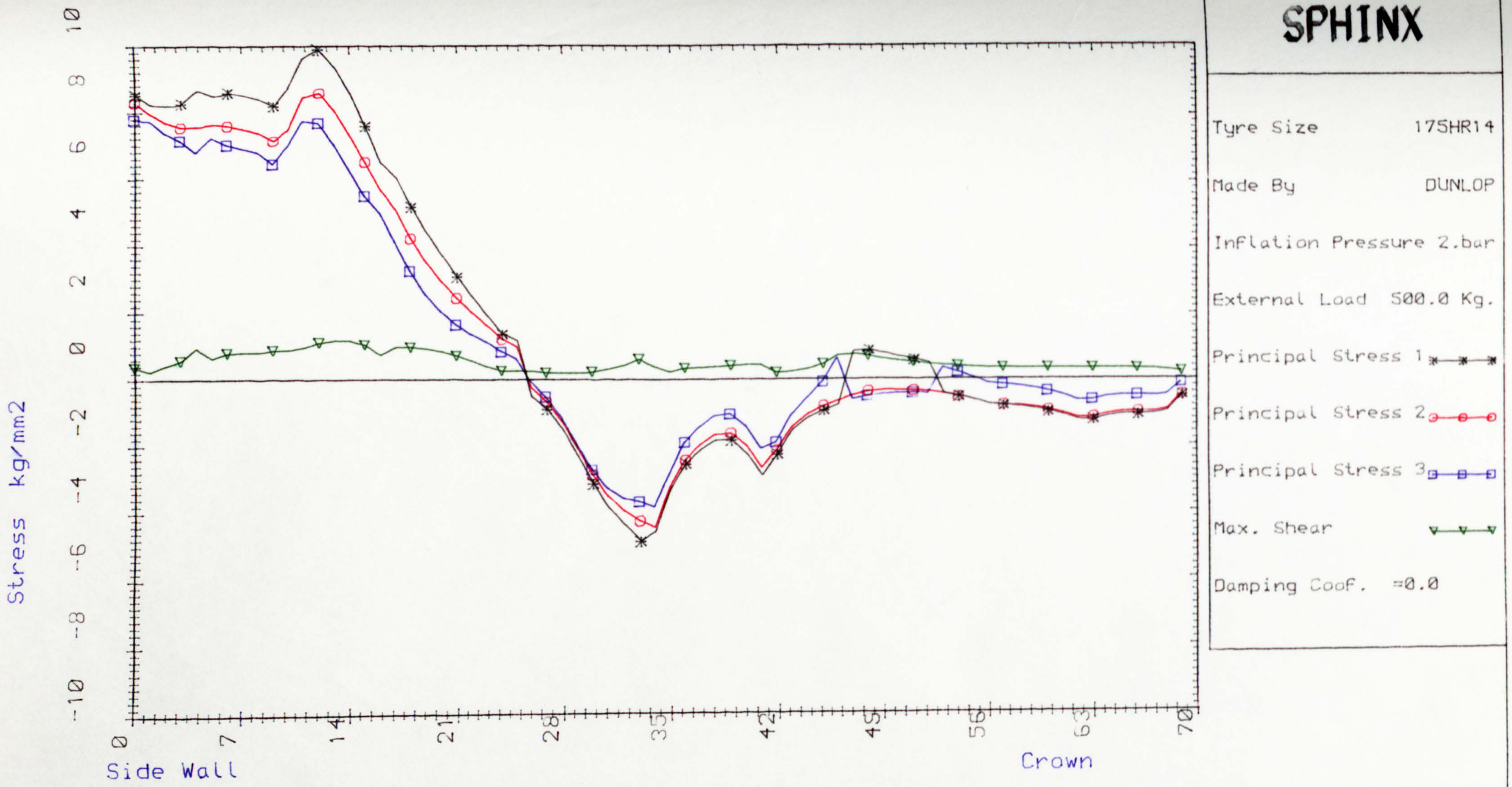


Fig.(8.25 b)Principal Stress Distribution in A Casing Ply

Of An Externally Loaded Radial Tyre

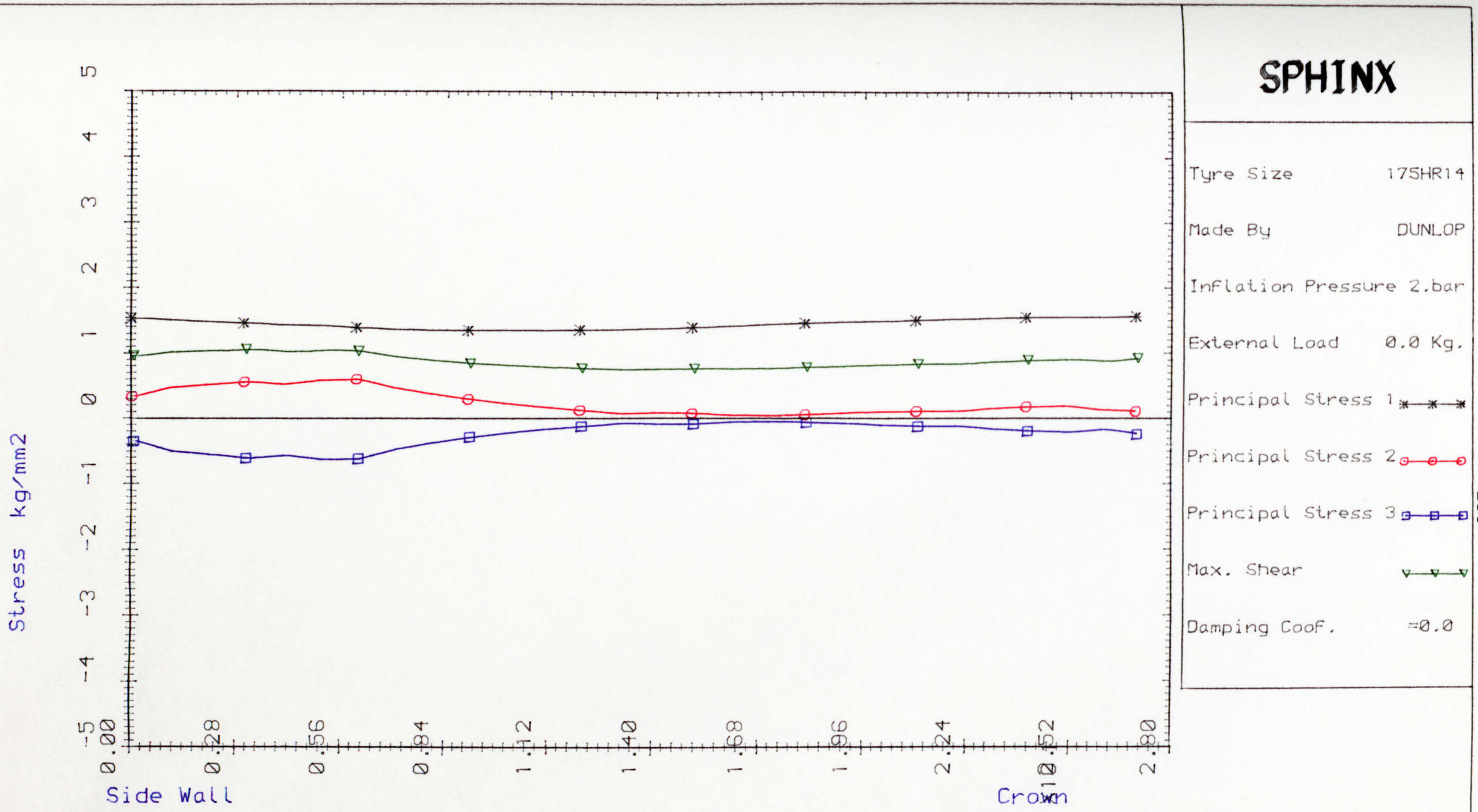


Fig.(8.26 a)Principal Stress Distribution in Breaker 1

Of Inflated Radial Tyre

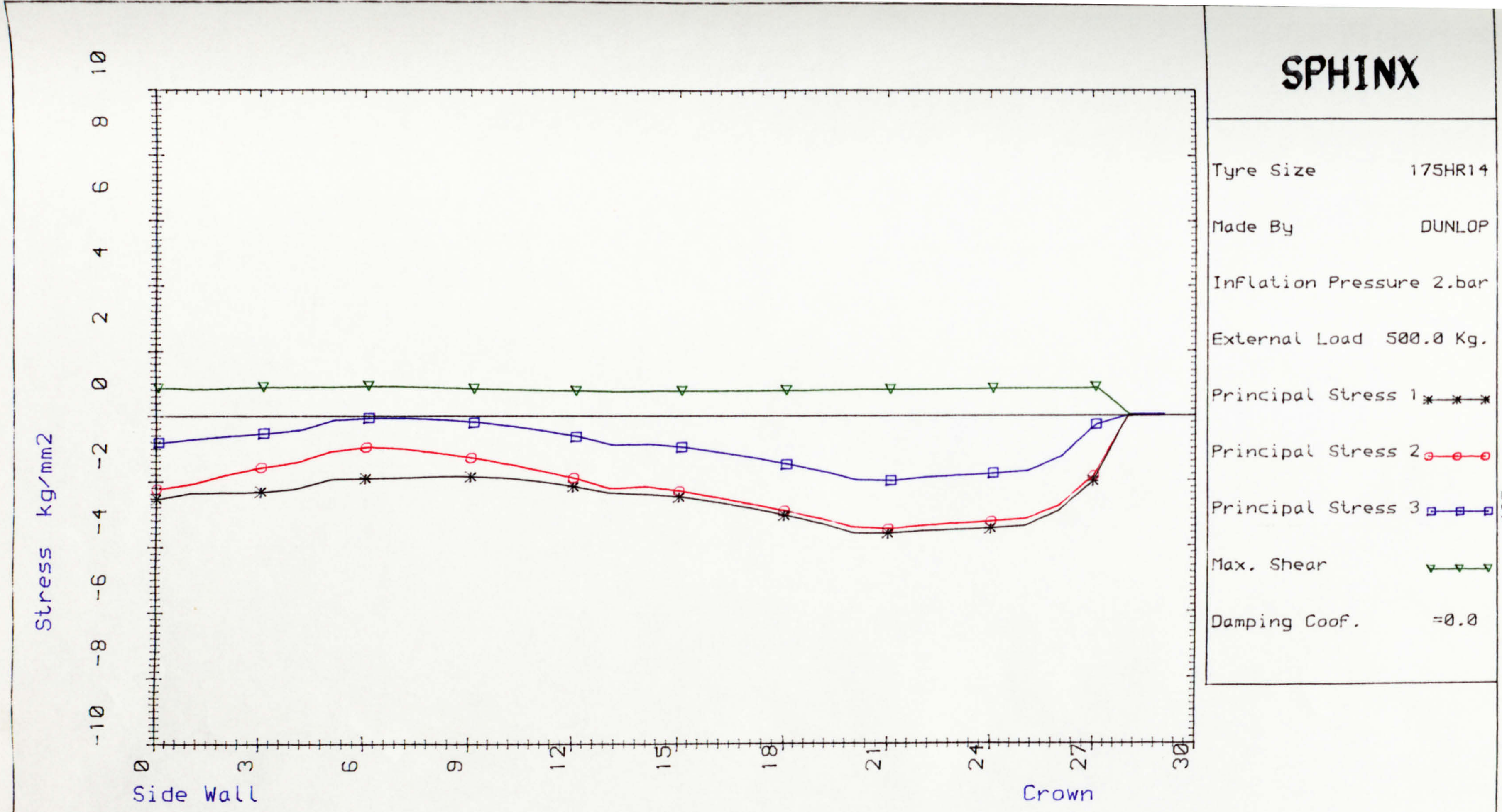


Fig.(8.26 b)Principal Stress Distribution in Breaker 1

Of An Externally Loaded Radial Tyre

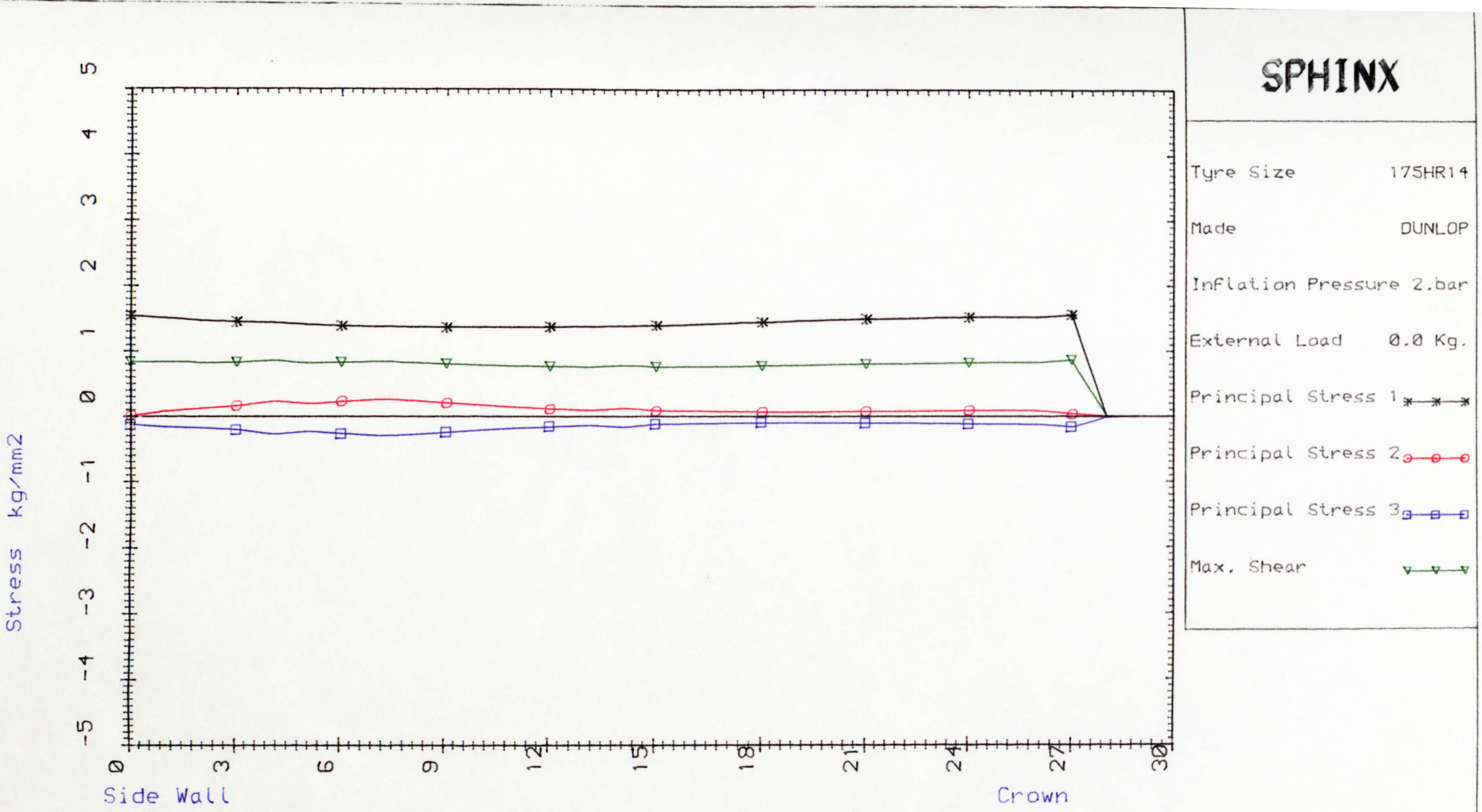


Fig.(8.27a)Principal Stress Distribution in Breaker 2 of Inflated Radial Tyre

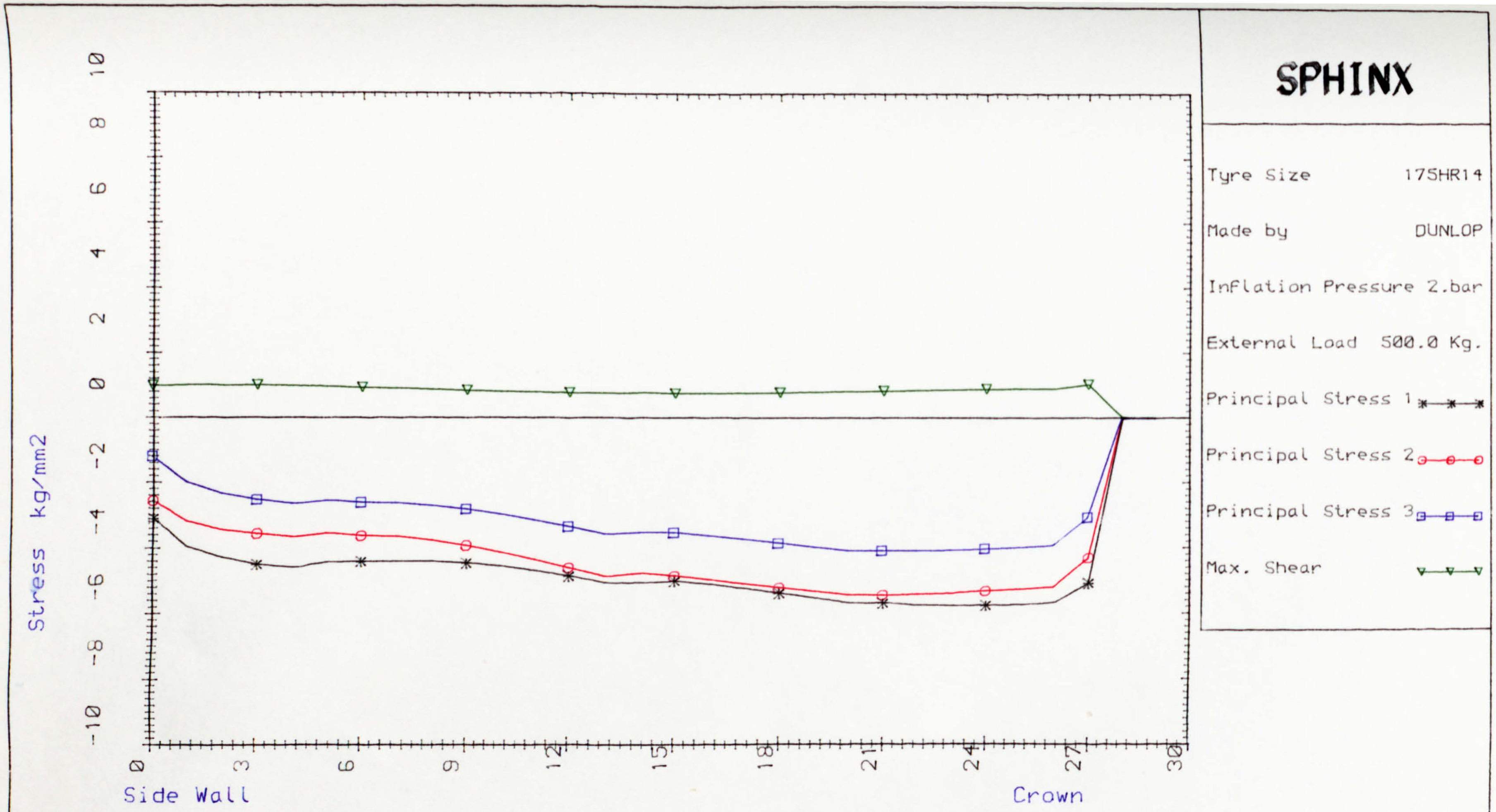


Fig.(8.27 b)Principal Stress Distribution in Breaker 2
of An Externally Loaded Radial Tyre

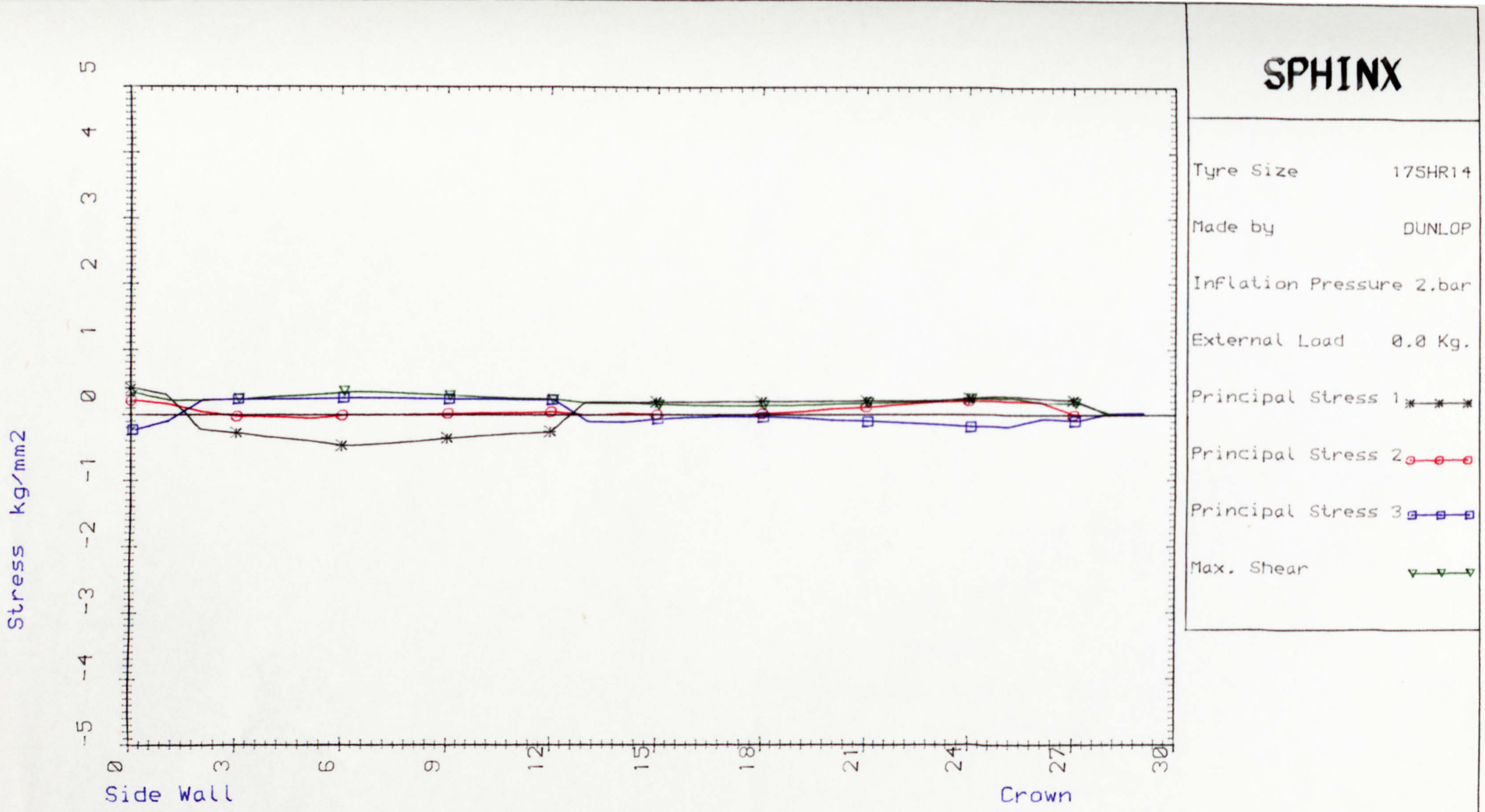


Fig.(8.28a)Principal Stress Distribution in Breaker 3
of An Inflated Radial Tyre

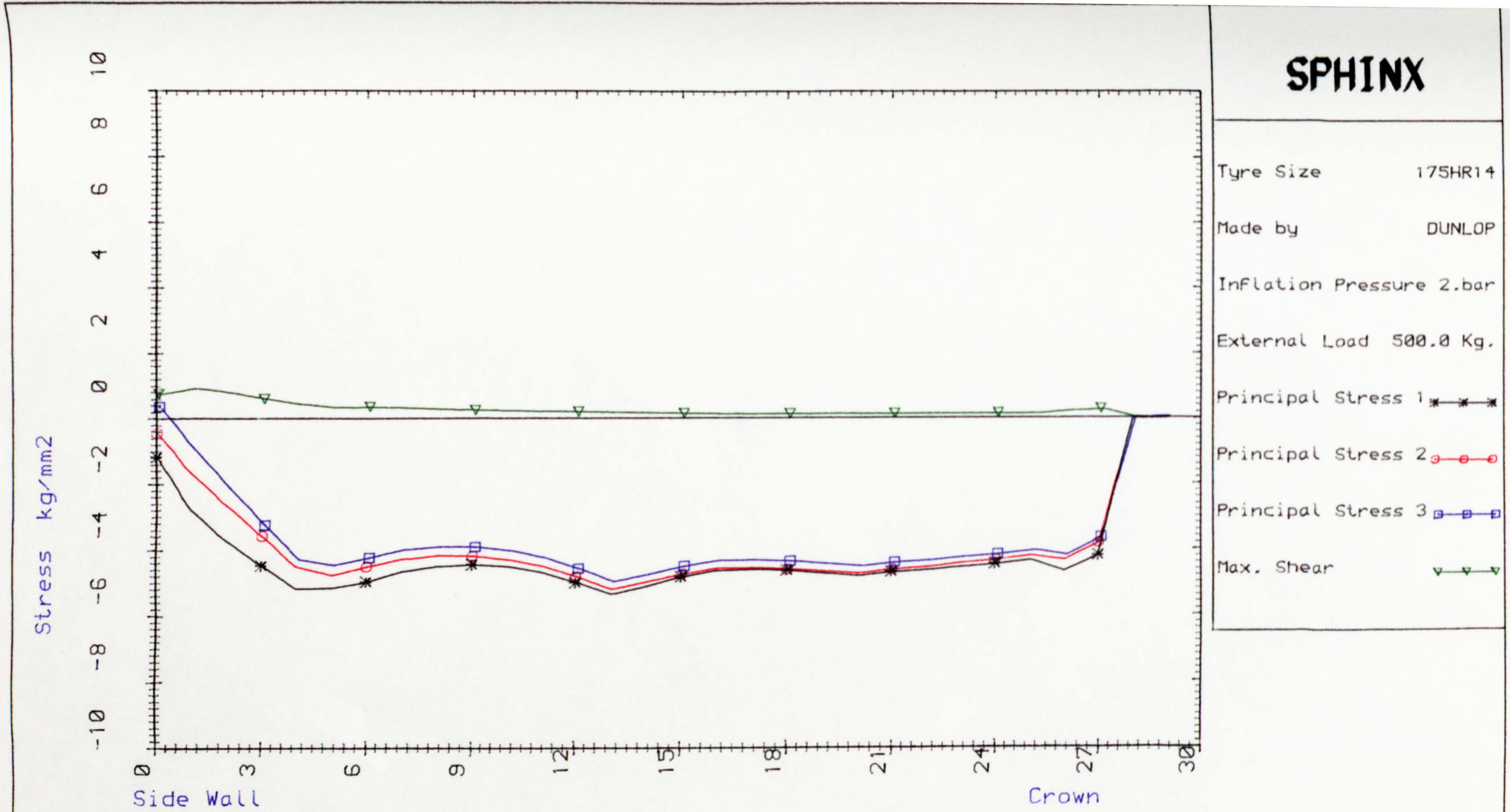


Fig.(8.28 b)Principal Stress Distribution in Breaker 3
of An Externally Loaded Radial Tyre

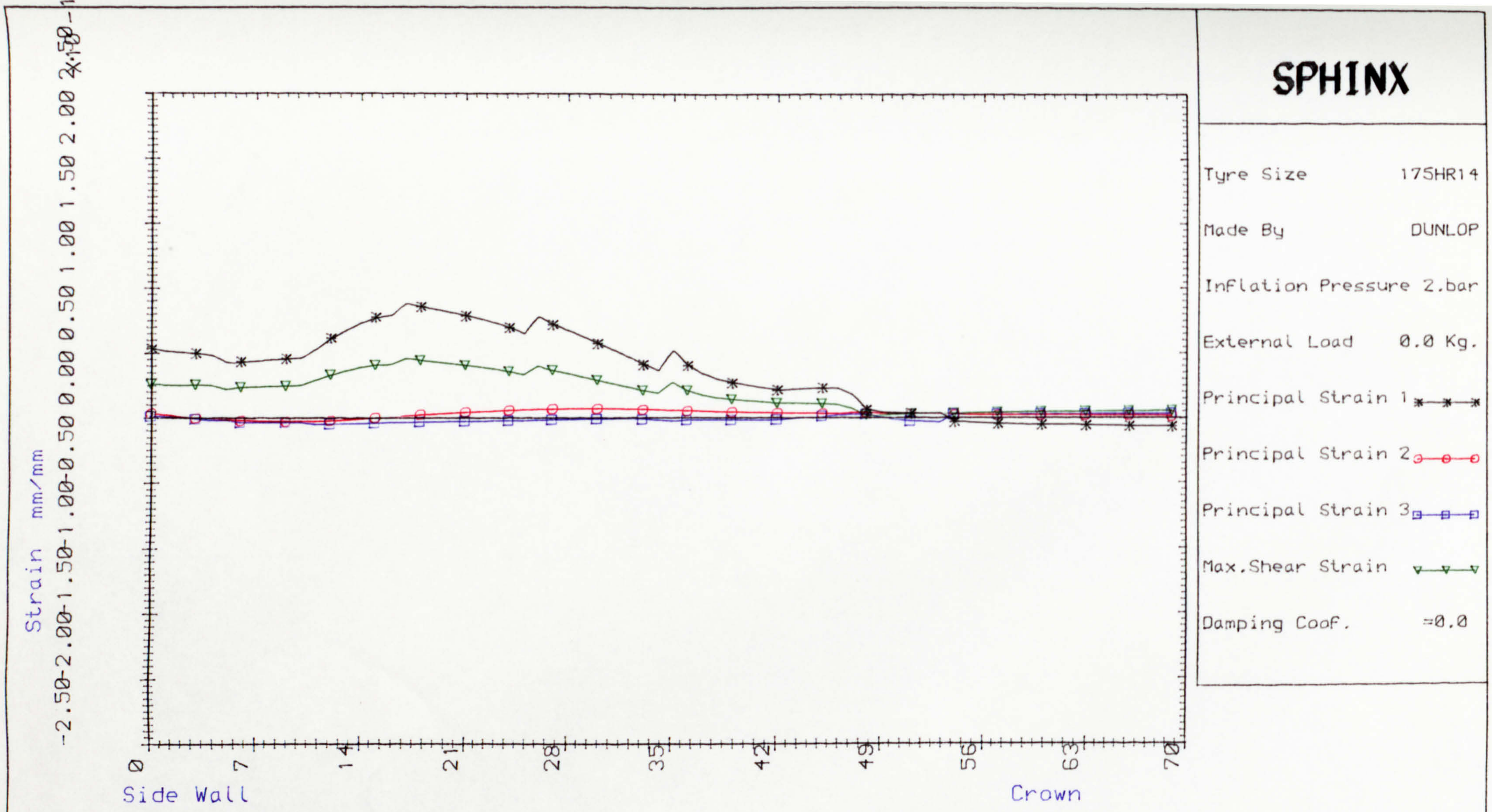


Fig.(8.29 a)Principal Strain Distribution in A Casing Ply
Of An Inflated Radial Tyre

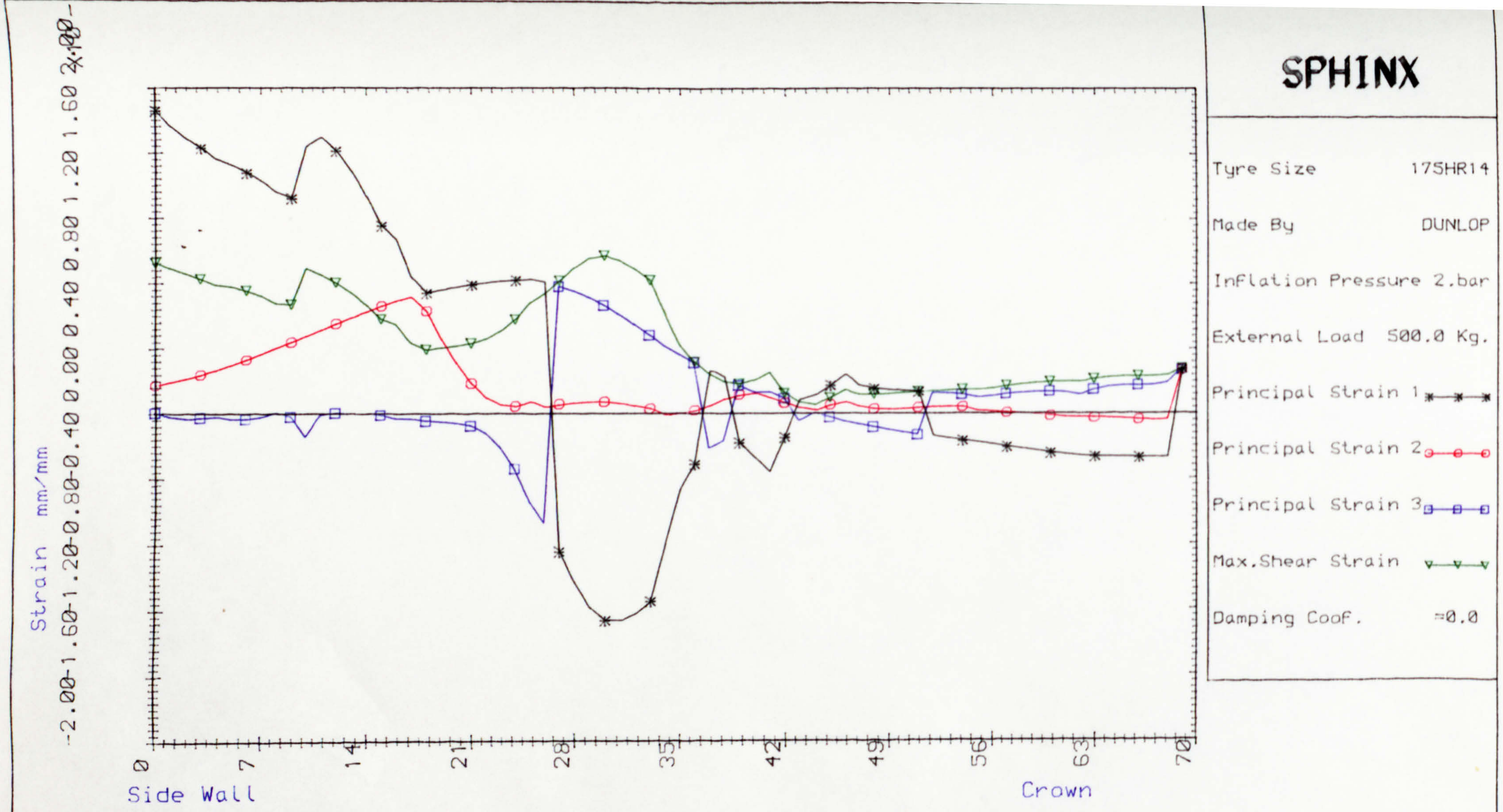


Fig.(8.29 b)Principal Strain Distribution in A Casing Ply
Of An Externally Loaded Radial Tyre

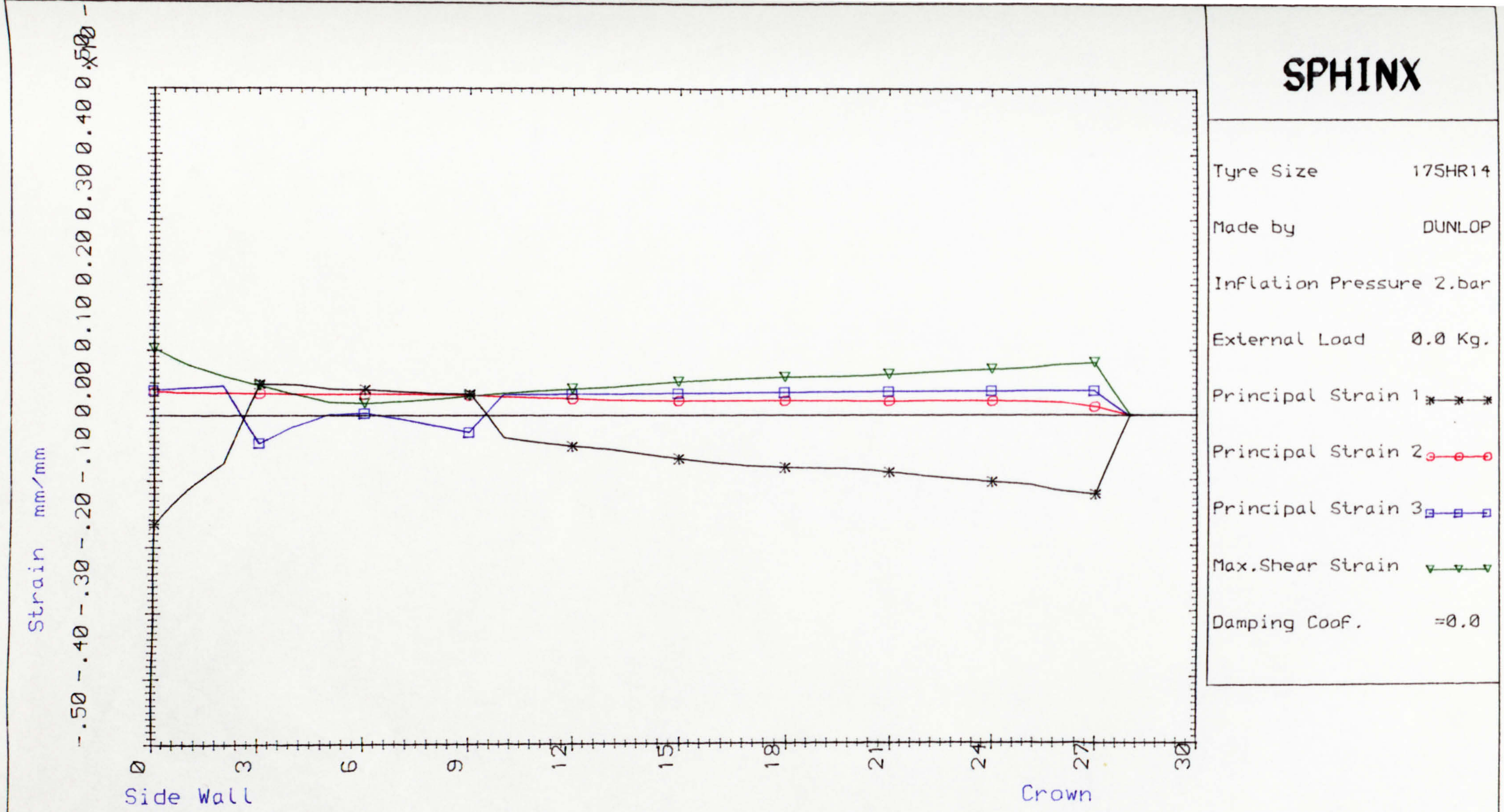


Fig.(8.30a)Principal Strain Distribution in Breaker 1

OF An Inflated Radial Tyre

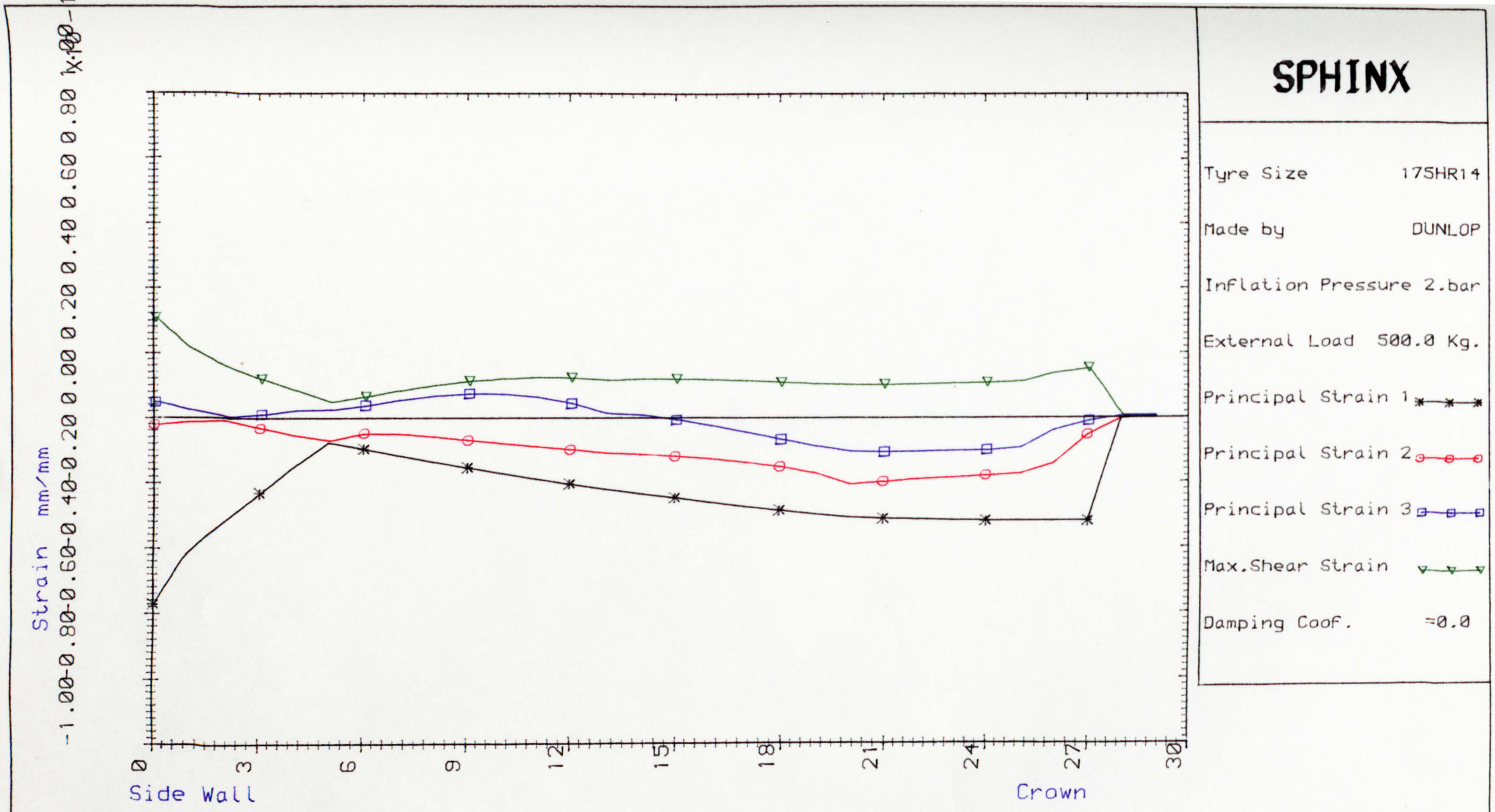


Fig.(8.30b)Principal Strain Distribution in Breaker 1

Of An Externally Loaded Radial Tyre

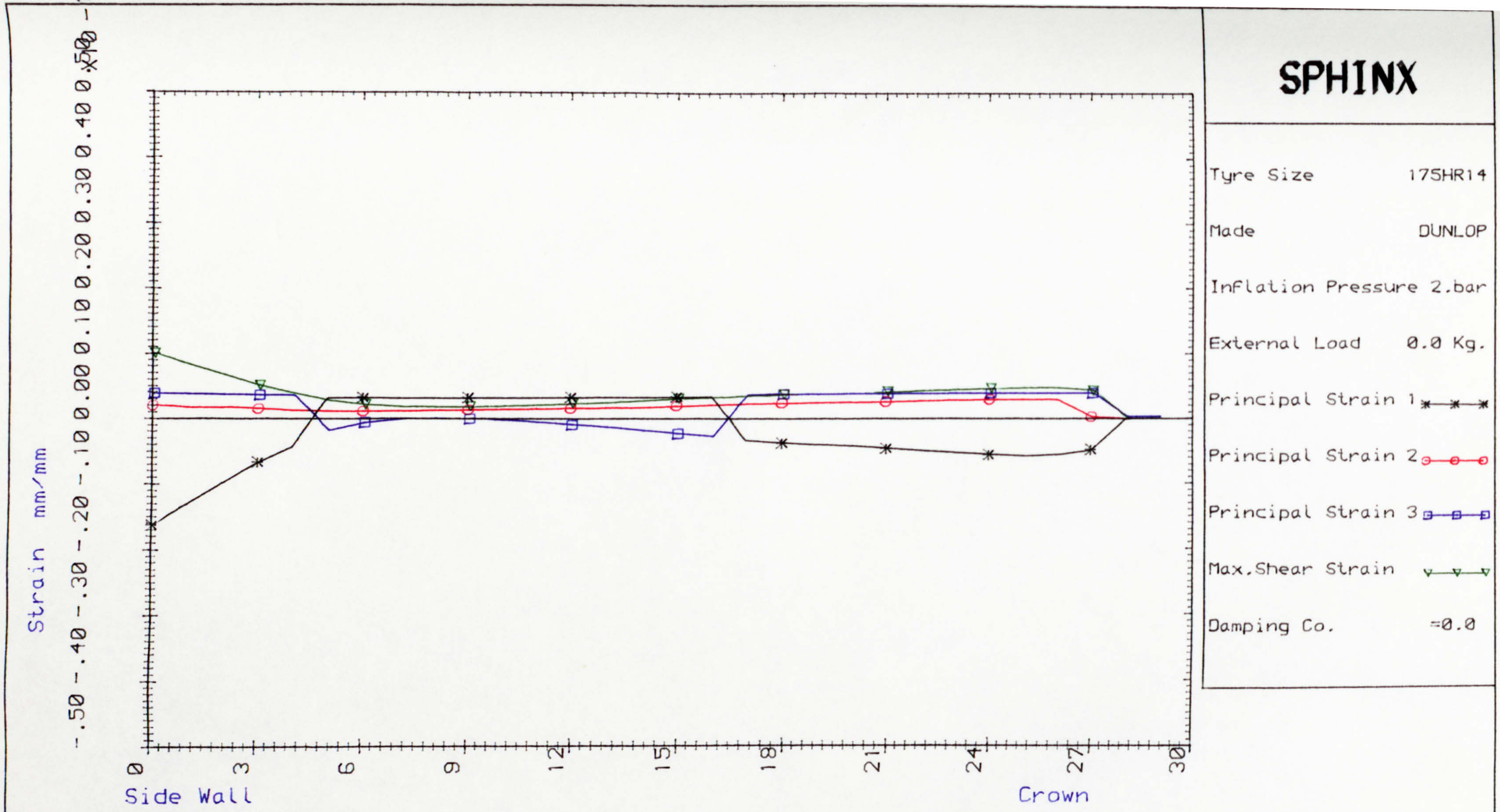


Fig.(8.31a)Principal Strain Distribution in Breaker 2
Of An Inflated Radial Tyre

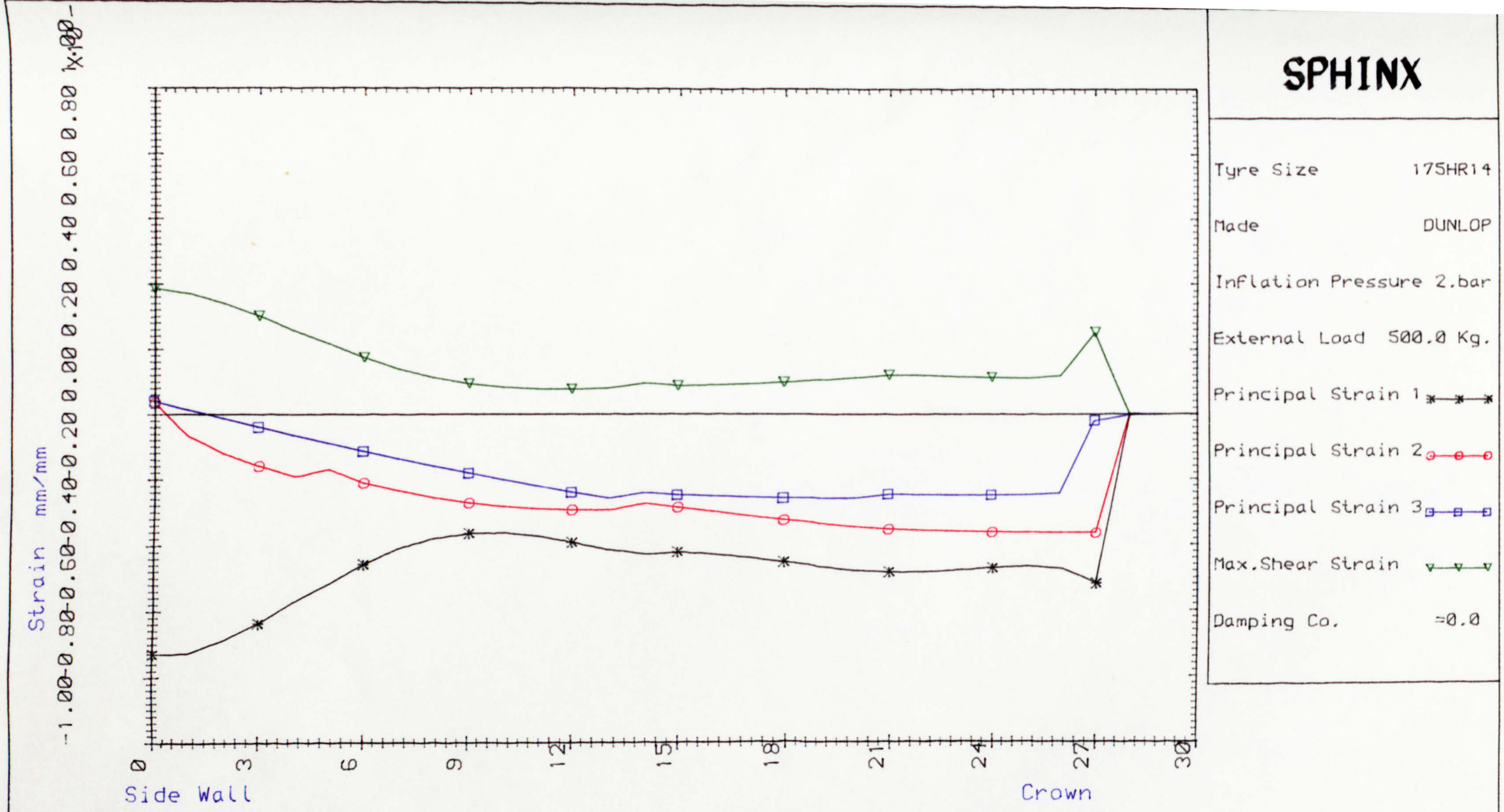


Fig.(8.31b)Principal Strain Distribution in Breaker 2
Of An Externally Loaded Radial Tyre

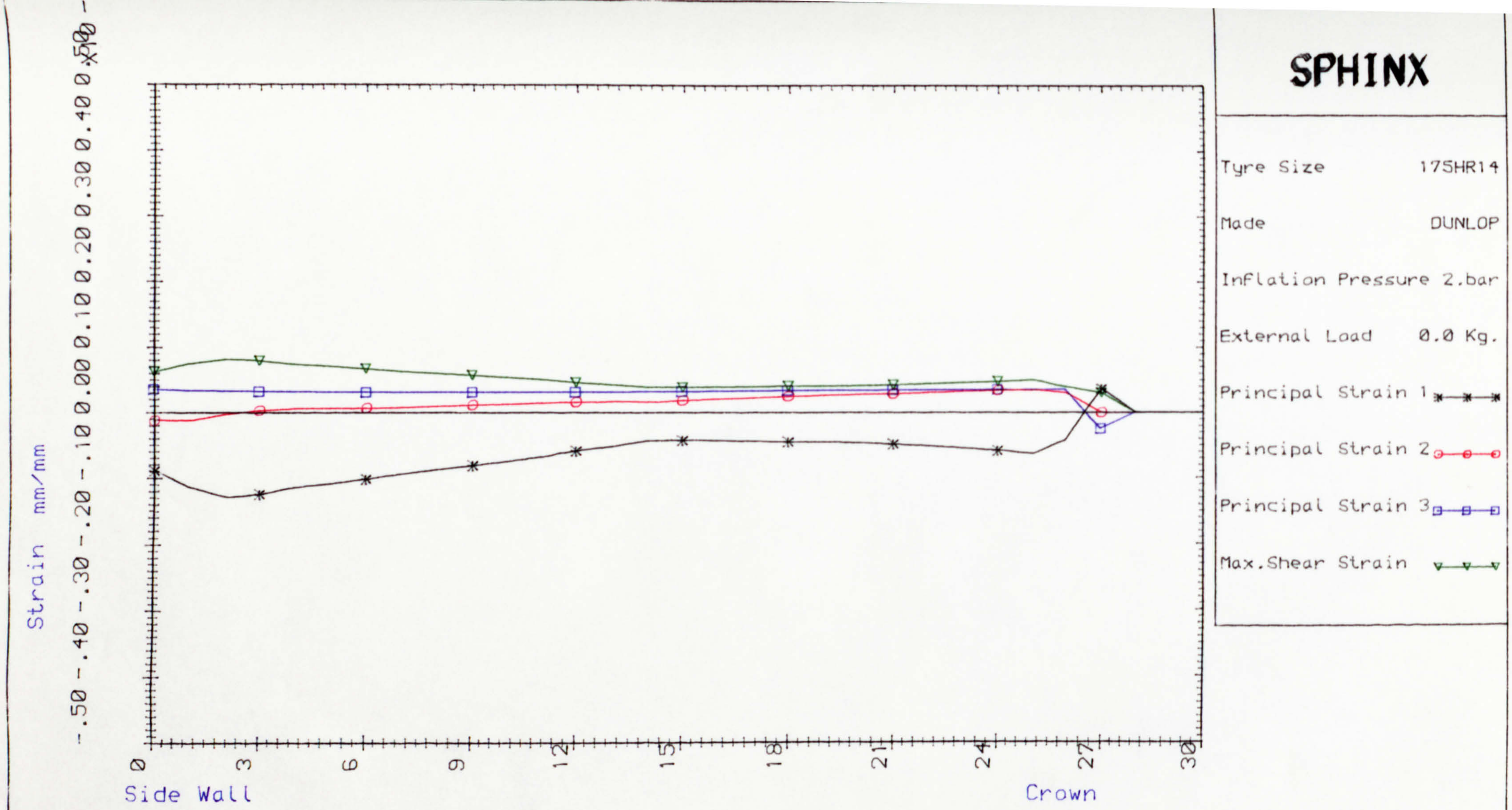
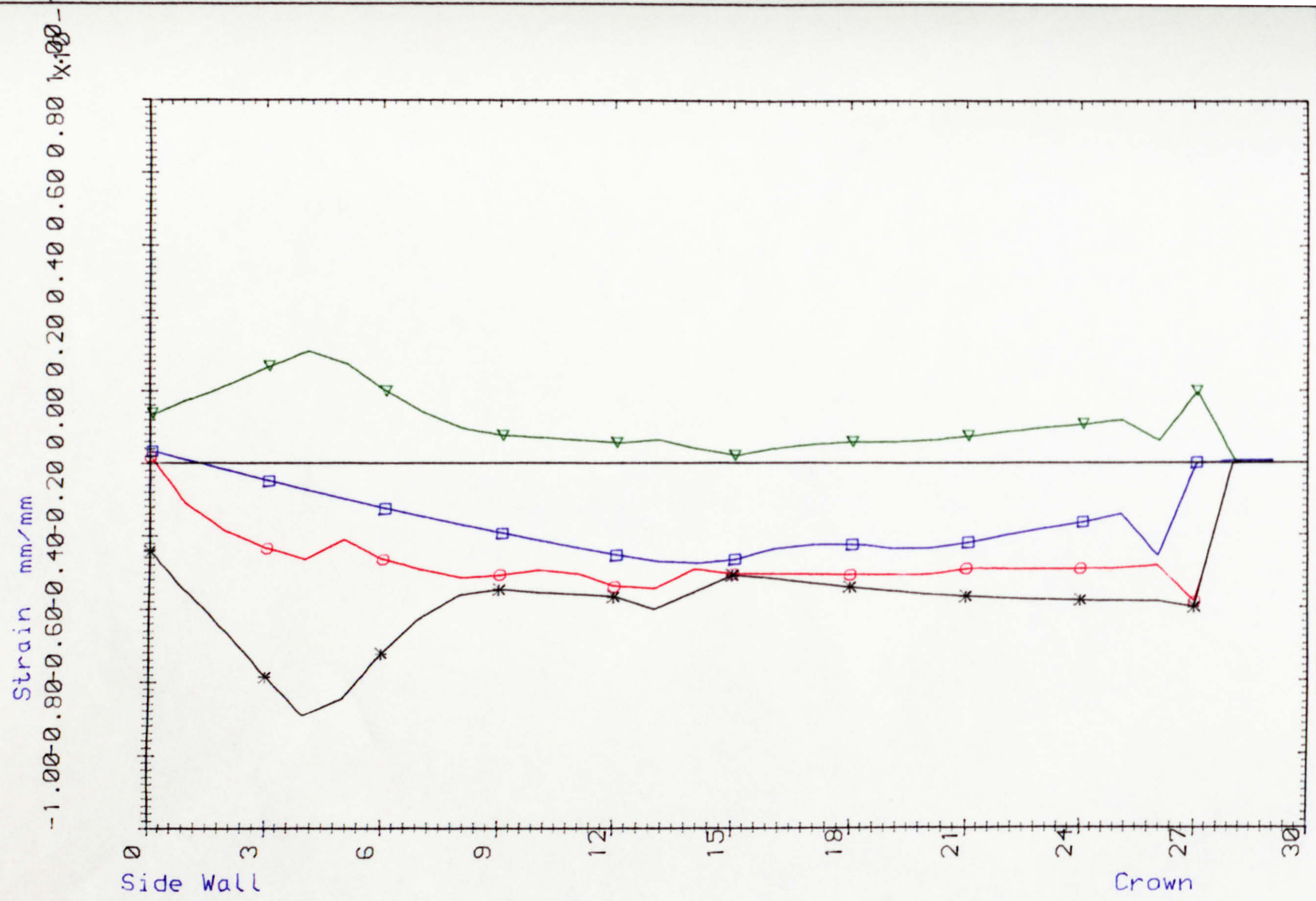


Fig.(8.32a)Principal Strain Distribution in Breaker 3
of An Inflated Radial Tyre



SPHINX

Tyre Size	175HR14
Made by	DUNLOP
Inflation Pressure	2.bar
External Load	500.0 Kg.
Principal Strain 1	
Principal Strain 2	
Principal Strain 3	
Max.Shear Strain	

Fig.(8.32b)Principal Strain Distribution in Breaker 3
of An Externally Loaded Radial Tyre

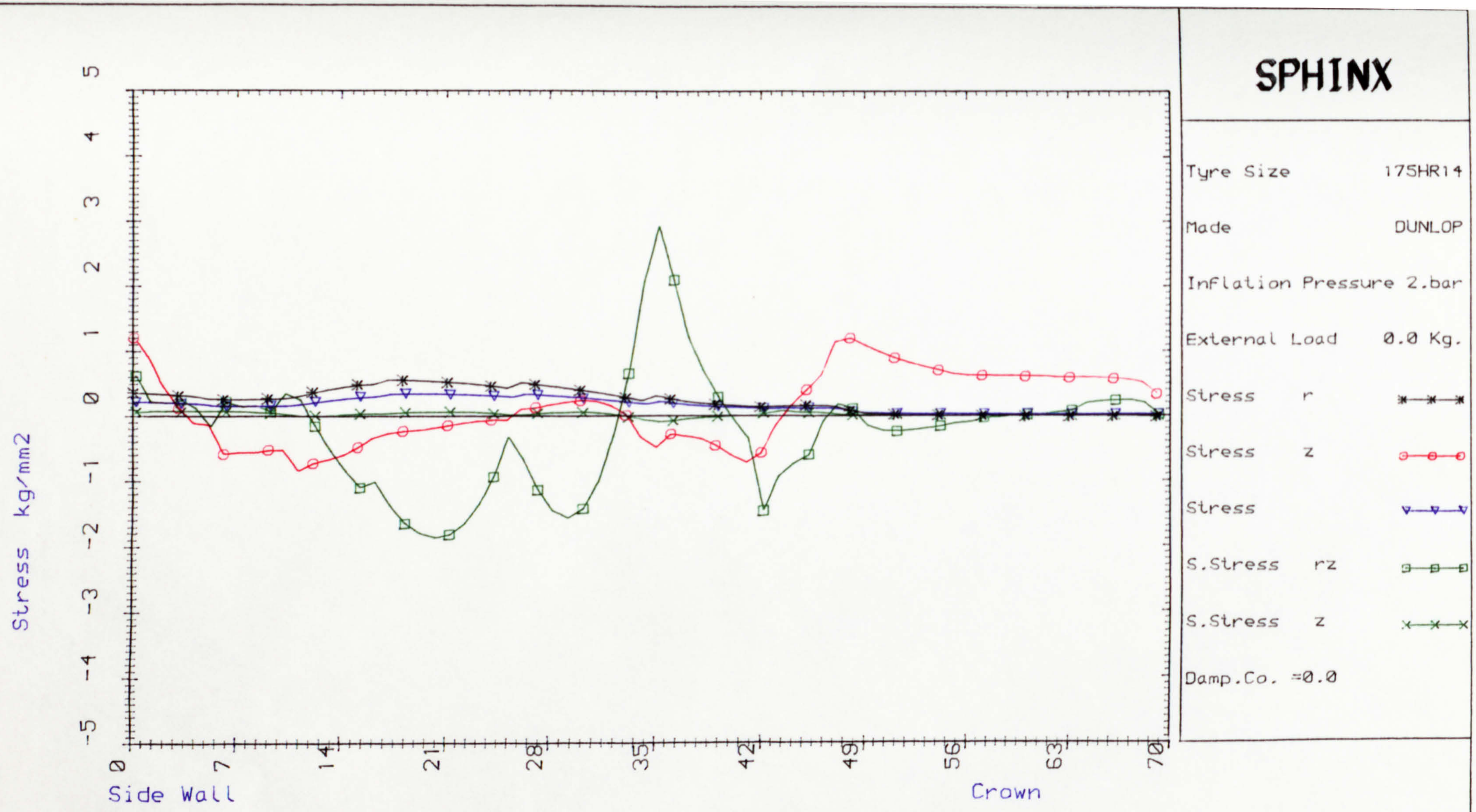
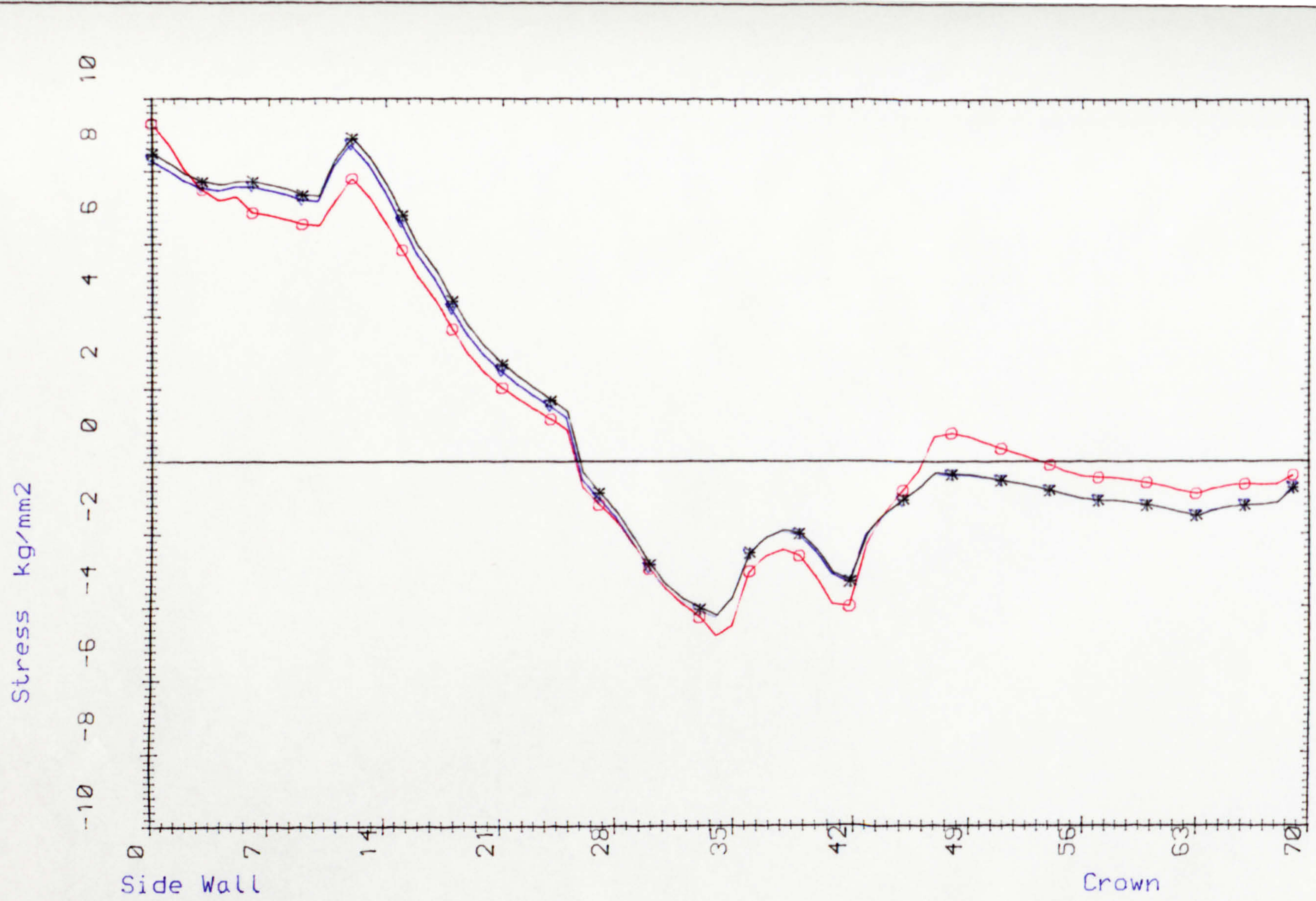


Fig.(8.33a)Stress Distribution in A Casing Ply
Of An Inflated Radial Tyre



SPHINX

Tyre Size	175HR14
Made by	DUNLOP
Inflation Pressure	2.bar
External Load	500.0 Kg.
Stress r	
Stress z	
Stress	
Damp.Co.	=0.0

201

Fig.(8.33 b)Stress Distribution in A Casing Ply
Of An Externally Loaded Radial Tyre

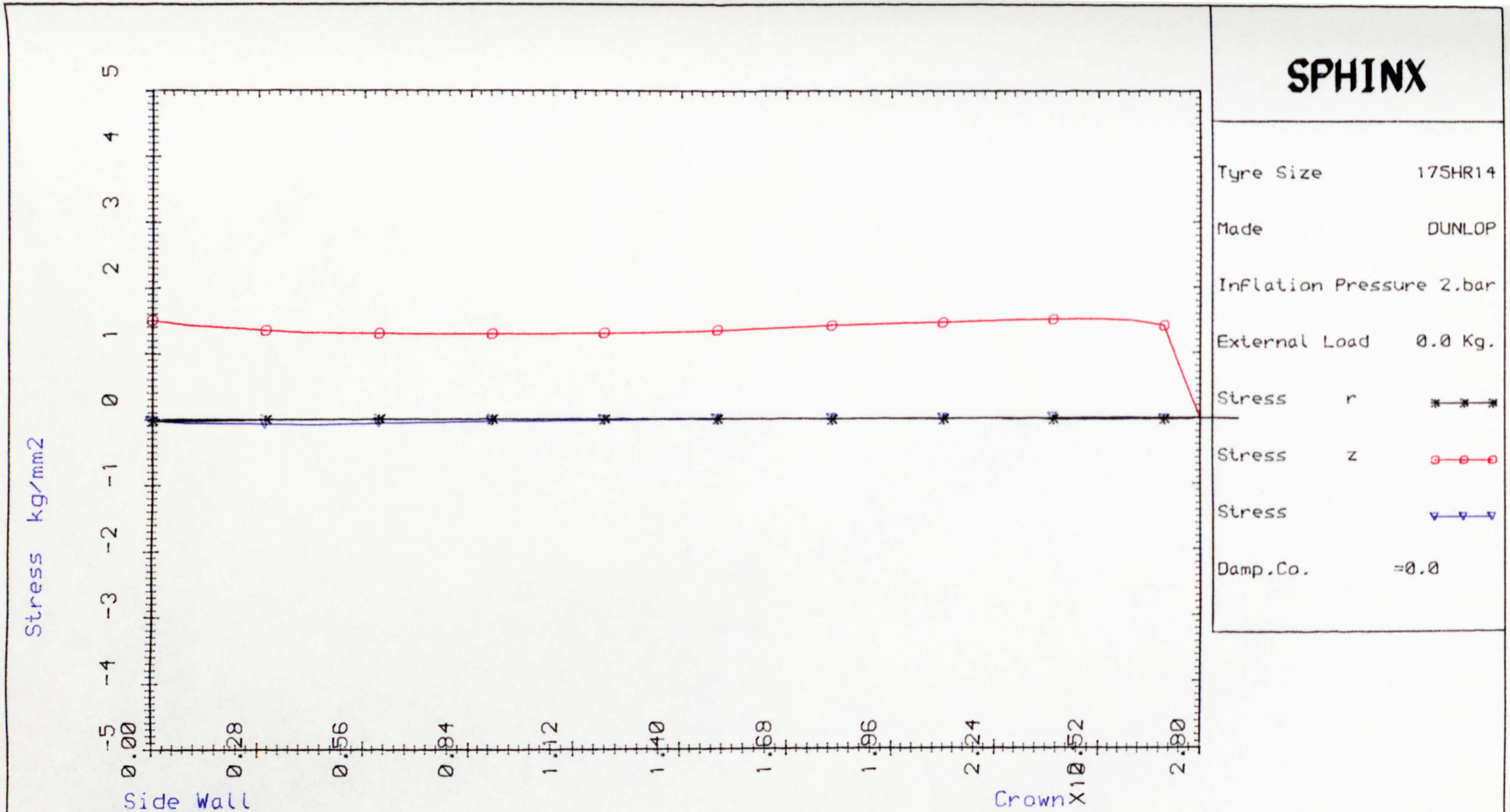


Fig.(8.34a)Stress Distribution in Breaker 1
of An Inflated Radial Tyre

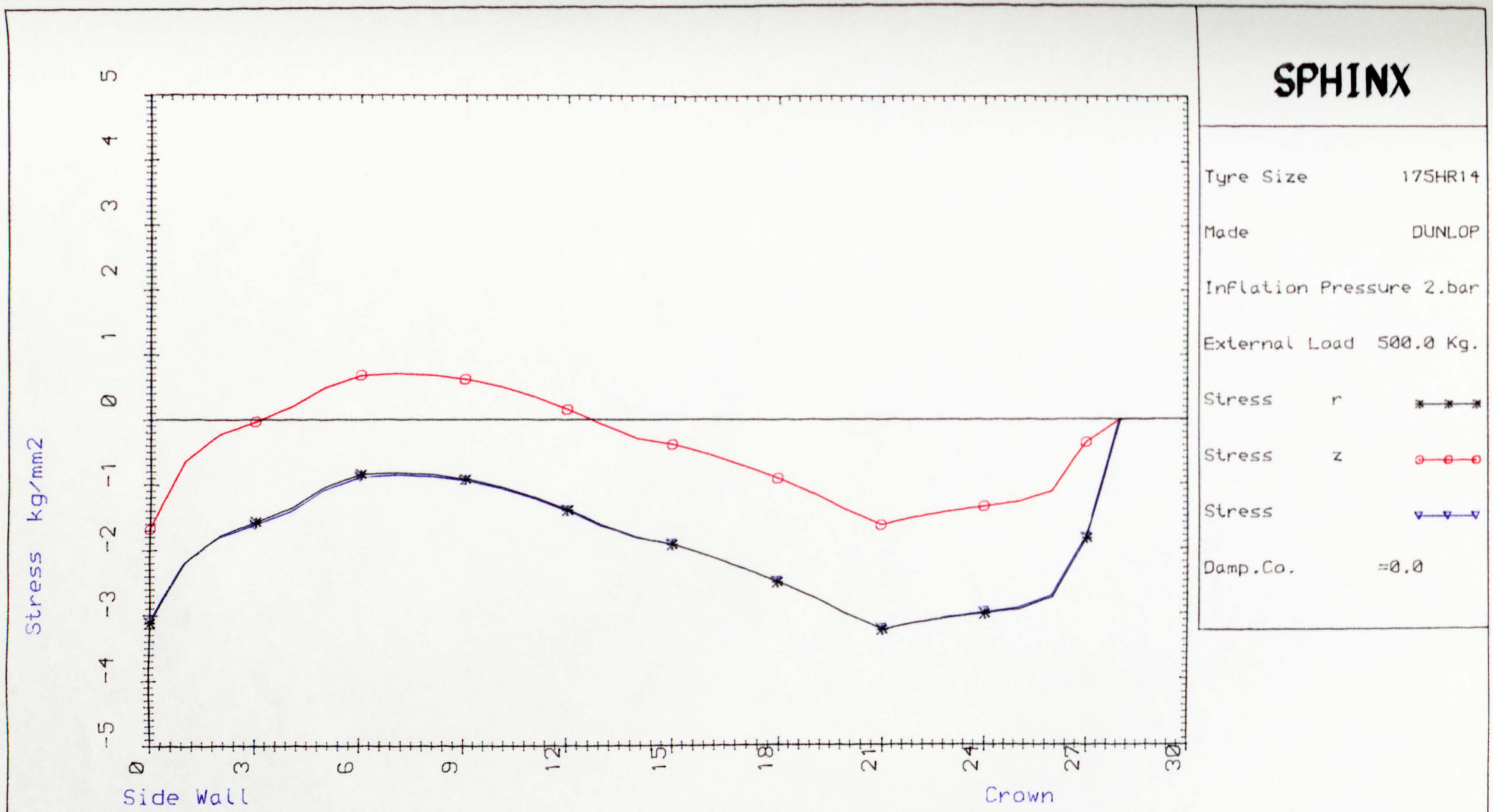


Fig.(8.34 b)Stress Distribution in Breaker 1
of An Externally Loaded Radial Tyre

SPHINX

Tyre Size 17SHR14

Made DUNLOP

Inflation Pressure 2.bar

External Load 0.0 Kg.

Stress r

Stress z

Stress

Damp.Co. =0.0

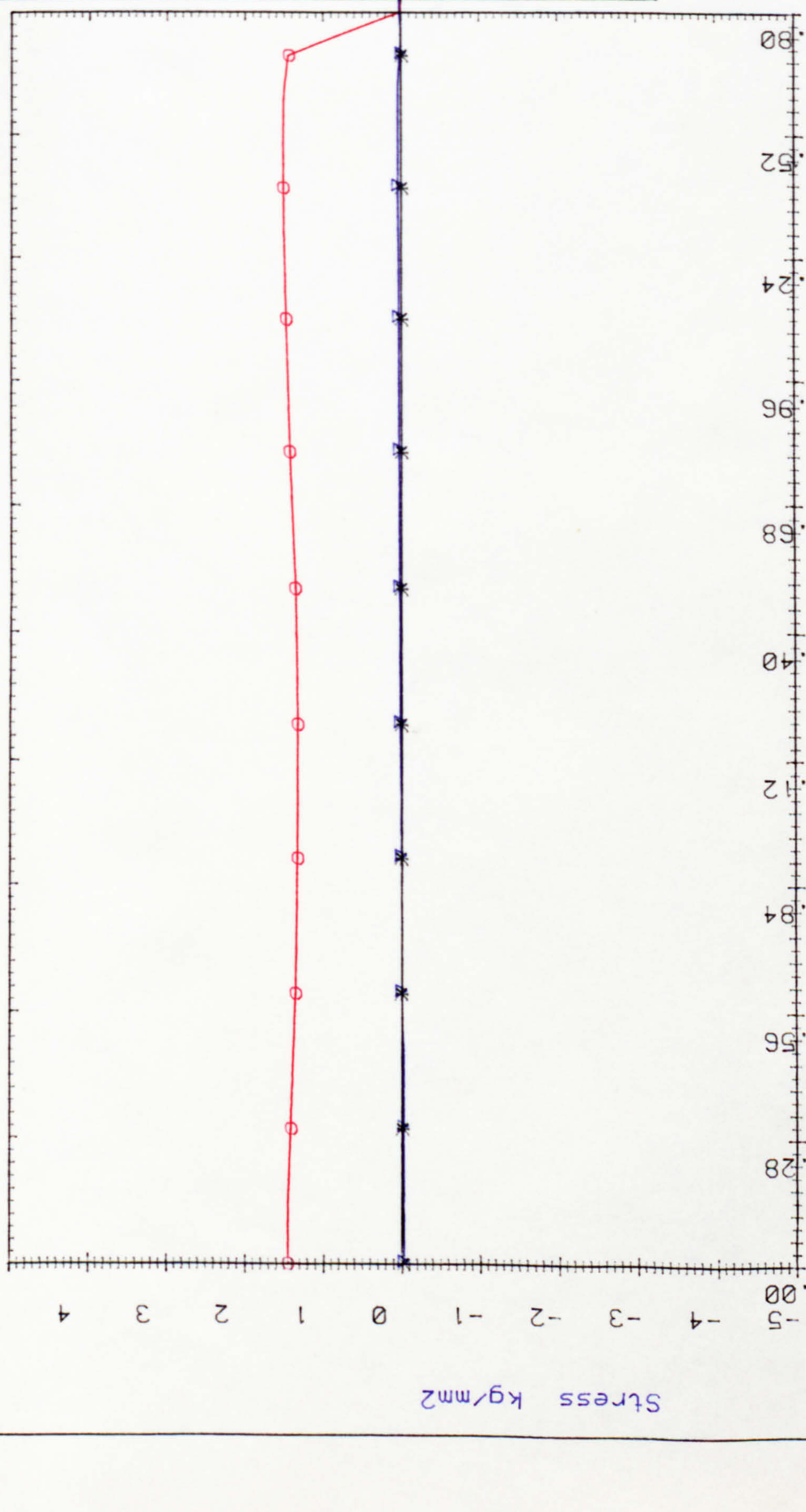


Fig.(8.35a)Stress Distribution in Breaker 2 of An Inflated Radial Tyre

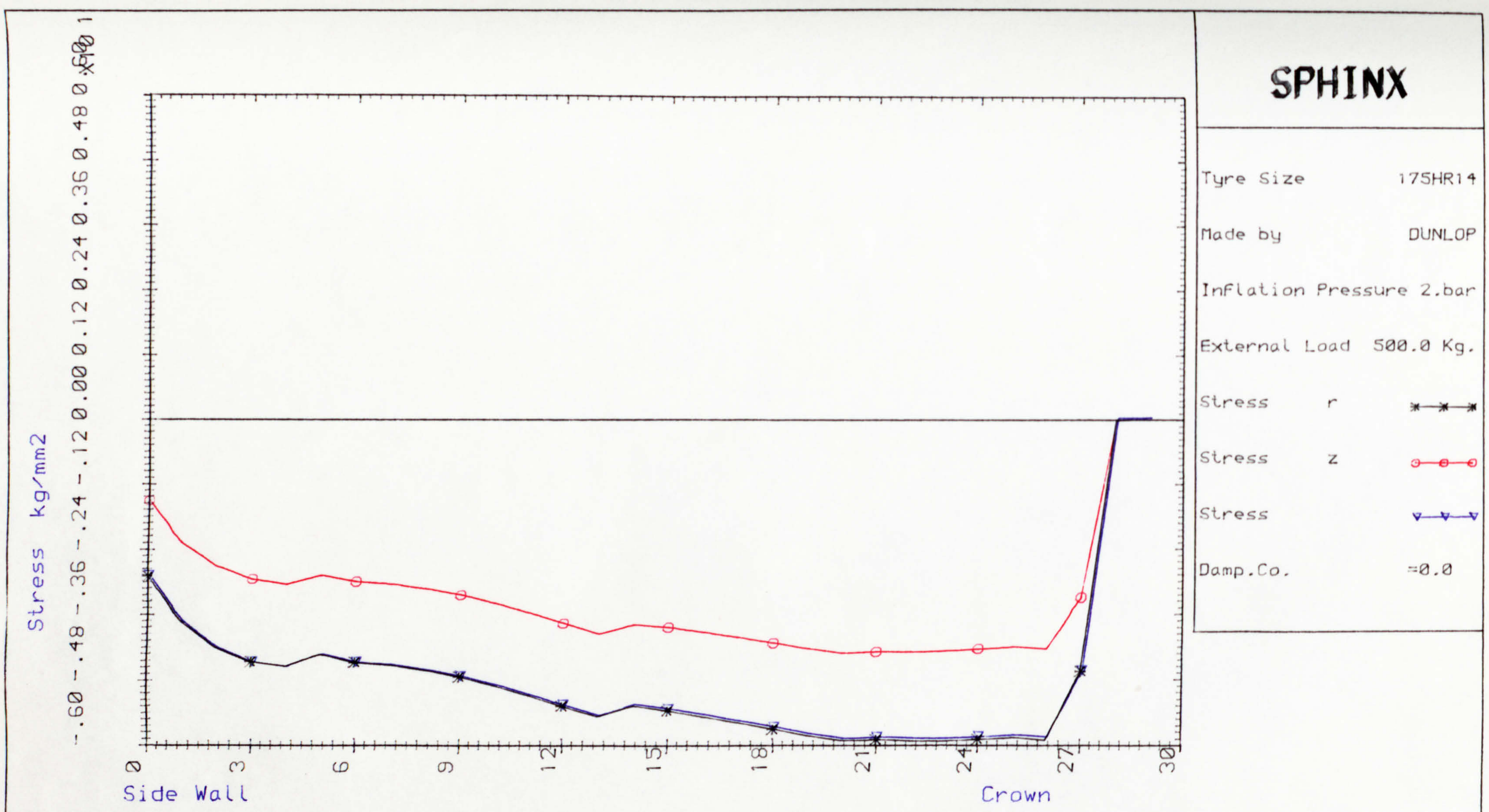


Fig.(8.35b)Stress Distribution in Breaker 2
of An Externally Loaded Radial Tyre

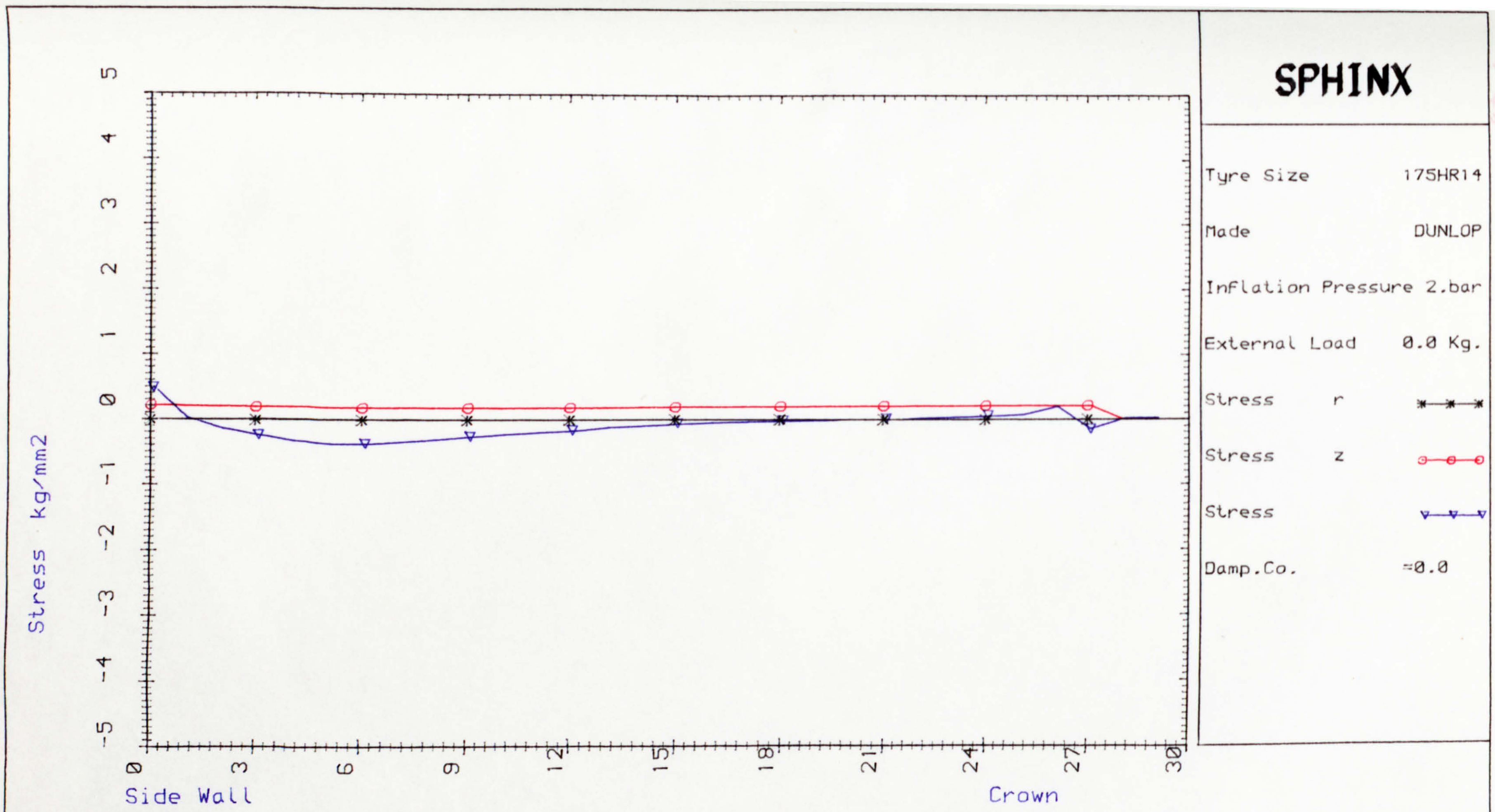


Fig.(8.36 a)Stress Distribution in Breaker 3
of An Inflated Radial Tyre

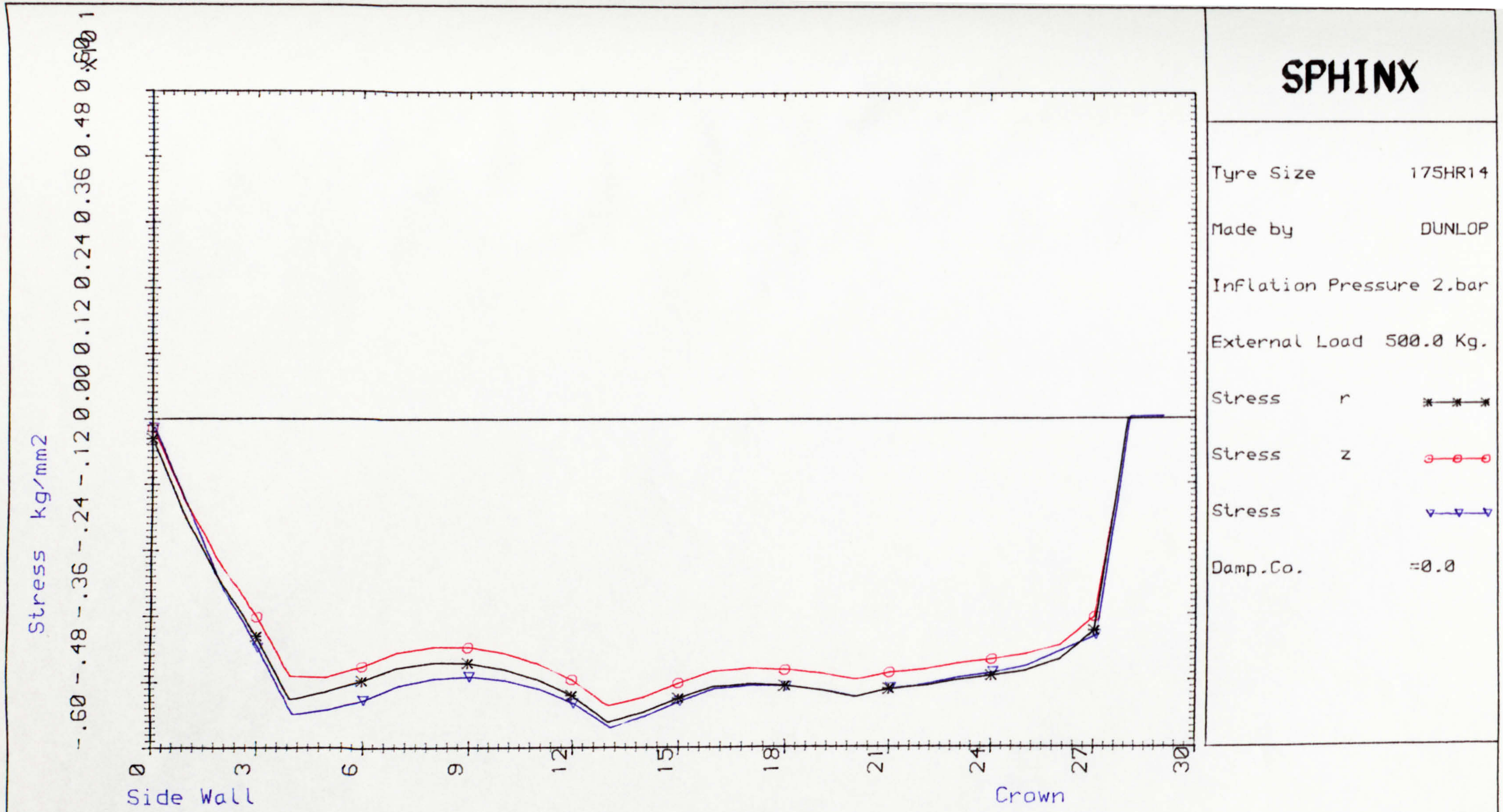
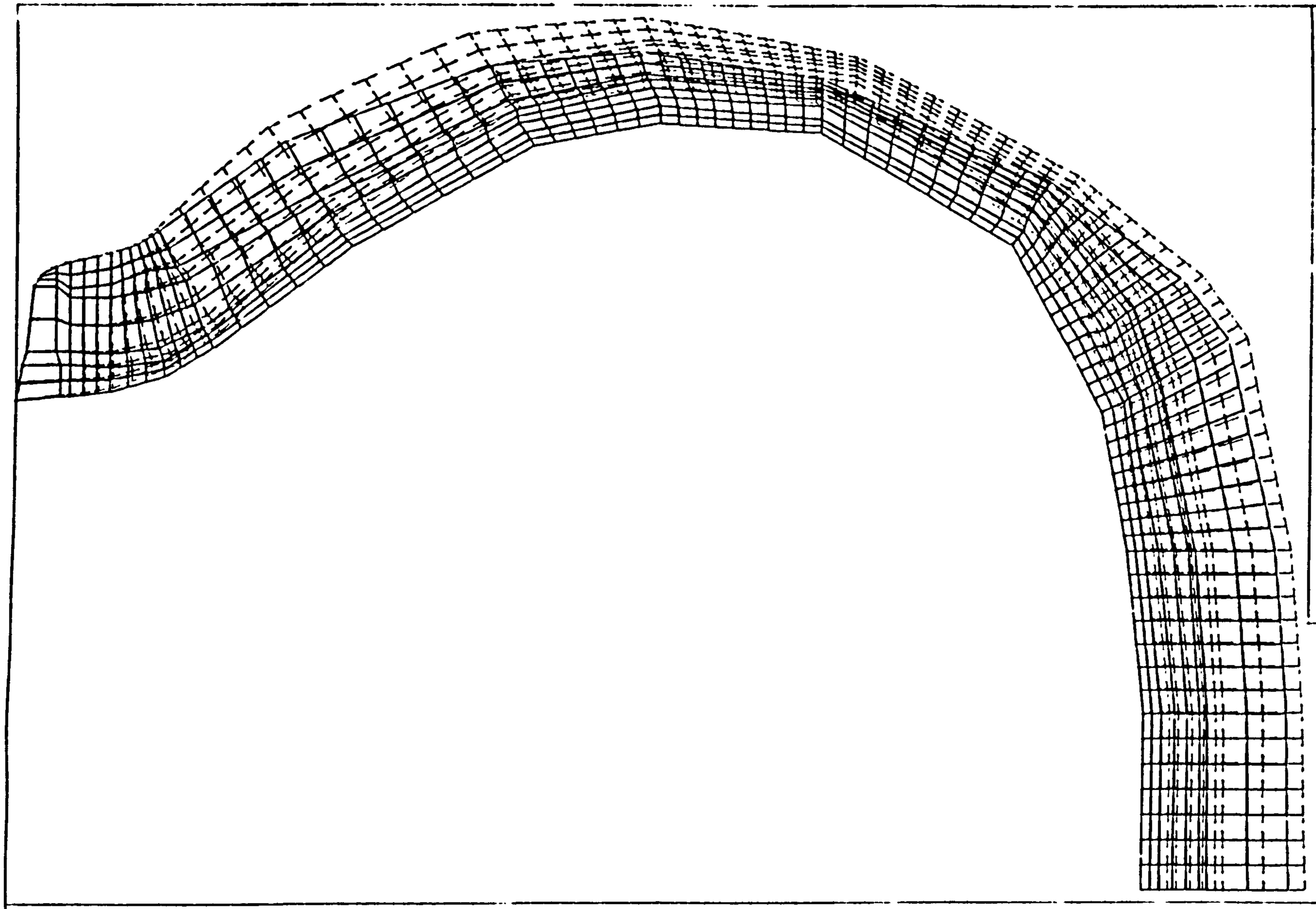


Fig.(8.36 b)Stress Distribution in Breaker 3
of An Externally Loaded Radial Tyre



SPHINX

Tyre Size 175HR14

Made by DUNLOP

Inflation Pressure bar

------ I.P.=0.0

- - - I.P.=2.0

Radial Load =0.0 Kg

Damp.Coof. =0.2

Fig.(8.37) Deformed Shape of An Inflated Radial Tyre

With Viscous Effect

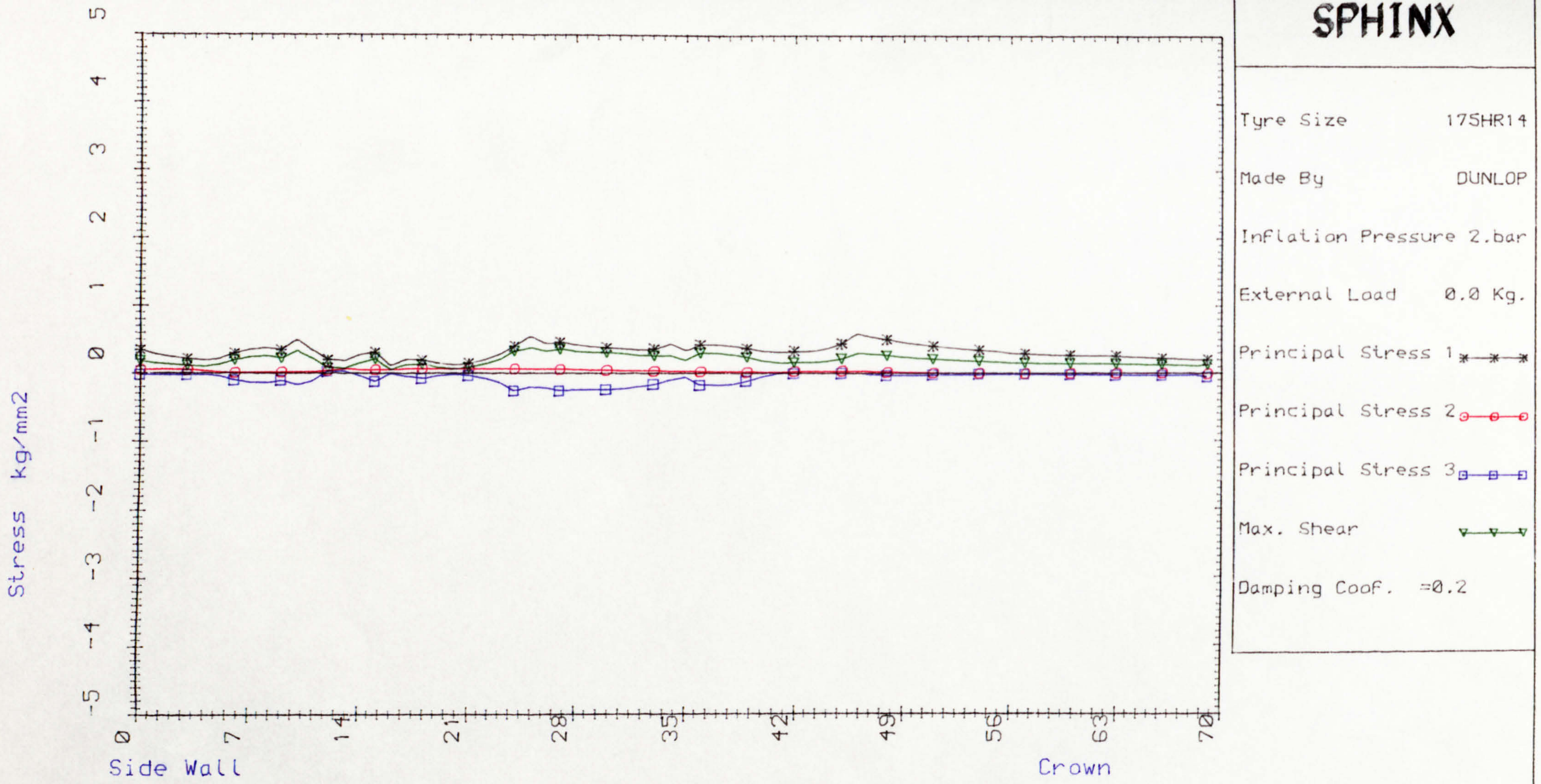


Fig.(8.38)Principal Stress Distribution in A Casing Ply

Due to Inflation and Viscous Effect

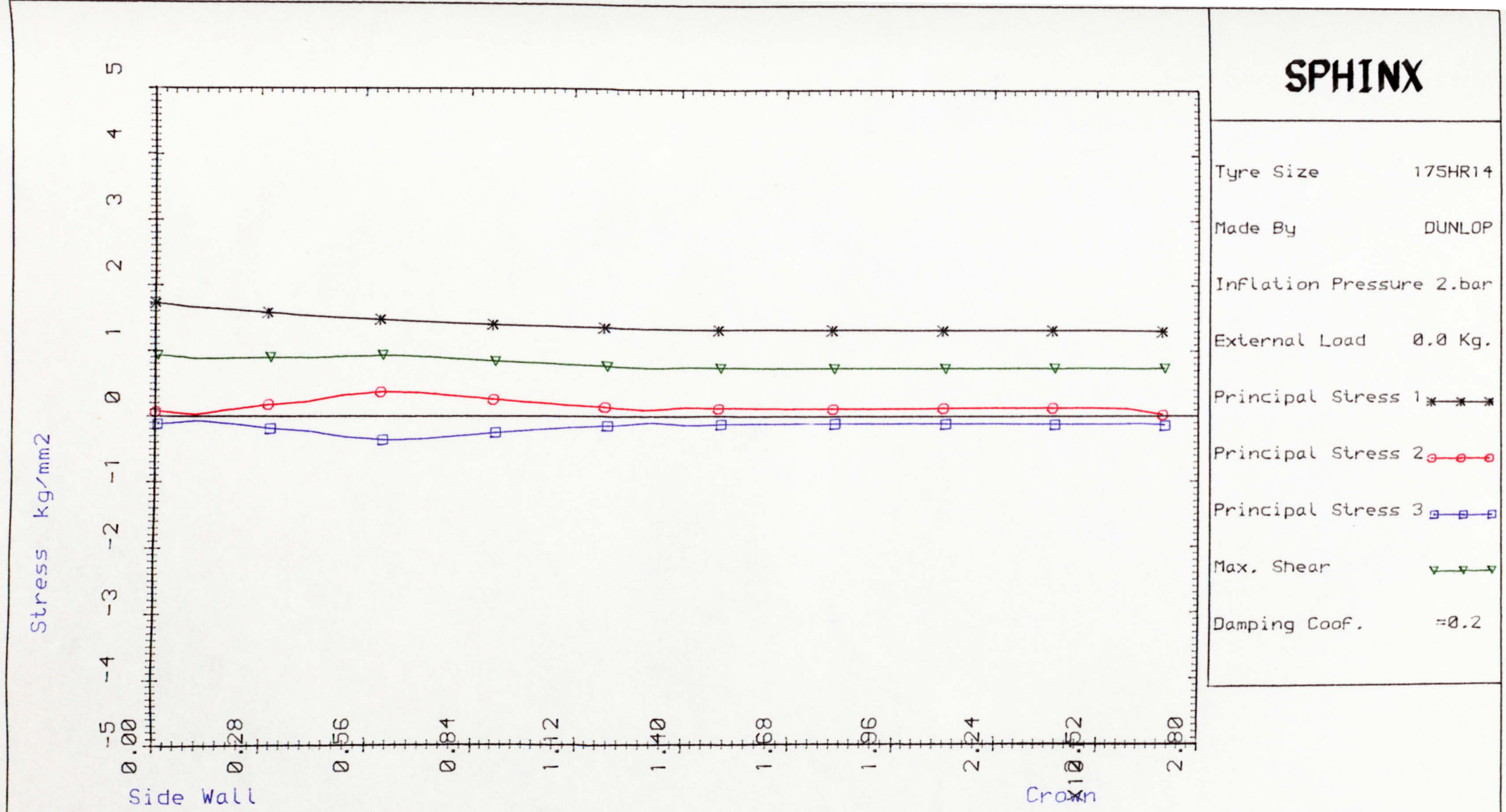


Fig.(8.39)Principal Stress Distribution in Breaker 1

Due to Inflation and Viscous Effect

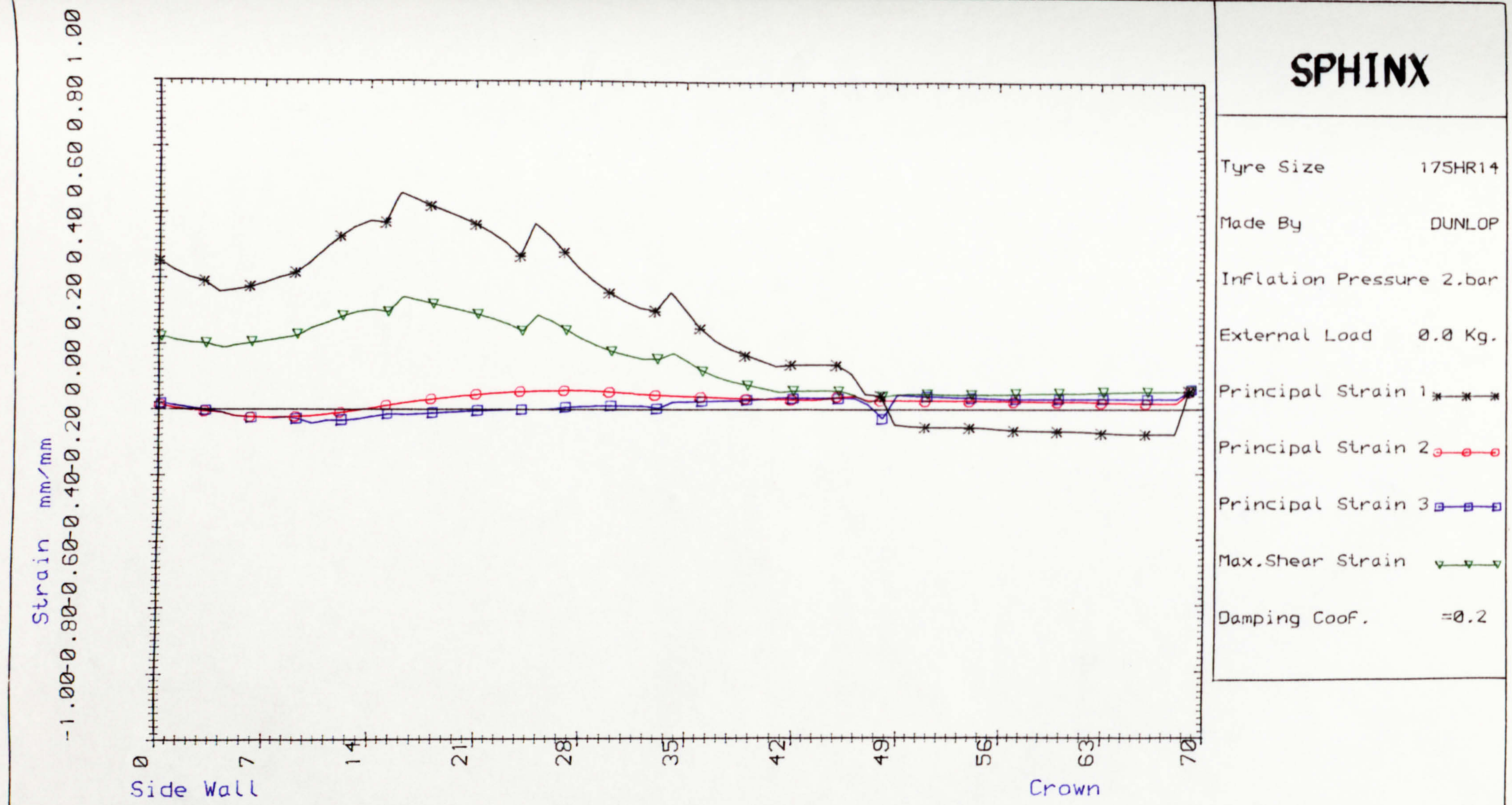


Fig.(8.40)Principal Strain Distribution in A Casing Ply
Due to Inflation and Viscous Effect

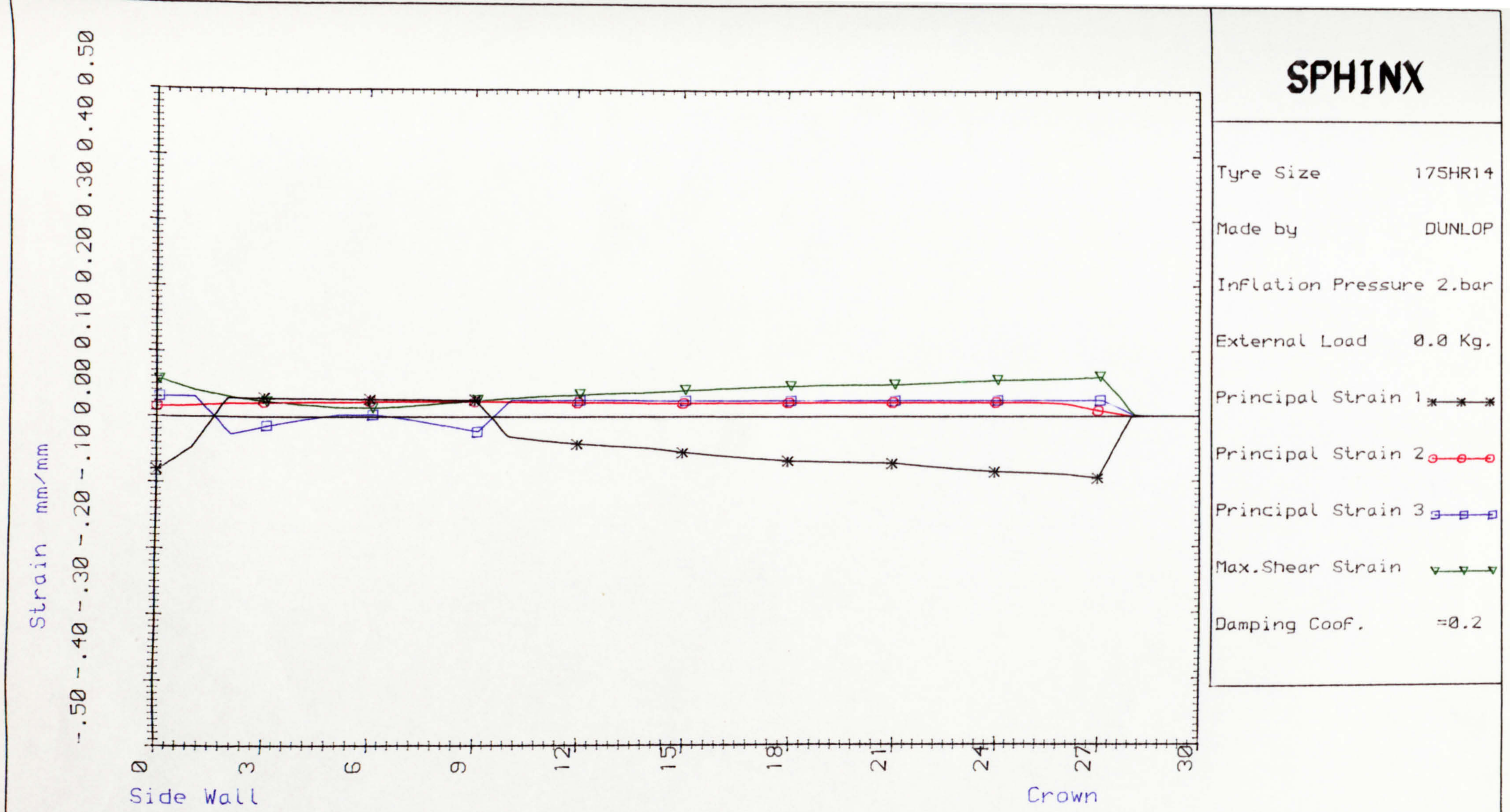


Fig.(8.41)Principal Strain Distribution in Breaker 1

Due to Inflation and Viscous Effect

SPHINX

Tyre Size 175HR14

Made by DUNLOP

Mode Shape No. 1

Frequency 1.515 Hz

Magnification =200

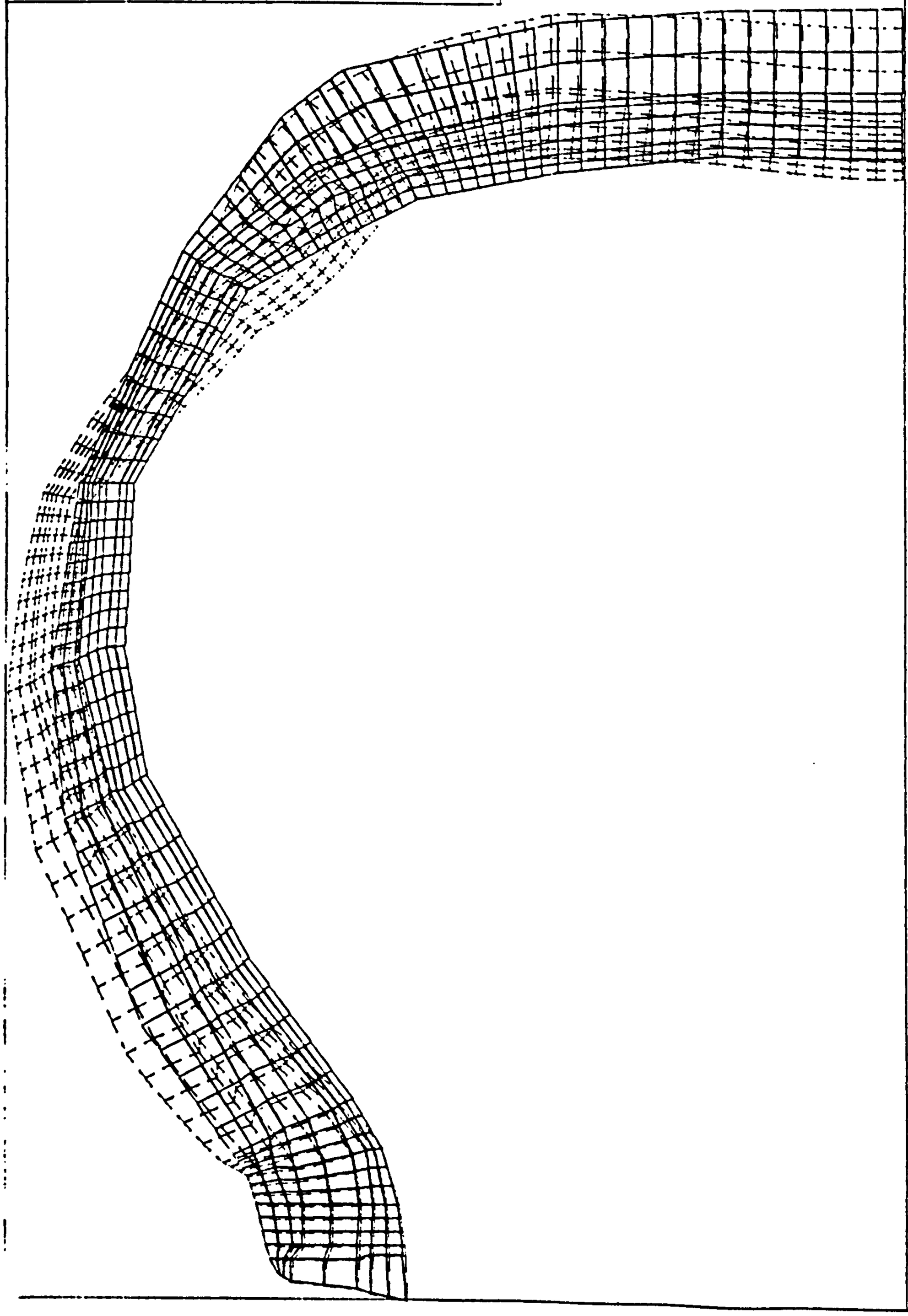
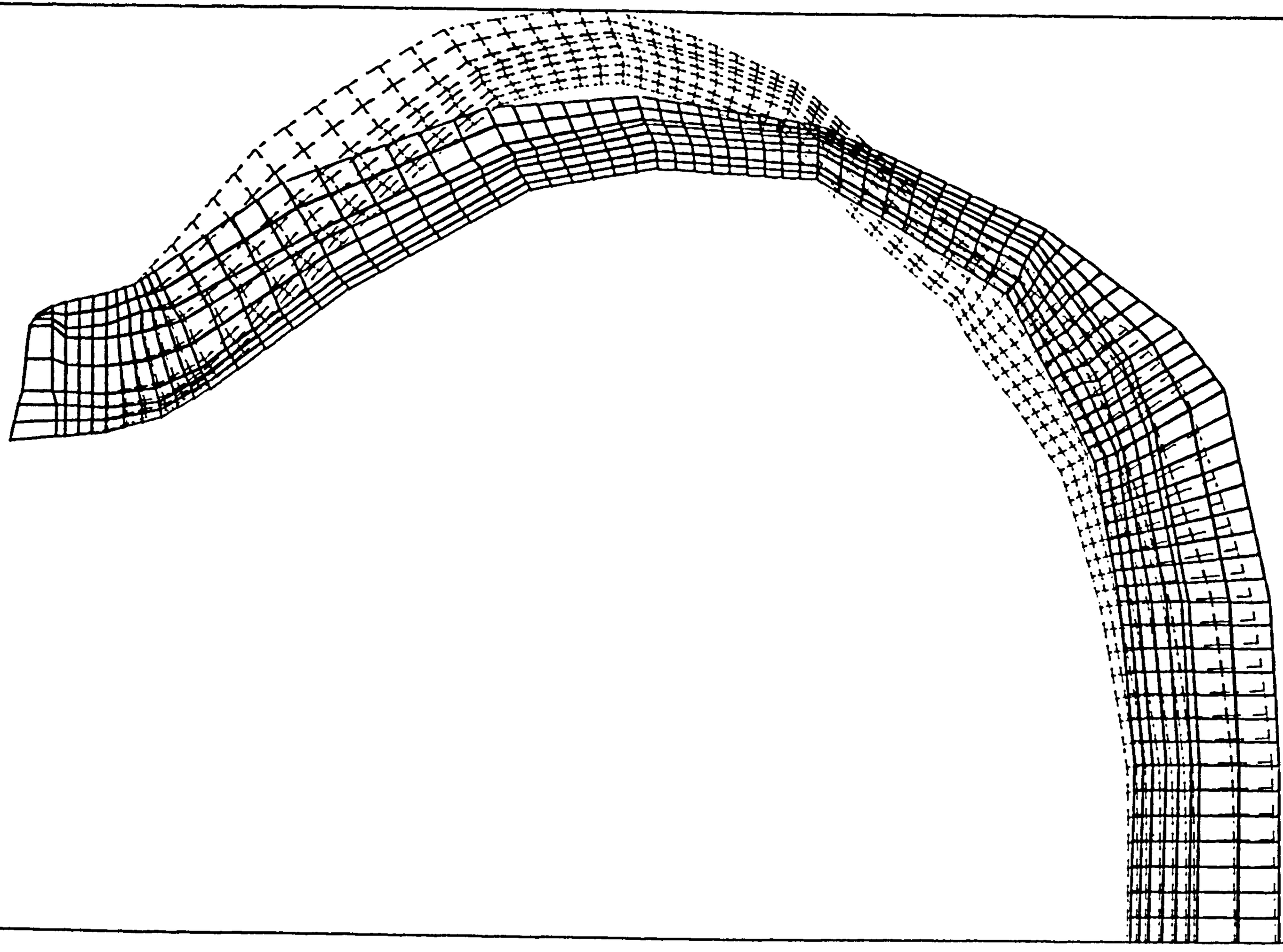


FIG. (8.42) FIRST MODE SHAPE OF RADIAL TYRE



SPHINX

Tyre Size	175HR14
Made by	DUNLOP
Mode Shape No.	2
Frequancy	2.581 Hz
Magnification	=10

FIG.(8.43)SECOND MODE SHAPE oF RADIAL TYRE

SPHINX

Tyre Size 175HR14
Made by DUNLOP
Mode Shape No. 3
Frequancy 3.288 Hz
Magnification =10

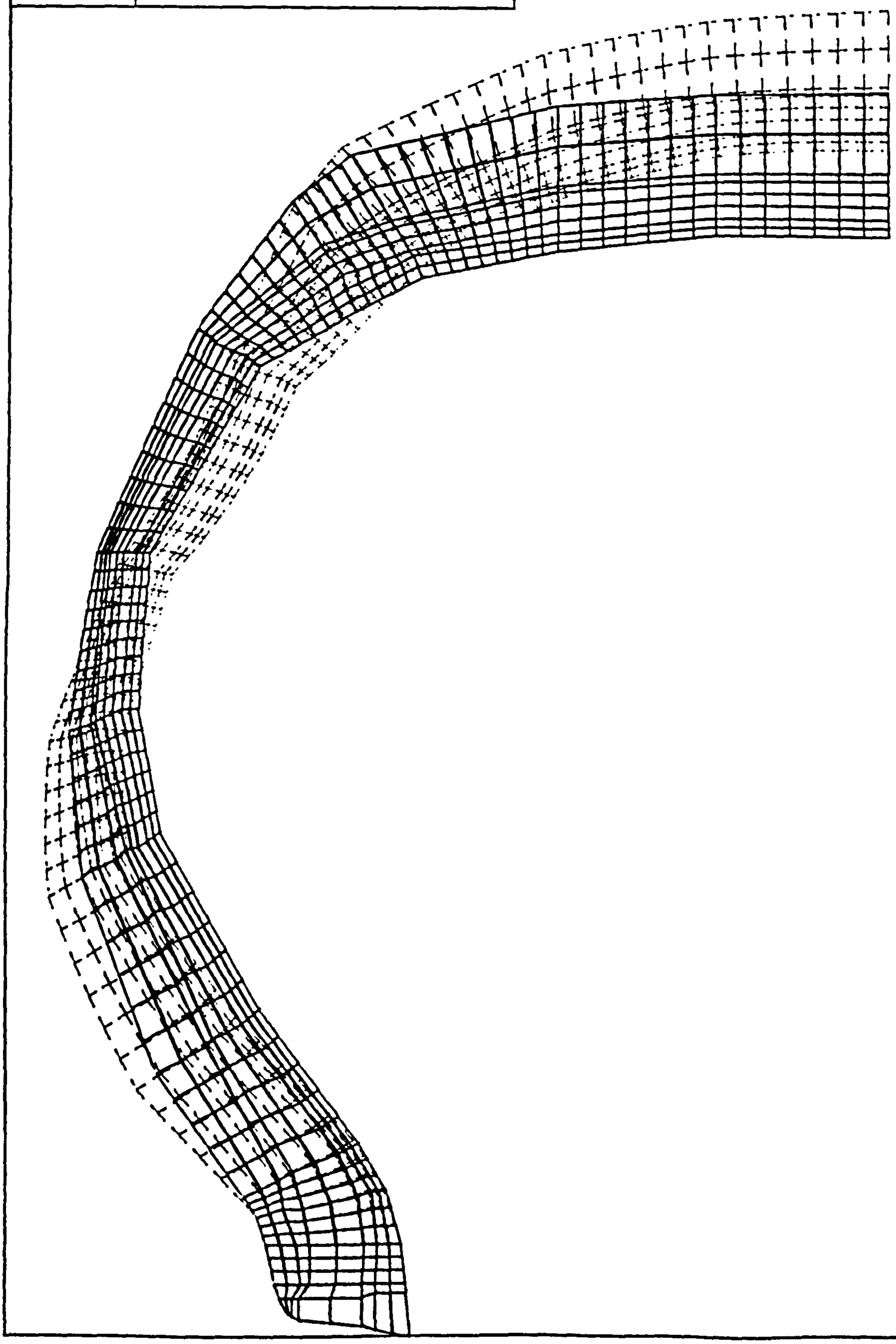


FIG.(8.44)THIRD MODE SHAPE OF RADIAL TYRE

SPHINX

Tyre Size 175HR14

Made by DUNLOP

Mode Shape No. 4

Frequancy 3.807 Hz

Magnification =10

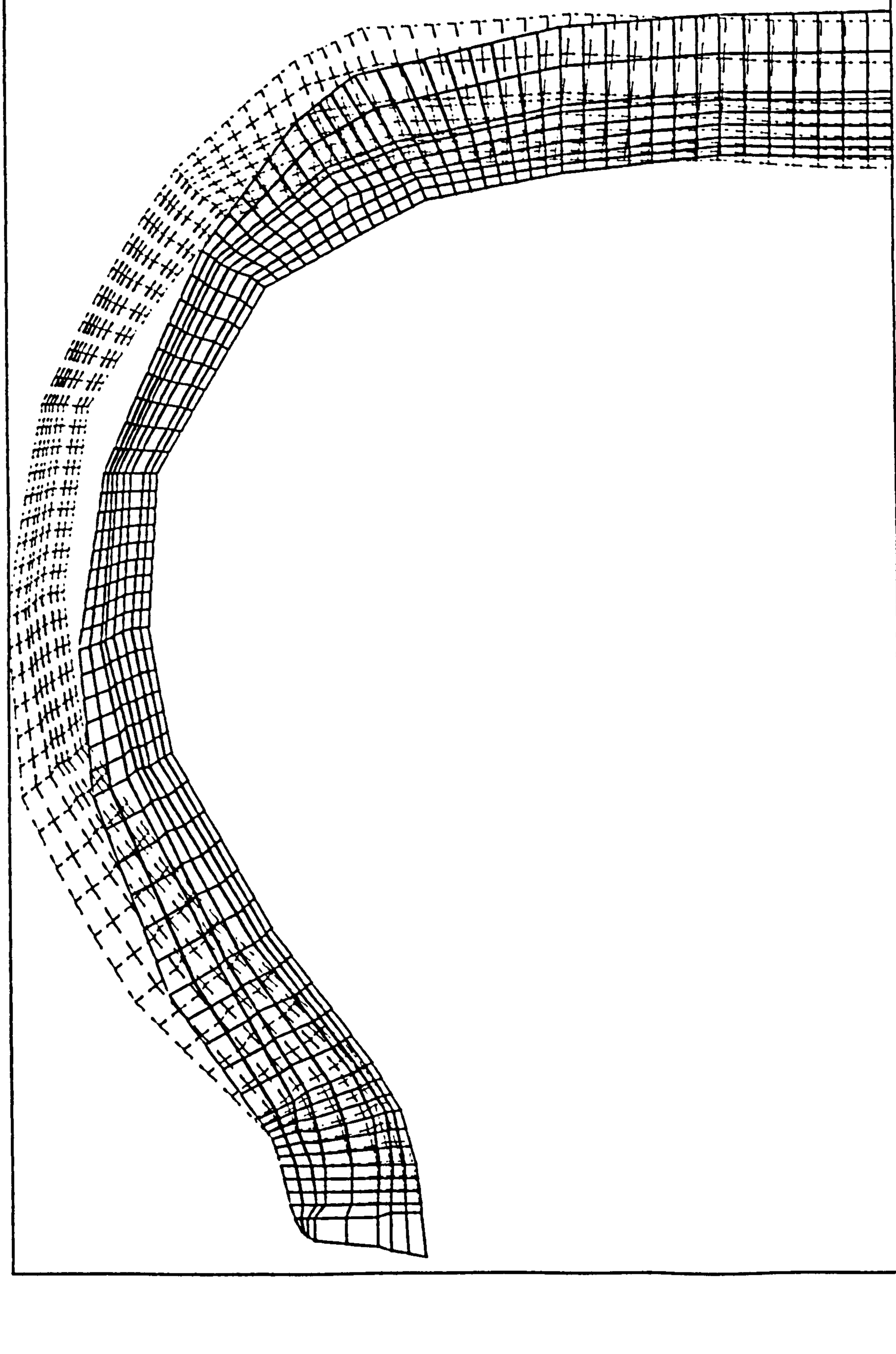
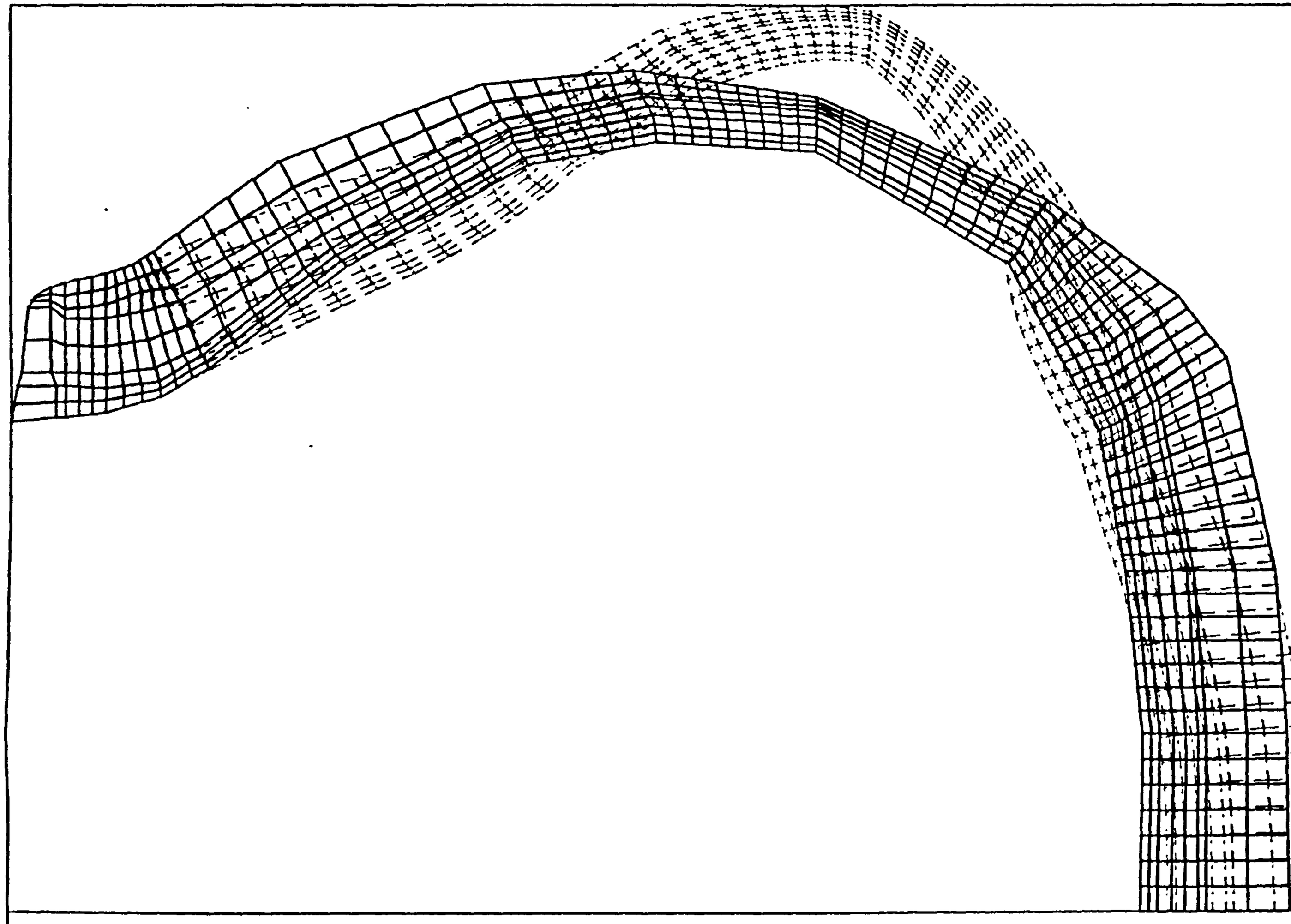


FIG.(8.45) FORTH MODE SHAPE OF RADIAL TYRE



SPHINX	
Tyre Size	175HR14
Made by	DUNLOP
Mode Shape No.	5
Frequancy	4.759 Hz
Magnification	=10

FIG.(8.46)FIFTH MODE SHAPE oF RADIAL TYRE